Overview of Lightning Hazards to Aircraft

Pierre Laroche
Scientific Adviser
Physics and Instrumentation Department

Since its early age, civil and military aviation had to face atmospheric events of unexpected dangerousness. At that time, lightning was certainly the most unrecognized and misunderstood atmospheric hazard to aviation. How and where an aircraft is struck by lightning, what the expected consequences for flight safety are and what damages could be anticipated, were still open questions at the very beginning of the 1980s. Up until this period, lightning safety on aircraft was ensured by oversized metallic protection and by considering the greatest lightning threat known. At the edge of the modern age of aviation, for which performances and safety were about to become of paramount importance, this approach was no longer valid. Awareness of the need for an in-depth knowledge and understanding of the entire physical aspect of the interaction between lightning and aircraft arose at that time.

The twelve articles gathered in this special issue are aimed at addressing the entire aspect of the interaction between aircraft, launchers and lightning, from the state of the art on storm electrification and lightning phenomenology, up to the advance lightning zoning method on aircraft and the electromagnetic topology of the threat.

Understanding where an aircraft encounters lightning begins with knowing the electrical characteristics created by a storm cloud in its vicinity. A storm cloud acts as a giant electrostatic machine, generating a mean current of few amps in magnitude and developing an electrical potential of tens of megavolts from the ground up to the level of the tropopause. Lightning flashes generated by storm clouds need to be known and understood. An aircraft struck by a lightning flash is connected to kilometer long arc channels: a quantitative evaluation of the threat to aircraft is obtained through the knowledge of the characteristics of the flash.

The state of the art on storm electrical environments is given in [1] and is illustrated by an example of in situ measurement reported in [2], showing the relation between the microphysics and atmospheric electricity within a convective cloud. Natural lightning properties are derived from a remote detection and mapping system [3], which contributes to obtaining important macroscopic information on lightning flashes, such as their length, energy, speed and current.

To be authorized to fly, aircraft and helicopter need to be protected against the effect of a lightning flash. The certification against lightning is a complicated process, which is still today based on a semi-empirical approach consisting of standardization and testing. Standardization is the result of a pragmatic synthesis between the general knowledge on lightning and the in-flight experiences of airline companies. Aircraft certification relies also on testing, whose adequacy and representativeness are key issues of the process [11].

The behavior of natural lightning flashes is determined by precursor discharges, which cannot be easily observed since they involve low currents and low light emission. Some types of these discharges play a major role in the behavior of lightning interaction with aircraft [4]. Laboratory experiments involving short atmospheric discharges, whose length is limited to about 10 meters, had contributed a lot of information on the physics of these precursor discharges. The gap of knowledge between few-meter-long discharges and kilometer-long natural lightning channels is filled with experiments on artificially

triggered flashes, which offer the opportunity of close-by observation of different types of precursors [5]. Triggered discharges and laboratory discharges were used to validate the physical modeling. Fundamental physical concepts were used to derive a simplified simulation of the attachment processes of lightning channels on aircraft [7] and to evaluate the surface distribution of different lightning hazards on an aircraft [8]. The design and the validation of the modeling depend on the in-flight observation of real events. From the mid-seventies up until the end of the eighties, three aircraft were instrumented to gather in-flight information on direct and indirect lightning strike events [6]. These validated simulations are used to design advance tools for a detailed description of the threat and the future advance approach in the Certification process at the aircraft design level [8].

The description and evaluation of the direct local effects of a lightning strike to the surface of the aircraft can be obtained by complex physical simulations [9]. Such a modeling approach is important for the design and the validation of the lightning protection for Carbon Fiber Composite aircraft.

A direct and nearby lightning strike induces strong electromagnetic coupling with the aircraft systems over a large frequency range, from a fraction of a kHz up to a few tens of MHz. 3D modeling of the coupling taking into account the actual waveform of the lightning signal is necessary to evaluate and mitigate this indirect threat [10].

In general, space launchers cannot be protected against the effect of a direct lightning strike. For that reason, special protection of the launching site and dedicated launching procedures are required to prevent any risk of a direct lightning strike [12] ■

References

[1] S. SOULA - *Electrical Environment in a Storm Cloud*. Aerospace Lab Issue 5, December 2012

[2] A. DELANNOY, P. GONDOT - *Airborne Measurements of the Charge of Precipitating Particles Related to Radar Reflectivity and Temperature within Two Different Convective Clouds*. Aerospace Lab Issue 5, December 2012

[3] Z. KAWASAKI - *Review of Location of VHF Pulses Associated with Lightning Discharge*. Aerospace Lab Issue 5, December 2012

[4] E. WILLIAMS, S. HECKMAN - *Polarity Asymmetry in Lightning Leaders: the Evolution of Ideas on Lightning Behavior from Strikes to Aircraft*. Aerospace Lab Issue 5, December 2012

[5] X. QIE, R. JIANG, P. LAROCHE - *Triggering Lightning Experiments: an Effective Approach to the Research of Lightning Physics.* Aerospace Lab Issue 5, December 2012

[6] P. LAROCHE, P. BLANCHET, A. DELANNOY, F. ISSAC - *Experimental Studies of Lightning Strikes to Aircraft*. Aerospace Lab Issue 5, December 2012

[7] P. LALANDE, V. MAZUR - *A Physical Model of Branching In Upward Leaders*. Aerospace Lab Issue 5, December 2012

[8] P. LALANDE, A. DELANNOY - *Numerical Methods for Zoning Computation.* Aerospace Lab Issue 5, December 2012

[9] L. CHEMARTIN, P. LALANDE, B. PEYROU, A. CHAZOTTES, P.Q. ELIAS - *Direct Effects of Lightning on Aircraft Structure ; Analysis of the Thermal, Electrical and Mechanical Constraints.* Aerospace Lab Issue 5, December 2012

[10] J.-P. PARMANTIER, F. ISSAC, V. GOBIN - *Indirect Effects of Lightning on Aircraft and Rotorcraft.* Aerospace Lab Issue 5, December 2012

[11] D. MORGAN, C. J. HARDWICK, S. J. HAIGH, A. J. MEAKINS - *The Interaction of Lightning with Aircraft and the Challenges of Lightning Testing*. Aerospace Lab Issue 5, December 2012

[12] F. ISSAC, E. BACHELIER, D. PROST, V. ENJALBERT, L. MOHEDANO - *Space Launching Site Protection against Lightning Hazards.* Aerospace Lab Issue 5, December 2012

S. Soula
(Laboratoire d'Aérologie, Université de Toulouse/CNRS)

E-mail: serge.soula@aero.obs-mip.fr

Electrical Environment in a Storm Cloud

This article gives an overview of the electrical characteristics of the thundercloud and the predominant mechanisms that are at the origin. The specific cloud that can produce lightning is described and the parameters that control its development and its organization are discussed. According to the variety of the scales of time and space associated with the mechanisms that occur within the thundercloud, it is difficult to simulate them both experimentally and numerically. Thus, the advances in the knowledge of the thunderstorm electricity have been sometimes relatively slow and have raised a lot of debates. Furthermore, in-situ observation remains difficult because of the hostility of the thundercloud medium for instrumentation, sensors, aircraft or other carriers of sensors. The responses to the questions in the domain of thundercloud electricity can sometimes remain speculative. However, recent detection techniques and laboratory experiments allow a better knowledge of the cloud electrical environment to be obtained. All aspects about lightning flashes and electrical discharges will be covered by other contributions in this issue.

History of the thundercloud electrical description

For most researchers, meteorologists and official organizations, lightning and thunderstorms are completely interdependent. Since the time of Benjamin Franklin, during the eighteenth century, it has been understood that the lightning flash is of electrical nature and therefore the thunderstorm that produces it is the seat of electrical processes. The first experiments simply showed that negative charge was present within thunderclouds and especially in their lower part. The difficulty in making in-situ observations has differed the understanding of the nature and causes of thundercloud electrification. Later, at the beginning of the twentieth century, C.T.R. Wilson, a famous scientist known for the Wilson cloud chamber used to follow trajectories of ionizing particles, showed that the thundercloud could hold both signs of charge by performing measurements with new sensors on the ground [1]. The charge structure as a positive dipole (positive charge above negative) of the storm was pointed out. However, all thunderclouds did not correspond with this scheme and reverse structures were sometimes observed from in-situ measurements [2]; [3]. In the second half of the last century, a lot of theories of charging have been proposed, along with some experiments of cloud exploration with new sensors using modern electronics and carried by aircraft or balloons. In parallel, laboratory experiments have simulated cloud microphysics and charge separation at small scale between particles. Resulting from these advances, the question of the effective contribution of the charging processes to the cloud electrification has fed a lot of discussions between researchers in the community of atmospheric electricity [4]; [5].

To return to the electrical cloud structure, a third and smaller charge center was also observed within many storms [6]. Charge was also observed at the periphery of the cloud as screening layers, especially at the cloud top [7]; [8], which was also confirmed theoretically. Finally, more complex charge structures have been observed with repeated experiments of cloud soundings and techniques derived from lightning mapping, or obtained with electrified cloud modeling (see in the following). This paper reviews current knowledge in the electrical characteristics of thunderclouds. The first section describes the thermodynamics and the microphysics of different categories of storms. The second section is devoted to the charging processes that can take part within the thundercloud electrification. The third section describes the main electrostatic structures observed or simulated within thunderclouds.

Thundercloud development and organization

Thunderclouds are the result of air convection combined with substantial humidity. The convection can initiate when conditional instability is released. In order to describe the conditional instability, the parcel theory is used: when a parcel of air moves in an upward vertical direction, it follows an adiabatic process – no energy is exchanged between the parcel and the surrounding air – which reduces its temperature at a rate of about 10°C every kilometer. If the parcel is found to be less cold than the surrounding air at its new altitude,

it can continue to rise because of an upward buoyancy force. Furthermore, if the parcel air saturates during its ascent, its temperature decreases more slowly because of the latent heat of condensation released. Under these conditions, the vertical motion of saturated air is called 'moist convection' and it happens on a large scale within the thundercloud. Thus, chances for moist convection are determined by the amount of moisture and high temperature in the lowest kilometers of the atmosphere, together with a strong decrease of temperature with height (colder air above) in the 2-5km layer. Additionally, if atmospheric circulations are present, they can adiabatically cool down (by lifting) mid-level layers and force parcels from lower levels to ascend, so that they become warmer than their surrounding air and will continue to rise by themselves (after having reached the Level of Free Convection). The atmosphere capability to produce 'buoyancy' can be expressed thanks to criteria, for example, the Convective Available Potential Energy (CAPE), which is a potential energy in J kg^{-1}:

$$CAPE = \int_{LFC}^{EL} g\left(\frac{T_v^{parcel} - T_v}{T_v}\right) dz$$

Where EL and LFC are the equilibrium and free convection levels, respectively; i.e. the heights between which a parcel is warmer than its surrounding air. T_v indicates the virtual temperature (temperature corrected for moisture content, so that densities can be compared). Figure 1 illustrates the calculation of this criterion. CAPE can be converted to kinetic energy in the form of a convective updraft, the velocity w of which is generally proportional to the square root of the CAPE:

$$w = \sqrt{2 \cdot CAPE}$$

However, on one hand, precipitation can prevent the calculated upward velocities from being attained and, on the other hand, other factors such as wind shear interactions with the updraft can increase the strength of wide updrafts. Also, CAPE in a certain area will eventually be consumed if released because, in effect, the troposphere is mixed towards a neutral thermal stratification. Thus, thunderstorm activity may last longer in areas with steeper lapse rates and higher CAPE.

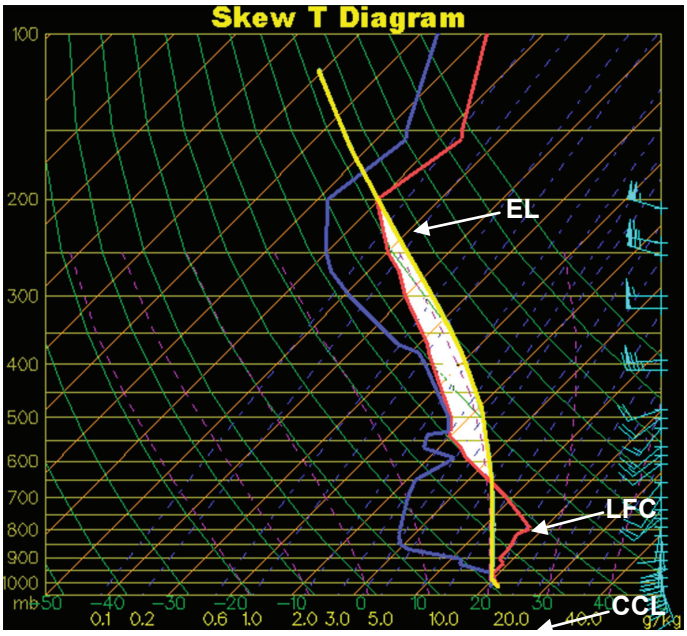

Figure 1 - CAPE from a skew-T thermodynamic diagram: the white shaded region on the sounding below is the CAPE area. The red line is the atmosphere sounding and the thick yellow vertical line is the parcel sounding. CAPE is especially important when air parcels are able to reach the (LFC) or Layer of Free Convection. The white region ("positive energy" region) is called CAPE and is expressed in Joules/kg. A CAPE value more concentrated in the lower half will produce a stronger updraft than an equal CAPE value that is stretched higher and narrower.

The thundercell is the basic organizational structure of all thunderstorms, as previously depicted by Byers and Braham [9] and this notion became the fundamental paradigm for thunderstorms. A typical cell lives for about 15-60 minutes, including the three stages illustrated in figure 2: growth stage as towering cumulus, mature stage with both updraft and downdraft, and dissipation as cool outflow cuts off the base of the updraft from its supply of warm air. At its mature stage, it consists of an updraft, where warm moist air rises and water vapor condenses into cloud particles from which precipitation-sized particles may grow; and a downdraft, where precipitation falls and drags the surrounding air downward, helped by evaporative cooling of cloud and precipitation particles near the top and sides of the cloud. The interaction of vertical wind shear with buoyant bubbles is responsible for enhancing updraft and downdraft velocities, which has a consequence on the longevity of the convective cell.

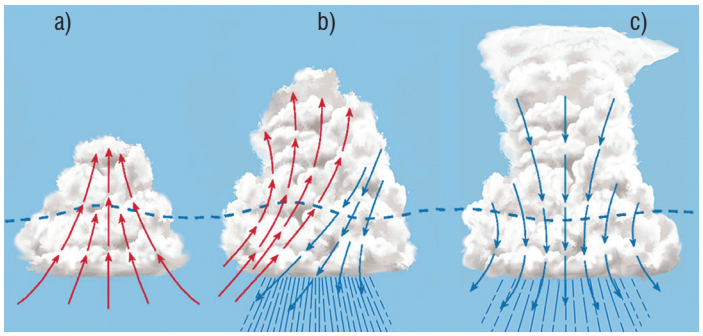

Figure 2 - The thundercell at different stages of its lifetime: a) development stage, when only updrafts are generated; b) mature stage, when updrafts and downdrafts coexist; c) dissipating stage, when only downdrafts subsist.

In the cases of strong vertical shear (>15 m/s shear vector between 0-6 km altitude) and clockwise turning of layer shear vectors at heights within the lower kilometers, a storm cell may acquire rotation as it ingests vorticity via the winds that it ingests. These special cases of cells are called 'supercells' and typically produce large hail (2-6 cm or even larger) as evidence of their exceptional updraft strength, as well as tornadoes and downbursts of damaging winds (figure 3a). As proposed by Browning [10], the supercell model initially was conceived as a quasi-steady form of an ordinary cell. Browning [11] later developed a new definition of a supercell, as a convective storm having a mesocyclonic circulation. The mesocyclone creates the radar reflectivity morphology ("distinctive" features [12], such as hook echo structures and Line Echo Wave Patterns (LEWPs)) typically associated with supercells (figure 3b). Thus, supercells can have strong updrafts, even when the static instability, as measured by CAPE, is modest [13]. Because the mass continuity requires compensating subsidence around the updraft and the convective downdrafts typically do not process as much mass as the updrafts [14], the most intense updrafts will virtually always be isolated. Thus, supercells are relatively rare as well as isolated storms, and are predominantly a mid-latitude phenomenon. Tropical environments usually do not have adequate shear to develop deep, persistent convective mesocyclones [15].

Figure 3a - Picture of a supercell.

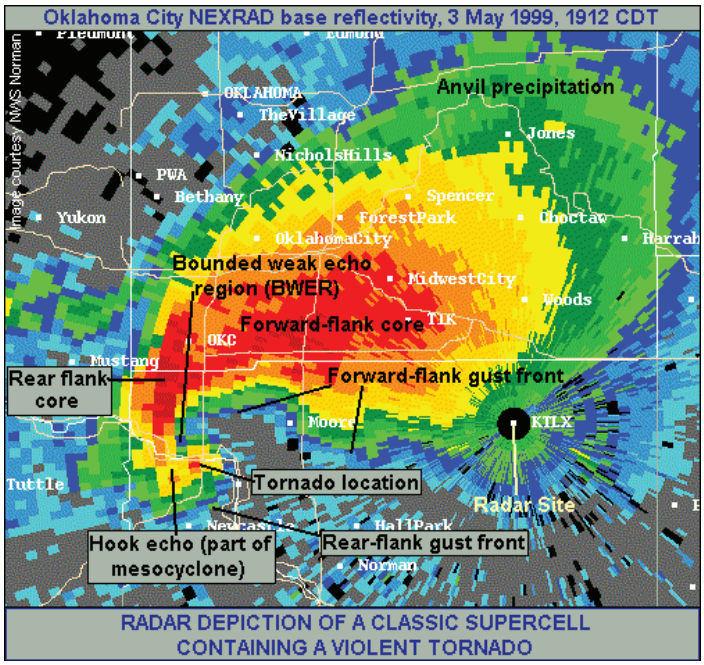

Figure 3b - A radar image of a violently tornadic classic supercell near Oklahoma City, Oklahoma, USA on the 3rd of May 1999. (http://www.spc.noaa.gov/faq/tornado/radscel.htm)

A multicellular thunderstorm cluster is a thunderstorm that is composed of multiple cells, each at a different stage in the life cycle of a thunderstorm [16]. These old cells dissipate as new cells form and continue the life of the thunderstorm system, with each cell taking a turn as the dominant cell in the group. New cells usually form in the upwind (usually western or southwestern) part of the storm, mature cells are usually in the center of the storm and dissipating cells are usually in the downwind (usually eastern or northeastern) part of the storm. The picture in figure 4 illustrates such organization of cells. The multicellular storm cluster can last for hours, while each individual cell should only last for about 20 minutes. These storms can sometimes be severe and sometimes have awkward paths due to the thunderstorm sometimes not following the path of the cells that compose it. Any severe activity in one of these storms will most likely come from the dominant cell near or after its peak updraft strength.

Figure 4 - A multicell cluster consists of a group of cells at different stages of the life cycle, moving as a single unit. New cells tend to form along the upwind and individual cells take turns at being the most dominant. (© Harald Edens).

Figure 5 - Picture of a squall line (© Oscar van der Velde). A squall line is a line of severe thunderstorms containing heavy precipitation, hail, frequent

Linear organization is often observed in the convective systems. As a matter of fact, since outflow is an effective mechanism for lifting near-surface parcels to their LFCs, it can have a dominant role in the development of subsequent cells when it develops. If the horizontal convergence along outflow boundaries has a value of 10^{-2} s^{-1} through a layer as deep as one km, the resulting upward motions at a height of one km are of an order of 10 ms^{-1}, which can initiate deep convection [15]. As convection continues, new outflows merge with old ones, resulting in an expanding pool of cold, stable air at low levels, often with new convection on its leading edge, as the outflow pushes into untapped, potentially buoyant air ahead of the outflow. Such systems are organized linearly and include mesoscale convective systems (MCSs), such as for example squall lines (figure 5). A related factor in developing a linear structure is the nature of the process responsible for the first convective cell initiation. When the lifting mechanism is a front, a dryline, or a pre-frontal trough, there are along-line variations in the lift resulting from these processes. Also, there is variability in the thermodynamic characteristics of the lifted air. Thus, the first convective developments can occur separately to form individual cells but rapidly, convective elements develop along the line and merge because of the overall linear nature of the initiating mechanism for

thunderstorms. The subsequent development of cold outflows serves to reinforce this evolution; hence, the high frequency of this sort of organization to convective systems.

The electrification processes

One of the longest-standing questions is how convective clouds become electrified in order to produce lightning. To answer this question, researchers have performed laboratory experiments and field observations, but it is difficult to obtain a definitive explanation because of the range of the distance scale between the microscale of the physical processes concerning the cloud hydrometeors (water particles) and the size of the thundercloud for the charge structure. Likewise, the multiple processes taking part in the charge and discharge phenomena within the thundercloud cover a very large range of time. Furthermore, it is very difficult to make *in situ* measurements, because the storm conditions are hostile to the instrumentation. Some mechanisms are described here that can take part in the cloud electrification, either as a process to initiate and sustain it, or as complementary processes to reinforce it.

Non-inductive ice-ice charging mechanism

Of all charging mechanisms proposed during past century, the one considered as the best able to start the electrification within the cloud and to reproduce the vertical charge layering and the amount of charge observed, involves rebounding collisions between ice crystals and graupel pellets. The graupel pellets can be described as small porous hail and grow as small supercooled cloud droplets freeze to their surface (riming). This mechanism is non-inductive, i.e., it does not need an external electric field to create charge on a particle. To study this kind of mechanism, researchers use laboratory experiments to empirically analyze the different aspects of the electrical properties of particles in a controlled environment that can reproduce that of the thundercloud. Early on in these experiments, it was found that the result of the mechanism strongly depends on several parameters. Takahashi [5] showed that according to the ambient temperature and the liquid water content, riming particles charged positively (for higher temperatures and for either very high or low cloud water content), or negatively (for colder temperatures and for the mid-range of cloud liquid water content). Similar experiments performed by a University of Manchester (UMIST) group led to slightly different results: there indeed was a charge reversal temperature below which the riming particle acquires negative charge, but this temperature decreased in their case as effective cloud water content increased, meaning that positive charging becomes more likely [17], [18], [19]. The largest difference was a reversed polarity for the riming particle at low effective water content, negative for Takahashi's results [5] and positive for [18]. Both results are shown in figure 6. It was found that the charge amount transferred during a collision depends on the size of the ice crystal [20] and that for a large amount of liquid water content, the droplet size distribution can modify the sign of the charge of the riming particle [21]. Recently, researchers from Argentina [22] obtained results that show that at a temperature > -19°C, the magnitude of the charge transferred decreases as the liquid water content increases.

The experimental setups can be a major cause of the different laboratory results. For example, the use of a single cloud of water and ice particles (UMIST experiment), instead of mixing two separate clouds of water and ice particles shortly before encountering the riming

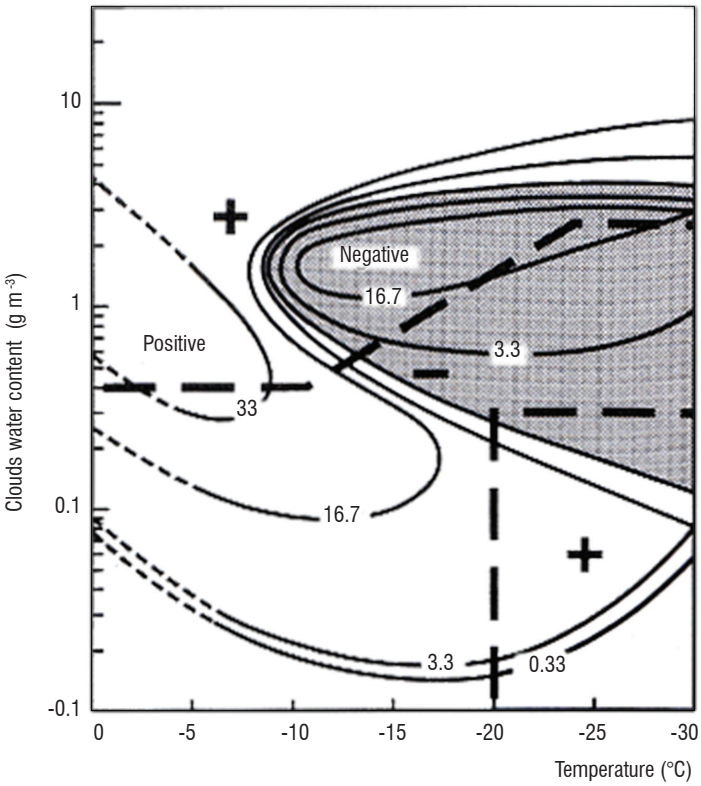

Figure 6 - Polarity of charge gained by rimed graupel after a collision with an ice crystal, as a function of ambient temperature and liquid water content for the Takahashi [5] experiment (curves) and for the Saunders et al. [18] experiment (lines). The dashed bold lines outline the temperature and liquid water content values at which the charge of the graupel changes its polarity. (From MacGorman and Rust [30]).

target, small ice particles grow at the cost of cloud droplets and the saturation (relative humidity) will be smaller with respect to liquid water ([23], [24]. Lower relative humidity at temperatures around -15°C means higher saturation with respect to ice than to water, which leads to the depletion of vapor from liquid surfaces to ice and a more neutral to positive charge on the riming target [25]. Concentrations of different aerosols, which influence the formation of cloud droplets, may also affect the resulting charge for a given temperature-humidity regime. For example, aerosols can lead to charge reversal, by suppressing the precipitation in the cloud and leaving a greater amount of supercooled cloud water at greater heights and lower temperature [26]. At a large scale, cloud condensation nuclei (CCN) aerosol particles could play a significant role in differences in lightning production between maritime and continental thunderstorms, but no observational evidence could be obtained because of the associated thermodynamic differences. Yuan et al. [27] showed lightning enhancement in the presence of increased aerosol produced by volcanic activity, while the meteorology conditions did not change.

A possible explanation for the difference of the charge polarity on the graupel pellet is given by the laboratory experiments performed by Baker et al. [28] and later by Emersic and Saunders [29]. They found that the target simulating the ice particle involved in the collision with ice crystals was positively charged when its surface was growing more rapidly from the vapor than from the ice crystals, and negatively in the opposite case. However, for the same growth regime of the ice particle, all experiments do not provide the same result and the question is still open even after several series of experiments. Actually, one set of experiments showed that the individual charge gained by

a rimed graupel could be either positive or negative [21], and others, while most previous experiments considered the average charge. Despite a lot of questions for this non-inductive mechanism, some agreements can be noted about its contribution to the thundercloud charge, as indicated by MacGorman and Rust [38]: the simultaneous presence of riming larger ice particles and at least a small amount of liquid water is required; For large amounts of liquid water content, the graupel is positively charged and for intermediate amounts it is negatively charged, which explains the main negative charge pole within the cloud; If the temperature is less cold (near zero) the graupel becomes positive, regardless of the liquid water content. Finally, the non-inductive ice-ice charging mechanism matches well with the overall tripole-charge structure often observed. The role of graupel particles in the charging processes is confirmed with in-situ observations, especially when the total lightning activity is detected and the microphysics species are inferred from radar observations (see for example [31]).

Inductive charging mechanisms

All mechanisms of this category cannot explain the charge to produce the primary electrostatic field within the thundercloud. Ion capture is one of the earliest to be suggested, especially by Wilson [1]. It works between ions and falling frozen or liquid hydrometeors in the presence of an electric field, which makes the particle polarized (figure 7a). The ions involved in the process could be mainly produced by lightning flashes [32]. The precipitating particle captures the ions with polarity opposite to the charge of its bottom and repels the ions with the same polarity. Thus, if the direction of the electrostatic field is downward within the cloud, negative ions are captured by the hydrometeor, which becomes charged negatively. The motion of the ions can be driven either by the electric forces, or by the updrafts. The efficiency of the mechanism is related to the relative velocities of both ion and particle. For example, if the particle velocity is low, ions repelled by the bottom of the hydrometeor can be attracted by its top and finally captured, which reduces the efficiency. The capture of charge by the bottom causes a migration of an opposite charge from the top, which reduces the capability for attracting additional charge. The magnitude of the ambient electrostatic field is therefore an important parameter to sustain the mechanism, which does not assign a major role in the primary cloud electrification. For a normal dipole structure (positive charge above negative charge) ion capture tends to transfer a negative charge to the precipitating particles between both poles, which increases the negative charge of the main pole. Ion capture is selective in the presence of an electric field, but it can work for both ion polarities in its absence. If one of the charged ions is predominant, as for example below the thundercloud, the particles can acquire charge by this process.

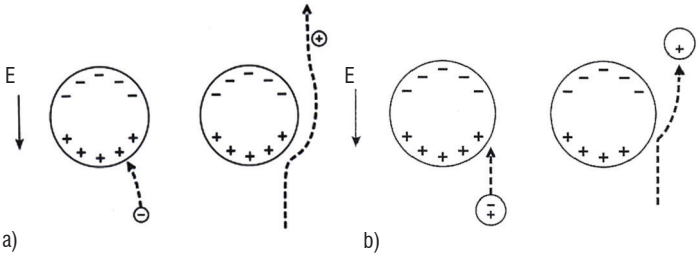

Figure 7 - a) Selective ion capture by a polarized drop. The lower side of the drop attracts the negative ion and repels the positive ion. b) Inductive charging of the rebounding polarized drop and droplet. E is the electrostatic field. From MacGorman and Rust [30].

Another inductive charging mechanism can work between colliding and rebounding particles. If particles have different vertical velocities, the collision between them can occur as described in figure 7b. Particles of different sizes, including precipitating particles and cloud droplets, can be actors of this mechanism. In the presence of an electric field, both particles are polarized and they collide by their bottom for the larger one and the top for the smaller one, i.e., by their oppositely charged sides. After rebounding, both particles carry a net charge, negative for the precipitating one and positive for the one that rises. As for the selective ion capture, this mechanism can reinforce the main negative charge of the cloud.

Other processes

Finally, many other processes were proposed, but it is really difficult to properly estimate their existence under the thundercloud conditions and their relative contribution to the storm electrification. One of these processes is the convective electrification theory, which is completely different from the others, since it does not involve the hydrometeors to create charge within the cloud. It is also called ″Vonnegut convective electrification″ [33] and explains the presence of positive charge at the top of the cloud with the ions entrained by upward air motion. The presence of negative charge at lower levels should be due firstly to being attracted from the cloud environment by the positive charge at upper levels and then carried down by the subsidence. However, quantitative estimations show that the amount of charge and the time delay involved in such a process are not consistent with the observations at the scale of the thundercloud [4], [34], [54]. Ice particles or liquid hydrometeors can gain charge by many other processes, especially during melting for the ice, or evaporation or condensation for the water. Drops can also become charged when they splash. None of these mechanisms can be efficient enough to be taken into account in the storm electrification.

The charge structure of the thundercloud

The tripole vertical structure was proposed early on, but though it is generally well adapted to the thundercell it is not suitable for complex and big storms structures [35]. In a normal storm, negative graupel pellets form the lower of both main poles, while positive lighter ice crystals are advected to greater heights and form the upper pole. A secondary and small positive pole occurs at the cloud base because of the warmer temperatures and possibly because screening layer charge at the bottom of the cloud is ingested.

Normal charge structure

One of these methods involves measuring the electrostatic field (E) within the thundercloud, because it is linked to the overall charge structure and it is difficult to directly measure the charge carried by all types of hydrometeors within the whole thundercloud. Extensive *in situ* measurements of E have been performed with airplanes and balloons, each one providing different characteristics of this parameter. Thus, soundings with balloons provide vertical profiles and airplanes tend to provide horizontal variations at given altitudes. Some measurements have also been made with rockets, with the advantage of obtaining an instantaneous state of the structure. However, most of the works that have been published are based on balloon soundings performed when the thundercloud electrification has been initiated. Thus, the maximum rarely exceeded 200 kV m^{-1}, even though

horizontal and vertical components were measured [30]. The vertical soundings of E have been used to infer the charge density in the region crossed by the balloon, thanks to Gauss's law with a one-dimensional approximation [36]. This method allows the net charge to be determined, without identifying the nature of the charge carrier (ions, precipitation, ice particles, etc.).

By using several soundings performed within three different kinds of convective systems (supercell, MCS and mountain storm), Stolzenburg et al. [36] proposed a structure for the convective region of the storm (figure 8). All regions of charge are found to have horizontal dimensions much larger than the vertical ones. The convective updrafts have four charge regions: the lowermost is weak and positive; a main negative charge above this one forms the main dipole with an upper positive charge; a shallow layer of negative charge is added near the upper cloud boundary. Outside this updraft region, six different charge layers are generally observed, with the uppermost still negative and the others with alternating polarity down to the lowermost. However, the latter structure can frequently vary from one storm to another [37].

The altitude of the charge regions within the updrafts change from one convection type to another and the main negative region is related to the average updraft speed. While it can be found at about 9 km in a supercell, it is only at about 7 km in an MCS and about 6 km in a mountain storm. When individual charge measurements were made, the main charge carriers were identified as precipitating particles in the positive lower and the main negative charge regions for the updrafts region, while they corresponded rather with cloud particles above the main negative charge [36], [38], [39]. This kind of structure can evolve into more complex ones after lightning flash production and when the updrafts decline [40]. Generally, intracloud and negative cloud-to-ground flashes are produced from these regions of the storm, the latter requiring intense electrostatic field values at low altitude, generally allowed by the presence of the lower positive charge.

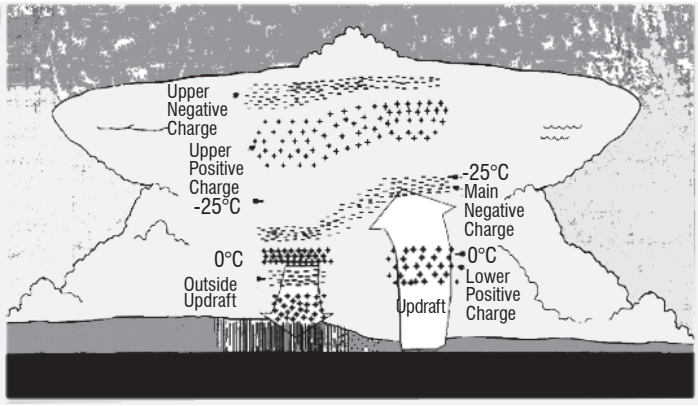

Figure 8 - Charge structure in the updrafts and the downdrafts of a thunderstorm. From Stolzenburg et al., [56].

Large amounts of positive charge have been observed [57] within the stratiform regions associated with the MCSs. According to the long time of activity of a MCS, the charge structure within the stratiform characterized by weak updrafts, a horizontally extended melting region and dying cells, may be complex. Marshall and Rust [57] identified two kinds of structure, one with five vertically-distributed charge regions, sequentially positive and negative, and one with only four regions. The most dense charge region is around the 0°C level in each case and can be positive or negative. Another type of structure, called "anvil-type", is characterized by a cloud base above the melting level, a deep positive charge within the cloud, a lower negative screening layer and a possible upper negative layer. The reservoir of positive charge located at or above the melting level can provide charge for positive flashes with large peak currents and/or large charge moment changes, which are generated close to the convective region and at the origin of sprites [41].

Inverted charge structure

Data from lightning mapping systems displays the path of the flashes, thanks to the VHF radiation produced by their leader phases [42]. In a normal charge structure, intracloud flashes move through two layers of charge: positive charge above negative charge. Because the negative leader radiates more than the positive one, the thunderstorm charge structure can be inferred by examining a composite of the charge structures of many individual flashes within a storm [31]. In specific storm cases, inverted-polarity intracloud flashes move through two layers of charge in the opposite configuration: negative charge above positive charge [43]. Thus, the main dipole exhibits a negative charge above a positive charge [44]. These storms tend to produce predominately positive cloud-to-ground lightning flashes and inverted-polarity intracloud flashes, and they can occur preferentially in some regions as US high plains region[45].

The Severe Thunderstorm Electrification and Precipitation Study (STEPS) took place in the early summer of 2000, in order to study severe storms occurring within this region and to describe their charge structure [44]. Balloon field soundings and data from a lightning mapping array (LMA) were used during the experiment. The LMA stations use a time-of-arrival technique to provide three-dimensional location and time of sources of very high frequency (VHF) radiation pulses produced by the electrical breakdown during the lightning channel propagation [46], [47]. For a lightning flash, the LMA may locate hundreds to thousands of such VHF sources, which allows the lightning path and the total lightning activity to be mapped in detail. Several cases of storm were analyzed with both means of electrical investigation associated with radar observations (see for example [37] for a multicell storm). Four sections of this multicell structure storm were analyzed at different periods of its lifetime. The electrical structures of each of these sections differed from the others during all or part of the analyzed periods.

Figure 9 displays the charge structure provided by the LMA within four regions of the storm system at the first period analyzed. The information is qualitative, since any charge density value may be evaluated and it shows the location of the charge regions. Thus, the regions are also found to have a much greater horizontal extension and the number of regions is comprised between two and four. One section (A) has a normal dipole, while three others display the inverted structure. From the same case study, Weiss et al. [37] made a comparison of both methods (balloon and LMA) of charge structure investigation and the result is displayed in figure 10 for the most complex charge structure found in a convective section of the storm. The same vertical distribution of charged layers is found by both methods, with some differences in the heights. The intracloud lightning flashes concentrated within the regions with large radar reflectivity values and the rate of cloud-to-ground flashes, predominantly positive, increased when reflectivity cores descended to lower heights.

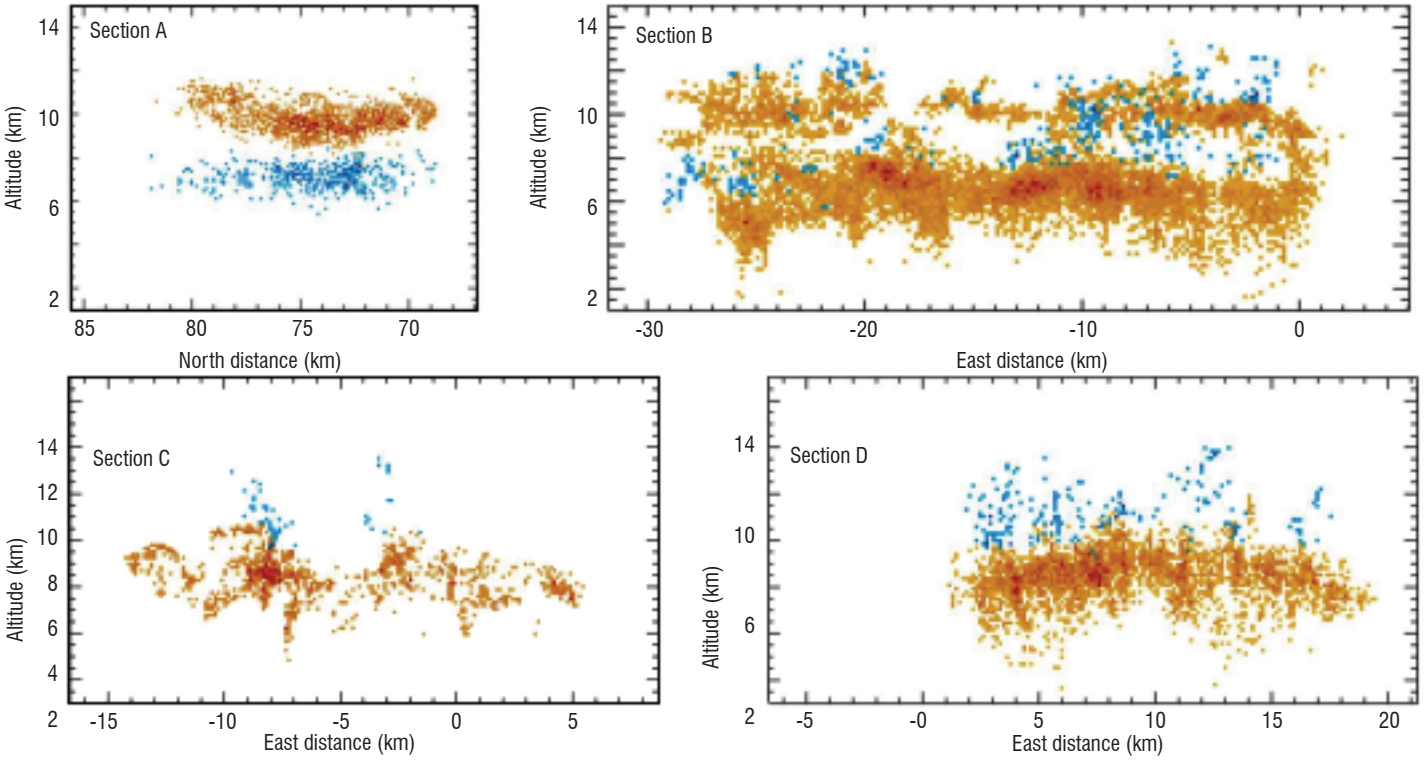

Figure 9 - Density of VHF sources inferred from LMA data and produced by flashes during 10 minutes in four different regions of a storm. Blue indicates negative storm charge and orange indicates positive storm charge. Darker colors represent larger source densities. From Weiss et al. [37].

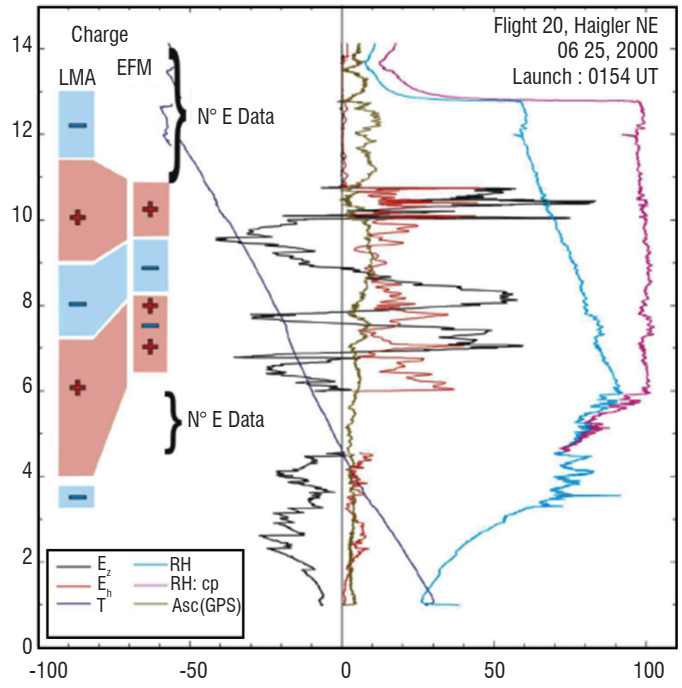

Figure 10 - Comparison of the charge structure (left side) for a storm documented during STEPS with a LMA system and with balloon soundings of electric field and thermodynamic parameters. The negative charge inferred in the EFM data at 7.5 km was likely due to charge deposited by lightning. From Weiss et al. [37].

Simulation of cloud charge structure

Three-dimensional dynamic cloud model incorporating airflow dynamics, microphysics and thunderstorm electrification mechanisms are used to examine the relationships between flash rate and other storm properties [49],[48]. Several parameterizations of the non-inductive charging process are generally used in cloud models and the inductive charging process can be included as well. The electric charges are transported along the airflow by the hydrometeor categories, which are involved in the charging processes. They are exchanged according to the various microphysical mass transfer rates and by assuming some charge–dimension relationships. The electric field is obtained by inverting the Gauss equation. When the electric field locally exceeds a given threshold a lightning flash is triggered and its propagation is driven by the electric field according to the theory of the bi-leader [50]. It propagates in two opposite directions until the magnitude of the electric field falls below a prescribed value. A charge amount is neutralized according to specific parameterizations.

Numerical experiments show different kinds of charge structure with a high sensitivity to the parameterization of the non-inductive charging process [51],[52], [48]. Figure 11 displays the vertical cross sections of the total charge density performed with the Meso-NH model at different stages of the storm documented during STERAO [53]. In this case, a negative dipole was first generated (negative charge above positive charge) and then the structure became more complex, with the normal tripole in the convective regions and a negative screening layer at the top of the cloud. Mansell et al. [48] used a three-dimensional dynamic cloud model and compared five laboratory-based parameterizations of non-inductive graupel-ice charge separation. Three of these schemes produced a normal polarity charge structure, consisting of a main negative charge region with an upper main positive charge region and a lower positive charge region. The other two schemes, which are dependent on the graupel rime accretion rate, tended to produce an initially inverted polarity charge structure and + CG flashes. Figure 12 illustrates the result of two schemes, in terms of charge structure, with a different number of charge regions.

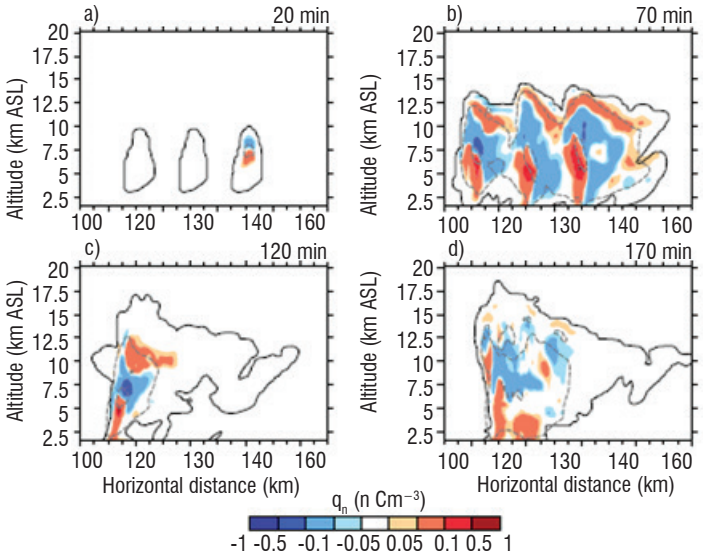

Figure 11 - Simulation of a STERAO case of storm: Vertical cross-sections of the total charge density (colors; in n Cm^{-3}) along (a) 20 min, (b) 70 min, (c) 120 min and (d) 170 min. The black solid line corresponds to the cloud contour. Dashed gray contours show the electric field module (10 and 50 kVm^{-1} contours). From Barthe et al. [53].

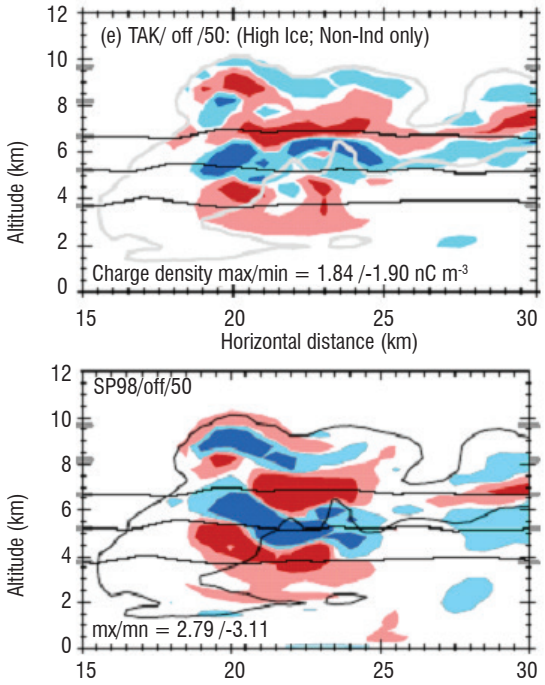

Figure 12. Charge structure of a multicell storm obtained by modeling with two non-inductive charging schemes: upper panel, [5] and lower panel, [19]. Red and blue shading denotes positive and negative charge regions, respectively. From Mansell et al. [48].

Conclusion

Some aspects of thundercloud development and its electrical characteristics have been described in this paper. For more complete information, the reader can refer to [30], [54] and [55]. The complexity of the mechanisms that contribute to the cloud charge structure and their scale diversity in terms of space, time and magnitude, makes their numerical representation difficult. A lot of effort has been made over the last decades, especially with laboratory experiments, in order to evaluate and understand the different factors that influence the sign and magnitude of the charge transfer. Another effort has been spent in the development of new lightning detection systems. In this sense, measurements from LMA have considerably advanced our knowledge of the electrical structure of storms and the cloud environment where lightning occurs and propagates. The LMA allows research with multiple applications to be developed, to understand the physics of lightning and storm electrification and for operational meteorology. ■

References

[1] C. T. R. WILSON - *Some Thundercloud Problems*. J. Franklin Inst., 208, 1-12, 1929
[2] SIR G. SIMPSON and F. J. SCRASE - *The Distribution of Electricity in Thunderstorms*. Proc. Roy. Soc. Lond., A, 161, 309-52, 1937
[3] T. W. WORMELL - *The effect of Thunderstorms and Lightning Discharges on the Earth's Electric Field*. Phil. Trans. Roy. Soc. Lond., A, 328, 249-303, 1939.
[4] J. LATHAM - *The Electrification of Thunderstorms*. Quart. J. Roy. Meteor. Soc., 107, 277-98, 1981
[5] T. TAKAHASHI - *Riming Electrification as a Charge Generation Mechanism in Thunderstorms*. J. Atmos. Sci., 35, 1536–1548 , 1978
[6] T. C. MARSHALL and W. P. WINN - *Measurements of Charged Precipitation in a New Mexico Thunderstorm: Lower Positive Charge Centers*. J. Geophys. Res., 87(C9), 7141–7157, 1982, doi:10.1029/JC087iC09p07141.
[7] B. VONNEGUT, C. B. MOORE, R. G. SEMONIN, J. W. BULLOCK, D. W. STAGGS, and W. E. BRADLEY - *Effect of Atmospheric Space Charge on Initial Electrification of Cumulus Clouds*. J. Geophys. Res., 67(10), 3909–3922, 1962, doi:10.1029/JZ067i010p03909.
[8] T. C. MARSHALL, W. D. RUST, W. P. WINN, and K. E. GILBERT - *Electrical Structure in Two Thunderstorm Anvil Clouds*. J. Geophys. Res., 94(D2), 2171–2181, doi:10.1029/JD094iD02p02171, 1989
[9] H.R. BYERS and R.R. BRAHAM, Jr. - *The Thunderstorm, U.S. Government Printing Office*. Washington, D.C., 287 pp. 1949
[10] K.A. BROWNING - *Airflow and Precipitation Trajectories within Severe Local Storms which Travel to the Right of the Winds*. J. Atmos. Sci., 21, 634-639, 1964
[11] K.A. BROWNING - *The Structure and Mechanism of Hailstorms*. Meteor. Monogr., 38, 1-39, 1977
[12] G.S. FORBES - *On the Reliability of Hook Echoes as Tornado Indicators*. Mon. Wea. Rev., 109, 1457-1466, 1981
[13] E.W., Jr. McCaul - *Observations and Simulation of Hurricane-Spawned Tornadic Storms.* The Tornado: Its Structure, Dynamics, Prediction, and Hazards (C. Church et al., Eds), Geophys. Monogr. 79, Amer. Geophys. Union, 119-142, 1993
[14] P.J. WETZEL, W.R. COTTON and R.L. MCANELLY - *A Long-Lived Mesoscale Convective Complex. Part II: Evolution and Structure of the Mature Complex*. Mon. Wea. Rev., 111, 1919-1937, 1983
[15] C. T. A. Doswell III - *Severe Convective Storms - An Overview, in Severe Convective Storms*. Meteorological Monograph, published by The American Meteorological Society. 2001
[16] G. B FOOTE and H. W. FRANK - *Case Study of a Hailstorm in Colorado. Part III: Airflow from Triple-Doppler Measurements*. J. Atmos. Sci., 40, 686-707, 1983
[17] E. R. JAYARATNE, C. P. R. SAUNDERS, and J. HALLETT - *Laboratory Studies of the Charging of Soft hail During ice Crystal Interactions*. Quart. J. Roy.

Meteor. Soc., 109, 609-630, 1983
[18] C. P. R. SAUNDERS, W. D. KEITH, and R. P. MITZEVA - *The Effect of Liquid Water on Thunderstorm Charging*. J. Geophys. Res., 96, 11 007–11 017,[19]
[19] C. P. R. SAUNDERS AND S. L. PECK - *Laboratory Studies of the Influence of the Rime Accretion Rate on Charge Transfer during Crystal/Graupel Collisions*. J. Geophys. Res., 103, 13,949–13,956,1998
[20] W. D KEITH and C. P. R. SAUNDERS - *Charge Transfer During MultipleTarge Ice Crystal Interactions with a Riming Target*. J. Geophys. Res., 94(D11), 13,103–13,106, doi:10.1029/JD094iD11p13103, 1989
[21] E.E. ÁVILA, G.M. CARANTI, N.E. CASTELLANO, C.P.R. SAUNDERS - *Laboratory Studies of the Influence of Cloud Droplet Size on Charge Transfer During Crystal - Graupel Collisions*. J. Geophys. Res., 103, 8985–8996, 1998
[22] R. G. PEREYRA, R. G., R. E. BÜRGESSER and E. E. ÁVILA - *Charge Separation in Thunderstorm Conditions*. J. Geophys. Res., 113, D17203, doi:10.1029/2007JD009720, 2008.
[23] R. G. PEREYRA, E. E. AVILA, N. E. CASTELLANO and C. SAUNDERS - *A laboratory Study of Graupel Charging*. J. Geophys. Res., 105, 20803-20812.3. 2000
[24] C.P.R SAUNDERS, H. BAX-NORMAN, E.E. ÁVILA, and N.E. CASTELLANO - *A Laboratory Study of the Influence of Ice Crystal Growth Conditions on Subsequent Charge Transfer in Thunderstorm Electrification*. Q. J. R. Meteorol. Soc. 130, 1395–1406, 2004
[25] P. BERDEKLIS and R. LIST - *The Ice Crystal - Graupel Charging Mechanism of thunderstorm Electrification.* J. Atmos. Sci., 58, 2751–2770, 2001
[26] D. ROSENFELD AND W.L. WOODLEY - *Deep Convective Clouds with Sustained Supercooled Liquid Water Down to -37.5°C*. Nature, 45, 440-442, 2000
[27] T. YUAN, L. A. REMER, K. E. PICKERING, and H. YU - *Observational Evidence of Aerosol Enhancement of Lightning Activity and Convective Invigoration.* Geophys. Res. Lett., 38, doi:10.1029/2010GL046052, 2011
[28] B. BAKER, M. B. BAKER, E. R. JAYARATNE, J. LATHAM and C. P. R. SAUNDERS - *The Influence of Diffusional Growth Rates on the Charge Transfer Accompanying Rebounding Collisions Between ice Crystals and Soft Hailstones*. Quart. J. Roy. Meteor. Soc., 113, 1193-1215, 1987
[29] C. EMERSIC and C. P. R. SAUNDERS - *Further Laboratory Investigations into the Relative Diffusional Growth rate Theory of Thunderstorm Electrification.* Atmos. Res., 98, 327-340, doi:10.1016/j.atmosres.2010.07.011, 2010
[30] D. R. MACGORMAN and W. D. RUST - *The Electrical Nature of Storms*. Oxford Univ. Press, New York, pp. 118–162 1998
[31] K. C. WIENS, S. A. RUTLEDGE and S. A. TESSENDORF - *The 29 June 2000 Supercell Observed during STEPS. Part II: Lightning and Charge Structure.* J. Atmos. Sci., 62, 4151-4177, 2005
[32] J. H. JR. HELSDON, S. GATTALEERADAPAN, R. D. FARLEY, and C. C. WAITS - *An Examination of the Convective Charging Hypothesis: Charge Structure, Electric Fields, and Maxwell Currents*. J. Geophys. Res., 107, 4630, doi:10.1029/2001JD001495, 2002
[33] B. VONNEGUT - *Some Facts and Speculations Concerning the Origin and Role of Thunderstorm Electricity*. Meteorol. Monogr. 27, 224–241, 1963
[34] S. CHAUZY and S. SOULA - *Contribution of the Ground Corona ions to the Convective Charging Mechanism.* Atmos. Res., (51), 279-300, 1999
[35] E. R. WILLIAMS - *The Tripole Structure of Thunderstorms*. J. Geophys. Res., 94, 13151-13167, 1989
[36] M. STOLZENBURG and T. C. MARSHALL - *Charged Precipitation and Electric Field in Two Thunderstorms*. J. Geophys. Res., 103(D16), 19,777–19,790, 1998 , doi:10.1029/98JD01675.
[37] S. WEISS, W. D. RUST, D. R. MACGORMAN, E. BRUNING, and P. KREHBIEL - *Evolving Complex Electrical Structure of the STEPS 25 June 2000 Multicell Storm*. Mon. Wea. Rev., 136, 741–756, 2008
[38] T. C. MARSHALL, and S. J. MARSH - *Negatively Charged Precipitation in a New Mexico Thunderstorm*. J. Geophys. Res., 98(D8), 14,909–14,916, doi:10.1029/93JD00420, 1993
[39] M. G. BATEMAN, T. C. MARSHALL, M. STOLZENBURG, and W. D. RUST - *Precipitation Charge and size Measurements inside a New Mexico Mountain Thunderstorm*. J. Geophys. Res., 104, 9643-9653, 1999
[40] D.R. MACGORMAN, W.D. RUST, P. KREHBIEL, W. RISON, E. BRUNING, and K. WIENS - *The Electrical Structure of Two Supercell Storms during STEPS*. Mon. Wea. Rev., 133, 2583–2607, 2005
[41] T. J. LANG, S. A. RUTLEDGE, and K. C. WIENS - *Origins of Positive Cloud-to-Ground Lightning Flashes in the Stratiform Region of a Mesoscale Convective System*. Geophys. Res. Lett., 31, L10105, doi:10.1029/2004GL019823, 2004
[42] X. M. SHAO and P. R. KREHBIEL - *The Spatial and Temporal Development of Intracloud Lightning.* J. Geophys. Res., 101, 26,641–26,668, 1996
[43] W. D. RUST and Co-authors - *Inverted-Polarity Electrical Structures in Thunderstorms in the Severe Thunderstorm Electrification and Precipitation Study (STEPS)*. Atmos. Res., 76, 247–271, 2005
[44] W. D. RUST, and D. R. MACGORMAN - *Possibly Inverted-Polarity Electrical Structures in Thunderstorms during STEPS*, Geophys. Res. Lett., 29(12), 1571, doi:10.1029/2001GL014303, 2002
[45] L. D. CAREY, S. A. RUTLEDGE, and W. A. PETERSEN - *The Relationship B-between Severe Storm Reports and Cloud-to-Ground Lightning Polarity in the Contiguous United States from 1989 to 1998*. Mon. Wea. Rev., 131, 1211–1228, 2003
[46] W. RISON, R. J. THOMAS, P. R. KREHBIEL, T. HAMLIN, and J. HARLIN - *A GPS-Based Three-Dimensional Lightning Mapping System: Initial Observations in Central New Mexico*. Geophys. Res. Lett., 26, 3573–3576, 1999
[47] R. THOMAS, P. KREHBIEL, W. RISON, S. J. HUNYADY, W. P. WINN, T. HAMLIN, and J. HARLIN - *Accuracy of the Lightning Mapping Array*. J. Geophys. Res., 109, D14207, doi:10.1029/2004JD004549, 2004
[48] E. R. MANSELL, D. R. MACGORMAN, C. L. ZIEGLER, and J. M. STRAKA - *Charge Structure and Lightning Sensitivity in a Simulated Multicell Thunderstorm*, J. Geophys. Res., 110, D12101, doi:10.1029/2004JD005287, 2005
[49] C. BARTHE, G. MOLINIÉ and J.-P. PINTY - *An Explicit Electrical Scheme for Use in a Cloud Resolving Model.* Atmos. Res., 76, 95-113, 2005.
[50] D.R. MACGORMAN, J.M. STRAKA, C.L. ZIEGLER - *A Lightning Parameterization for Numerical Cloud Models.* J. Appl. Meteorol., 40, pp. 459–478, 2001
[51] J. H. Jr., HELSDON, W. A. WOJCIK, and R. D. FARLEY - *An Examination of Thunderstorm-Charging Mechanisms Using a two-Dimensional Storm Electrification Model*. J. Geophys. Res., 106, 1165-1192, 2001
[52] J.-P. PINTY, and C. BARTHE - *Ensemble Simulations of the Variability of Electrical Activity with a Mesoscale Mode*l. Mon. Wea. Rev., 136(1), 380-387, 2008.
[53] C. BARTHE, M. CHONG, J.-P. PINTY, C. BOVALO, and J. ESCOBAR - *Updated and Parallelized Version of an Electrical Scheme to Simulate Multiple Electrified Clouds and Flashes over Large Domains.* Geosci. Model Dev., 5, 167-184, doi:10.5194/gmd-5-167-2012.
[54] M. STOLZENBURG and T. C. MARSHALL - *Charge Structure and Dynamics in Thunderstorms*. Space Sci. Rev., 137, Nos 1–4. DOI: 10.1007/s11214-008-9338-z, 2008
[55] C. P. R. SAUNDERS - *Charge Separation Mechanisms in Clouds.* Space Sci. Rev., 137, 335--353, doi:10.1007/s11214-008-9345-0, 2008
[56] M. STOLZENBURG, W. D. RUST and T. C. MARSHALL - *Electrical Structure in Thunderstorm Convective Regions*, 3. Synthesis, J. Geophys. Res., 103, 14,097– 14,108, 1998.
[57] T. C. MARSHALL and W. D. RUST - *Two Types of Vertical Electrical Structures in Stratiform Precipitation Regions of Meoscale Convective Systems.* Bull. Am. Meterol. Soc. , 70, 2159-2170, doi: 10.1175/1520-0477(1993) 074<2159/TTOVES>2.0.CO; 2

Acronyms

CAPE (Convective Available Potential Energy)
EL (Equilibrium Level)
LFC (Level of Free Convection)
LEWPs (Line Echo Wave Patterns)
MCSs (Mesoscale Convective Systems)
UMIST (University of Manchester Institute of Science and Technology)
CCN (Cloud Condensation Nuclei)
VHF (Very High Frequency)
STEPS (Severe Thunderstorm Electrification and Precipitation Study)
LMA (Lightning Mapping Array)
STERAO (Stratospheric-Tropospheric Experiment Radiation, Aerosols and Ozone)

AUTHOR

Serge Soula graduated from Paul Sabatier University (Toulouse). He obtained his PhD in Atmospheric Physics in 1986 and his Habilitation à Diriger des Recherches (HDR) in 1998. He works at Obervatoire Midi-Pyrénées (OMP) as a researcher in storm electricity. His research has been focused on mechanisms of charge transfer within the thundercloud and its environment. He is now involved in research on the physics of Transient Luminous Events (TLE) above thunderstorms (sprites, elves, jets, etc.).

A. Delannoy †
(Onera)
P. Gondot
(Airbus)

E-mail: pascal.gondot@airbus.com

Airborne Measurements of the Charge of Precipitating Particles Related to Radar Reflectivity and Temperature within two Different Convective Clouds

Simultaneous ground based radar reflectivity measurements and airborne electric parameters (electrostatic field and charged particles) are presented. They are used to investigate the charging processes acting in convective cells. Within the two thunderclouds presented in this work, both signs are found on large hydrometeors. It is shown that negative particle charging exists at high levels in classical vertically developed cells. There is some evidence that positive charging of precipitating particles is occurring in the lower parts of the clouds.

Introduction

The charge separation, which occurs when an ice particle collides with a graupel, has received increased attention over the last few years, as a possible mechanism for the electrification of thunderstorms. Laboratory studies following the pioneering work of Reynolds et al. (1957)[1] have provided evidence for a viable ice collisional charging mechanism. The works of Takahashi (1978) [2], Jayaratne et al. (1983) [3] and, more recently, Emersic and Saunders, (2010) [4] pointed to the dependence of sign and magnitude of charging efficiency on temperature, cloud liquid water content (LWC), particle size and velocity. Note: many papers on this topic have been published since 1983 - this 2010 paper includes references to most of them.

An important general result of these experiments is the existence of two domains for graupel charging: positive charging at a higher temperature and higher LWC, and negative charging at a lower temperature and LWC. Under natural realistic conditions, the transition between these two domains depends on cloud water content and could occur at temperatures typically between -20° C and -10° C. Note: both studies give a range of charge sign reversal temperatures and liquid water contents - and we now know that this depends on supersaturation too.

Aircraft observations of convective clouds reported evidence of the association of electric charge with ice particles. Generally, the highest charge densities are coincident with regions of high graupel concentration (Gardiner et al., 1985) [5]. Dye et al. (1988)[6] observed two electrified regions during initial thunderstorm electrification. In both regions, supercooled water and ice particles, including graupel, were present and solid particle concentrations, sizes, and collision rates were at a relative maximum. A great number of observations were related to the negative charge center of the cloud, but in all cases particle charge measurements reported the presence of both signs at the same location.

Thus, the combined information from laboratory and *in-situ* measurements suggests that charge generation is probably associated with ice particle collisions. From a schematic point of view and according to the classical picture, the smallest positively charged ice particles, ice crystals, are carried by updrafts to the top of the cloud and the largest negatively charged riming particles, like graupel grow near the -15° C level, thus developing the classical thunderstorm electrostatic dipole.

Our purpose in this paper is to report observations, which could be discussed and analyzed within the context of particle charging in thunderstorms. During Summer 1984, in the South-West of France, *in-situ* measurements of electrostatic field, precipitation charge and size were collected in two quite different convective situations. On June 6th, an exceptional meteorological situation was observed by an instrumented aircraft and by a meteorological radar system. In order to point out the main electrical features of these convective cells, it seems interesting to compare observations on June 6th with a more classical case encountered a few days later, on June 24th.

The most important feature pointed out in this paper concerns electrical parameters, precipitation charge measurement in particular. The net charge carried by precipitation observed in the same range of flying levels was of opposite sign in the two kinds of convective cells. A preliminary report of these observations was made by Delannoy et al. (1988)[9].

The airborne observations described here were made during the Landes-Fronts '84 experimental program, which covered a large set of complementary measurements, including a ground-based network, in order to be able to analyses frontal or isolated convective cells. More details were reported in several publications, for instance, see Laroche et al. (1985) [7] or Laroche et al. (1986) [8].

Among the experimental capabilities was a C160 Transall aircraft, which was first dedicated to triggering lightning and recording electromagnetic parameters, but was also used to make electrical and microphysical basic measurements in and around the clouds. The aircraft was fitted with several types of sensors: a network of five field-mills, a complete set of PMS (Particle Measuring Sensor) probes and an induction ring to measure particle charges. A short account of this last sensor is presented in box 1. The locations of the main sensors on the aircraft are reported in box 2.

Many flights of the Transall were made in conjunction with radar reflectivity measurements. The aircraft location was determined with the inertial system rechecked with a tracking radar, to give an accuracy of about 100 meters on the aircraft trajectory. This enables us to make good spatial correlations between *in-situ* measurements and radar reflectivity data.

Comparison of data obtained on June 6th, during flight A and on June 24th, during flight B

Figure 1b presents radar reflectivity obtained during flight B. It indicates that the convective cells in the scanning region have a strong precipitation core (more than 40 dBz) with a vertical extent of 7 kilometers. Such clouds were currently observed during the entire campaign.

On the other hand, the convective situation encountered on June 6th (flight A) was exceptional: a thick layer of cirrus clouds were visually observed above the site between 5 and 7 kilometers. The vertical convective motion was stopped below this level. Typical reflectivity obtained during this flight is presented in figure 1a. From the vertical cross section, it can be seen that the precipitation core was entirely below the 4 kilometer level. Precipitating particles were all below the -20° C isotherm. All of the cells scanned during this flight exhibited the same characteristics.

In figure 2, we present charge measurements collected during these two flights. One must keep in mind that the main goal of the campaign was to trigger lightning by the aircraft itself. This implied that the clouds were crossed as frequently as possible, the flight path being determined by electric field measurements. Due to aircraft limitations, most of the penetrations took place between the 2 km and 5 km levels. The cells identified in figures 1a and 1b were crossed several times at several levels in this interval. Other similar cells in their vicinity were sampled too.

For each pass through the cloud, a histogram shows all of the charged particles detected by the induction ring. The histogram is made up of 32 classes, 16 for each sign. The width of every class is $15\ pC$. The two first classes $(|q| < 15\ pC)$ are empty because of the choice of a threshold value of $15\ pC$ (see box 1). The two highest classes $(|q| > 225\ pC)$ are incremented even if the measured charge is greater than $240\ pC$: in such cases, the amplifier is saturated and the charge value is not correctly measured, but we are interested in the counting of highly charged particles, which is always normally operating.

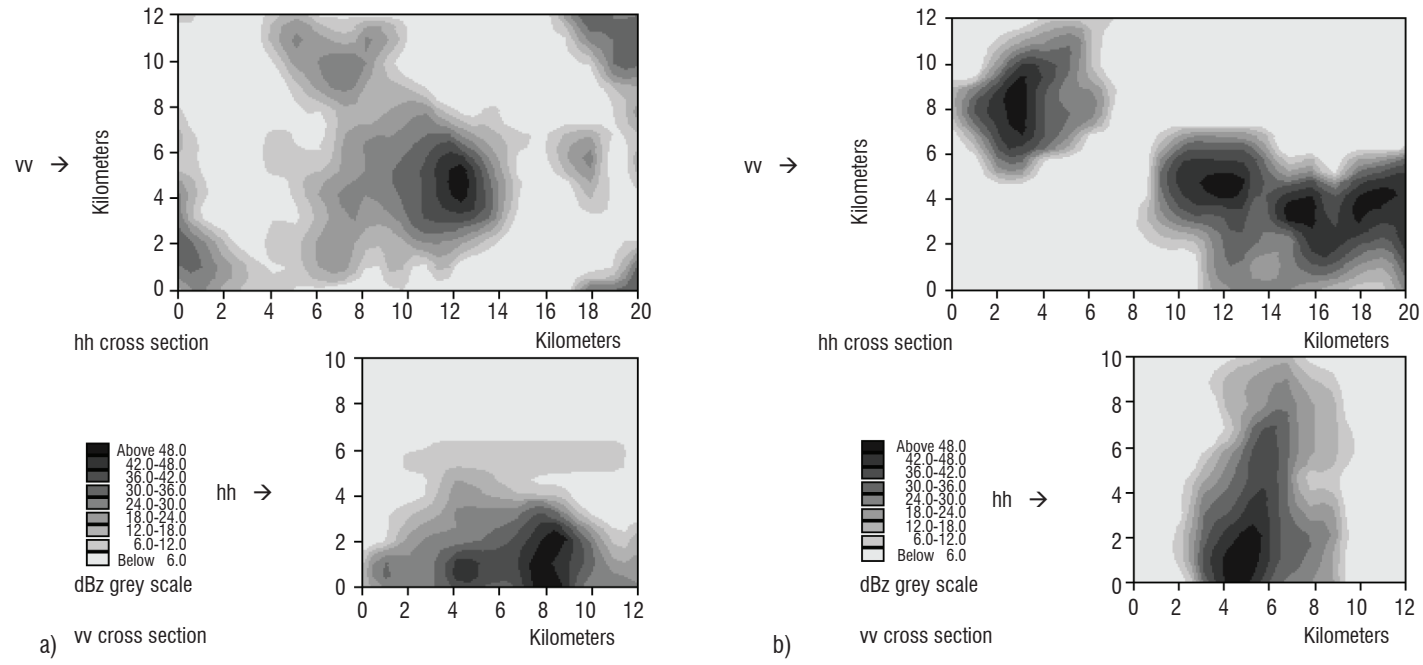

Figure 1- Radar reflectivity cross-sections obtained during flight A and flight B

Box 1 - Measurements of electric charges carried by large hydrometeors

The electric charge of precipitating particles is measured using an induction ring (FARADAY cylinder), which is described in figure B1. The sensing electrode is dimensioned so as to contain no more than one particle at a time. It is mainly concerned by the same class of particles as the PMS 2 DP probe. The volume of cloudy air sampled at a true airspeed of 100 m/s is around 70 l/s.

Special care is taken to avoid corona discharges from leading edges and the sensing part of the device is shielded and insulated. The shape of the guard rings and of the electrode is conical, to minimize collision efficiency between precipitation particles and the inner side of the sensor.

a)

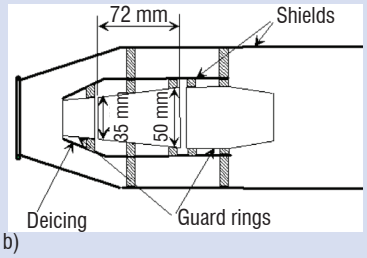

b)

Figure B1-1
a) The induction ring on the left pod, under a PMS probe
b) dimensions of the sensing electrode

The sensor is located on a pod under the wing in the same vertical plane as the propeller, at about 10m from it. (see figure B2 - 1)

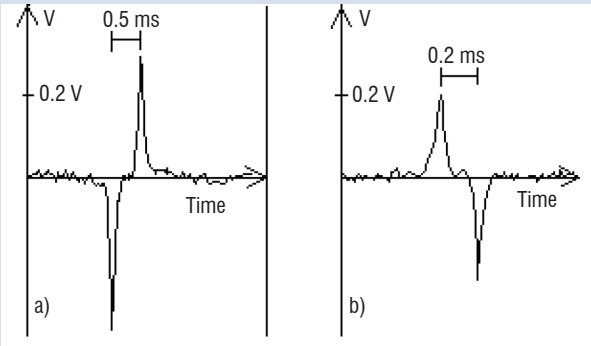

Figure B1-2 Signals obtained with a positive (a) and a negative (b) particle

The detector electronics are made with low noise and high gain amplifiers. Typical signals of both signs are shown in figure B1-2. If the current peak value is greater than a threshold value S, the signal enters a process unit. To be accepted, the pulses generated by a particle passing through the device must be symmetric (the extremes are inverted when the particle goes in and out the induction ring without colliding) and the time interval between the two sharp extremes must be equal to the length of the electrode (72 mm) divided by the particle relative velocity, which is not very different of the airspeed.

If one of these conditions fails, the pulse is rejected. Counting of such events is performed. If both conditions are true, it is assumed that a single particle has penetrated the device and exited without colliding. Spurious signals are found to be less than 5% of the acquired signals.

When a pulse is valid, the charge carried by the particle is calculated by the formula:

$$q = \alpha . \Delta i . \Delta t$$

where:
Δi is the difference of intensity between two extremes values
Δt is the time interval between two peak values coefficient deduced from laboratory calibrations.

According to its charge value, the particle enters under 32 classes (16 for each sign).The full process lasts for 4ms and is initialized at each time a “significantly charged” particle enters the probe bin. The error rate for classifying is 10%. However, if there are more than 3 valid events per liter (less than 4ms between two consecutive events), some of them are ignored by the processing system and counting is underestimated. The choice of a threshold value is a convenient way of limiting the number of events to be taken into account by the processing unit. With $S = 15\ pC$, the maximum number of detected charges is about 100 per second for the entire campaign, that is, less than two “significantly charged” particles per liter.

Box 2 -Electric field measurements on the aircraft

Electric field measurements are made at five locations on the fuselage. The sensors are of the field-mill type. Their location is displayed in figure B2-1b. Laboratory calibrations were made on a scale model aircraft, to assess the amplification coefficients resulting from the curvature of the fuselage.

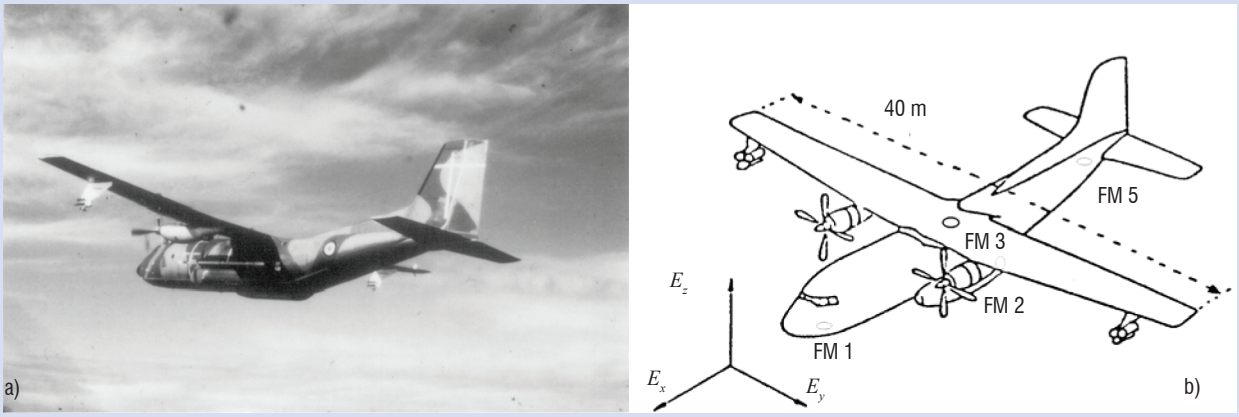

Figure B2- 1 The instrumented C160 aircraft end the locations of its five field-mill sensors

These coefficients can also be deduced by numeric integration of Poisson's equation on a modeled structure. The three atmospheric electric field components and the electrostatic potential of the aircraft are retrieved from the five measured signals, by means of a least square method (see Laroche et al., 1985)[7].

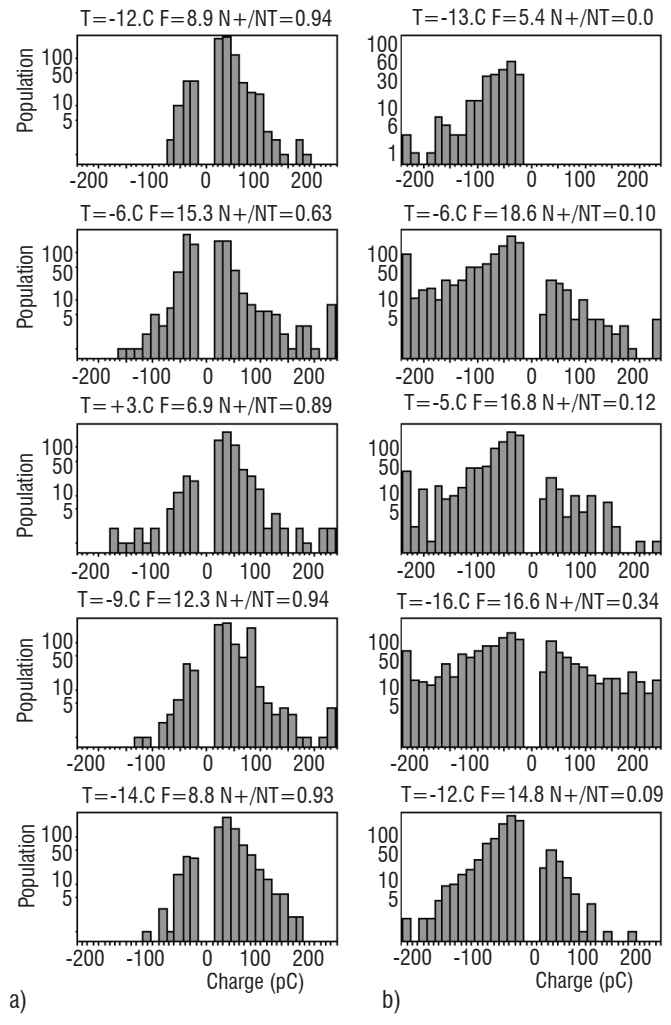

Figure 2 - Histograms of charges recorded during flight A and flight B

The histograms presented in figure 2 have been chosen from a larger set (approximately 20 penetrations per flight) to illustrate the charge distribution at different levels in two different meteorological situations. The duration Dt of each pass through the cloud is variable, depending on the in-cloud path of the aircraft and its velocity. Knowing the total number NT of charged particles encountered during a penetration, we define an average rate F of charged particles per second $(F=NT/Dt)$. The ratio $N+/NT$ indicates the proportion of positively detected charged elements. The histograms collected during flight A are referenced in column a (flight B, in column b). The average density of detected charged particles can be deduced from F and from the aircraft velocity and the collecting surface of the induction ring:

$$D = K^{-1}.F$$

with

$$K = Vp.\,Se$$

D is the average density in m^{-3}, Vp is the aircraft velocity in m/s and Se is the collecting surface of the induction ring in m^2. For flight A and B, K is close to 0.07.

We observe that, in most cases, positive and negative charges are both detected simultaneously, located at a given altitude in the range of our flying levels. Temperature measurements indicate that these levels are between the -16° C and +3° C isotherms. Obviously, most of the charges are positive in the data obtained during flight A; they are negative for flight B, although they were sampled within the same range of altitudes.

The population of the classes decreases when the absolute value of the corresponding charge increases, but the highest classes $(|q| > 225\,pC)$ often contain a high number of particles. Close examination of the data indicates that the filling up of those highest classes is always achieved in a few consecutive seconds, that is, during the crossing of a n unique narrow vertical layer.

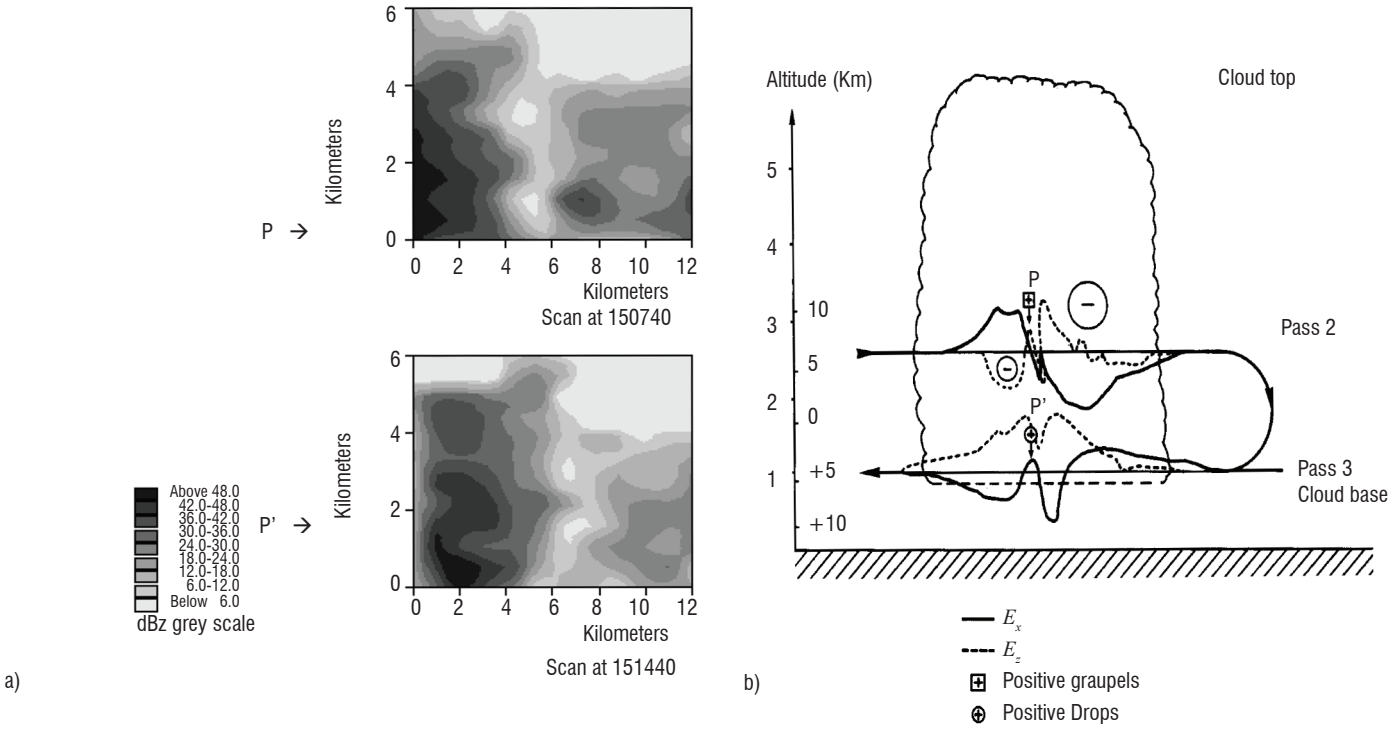

Figure 3 – Two scans and two flight paths through the same cell. a)Vertical scans of the cell, with indication of the two penetrating levels. b) Vertical cross-section in the cloud reference frame

The mean value of F for the 5 data sets of flight A is $F_A = 10 \pm 3$. The corresponding value for flight B is $F_B = 14 \pm 5$. The mean flow of charged precipitation through the induction ring is not so different from one situation to the other. It may be noticed that we detected more natural lightning during flight B than during flight A. Nevertheless, the intensity of the radar reflectivity, the total number of charged particles and the absolute value of the charges carried by precipitation are within the same order of magnitude for both of the kinds of cells under examination. They differ mainly by the vertical extent of their 50 dBz cores, by the temperature level reached by their tops, and by the dominant sign of their charged precipitating particles. For flight A the $N+/NT$ ratio lies between 0.63 and 0.94; for flight B , between 0.0 and 0.34.

Comparison of data obtained in two consecutive crossing of a single cell during flight A

We now present data from a cell which was penetrated during flight A at 150830 UT. The altitude of the aircraft was around 2700 m (level *P* in figure 3a, $T = -6° C$).The corresponding histogram of charges is presented in figure 2a. At this time, the cell was just entering the scanning region of the radar. As can be seen in figure 3a, the precipitation core (more than 40 dBz) reaches the 4 km level. At 15:15:00 UT, the cell was crossed again at a lower flying level (level P' in figure 3a, 1600 m, $T = +3° C$, corresponding histogram in figure 2a). From figure 3, we observe that the cell has moved between two consecutive radar scans. The two vertical planes of the reflectivity cross section are chosen according to the horizontal velocity of the cell. The top of the 40 dBz core is now under the 3 km level. Referring to the reflectivity data and to the tracking of the aircraft it can be established that this pass is just below the preceding one in the cloud frame of reference (figure 3b). The ratio $N+/NT$ is 0.63 for the first pass and 0.89 for the second one. Thus, while the cell is descending, the flying level of the aircraft is lowering too and there are fewer negatively charged particles. The distribution of positive charges is not clearly different from figure 2a ($T = -6° C$ and $T = +3° C$) when integrated over the whole path through the cloud.

In figure 4, these two consecutive penetrations are examined in more detail. The use of electrostatic data allowed us to identify different zones, which can be analyzed with a better spatial resolution. In this paper, we do not try to calculate charge distributions, which would give rise to the observed electric field components. Nevertheless, looking at the E_x component in figure 4a, we observe that it has a smooth shape on which an event (marked P) identified by the important positive slope of E_x is superimposed. This happens at 15:09:08 UT; the dimension of this zone along the trajectory of the aircraft is about 300 m. At this time, the aircraft is flying through a high reflectivity region. Graupel with sizes of up to 3 mm are sampled by the 2 DP probe.

In the lower part of figure 4a, the time interval during which the higher classes of the histogram are incremented, is marked. Event P occurs during this time. Only 8 particles carrying a charge greater than *200 pC* are detected by the induction ring.

E_x and E_z components are affected by event P in such a way that it is coherent to localize a region of positive charge in this part of the cloud. Triboelectric charging by impact of solid particles usually consists in negative charging of the aircraft and in a decrease in its electrical potential toward high negative value. This is observed in our case, when the aircraft fly through this region characterized by a high concentration of large and solid precipitating particles.

Data sampled by PMS 2DP probe during the P event 6400 μm

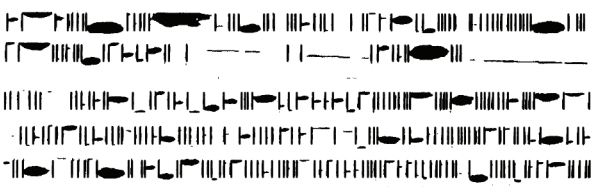

Data sampled by PMS 2DP probe during the P' event 6400 μm

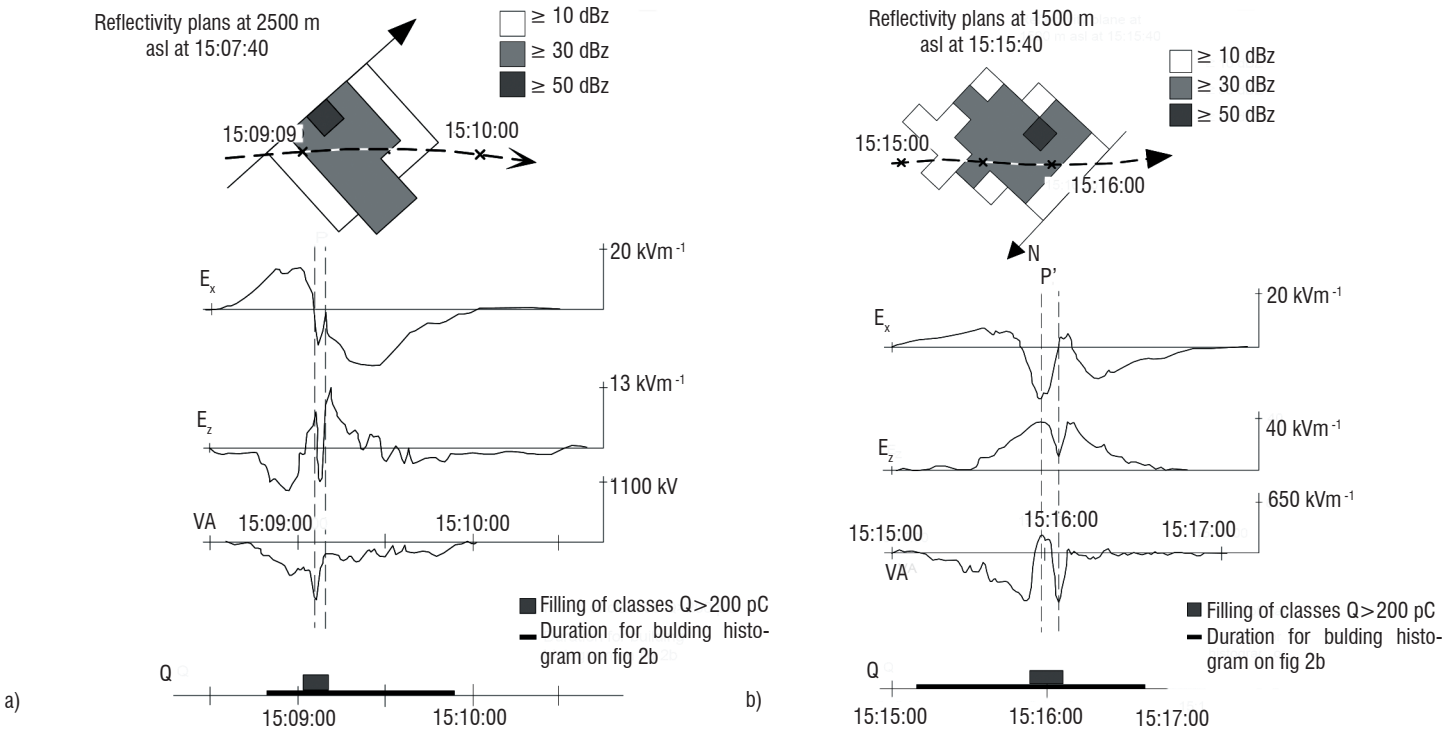

Figure 4 - Detailed data obtained during two flight legs: 2DP PMS, horizontal cross-section of radar reflectivity, electrostatic components E_x, E_z and potential, duration of the collection of charged hydrometeors.

There was no simultaneous measurement of the size and of the charge of an individual particle, the volumes sampled by the induction ring and by the 2 DP PMS being different. Thus, we may summarize what we have learnt on region P in the following manner: a narrow region of positive charge, with large precipitating hydrometeors, including few elements carrying positive charge higher than anywhere else along the trajectory.

Data obtained during the second crossing is displayed in figure 4b. We can notice that in a similar manner, an event marked P' characterized by a strong positive slope is superimposed on a regular evolution of E_x component. The vertical component E_z decreases and then increases again, while the slope of E_x remains positive: a region of positive charge is entered when E_x reaches its minimum value at 15:15:58 UT; its horizontal extension along the path is about 800 meters.

Event P' is encountered roughly 1000 meters below event P. It can be seen on data from the $2\ DP$ probe, that large solid particles are sampled with the addition of some large liquid drops. By splashing on the device, they produce a thin trail visible on the frame at the top of figure 4b. The triboelectric effect is inverted from event P to P': the aircraft's potential is increasing during the crossing of this region. This may be the result of crossing a liquid precipitation zone, as the splashing of large water drop produces negatively charged droplets, which are transported by air flow, the impact process charging the aircraft positively.

Simultaneously, the induction ring detects highly charged elements; the time during which the higher positive classes are filled is plotted on the lower part of figure 4b. Event P' appears to be similar to event P, with a larger extension along the aircraft's path. The reflectivity echoes and the precipitation rate are of the same order of magnitude for both passes, but the horizontal variations of electrostatic field's components are slower during the second crossing. This may result from the lower flying level and from the subsidence of the explored cell, as it is displayed on figure 3.

For a better comparison between the charge distribution during event P and P', it is useful to build histograms of the same duration including the two intervals of filling of the higher classes. These are presented in figure 5. The total number of charged particles detected in 16 seconds decreases from 380 to 180 and the ratio $N+/NT$ increases from 0.60 to 0.92. The number of negatively charged particles in the two corresponding regions defined by a positive slope of Ex undergoes a sharp drop between the two temperature levels $T=-6°\ C$ and $T=+3°\ C$, while the precipitation core of the cell is descending.

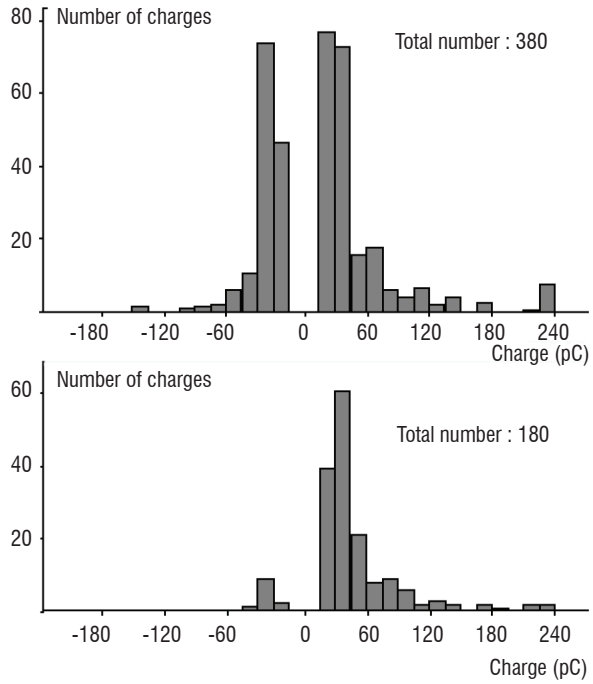

Figure 5 - Histograms collected during events *P* and *P'*

A concluding remark may be that most of the positively charged particles in this core carry less than $100\ pC$, but a narrow region exists with a noticeable vertical extension where few highly charged elements are found.

Concluding discussion

The charge acquired by a particle is not defined by the location at which it is sampled. It reflects its history in the cloud and depends on its travel during its entire life. Everywhere in the cells explored during flight A and B, we find the simultaneous presence of positive and negative charges on particles, but the higher the top of the cloud is, the more numerous negatively charged elements are at every level between 2 km and 5 km.

Cells of flight A and B differ mostly by the temperature of their top, the precipitation rates being not so different. For all of the cells explored during flight A, $N+/NT$ lies between 0.63 and 0.94, indicating that at all flying levels negatively charged particles detected are less numerous than positive ones. Conversely, during flight B $N+/NT$ is less than 0.34. Following our observations, a precipitation core confined in a range of temperatures warmer than -20° C seems to result in an important deficit in the negative population of the lower part of the cloud. The level at which precipitating particles appear may determine the sign of their initial charging, the colder tops of clouds being likely to promote negative charging.

In addition, negatively charged precipitation particles are less and less numerous when we sample particles at warmer levels, while the top of the cell is descending (flight A). It indicates that a positive charging mechanism is acting on precipitation in the range of altitudes of our explorations. This mechanism increases the ratio $N+/NT$: focusing on events P and P' or considering the whole passes at two flying levels, this positive charging acting in the lower part of the cell increases $N+/NT$ from 0.6 to 0.9 when the temperature increases from -6° C to +3° C. No values smaller than 0.6 are found for this ratio during flight A. This may be related to the little vertical extension of the upper region in which a negative charging may be efficient. In the regions that were explored during flight B, positive charging is working against the negative one, which is supposed to have worked at levels above the aircraft's passes. The histograms in figure 2b are obtained from crossings of different cells at different stages of their evolution, so they are not suitable for comparison between them. However, since we find much more negative charges than during flight A at the same altitude, we may conclude that the vertical extension of the negative charging zone is large enough to build an important population of negatively charged precipitation. The action of the positive charging all along the travel of the particles in the warmer part of the clouds is not sufficient to shift most of the observed charges to positive values: $N+/NT$ remains relatively low.

Because we have no direct measurements of the particle charge flux (which is the main point of interest in terms of the microphysical process), our data must be used with some assumptions, if we want to relate it to laboratory experiments. These assumptions may be rejected, but taking into account that we had the opportunity to observe an exceptional electrified cloud warmer than -20° C, these observations build a consistent description of a natural medium where a charging process depending on temperature is likely to act on solid precipitating particles. They argue for a reversal temperature. This charge-sign inversion occurs at altitudes higher than our flying levels, since positive charges are detected everywhere (with one exception, see figure 2b, T=-13° C). Negative charging occurs in the colder part of typical cells and if this upper part is not very tall, negatively charged particles at lower levels are fewer. Furthermore, these observations give us the opportunity to indirectly detect the positive charging acting in this lower part. Thus, the two distinct regions for charging pointed out by laboratory experiments seem to be efficient in natural conditions, and the whole microphysical process may be of major importance for the electrification of convective clouds ■

References

[1] S.E. REYNOLDS, M. BROOK and M.F. GOURLEY - *Thunderstorm Charge Separation.* J. Meteo., 14, 426-436, 1957

[2] T. TAKAHASHI - *Riming Electrification as a Charge Separation* . J. Atmos. Sci., 35, 1536-1548, 1978

[3] E.R. JAYARATNE, C.P.R. SAUNDERS and J. HALLETT - *Laboratory Studies of the Charging of Soft Hail During Ice Crystal Interactions.* Q. J. R. Meteo. Soc., 109, 609-630, 1983

[4] C. EMERSIC and C.P.R. SAUNDERS - *Further Laboratory Investigations into the Relative Diffusional Growth Rate Theory of Thunderstorm Electrification.* Atmos. Res. 98, 327-340, 2010

[5] B. GARDINER, D. LAMB, R.L. PITTER and J. HALLETT - *Measurements of Initial Electric Field and Ice Particle Charges in Montana Summer Thunderstorm.* J. Geophys. Res., 90, 6079-6086, 1985

[6] J. E. DYE, J. J. JONES, W. P. WINN, T. A. CERNI, B. GARDINER, D. LAMB, R. L. PITTER, J. HALLETT and C. P. R. SAUNDERS - *Early Electrification and Precipitation Development in a Small Isolated Montana Cumulonimbus*. J. Geophys. Res., 91, 1231-1247, 1986

[7] P. LAROCHE, M. DILL, J. F. GAYET and M. FRIEDLANDER - *In-Flight Thunderstorm Environmental Measurements During the Landes 84 Campaign.* 10th Int. Aerospace and Ground Conf. on Lightning and Static Electricity, PARIS, 1985

[8] P. LAROCHE, A. DELANNOY, P. GONDOT, F. HELLOCO and J. F. GAYET - *Airborne Observation of Small Scale Fluctuation of Microphysical Dynamic and Electrical Properties in Convective Clouds.* 23rd Conf. on Radar Meteorology and Cloud Physics, SNOWMASS, COLORADO, 1986

[9] A. DELANNOY, P. GONDOT, F. HELLOCO and P. LAROCHE - *Airborne Precipitation Charge Measurement Related to Local Electrostatic Field and Temperature.* 8th Int. Conf. on Atmospheric Electricity, UPSSALA, 1988

Acronyms

PMS (Particle Measuring Sensor)

AUTHORS

Alain Delannoy † *(1951-2012*) received a PhD in Atmospheric Physic from University Paris 6 in 1979. He joined Onera in 1980 and was engaged in research on Atmospheric Electricity, Cloud microphysic and Physic of Lightning. His interest focused on in situ electrical measurements in cloud for what he setup specific instrumentations. He was engaged in lightning strike experiment on aircraft. Alain Delannoy was author and co-author of numerous articles and reports on Atmospheric Electricity and Lightning.

Pascal Gondot received a PhD in Atmospheric physic from University Paris 6 in 1985 and a PhD in Physical Meteorology from University of Clermont-Ferrand in 1988. After 5 years at Onera he joined the EADS Corporate Research Centre (Innovation Works) where he became the head of EMC and Lightning Department and EADS Senior Expert in Hardening of systems. He is now in charge of the development of R&T Partnerships and Co-operations for Airbus Operation SAS.

Z. Kawasaki
(E-JUST and Osaka University)

Review of the Location of VHF Pulses Associated with Lightning Discharge

E-mail: zen@comm.eng.osaka-u.ac.jp

This article gives a brief summary on VHF pulse radiation associated with lightning discharges and its location. There are two independent techniques: Time of Arrival and Interferometry. VHF pulses are believed to be emitted during all of the processes of a lightning discharge. Thus, the mapping of VHF pulses associated with lightning yields information not only on lightning channel, but also on the charge distribution. On the other hand, both systems have advantages and disadvantages over each other, and this article summarizes both principles.

Introduction

Lightning discharges radiate electromagnetic waves in a broadband frequency range, from ELF/VLF up to VHF/UHF/SHF. Moreover, Gamma and X-ray radiation have been recorded recently during lightning activity, and the physical mechanism of their generation has become a current topic among the researchers involved with these. The cause of each frequency range radiation is related to an individual lightning discharge process and its progression. Though lightning discharges are phenomena that last only one or two seconds, they consist of processes such as preliminarily breakdown, stepped leader progression, first return stroke, junction process, dart leader progression and subsequent return stroke in the case of a cloud-to-ground flash. In addition, a cloud flash includes the processes of preliminarily breakdown, leader progression, leader encountering a highly charged region, K process and recoil streamer. Among these various processes, ELF/VLF radiation is mainly associated with lightning return strokes and VHF/UHF/SHF radiation is believed to be related to the progression of the tip of a breakdown. In other words, VHF/UHF/SHF radiation is expected to be detectable throughout a lightning discharge, from its very beginning up until its termination and dying-out. Additionally, the detection and location of VHF emissions associated with lightning discharges can be an early warning and alert for rocket launching, as evidenced by the success of Lightning Detection and Ranging systems (LDAR). Thus, the objective of this review article is to offer a brief discussion, in particular on VHF observations from the aspect of lightning location technology development. The technologies reviewed in this article are “Time of Arrival” and “Interferometry”. Physical interpretations of VHF radiation unveiled recently are also introduced.

Time of arrival

Lightning location systems by a time-of-arrival (TOA) technique detecting VHF pulses associated with lightning discharges are categorized into two groups: a very-short-baseline with antenna separation of the order of ten meters and a short-baseline with antenna separation of the order of ten kilometers. In the case of short-baseline TOA for three-dimensional locations, at least four antennas are required and, generally speaking, a TOA system consists of more than five antennas, for redundancy, to obtain the higher imaging accuracy with the aid of a chi-square goodness-of-fit test for example.

The very-short-baseline TOA system is considered. The antenna separation for this technique is 30 to 300 m, receiving a frequency range from 30 to 100 MHz [1]. Though the VHF pulses, which are detected by several antennas, are not easy to identify and/or discriminate from each other, the very-short-baseline technique may overcome this difficulty because, given the velocity of electromagnetic waves, the closely spaced antennas can be considered to have almost identical positions, with the pulses arriving at all antennas within an amount of time that is very short compared to the time interval between pulses. Basically, the very-short-baseline technique is useful for estimating the azimuth and elevation of VHF sources. The very-short-baseline technique led to the development by the author’s group in the 1990s of the broadband interferometer, which will be presented in detail in § “ Lightning Mapping Array (LMA) and Digital Interferometer (DITF) “

The short-baseline technique had been used for the development of two independent systems. The first is the short-baseline time of arrival system presented by Proctor [2], [3]. He deployed five VHF antennas with operating frequencies of 253 and 355 MHz, with baselines ranging from 10 to 40km. At that time, automatic time synchronization between antennas was not available because of it being the pre-GPS era and his laborious work is really respectable. With his own eyes and his wide experience, he conducted the identification of numerous VHF pulses recorded on magnetic tapes at five different locations. His series of papers give rather clear images of the time sequence of lightning initiations, leader propagations and return strokes. He showed the typical velocity of the stepped leader progression and return stroke. One of the most impressive results of lightning location is shown in figure 1.

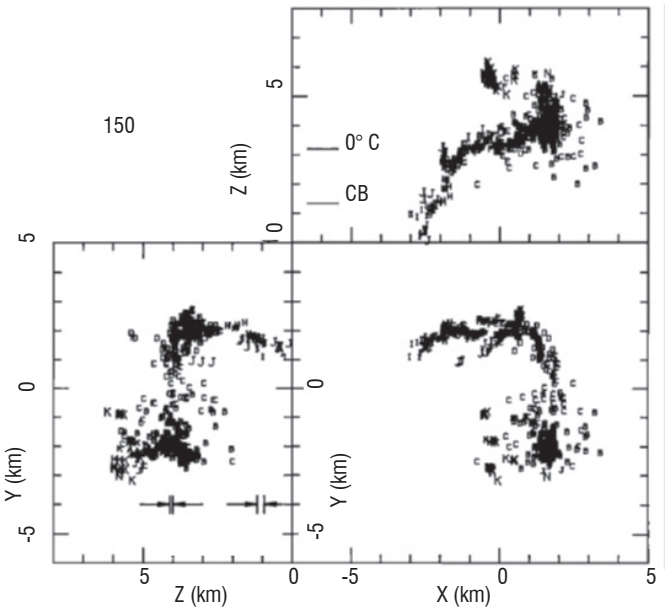

Figure 1 - VHF source locations in a plane view and two elevation views of a flash (adapted from [3]).

The second type of TOA equipment is the Lightning Detection and Ranging (LDAR) system operated at a central frequency range of between 56 and 75 MHz. LDAR was deployed for practical purposes by Lennon and Pochler [4]. According to the author's understanding, LDAR was designed for assessing the threat of triggered lightning to launches at the time of the Apollo-Soyuz mission, as a quasi-real-time operation system. As described before, the identification of VHF pulses is the key procedure for real-time operation. For this, time synchronization is accomplished by common triggering using radio signals for LDAR. However, LDAR still has the disadvantage of not allowing location for VHF burst pulses emitted by processes like K-changes or recoil streamers. As the author has described, the key point of the short-baseline time-of-arrival technique is the identification of VHF pulses and this is why this technique is mainly effective for isolated VHF pulses associated with leader progressions. Figure 2 gives an example of a LDAR observation result.

Interferometry

The interferometry technique is the alternative method to locate VHF pulses associated with lightning discharges. The principle of the interferometer is to measure the phase difference between VHF pulses received by pairs of appropriately spaced antennas. In other words, this technique is principally the same as an FM broadcasting receiver. Since the VHF pulses emitted by lightning discharge do not include the carrier frequency, two antennas are required to estimate the phase difference.

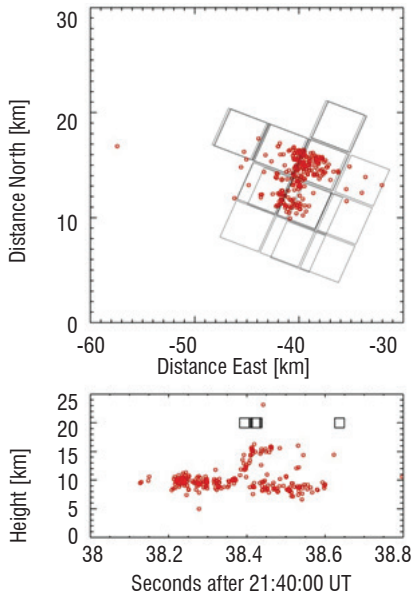

Figure 2 - Example of a cloud flash at 21:40:36 (UTC) on the15th of August 1998 with an overlay of LDAR sources and TRMM/LIS events. Circles and rectangles indicate the LDAR sources and LIS events, respectively. (Adapted from [5])

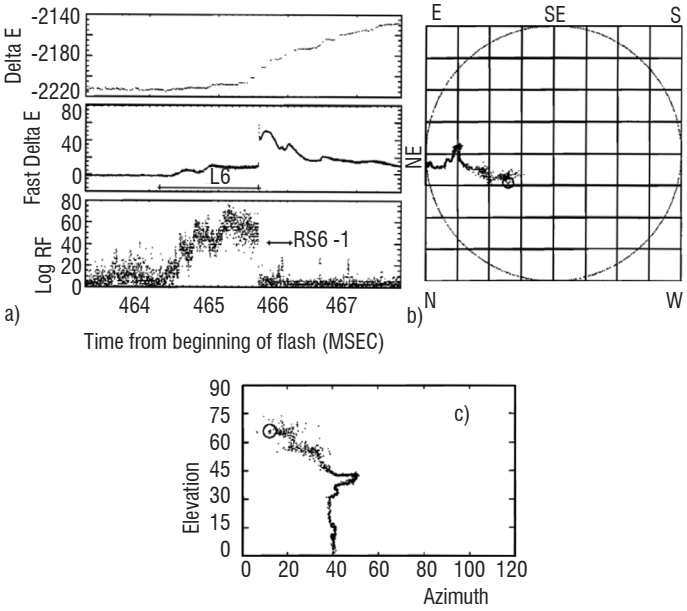

Figure 3 - Observations for a sixth stroke of a cloud-to-ground flash; (a) delta E, fast delta E, and log RF waveforms, (b) VHF source locations in a projection plane and (c) VHF source locations in an azimuth-elevation format. (adapted from[8]).

The first interferometer was designed by Hayenga and Warwick [6], [7]. The operating frequency of their interferometer was 34.3 MHz with a 3.4 MHz bandwidth. The interferometer consisted of three antennas installed at the three apexes of an isosceles right triangle. The spacing between two interferometer antennas is about 15 m, which corresponds to two wavelengths of the center frequency. Two pairs of antennas are able to measure the phase differences and these are

recorded on magnetic tape. We can derive the VHF pulse incidence angle relative to the interferometer as the azimuth and elevation. In the early 1990s a series of papers by the New Mexico Institute of Mining and Technology (NMIMT) introduced a new version of their interferometer as a more practical system. Moreover, they applied the idea of combining two baseline lengths to overcome the fringe ambiguity. The series of papers showed the various scientific interpretations of the lightning mechanism and phenomena such as charge distributions, leader progressions including attempted leader, cloud discharges and K events. One of the NMIMT interferometer observations is shown in figure 3 [8].

The Office National d'Études et de Recherches Aérospatiales (Onera) group also developed their own interferometer independently from NMIMT in the 1980s [9], [10]. Figure 4 shows a block diagram for the concept of Onera's interferometer. Normally, using one set of three and/or several antennas for the interferometry (the term 'interferometer unit' is used hereafter) gives us only the VHF pulse incidence angle relative to the observation site in azimuth and elevation. Then Onera group used the GPS time synchronization technique, with a spacing of tens and/or hundreds kilometers between several interferometer units, and two-dimensional mapping of VHF pulses on the ground plane was available for monitoring lightning activity. Moreover, three-dimensional images of lightning progression were obtained for scientific investigation. It may be noticed that an ordinary triangulation was applied for both two and three-dimensional mapping. The triangulation is a weak point of the interferometer for three-dimensional imaging of lightning. However, the Onera system finally became commercially available with an operational system named SAFIR, the operating frequency of which ranges from 110 MHz to 118 MHz, because this frequency band is dedicated to aviation and there is less contamination by artificial signals and noises. Many SAFIR systems are currently deployed all over the world.

The author's group operated SAFIR as the first user outside of France and showed that the location of VHF pulses and thunder cloud development were highly correlated, as a function of time and space [11]. It was possible to conclude that the total number of VHF pulses detected by an interferometer was linearly proportional to the possible amount of precipitation. In addition, the VHF pulse location may sometimes imply the location of solid precipitation particles such as graupel and hail. This fact has led the author and others to assess the ability of VHF lightning mapping to identify charge distribution and polarity within electrified clouds. The rimming electrification theory [12] for charge separation within thunderclouds is considered to be consistent with the VHF source distributions.

Then NMIMT group has been engaged in Lightning Mapping Array (LMA) and the author's group has been working on a broadband interferometer. Moreover their achievements are highly owed to the digital signal processing techniques recently developed in 1990s. The author understands that both NMIMT LMA and Osaka BDITF are the standing digital processing techniques and, from this aspect, there is some discrepancy between these two systems and the previously developed VHF mapping systems. These issues will be presented in the next chapter with scientific discussions.

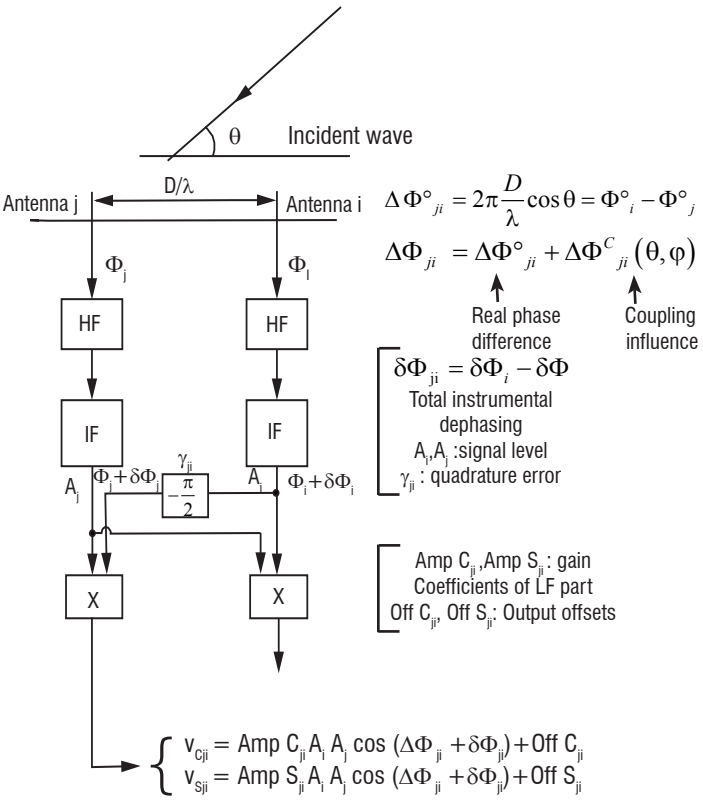

Figure 4 - Modeling of an interferometric couple with amplitude and errors. (adapted from [9]).

Lightning Mapping Array and Digital Interferometer

At the very beginning of this section, the author lists the four possible VHF radiation mechanisms associated with lightning discharges. These are: (1) a negative breakdown penetrating into a positive charge region, (2) a negative breakdown propagating in a free space, (3) a positive breakdown penetrating into a negative charge region, and (4) a positive breakdown propagating in a free space. The knowledge about the radiation intensity discrepancy between a negative and positive breakdown is additionally important. The intensity due to a negative breakdown is about 20 dB stronger than that of a positive breakdown [13], [14]. Since a bidirectional breakdown progression is expected for lightning discharges in the air, that means discharges without metal electrodes, the VHF radiation associated with a positive breakdown is not normally noticeable at the early stage of a discharge because of the masking effect. On the other hand, the progression velocity of a negative breakdown is about ten times faster than that of a positive breakdown and this is why the positive breakdown may still continue after a negative breakdown encounters the positive charge dominated region. Thus, the VHF radiation by a positive breakdown during the late stage of progression may be detectable. If all of these conditions are taken into account, the following interpretations are concluded. A large volume of locations with rather strong VHF pulse emission may correspond to a positive charge region. A time sequence of successive locations organized as a thin filament with a strong emission of VHF pulses may correspond to a negative breakdown, or we can say leader progression, in free space. A mass of weak VHF pulse emissions may correspond to a negative charge

region. Finally, a time sequence of successive locations organized as a thin filament of rather weak VHF pulse emissions may correspond to a positive leader progression in virgin air.

The VHF emission by a return stroke is much less, since the return stroke runs along the pre-ionized channel. It should be noticed that automatic discrimination and grouping for four categories cannot be performed yet, because the intensity of the VHF pulses is relative. The above mentioned conceptual idea should be kept in the reader's mind for the understanding of the latter part of this section.

Lightning Mapping Array (LMA) is principally based on TOA techniques. The NMIMT team deployed several VHF antennas with a receiving frequency of 60 MHz, and developed the portable LDAR [15]. The schematic diagram is presented in figure 5. As we may imagine from the title of the reference, LMA is accomplished by using GPS for the time synchronization between several antennas, to image three-dimensional mapping for lightning discharges. However, as described in a previous section, the one-to-one identification of detected VHF pulses at several sites is difficult, even if a received VHF impulse is isolated. Thus, the NMIMT conducted the enormous calculation for all physically possible combinations, in order to have the three-dimensional location of VHF pulses when they started the LMA project. The recent increase in computer capability and speed dramatically reduces the elapsed time necessary to locate VHF pulses. They introduce the cross correlation and an appropriate time window for data analysis to improve the LMA function, and LMA could be a quasi-operational system for lightning monitoring at this moment.

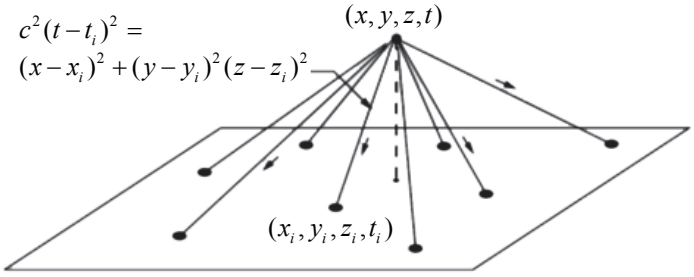

Figure 5 - Basic TOA technique. Measurements of the arrival times ti at N4 locations are used to determine the location and time of the source event *(x, y, z, t)*. (adapted from [16])

In late 1990s and early 2000s LMA showed many interesting observations by archived data analysis. One of the most important discoveries by LMA was the existence of an inverse charge distribution in a super cell thundercloud, as shown in figure 6. The NMIMT LMA found horizontally propagating lightning over a few tens of kilometers, and this lightning reached the ground at more than two locations (figure 7). The multi-point lightning strike over such a long distance presented in figure 7 may be a new subject to investigate and its physical interpretation is still controversial. The possible interpretation for "the bolt from the blue" is also presented and a variety of observations are shown on their website. On the other hand, LMA is still weak in regard to imaging for rapid progression phenomena such as a recoil streamer. VHF bursts associated with the K process cannot be imaged. Lojou [19] presented a detailed discussion of the advantages and disadvantages of TOA and Interferometry. Moreover, [20] suggested the necessity of calibration from the aspect of altitude for locations estimated by TOA because of the curvature of the earth.

The Osaka University group has been engaged in the VHF broadband digital interferometer (BDITF) [21]. The Osaka group's BDITF records a VHF pulse with a broadband frequency range between 30 to 100 MHz. As described in § "Time of Arrival", BDITF is principally similar to a very-shot-baseline TOA. However, the recent digital electronics allow a completely different and sophisticated system to be achieved as a quasi-real time system [22]. It must be noted that BDITF does not deal at all with the time difference between received VHF pulses. The phase difference for Fourier components with common time window is calculated. BDITF can estimate the azimuth and elevation of a VHF pulse incidence angle relative to the position of a BDITF unit, as has been done by the original very-short-baseline TOA system. Because of its broadband signal, a fringe ambiguity can be easily eliminated from the lower Fourier component through to the higher one successively. Schematic diagrams of antenna alignment and the fringe ambiguity elimination procedure are given in figures 8 and 9 respectively. For a recorded VHF pulse, each pair of VHF antennas estimates the incidence angles relative to its base-line (ϕ_1, ϕ_2 in figure 8) based on broadband digital interferometry. Finally, the BDITF allows the arrival angle (α: azimuth, β: elevation) of the VHF pulse to be obtained from the following equations:

$$\alpha = \tan^{-1}\frac{\cos\phi_2}{\cos\phi_1}$$

$$\beta = \cos^{-1}\frac{\cos\phi_1}{\cos\alpha}$$

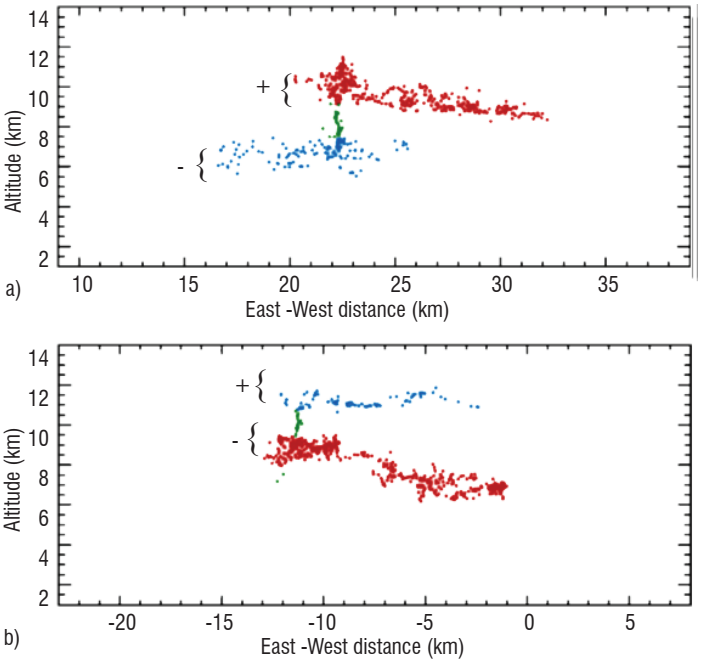

Figure 6 - Classification of the lightning radiation sources mapped by the LMA, in terms of the parent storm charge for the (a) normal-polarity and (b) inverted-polarity cloud flashes, respectively. The red dots indicate inferred positive charge in the storm, the blue dots indicate negative storm charge and the green dots connecting the two charge regions are not applicable to the inferred charge structure of the storm. (adapted from [17]).

The full details of the location technique are available in [24].

The BDITF has a disadvantage and some advantages over LMA. The disadvantage is the need to triangulate for three-dimensional mapping. Moreover, even if the time synchronization among BDITF units is

perfect, the lines-of-site from two or three interferometer units hardly intersect each other and this is why LMA can be superior to BDITF in this regard. NMIMT used to be engaged in BDITF [25], but they have changed their focus to a TOA system.

The advantages of BDITF are the availability of VHF burst pulse location, easy real-time operation for lightning monitoring and the freedom of antenna alignment, etc... [23]. Figure 10 shows the two-dimensional location of a cloud-to-ground stroke in azimuth and elevation format, obtained at most one second after the lightning strike. [25] were able to reveal the mechanism of a cloud discharge K process thanks to the advantage of VHF pulse burst imaging. The Osaka Group showed one of the possible interpretations for long propagating lightning channels, by combining BDITF and dual polarized RADAR observations [25]. According to their understanding, a negative breakdown progression is prevented from descending toward the ground by a positively charged layer and it propagates horizontally for a distance of over 15 kilometers. This interpretation is consistent with the well-known common sense obtained through many-years-field-observations.

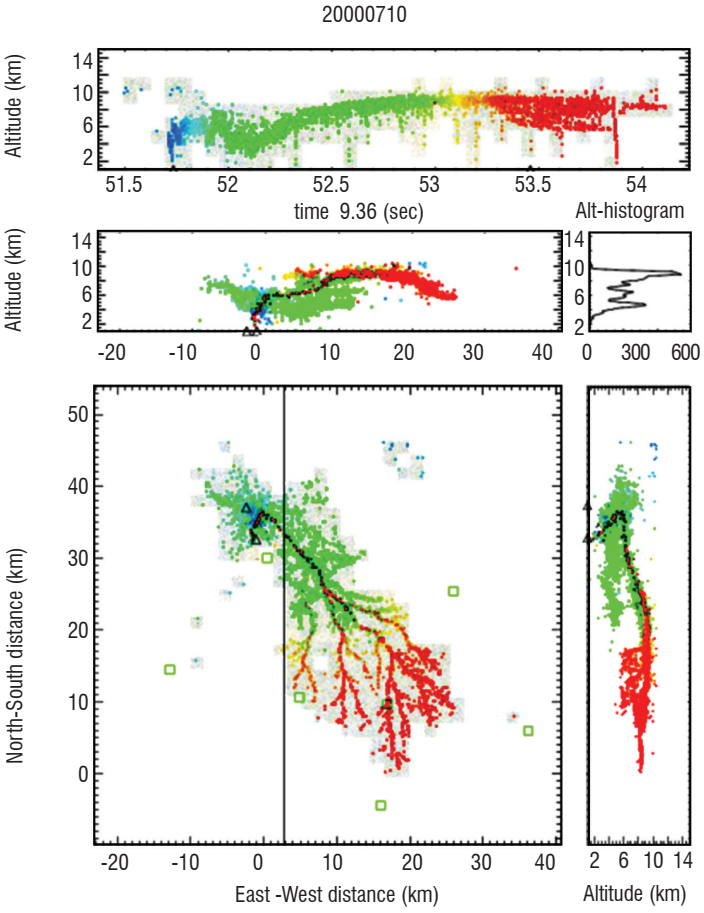

Figure 7 - A normal polarity, negative CG flash (negative charge descending to ground) that had a substantial (>50 km) incloud horizontal extent and a spectacular dendritic structure. The small triangles indicate the -CG strike points, as determined by the NLDN, but provide no indication of the overall size of the discharge (adapted from [18]).

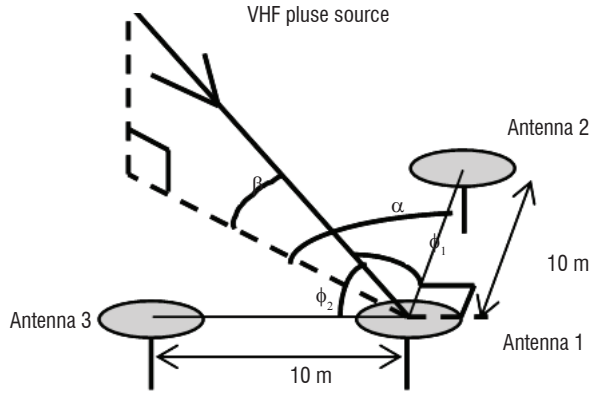

Figure 8 - Antenna arrangement of a perpendicular-baseline-interferometer for 2D mapping. Antennas 1 and 2 form one baseline, and antennas 1 and 3 form the other baseline.

NMIMT and Osaka University have been collaborating to evaluate each other's systems. LMA and BDITF have been installed in New Mexico and simultaneous observations are ongoing. According to the preliminary results, which were presented at the AGU fall meeting in 2011, both systems show an excellent correspondence in terms of the two-dimensional time sequence of mapping in azimuth and elevation, as shown in figure 11. However, as expected in the case of a rapid change like a recoil streamer, BDITF definitely maintains the advantage over LMA. On the other hand, LMA proves to be superior to BDITF for three-dimensional imaging.

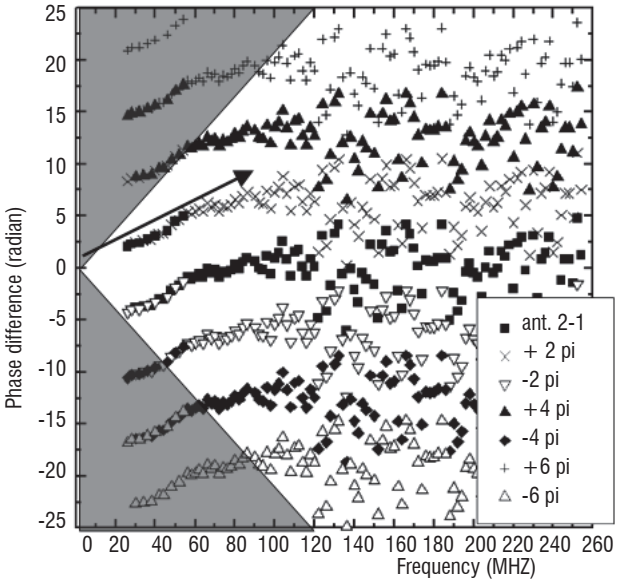

Figure 9 - Removing phase ambiguity by the displacement of phase differences θ_{12} with $\theta_{12}\pm2\pi$, $\theta_{12}\pm4\pi$, ... The shaded area is the contradictory area to the 10 m baseline. The series of phase differences follows the arrow.

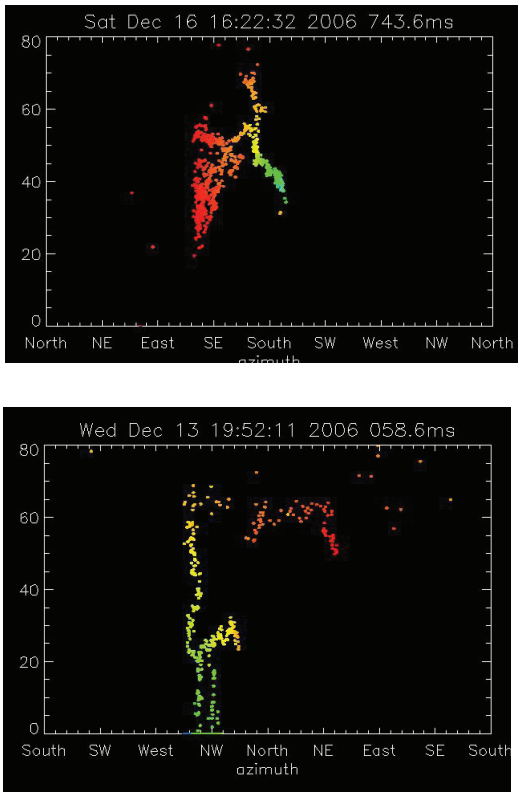

Figure 10 - (a) positive cloud-to-ground flash (b) negative cloud-to-ground flash. A video of two-dimensional VHF source locations of a cloud-to-ground flash in an azimuth and elevation format. In the case of a positive CG, the return stroke and breakdown inside the cloud are located, on the other hand, in the case of a negative CG the leader propagation can be imaged. For both cases we may see the negative breakdown.
(http://www.aerospacelab-journal.org/al5/review-of-the-location-of-VHF-pulses-associated-with-lightning-discharge)

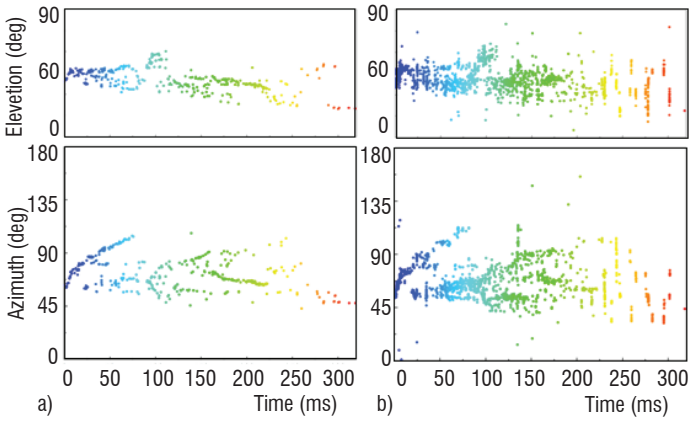

Figure 11 - The 2D mapping for IC flash recorded at 2258:03 UT on the 7th of September 2011 in New Mexico. Data is shown for (a) LMA, (b) BDITF. (adapted from [26])

Conclusions

This review article gives a brief summary of two VHF location system principles that have been developed since the 1970s. Because of recent advanced technology in digital electronics, lightning location systems are able to reveal new phenomena and interpretations, even though they are based on the same principle as in the 1970s or 1980s. For example, though the TOA technique was known originally, LMA contributes much for atmospheric electricians and lightning physicists. The BDITF is also based on the very-short-baseline technique and an operational quasi- nowcasting BDITF system has been developed. Moreover, LMA and BDITF are ultimately and principally equivalent, from the point of view of lightning channel imaging. The author expects that these two systems will be able to contribute to unveil the remaining problems. One of the expectations is the real-time and automatic discrimination between positive and negative breakdowns. Though at the moment discrimination is performed manually, using well trained eyes, an operational real-time system can be expected soon ■

References

[1] G. N. OETZEL AND E. T. PIERCE - *VHF Technique for Lightning Location*. Radio Science 4, 199-201, 1969.
[2] D. E. PROCTOR - *A Hyperbolic System for Obtaining VHF Pictures of Lightning*. J. Geophys. Res., 76, 1478-1489, 1971.
[3] D. E. PROCTOR - *Regions where Lightning Flashes Began*. J. Geophys. Res., 93, 5099-5112, 1991.
[4] C. L. LENNON and H. A. POCHLER - *Lightning Detection and Ranging.* Astronautics and Aeronautics, 20, 29-31,1981.
[5] T. USHIO, S. HECKMAN, K. DRISCOLL, D. BOCCIPPIO, H. CHRISTIAN, and Z-I. KAWASAKI - *Cross-Sensor Comparison of the Lightning Imaging Sensor (LIS)*. Int. J. Remote Sensing, 23, 2,703-2,712, 2002.
[6] C.O. HAYENGA and J. W. WARWICK - *Two-Dimensional Interferometric Positions of VHF Lightning Sources*. J. Geophys. Res., 86, 7,451-7,462, 1981.
[7] C. O. HAYENGA - *Characteristics of Lightning VHF Radiation near the Time of Return Strokes*. J. Geophys. Res., 89, 1403–1410, doi:10.1029/JD089i-D01p01403, 1984.
[8] X. M. SHAO, P. R. KREHBIEL, R. J. THOMAS, and W. RISON - *Radio Interferometric Observations of Cloud-to-Ground Lightning Phenomena in Florida*. J. Geophys. Res., 100, 2,749-2,783, 1995.
[[9] P., G. RICHARD. AUFFRAY - *VHF-UHF Interferometric Measurements, Applications to Lightning Discharges Mapping*. Radio Science, 20, 171-192, 1985.
[10] P., A. RICHARD, DELANNOY, G. LABAUNE, and P. LAROCHE - *Result of Spatial and Temporal Characterization of the VHF–UHF Radiation of Lightning*. J. Geophys. Res., 91, 1,248–1,260, 1986.
[11] Z-I. KAWASAKI, K. YAMAMOTO, K, MATSUURA, P. RICHARD, T. MATSUI, Y. SONOI and N. SHIMOKURA - *SAFIR operation and evaluation of its performance*. Geophys. Res. Letters, Vol.21, Issue 12 pages 1133-1136, June 1994.
[12] T. TAKAHASHI - *Rimming Electrification as a Charge Generation Mechanism in Thunderstorms.* J. Atmos. Sci., 35, 1,536-1,548. (1978)
[13] X. M. SHAO, C. T. RHODES and D. N. HOLDEN - *RF Radiation Observations of Positive Cloud-to-Ground Flashes*. J. Geophys. Res., 104, 9,601–9,608, 1999.
[14] Z-I. KAWASAKI, S. YOSHIHASHI and J. H. LEE - *Verification of Bi-Directional Leader Concept by Interferometer Observations*. J. Atmos. Elect., 22, 2, 55-79, 2002.
[15] W. RISON, R. J. THOMAS, P. R. KREHBIEL, T. HAMLIN, and J. HARLIN - *A GPS-Based Three Dimensional Lightning Mapping System: Initial Observations in Central New Mexico*. Geophys. Res. Letters, 26, 3573-3576. 1999.
[16] R. J. THOMAS, P. R. KREHBIEL, W. RISON, S. J. HUNYADY, W. P. WINN, T. HAMLIN, and J. HARLIN - *Accuracy of the Lightning Mapping* Array, J. Geophys. Res., 109, D14207, doi:10.1029/2004JD004549. 2004.

[17] W. D. RUST, D. R. MACGORMANA, E. C. BRUNING, S. A. WEISS, P. R. KREHBIEL, R. J. THOMAS, W. RISON, T. HAMLIN, J. HARLIN - *Inverted -Polarity Electrical Structures in Thunderstorms in the Severe Thunderstorm Electrification and Precipitation Study (STEPS)*. Atmospheric Research Vol. 76, Issues 1–4, July–August 2005, pp. 247–271.
[18] P. R. KREHBIEL, T. HAMLIN, Y. ZHANG, J. HARLIN, R. THOMAS, and W. RISON - *Three-Dimensional Total Lightning Observations with the Lightning Mapping Array*. International Lightning Detection Conference, Tucson, U.S.A., 2002.
[19] J. Y. LOJOU - *Total Lightning Mapping using both VHF Interferometry and Time-of-Arrival Techniques*. 19th Int. Lightning Detection Conf., 24-25 April, Tucson, USA, #36, 2006.
[20] W. J. KOSHAK, R. J. SOLAKIEWICZ, R. J. BLAKESLEE, S. J. GOODMAN, H. J. CHRISTIAN, J. M. HALL, J. C. BAILEY, E. P. KRIDER, M. G. BATEMAN, D. J. BOCCIPO, D. M. MACH, E. W. MCCAULC, M. F. STEWART, D. E. BUECHLER, W. A. PETERSEN, and D. J. CECIL - *North Alabama Lightning mapping Array (LMA): VHF Source Retrieval Algorithm and Error Analyses*. J. Atmos. Ocean. Tech., 21, 4, 543-551, 2004.
[21] T. USHIO, Z-I. KAWASAKI, Y. OHTA, and K. MATSUURA - *Broadband Interferometric Measurement of Rocket Triggered Lightning in Japan*, Geophys. Res. Letters, 24, 2,769–2,772, 1997.
[22] R. MARDIANA and Z-I. KAWASAKI - *A Broadband Radio Interferometer Utilizing a Sequential Triggering Technique for Locating Electromagnetic Sources Emitted from Lightning*. IEEE Trans. Instrum. Meas, 49, 376– 38, 2000.
[23] T. MORIMOTO, A. HIRATA, Z-I. KAWASAKI, T. USHIO, A. MATSUMOTO, and J. H. LEE - *An operational VHF broadband digital interferometer for lightning monitoring*, IEEJ Trans. Fundam. Mater., 124, 1,232–1,238, 2004.
[24] X. M. SHAO, D. N. HOLDEN, and C. T. RHODES - *Broad Band Interferometry for Lightning Observations*. Geophys. Res. Letters, 23, 1,917-1,920, 1996.
[25] M. AKITA, Y. NAKAMURA, S. YOSHIDA,T. MORIMOTO, T. USHIO, Z-I. KAWASAKI, and D. WANG - *What Occurs in K Process of Cloud Flashes?* J. Geophys. Res., 115, D07106, 2010.
[26] M. AKITA, S. YOSHIDA, Y. NAKAMURA, T. MORIMOTO, T. USHIO, Z-I. KAWASAKI, and D. WANG - *Effects of Charge Distribution in Thunderstorms on Lightning Propagation Paths in Darwin*. Australia, A. Met. Society, 68, 719-726, 2011.

Acronyms

DITF (Digital InTerFerometer)
LDAR (Lightning Detection And Ranging systems)
LMA (Lightning Mapping Array)
NMIMT (New Mexico Institute of Mining and Technology)
TOA (Time-Of-Arrival)

AUTHOR

Zen Kawasaki (M'72) received the B.S., M.S., and Dr. Eng. degrees in communications engineering from Osaka University, Osaka, Japan, in 1973, 1975,and 1978, respectively. In 1989, he joined the Department of Electrical Engineering, Osaka University, where he is currently a Professor in the Division of Electrical, Electronic and Information Engineering. His research mainly concerns the electromagnetic compatibility and atmospheric electricity. He is a Fellow of the IEE Japan and the President of the International CommissiAtmospheric Electricity (IUGG/IAMAS)

E. Williams
(MIT)
S. Heckman
(Earth Networks)

E-mail: earlew@ll.mit.edu

Polarity Asymmetry in Lightning Leaders: the Evolution of Ideas on Lightning Behavior from Strikes to Aircraft

This study is concerned with outstanding questions on the mechanism of lightning and its theoretical treatment as a bidirectional leader. Previous studies of lightning strikes to aircraft are reviewed to highlight the key physical phenomena: the simultaneous action of both positive and negative leaders, the frequent tendency for electrical current in certain channels to cut-off abruptly, and the subsequent tendency for recoil leaders to initiate in these previously cut-off channels to establish a new stroke in the flash.

Introduction

This study is concerned with outstanding questions on the mechanism of lightning and its theoretical treatment as a bidirectional leader. Previous studies of lightning strikes to aircraft are reviewed (§ "Evidence from aircraft lightning strikes") to highlight the key physical phenomena: the simultaneous action of both positive and negative leaders, the frequent tendency for electrical current in certain channels of the double-ended lightning 'tree' to cutoff abruptly, and the subsequent tendency for recoil leaders to initiate in these previously cutoff channels to establish a new stroke in the flash. The theoretical treatment of the asymmetrical bidirectional leader is reviewed in § "Theoretical treatment of the asymmetrical bidirectional leader", showing that current flow in the positive leader end will be consistently smaller than in the negative end. Two different physical mechanisms are presented to account for the current cutoff and recoil leader formation. They are compared and contrasted in § "Contrasting two explanations for current cutoff and formation of a subsequent stroke" with available observations as discussed in § "Comparison with available observations" toward distinguishing the two mechanisms.

Evidence from aircraft lightning strikes

Important physical evidence for bidirectional lightning development proposed theoretically by [1] came from studies of lightning interaction with aircraft [2]. Radar observations with the aircraft centered in the radar beam demonstrated that the aircraft served to trigger the bidirectional development, showing extension of the radar echo away from the pronounced metallic aircraft target in both directions along the fixed radar beam [2], leaving the aircraft in the 'trunk' of the evolving discharge with two distinct current contact points (one entry and one exit point) on the aircraft. Figure 1 shows an example of an aircraft in the trunk of a double-ended lightning tree, in this case beneath cloud base where the lightning geometry is clearly exposed.

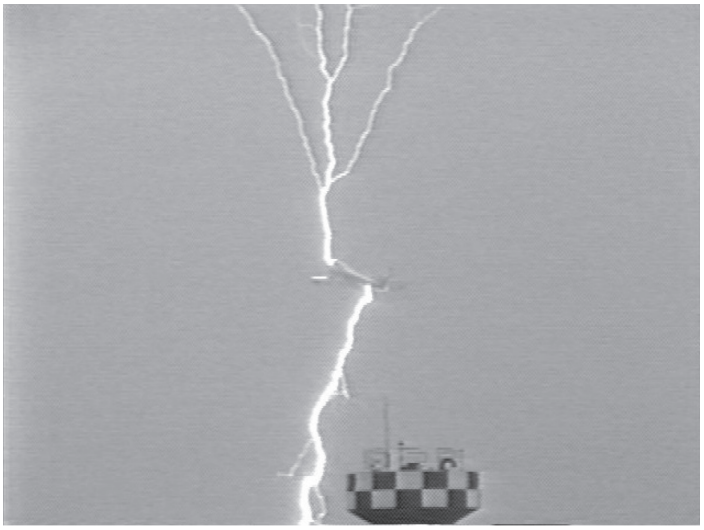

Figure 1 - Lightning strike to aircraft showing bidirectional leader development, with the aircraft in the 'trunk' of the 'tree' (from K. Michimoto and Z. Kawasaki).

A key feature of lightning polarity asymmetry [3]has also been documented in the case of lightning strikes to aircraft of the kind shown in figure 1. Recoil leader activity is confined to the positive end of the bidirectional leader [4], [5]. An antecedent condition for the recoil leader occurrence is a remarkable phenomenon also in common with natural lightning: complete cutoff of the channel current in those channels in which recoil leaders subsequently initiate [6], [7], [8].

The special location of the aircraft in series with the bidirectional leader in typical lightning aircraft interactions allows for unique observations of lightning both from within and on the surface of the aircraft.

Theoretical treatment of the asymmetrical bidirectional leader

Kasemir [1] seminal electrostatic treatment of lightning as a double-ended extension of a long, thin conductor aligned in a uniform electric field gave no preference to positive and negative ends. The shape of the analytically-tractable prolate spheroid conductor was identical at either end, as was the speed of extension in the electric field. As a consequence, the current is identical at both ends and the distribution of current in a prolate spheroid is uniform, consistent with recent applications of this model to observations of lightning [7], [9]. Both the positive and negative line charge densities $\lambda(z)$ increase linearly from midpoint of the conductor to their respective ends (figure 2).

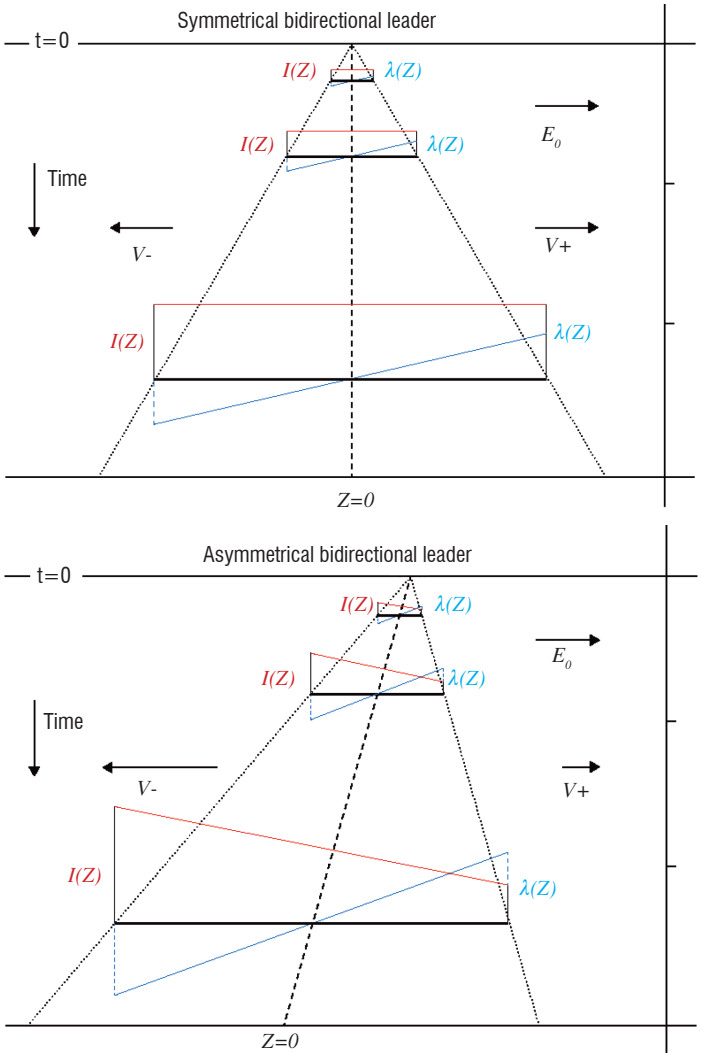

Figure 2 - Illustration of symmetrical and asymmetrical development of bidirectional leaders aligned with an imposed electric field [10].

Mazur and Ruhnke [7] first recognized and emphasized the polarity asymmetry in recoil leader development evident in both the aircraft-initiated bidirectional lightning and in natural lightning. They speculated that the "difference between negative and positive leader breakdown is the important factor involved". Recent studies by [10] have confirmed this earlier speculation by identifying evidence for a distinct contrast in the speed of positive and negative leader progression, and by generalizing the Kasemir [1] mathematical model to an asymmetrical bidirectional development. The behavior of the symmetrical (matched leader speeds) and asymmetrical case (faster negative leader speed) are contrasted in figure 2, where the variation of line charge density and current along the leader channel are also shown. The asymmetry in leader speed is consistent over a wide range of scales, from laboratory point-to-plane gap studies on meter scales [11], [12], [13], to 100 meter discharges with outdoor high voltage generators [14], [15], to rocket triggered lightning [16], [17] on kilometer scales into clouds of both polarities, to natural lightning strokes to towers [18], [19], [20], to detailed LMA analysis of leader propagation on thundercloud scales [21].

We do not have a fundamental quantitative explanation for the marked polarity asymmetry in leader speed, except to recall that a pronounced asymmetry in progression behavior is well established for negative and positive leaders, in both laboratory scale sparks [11], [12], [22] and in negative lightning stepped leaders [23], [24], [25]. On the scale of the respective leader "head", complicated streamer physics is controlling the leader extension. The negative progression is intermittent and discontinuous by virtue of the existence of "space leaders" that form out front of the main leader channel and which then extend in both directions to link with the main leader behind, setting up conditions for a new space leader, and so on. In contrast, the positive leader end progresses smoothly, led by positive streamers, generally with lower electric field thresholds for progression, and without the participation of space leaders. Evidently the jumpy progression at the negative end is faster despite the interruptions because the speed of space leader expansion is substantially greater than the positive streamers. The advent of ultra-high speed lightning imaging is likely to clarify this situation in the near future.

Returning to figure 2 in the symmetrical bidirectional leader, the current is constant with length, but in the asymmetrical case, the current varies linearly from the low speed positive end to the high-speed negative end. The current I at each end is given by

$$I = (2\pi\varepsilon_0/ln(L/r))\ E\ LV \qquad (1)$$

where L is the total length in meters, r is the semi-minor-axis of the prolate spheroid, E is the uniform electric field, and V is the leader tip speed at that end (in m/s). The distribution of line charge density $\lambda(z)$ remains symmetrical at any given time, assuring conservation of electric charge on the conductor. But the zero of line charge density translates in space at a speed which is half the difference of the two leader speeds.

Heckman [28] investigated the instability of lightning using an equivalent circuit consisting of three elements in parallel: a current source, a channel capacitance and a negative resistance. The current source represented the extension of the lightning conductor in the electric field of the thunderstorm. The channel capacitance, associated with charge and voltage on the conducting lightning channel, was represented analytically by

$$C = 2\pi\varepsilon_0 L/ln(L/r)$$

(with ε_0 the permittivity of free space, L the channel length and r the channel radius), an elementary result from electrostatics. The third circuit element is a negative resistance, based on observations of arc channels in air [26], [27] showing that for low current (generally <100 A), the channel voltage drop increases with decreasing current, and therefore exhibits negative differential resistance. The equivalent circuit described here is decidedly nonlinear by virtue of this third circuit element. [25] derived conditions for the linear instability of this circuit. These conditions, involving channel current and channel length, are shown in figure 2. The irregular black line boundary separates a stable region (upper left) for continuing current from an unstable region (lower right) in which the current is predicted to cutoff. The negative differential resistance plays a fundamental role here: reduced current imposes increased resistance, decreasing current and causing cooling of the arc, resulting in further increases in resistance, in a kind of runaway to vanishing arc current. Ordinary ohmic resistance does not behave in this way.

Based on the instability analysis of a long, thin current carrying arc with negative differential resistance, Heckman [28] produced a parameter space of current and arc channel length predicting when the current was stable (as a long continuing current) and when it was subject to cutoff. Additional strokes were made possible by the action of sustained leader extension into electric field, which then stressed the cutoff channel (by virtue of its reduced dielectric strength as a low density channel).

The unique current-length relationship (1) for the bidirectional leader was discussed previously in [10]. This relationship can be superimposed on the Heckman instability diagram, as shown in figure 3. Here the total range of (linearly varying) current in the asymmetrical bidirectional leader is shown, for propagation in a uniform field of 10^5 v/m, and with assumed positive and negative leader speeds of 10^4 m/s and 10^5 m/s, respectively. With this realistic selection of parameters, sections of the (slower) positive end of the bidirectional leader are predicted to be unstable, and hence prone to current cutoff, whereas the faster negative end remains stable. We will return to these predictions in interpreting the observations discussed in § "Comparison with available observations".

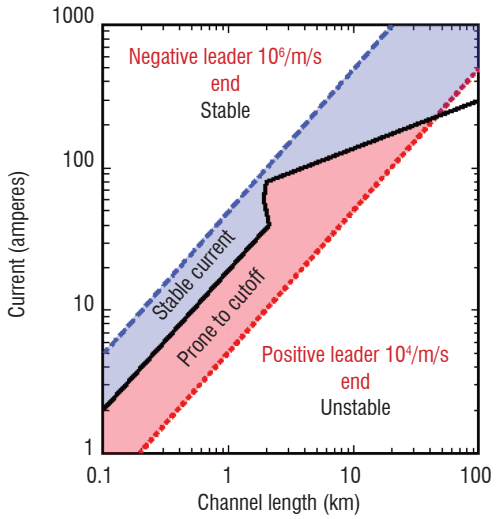

Figure 3 - Stability diagram for lightning (adapted from [10]), showing the range of current for every length of a asymmetrical bidirectional leader with negative tip speed of 105 m/s and a positive tip speed of 104 m/s.

Contrasting two explanations for current cutoff and formation of a subsequent stroke

Current cutoff

Previous sections have emphasized that the phenomena of current cutoff and subsequent recoil leaders leading to a new lightning stroke are common to lightning strikes to aircraft [5], [6], to rocket-triggered lightning [7] and to natural lightning as in figure 4 [29], [30], [31]. Twenty years ago, two distinct physical explanations for these phenomena were advanced, one by Mazur and Ruhnke [7] (with recent revision [32]) and one by Heckman [28]. Both the physical basis for current cutoff and for the subsequent breakdown to follow the same cutoff channel are distinctly different in these two treatments.

The physical picture of lightning in [7] and [32] (and subsequent work by the same authors) is based on the assumption that lightning leaders are isopotentials. Their mechanism for current cutoff is shown in figure 5 and is based on electrostatic shielding of the cloud electric field by these perfect conductors. Extensive lateral branching of the positive leader in advancing into negative space charge in the mid-region of thunderstorms leads to a reduction in the field in the channel connected to Earth. In a two-tiered development of the positive tree (see figure 5), the electric field lines terminating on the lower branches may be reduced as upper branches extend, thereby reducing the induced charge and enabling a current reversal from the side-branches to the main leader channel.

Figure 4 - Illustration of current cutoff in the channel to ground in a multi-stroke lightning flash [31]. Note the reproducibility of the fine structure of the channel tortuosity from stroke to stroke.

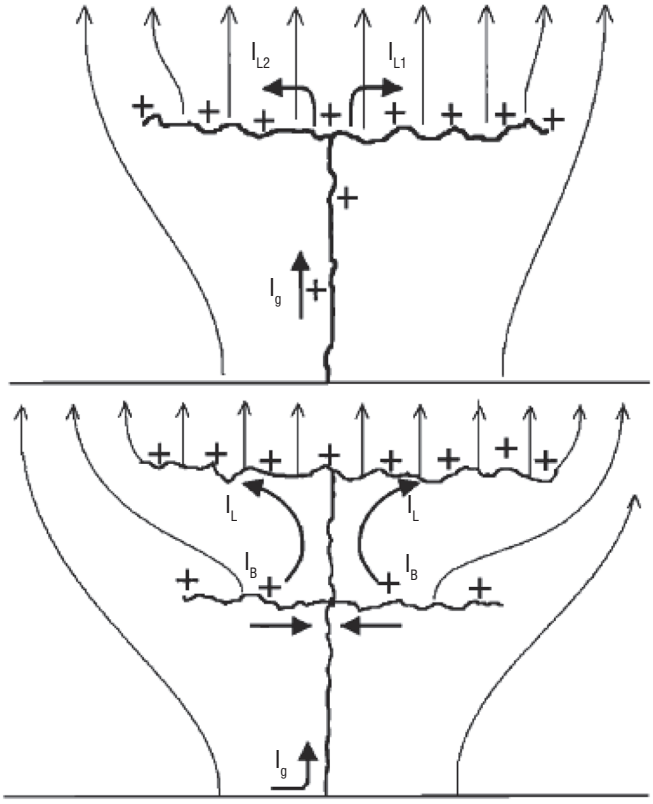

Figure 5 - Illustration of the mechanism of current cutoff by electrostatic screening, according to [7] and [37].

In contrast, the mechanism for current cutoff and current instability proposed by Heckman [28] is based on negative differential resistance in lightning channels (figure 6) and requires the departure of leader channels from the isopotential condition assumed by Mazur and Ruhnke [7], [9]). Heckman's work developed from the earlier suggestion of King [26] that "the negative resistance characteristics of the channel were important in causing the strokes to be discrete". Quantitative experiments with DC arcs in air ([33], [34], [26], [35]) show that the electric field in channels with current exceeding 100 amperes (and extending to current levels characteristic of lightning return strokes) is ~ 1 kV/m. For a leader channel length comparable to the size of a thunderstorm (~10 km), the estimated total voltage drop is 10 MV, already a significant portion of measured total potentials in thunderclouds [36]. But the mechanism for cutoff relies on the demonstrated tendency for arcs in air at currents less than 100 amperes (figure 6) to exhibit increasing channel field with decreasing current, the well-known characteristic of negative differential resistance [34], [26]. Heckman [28] and Williams [3] examined the stability of an analog electric circuit for lightning consisting of a long arc connected to a current source. This analysis established a boundary between stable and unstable lightning regimes shown in figure 3. The unstable regime leads to a diminishment of current, and the monotonic increase of arc channel electric field with decreasing current guarantees a complete current cutoff. In the lightning context, in contrast with the mechanism in [7] and [37], no branching of the arc channel is needed to produce current cutoff. This phenomenon is predicted whenever the interstroke extension of the positive leader provides less than the critical current [28].

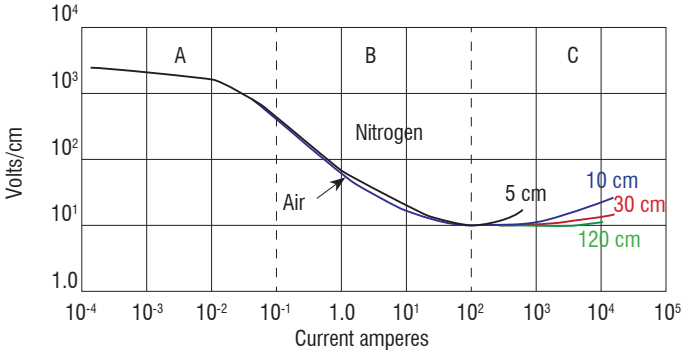

Figure 6 - Evidence for negative differential resistance in a DC arc in air [26].

Recoil leaders and subsequent strokes

The common ground in [7] and [28] is the mechanism for maintaining a current inside the thundercloud in the interstroke interval. Historically, the physical evidence for this "J-process" is indirect and was documented initially with electric field measurements by Malan and Schonland [38], showing that the negative charge increased overhead in the (cutoff) interval between strokes of a cloud-to-ground flash. Krehbiel's important contribution here [39],[30] was demonstrating that the interstroke current was predominantly horizontal rather than vertical, as [38] had argued earlier, consistent with a large body of contemporary evidence that the main negative charge region is relatively compact in the vertical in comparison with its horizontal extent. So in this context, the common mechanism for the maintenance of interstroke current is the continued progression of the positive leader(s) throughout the interstroke interval. As Mazur and Ruhnke [7] noted:

"*In their search for the origin of discrete strokes in CG flashes, Heckman and Williams[40] concluded that interstroke currents observed are entirely due to longitudinal channel extension, rather than corona envelope radial expansion. These findings concur with our concept of recoil streamer initiation.*"

Mazur and Ruhnke [7] and Heckman [28] also concur that the cutoff lightning channel becomes non-conducting, and this transition is essential for the increased voltage on the cutoff channel by the interstroke current which ultimately causes recoil leader initiation. Studies of the electrical conductivity of air versus temperature [41] show that the resistivity increases by more than 5 orders of magnitude between 3000 K (4.7 x 10^3 Ω.m) to 2000 K (1 x 10^9 Ω.m), leading Aleksandrov and al. [42] to conclude that "*such a high linear resistivity can be achieved only when in the current in the channel terminates*". This dramatic change goes hand-in-hand with the negative differential resistance with declining current depicted in figure 6. Mazur and Ruhnke [9] are noncommittal about why the subsequent recoil breakdown follows the same cutoff channel. In contrast, Heckman[28] is explicit in stating that the decayed channel is dielectrically weak because it is still warmer than ambient atmospheric temperature, and hence of low density. The cutoff channel may also be dielectrically weak because of the abundance of ions and their lower ionization potential in comparison with neutral species.

In both [7] and [28], the cutoff channel of lightning is electrically restressed by the increased voltage on the cutoff channel, caused in turn by the continued extension of the lightning 'tree'.

Comparison with available observations

Current cutoff

A large body of evidence for current cutoff between strokes of a lightning flash has accumulated, in the context of aircraft strikes, the rocket triggering of lightning and in all forms of natural lightning. It should be noted at the outset of this discussion that the common existence of discrete strokes superimposed on continuing current, a prevalent phenomenon in both aircraft lightning strikes and rocket-triggered lightning, is no indication that current cutoff played no role in the discrete stroke. It is only necessary that the current cutoff occur in a secondary branch also connected to the main channel in which the current is measured, and that the cutoff channel be at a different electrical potential than the main channel. A good example of this behavior is found in [9].

Evidence for cutoff in lightning strikes to aircraft is the absence of modification to the metallic skin of the aircraft as the current attachment point sweeps along the aircraft surface. Distinct pitting of the surface occurs at times of discrete strokes, but the surface is often unblemished in the interstroke intervals.

Pulse-to-pulse radar observations on lightning channels also provide evidence for current cutoff. Hewitt [43] noted systematic diminishments in radar returns during the latter portion of interstroke intervals in natural lightning. In commenting on these observations and their interpretation, Krehbiel and al. [39] noted the following:

"*An unresolved discrepancy between the present results and those of Hewitt concerns his observations that the interstroke echoes decreased in intensity during the latter portion of the interstroke period and that the next stroke generally did not occur until this decrease had taken place. If the echo intensity were an indication of the interstroke current, Hewitt noted, such a result would indicate that the current decreases substantially 10-20 ms priot to the subsequent stroke. Such an effect is not apparent in the electric field measurements, either of this investigation or others. Rather, the field changes uniformly throughout the interstroke interval, indicating that the dipole moment change (and hence current, assuming constant displacement) remains approximately constant.*"

A plausible resolution of this apparent discrepancy is that Hewitt's radar beam was aimed at the cutoff channel to ground and not the extending positive leader tips believed to maintain the interstroke current in other portions of the cloud. Radar observations on a rocket-triggered lightning channel at 10 m range [28], for which there is no ambiguity concerning the radar lightning target, indicate that current cutoff occurs on a time scale of milliseconds.

The complete disappearance of lightning channels to ground in optical/photographic observations of ground flashes is widely recognized [31]. Recent observations by Mazur and Ruhnke [9] also show evidence of channel disappearance, supporting current cutoff, in high speed video camera observations of upward lightning flashes from towers. In both cases, this darkening of the channels precedes the formation of recoil leaders. These inferred current cutoffs are not preceded immediately by the extensive multi-tiered branching envisaged in figure 5. It remains unclear how a screening process based on shielding by branching can succeed in complete suppression of the lightning current.

Recoil leaders

A distinct feature of recoil leaders, evident in lightning strikes to aircraft [4], [6], in rocket-triggered lightning [7], in lightning strikes initiated by towers [9], [44] and in natural lightning, both intracloud [45] and cloud-to-ground [30], is their marked polarity asymmetry. Recoil leaders are observed to initiate only in the positive end of the lightning 'tree'. In the words of Mazur [37]:

"*From the standpoint of physical interpretation, we should find out why recoil leaders are only of negative polarity, and positive recoil leaders have never been observed (or do not exist), in spite of seemingly similar conditions for the negative and positive breakdown at the end of the cutoff process.*"

Mazur and Ruhnke [9] later give emphasis to the "branching positive leader" as the "origin" of the recoil leader. However, many observations show that both ends of the lightning 'tree' are often highly branched (see figure 1 in this study and the cover photograph of the May 2012 issue of the Newsletter on Atmospheric Electricity [46]). On this basis, it seems unlikely that branching alone can account for the polarity asymmetry in recoil leader initiation. In contrast, a distinct polarity asymmetry has been identified in the speeds of lightning leaders [10], with implications for smaller currents in the positive end of the asymmetrical bidirectional leader (§ "Theoretical treatment of the asymetrical bidirectional leader"). According to the instability analysis of Heckman [28] and the arc behavior of figure 6, the instability to current cutoff based on negative differential resistance is more likely where current is smaller (all other things being equal), thereby favoring recoil leader initiation in the positive end of the lightning 'tree'.

The most detailed published observations on current cutoff in lightning channels that are subsequently re-illuminated by recoil leaders are those of Mazur and Ruhnke [9] and Warner and al. [44]. The observations come from high-speed video camera analysis with single-frame resolution of 139 μs and 18.5 μs, respectively. As with all other documented observations, the recoil leaders occur in the positive end of the lightning 'tree', on channels that typically disappear from detection in the high-speed imagery. In both cases, the recoil leaders show a bidirectional development (as speculated by [3]) and follow the same detailed channel form as the one inferred to be cutoff. A well-defined asymmetry in leader speed (x3 or greater), with larger speed on the negative end, is consistent with earlier evidence for polarity asymmetry in leaders [10]. The initiation locations for the bidirectional development are notably closer to the extending channel end than to the branch contact point on the continuously illuminated lightning 'tree', where the current prior to cutoff would be expected to be less and hence more susceptible to cutoff by negative differential resistance [28]. In both cases, the fully re-illuminated channel (following recoil leader extension) shows a greater extent away from its origin than was apparent for the channel prior to cutoff, consistent with the common view that the sustained channel extension in the electric field of the cloud was responsible for the re-stressing of the previously cutoff channel. One puzzlement in the observations of Mazur and Ruhnke [9] is why the distant end of the extending positive leader is not detectable in the high-speed imagery, despite the evidence in 'before' and 'after' image comparisons for such channel extension. This observation suggests that the disappearance of the channel in the imagery is no absolute guarantee that the channel current is zero. Further efforts aimed at the sensitivity to small currents in the video camera imagery are needed.

Conclusions

A wide variety of lightning observations have been revisited to support common features of bidirectional leader development in lightning strikes to aircraft, lightning triggered by wire-trailing rockets, lightning strikes to towers, and natural lightning (both intracloud and cloud-to-ground). Two long-standing mechanisms for current cutoff and the subsequent formation of a new stroke in the same tortuous channel have been reviewed and contrasted against the observational evidence. Current cutoff is more readily explained by negative resistance in the lightning channel as suggested initially by Krehbiel [30] than by electrostatic screening, because a real zero of current is guaranteed in the former situation and because lightning channels at low current (<100 A) cannot be accurately treated as isopotentials. The marked polarity asymmetry in recoil leader behavior is likewise more readily accounted for by the asymmetry in the antecedent leader speed than by polarity asymmetry in leader branching. The high speed video imagery reinforces the polarity asymmetry in leader behavior by showing a marked contrast in speeds of advance by the negative and positive ends of the bidirectional recoil leader.

Further progress in understanding lightning behavior will accrue from a return to video camera observations within lightning-stricken aircraft, equipped with high time resolution, where the trunk of the lightning 'tree' may be observed at very close range throughout the bidirectional development ■

Acknowledgements

Long-standing discussions on the topic of the lightning mechanism with Paul Krehbiel, Vlad Mazur, Vlad Rakov, and Lothar Ruhnke, are gratefully acknowledged. The invitation of Pierre Laroche to prepare this paper is also much appreciated.

References

[1] H.W. Kasemir - *A Contribution to the Electrostatic Theory of a Lightning Discharge,* J. Geophys. Res., 65, 1873-1878, 1960.
[2] V. MAZUR, B.D. FISHER, J.G. GERLACH - *Lightning Strikes to an Airplane in a Thunderstorm*. J. Aircraft, 21, 607-611, 1984.
[3] E.R. WILLIAMS - *Problems in Lightning Physics: the Role of Polarity Asymmetry*. Plasma Sources Science and Technology, 15, S91-S108, 2006.
[4] V. MAZUR - *Triggered Lightning Strikes to Aircraft and Natural Intracloud Discharges*. J. Geophys. Res., J. Geophys. Res., 94, 3311-3325, 1989.
[5] V. MAZUR, B.D. FISHER, P.W. BROWN - *Multistroke Cloud-to-Ground Strike to the NASA F-106B Airplane.* J. Geophys. Res., 96, 5471-5484, 1990.
[6] V. MAZUR, J.-P. MOREAU - *Aircraft-Triggered Lightning: Processes Following Strike Initiation that Affect Aircraft,* J. Aircraft, 29, 575-580, 1992.
[7] V. MAZUR, L.H. RUHNKE - *Common Physical Processes in Natural and Artificially Triggered Lightning*. J. Geophys. Res., 98, 12913-12930, 1993.
[8] A. LARSSON - *The Interaction Between a Lightning Flash and an Aircraft in Flight*. Comptes Rendus, 3, 1423-1444, 2002.
[9] V. MAZUR, L.H. RUHNKE - *Physical Processes During Development of Upward Leaders from Tall Structures*. J. Electrostatics, 69, 97-110, 2011.
[10] E.R. WILLIAMS, S. HECKMAN - *Polarity Asymmetry in Lightning Leader Speeds: Implications for Current Cutoff and Multiple Strokes in Ground Flashes*, Atmospheric Research (in review), 2012.
[11] LES RENARDIÈRES GROUP - *Positive Discharges in Long Air Gaps at Les Renardières*—1975 results and conclusions. Electra, 53, 1977.
[12] LES RENARDIÈRES GROUP - *Negative Discharges in Long Air Gaps at Les Renardières*—1978 results. Electra, 74, 1981.
[13] E.M. BAZELYAN, Y.P. RAIZER - *Lightning Physics and Lightning Protection*, Institute of Physics Publishing, 2001.
[14] J. MRAZEK - *Physics of Lightning Under Control of Big Scale Experiments*. Acta. Techn. CSAV, 52, 173-186, 2007.
[15] J. MRAZEK - *Modeling of Positive and Negative Lightning Channels*. International Conference on Grounding and Earthing and 3rd International Conference on Lightning Physics and Effects, Florianopolis, Brazil, November, 2008.
[16] R. Fieux, C. Gary, P. Hubert - *Artificially Triggered Lightning Above Land*, Nature (London). 257, 212, 1975.
[17] Y. KITO, K. HORII, Y. HIGASHIYAMA, K. NAKAMURA - *Optical Aspects of Winter Lightning Discharges Triggered by the Rocket-Wire Technique in Hokuriku District of Japan*. J. Geophys. Res., 90, 6147-6157, 1985.
[18] K. BERGER - *Novel Observations on Lightning Discharges: Results of Research on Mount San Salvatore*; J.Franklin Inst. 283: 478-525, 1967
[19] K. BERGER - *The Earth Flash.* In Lightning, vol. 1, Physics of Lightning, ed. R.H. Golde, pp. 119-190, New York Academic Press, 1977
[20] G. Diendorfer - *Lightning Flashes Measured at GBT With a Transferred Charge Exceeding 300 As.* presentation at GROUND 2010 & 4th LPE. Salvador, Brazil, November, 2010.
[21] P.R. KREHBIEL, W. RISON, S.J. HUNYADY, H.E. EDENS, R.G. SONNENFELD, G.D. AULICH - *Lightning Mapping and Electric Field Change Observations of a Stationary New Mexico Storm*. Presentation at Fall Meeting of the American Geophysical Union, San Francisco, December, 2010.
[22] I. GALLIMBERTI, G. BACCHIEGA, A. BOUNDIOU-CLERGERIE, P. LALANDE - *Fundamental Processes in Long Air Gap Discharges*. Comptes Rendus, Physique, 3, 1335-1360, 2002.
[23] C.J. BIAGI, D.M. JORDAN, M.A.UMAN, J.D. HILL, W.H. BEASLEY, J. HOWARD - *High-Speed Video Observaions of Rocket-and-Wire Initiated Lightning.* Geophys. Res. Lett., 36, L15801, doi:10.1-29/2009GL038525, 2009
[24] C.J. BIAGI, , M.A.UMAN, J.D. HILL, D.M. JORDAN, V.A. RAKOV, J. DWYER - *Observations of Stepping Mechanisms in a Rocket-and-Wire Triggered Lightning Flash.* J. Geophys. Res., 115, D23215, doi:10.1029/2010JD014616, 2010.
[25] J.D. Hill, M.A. Uman , D.M. Jordan - *High-Speed Video Observations of a Lightning Stepped Leader.* J. Geophys. Res., 116, D16117, doi:10.1029/2011JD01518, 2011.
[26] L.A. King - *The Voltage Gradient of the free Burning Arc in Air or Nitrogen*. Fifth International Conf. on Ionization Phenomena in Gases, 2, 871-877, 1961.
[27] Bazelyan, E.M. and Raizer, Y.P., Spark Discharge (ISBN 0849328683), 2000.
[28] S. HECKMAN - *Why Does a Lightning Flash have Multiple Strokes?* PhD thesis, Department of Earth, Atmospheric and Planetary Sciences, Massachusetts Institute of Technology, Cambridge, MA, June, 1992, 134 pp.
[29] D.J. MALAN, B.F.J. SCHONLAND - *Progessive Lightning: VII, Directly Correlated Photographic and Electrical Studies of Lightning from Near Thunderstorms*. Proc. Roy. Soc., London, Ser. A, 191, 483-503, 1947.
[30] P.R. Krehbiel - *An Analysis of the Electric Field Change Produced by Lightning.* Vol. I and II, Report No. T-11, New Mexico Institute of Mining and Technology, Socorro, New Mexico, 1981.
[31] V.A. RAKOV, M.A. UMAN - *Lightning Physics and Effects.* Cambridge University Press, 2003, 687 pp.
[32] L.H. Ruhnke - *Screening Effects on Branched Upward Leaders*, 2012 International Conf. on Lightning Protection (ICLP), Vienna, Austria, September, 2012.
[33] W. GROTRIAN - *Der Gleichstrom-Lichtbogen grosser Bogenlänge.* Ann. Physik, 47, 141-196, 1915.
[34] J.D. Cobine - *Gaseous Conductors: Theory and Engineering Applications.* Dover Publications, 1958, 606pp.
[35] K. SUNABE, T. INABA - *Electric and Moving Characteristics of DC Kiloampere High-Current Arcs in Atmospheric Air*, Electrical Engineering in Japan, 110, No. 1, 9-19, 1990.
[36] T.C. MARSHALL, M. STOLZENBURG - *Voltages Inside and Just Above Thunderstorms*. J. Geophys. Res., 106, 4757–4768, doi:10.1029/2000JD900640, 2001.
[37] V. MAZUR - *Physical Processes During Development of Lightning Flashes*. Comptes Rendus, 3, 1393-1409, 2002.
[38] D.J. MALAN, B.F.J. SCHONLAND - *The Electrical Processes in the Intervals Between the Strokes of a Lightning Discharge*. Proc. Roy. Soc., A, 209, 158-177, 1951.
[39] P.R. KREHBIEL, M. BROOK, R.A. MCCRORY - *An Analysis of the Charge Structure of Lightning Discharges to Ground.* J. Geophys. Res., 84, 2432-2456, 1979.

[40] S.J. HECKMAN, E.R. WILLIAMS - *Corona Envelopes and Lightning Currents.* J. Geophys. Res., 94, 13287-13294, 1989.
[41] J.M. Yos - *Transport Properties of Nitrogen, Hydrogen, Oxygen and Air to 30000 K*, AVCO Corporation Technical Memorandum RAD-TM-63-7, 1963.
[42] N.L. ALEKSANDROV, E.M. BAZELYAN, M.N. SHNEIDER - *Effect of Continuous Current During Pauses Between Successive Strokes on the Decay of the Lightning Channel.* Plasma Physics Reports, 26, 952-960, 2000.
[43] F.J. HEWITT - *Radar Echoes from Interstroke Processes in Lightning*, Proc. Phys. Soc. London, Sect. B 70, 961-979, 1957.
[44] T.A. WARNER, M.M.F. SABA, R.E. ORVILLE - *Characteristics of Upward Leaders From Tall Towers*, 22nd International Lightning Detection Conference, 2-3 April, Broomfield, CO., 2012.
[45] T. OGAWA, M. BROOK - *The Mechanism of the Intracloud Lightning Discharge*. J. Geophys. Res., 69, 5141-5150, 1964.
[46] Newsletter on Atmospheric Electricity Vol 23 n°1 May 2012. http://icae.jp/newsletters/pdf/icae-vol23-1-may2012bk.pdf.

Acronyms

DC (Direct Current)
CG (flashes: Cloud-to-Ground flashes)

AUTHORS

Earle Williams is a physical meteorologist, currently dividing his time between the MIT campus and the Aviation Weather group at MIT Lincoln Laboratory. He has been engaged in research on thunderstorm electrification and atmospheric electricity for nearly forty years. These interests have taken him to all of the predominant tropical thunderstorm regions (Africa (Niger), South America (Brazil) and the Maritime Continent (Northern Australia)) for radar field experiments. Williams is presently focused on the Earth's Schumann resonances, a naturally occurring electromagnetic phenomenon trapped between the conductive Earth and the ionosphere, and on the use of that phenomenon for the continuous monitoring of the global lightning activity.

Stan Heckman received his Ph.D. in atmospheric science from the Massachusetts Institute of Technology in Cambridge, Mass., for studies of lightning with radar. He received his bachelor's degree in physics from Michigan State University in East Lansing, Mich. He is the senior lightning scientist at Earth Networks and has recently been involved in developing the Earth Networks Total Lightning Network™ (ENTLN). He began his career by studying currents in rocket-triggered lightning at the United States Air Force Phillips Laboratory. During that time, he also worked to infer the global distribution of lightning and to estimate the global lightning rate from networks of ELF lightning sensors. Later, at the NASA MSFC Global Hydrology Resource Center, he compared data from lightning sensors. After that, he compared data from lightning satellites to radar and studied storm evolution with VHF lightning mapper data.

X. Qie, R. Jiang
(LAGEO)
P. Laroche
(Onera)

E-mail: pierre.laroche@onera.fr

Triggering Lightning Experiments: an Effective Approach to the Research of Lightning Physics

Artificial triggering lightning experiments by launching a small rocket trailing a thin wire toward a charged cloud overhead have been conducted since the 1960s. After decades of development, this has become an important means for investigating lightning physics and validating lightning protection and location techniques. Observations of the triggered lightning have provided considerable new insights into different aspects of lightning discharges. This paper presents an overview of worldwide artificial triggering lightning experiments by means of the rocket-and-wire technique. Some valuable results, including properties of upward positive leader (UPL), observational evidence for the leader stepping mechanism, return stroke currents, M component properties, and energetic radiation associated with the lightning discharges, are briefly reviewed.

Introduction

Lightning is a transient discharge event that occurs in the atmosphere during a thunderstorm. The high discharge current and intensive electromagnetic (EM) radiation of the lightning can cause severe damages to objects both on the ground and in the air. Knowledge of lightning physics and its EM fields in fine time resolution is very important not only from the view of scientific research objectives, but also from the view of lightning protection engineering, in particular with the wide utilization of the current micro-electronics and communications technologies.

Although most natural downward cloud-to-ground (CG) lightning flashes exhibit an overall direction from the thunderstorm to the ground, the corresponding strike points are always randomly determined. The randomness in time and space of lightning occurrences makes direct measurement of lightning difficult. Instruments installed at the top of high towers or buildings which have a greater chance of being struck have helped to overcome the difficulties in measuring the discharge current of lightning [1]. However, limitations still exist, owing to the temporal uncertainty and lower possibility of the downward lightning striking a high structure.

Since the 1960s, various techniques have been designed and tested to artificially trigger lightning discharge during thunderstorm events, such as rapidly extending a thin wire underneath a charged cloud, emitting laser beams from ground to cloud, water jets or firing transient flame, and so on. One of these is the rocket-and-wire technique, launching a small rocket that extends a thin wire (either grounded or ungrounded) into the gap between the ground and a charged cloud overhead, successfully triggering lightning [2]; [3]. After decades of development and improvement, the rocket-and-wire technique for triggering lightning has been used as an important means for investigating lighting physics and effects. In this paper, artificial triggering lightning experiments and some exciting results over recent decades are briefly reviewed.

The techniques and experiments of rocket-triggering lightning

The first successful triggering lightning discharge by artificial means was conducted on a research vessel at sea in the vicinity of St. Petersburg, Florida [2]. Then the triggering technique was improved and performed at Saint-Privat d'Allier, France, which was the first successful triggered lightning over land [3]. After that, artificial triggering lighting experiments over land have been continuously performed in different countries, e.g. in the United States of America [4]; [5]; [6];[7], in France [8], in China [9]; [10]; [11]; [12], in Japan [13]; [14];[15], and in Brazil [16]; [17].

In the rocket-triggering lightning experiment, the rockets are usually installed at a launching site, with a capability of launching several rockets during a thunderstorm event. Figure 1 shows a photo of the rocket launcher for the Shandong Artificial Triggering Experiment (SHATLE), China. The ascending speed of the rocket is usually about 200 m/s after ignition [18]; [19]. This speed guarantees a relatively rapid extending of the triggering wire that is trailed by the rocket, while

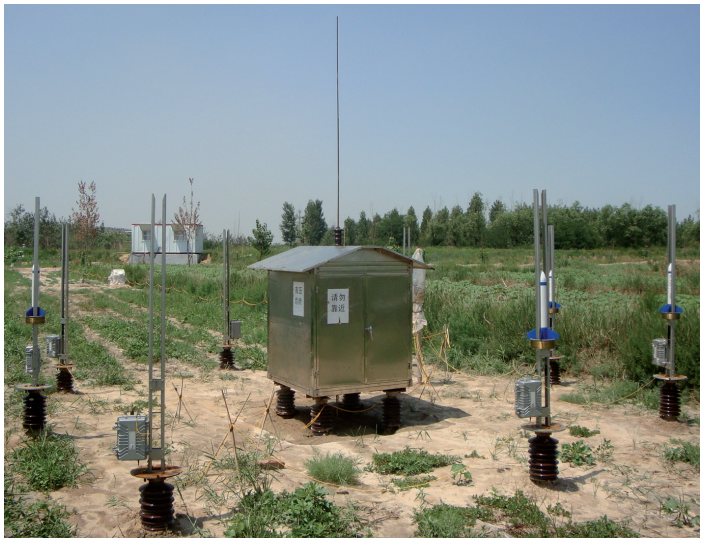

Figure 1 - Rocket launching site in Shandong Artificially Triggered Lightning Experiment (SHATLE), China.

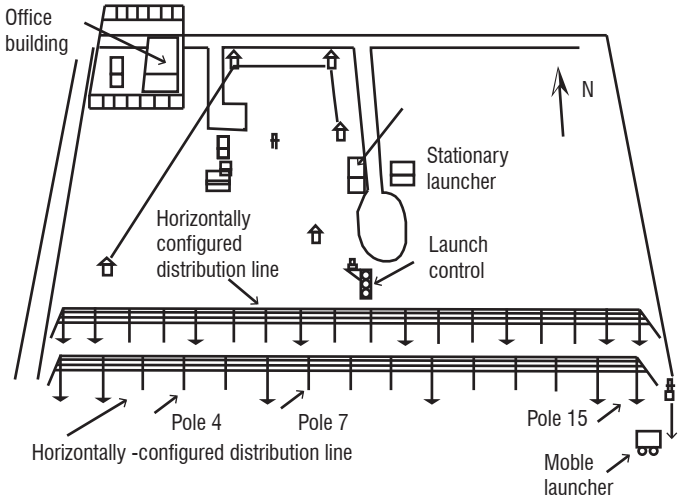

Figure 2 - Overview of the International Center for Lightning Research and Testing (ICLRT) in Florida, America. [21]

the associated pull force would not be too large to break the wire. Triggering wires (made of steel in China or copper in USA) with a diameter of approximately 0.2 mm are wound on a spool which is either fixed in the rocket or just installed on the ground. No matter where the spool is installed, one end of the triggering wire will ascend with the rocket. Due to the different grounding modes of the triggering wires, the techniques for triggering lightning are divided into conventional triggering and altitude triggering. For conventional triggering, the wire is well grounded, while for altitude triggering the rocket usually spools out 50-100 m of insulating Nylon followed by several hundred meters of conducting wire, so the triggering wire is not directly attached to the ground.

Various approaches to the observation of triggered lightning can be pre-designed and conducted close to the rocket launcher. Figure 2 shows an overview of the International Center for Lightning Research and Testing (ICLRT) in Florida, USA. In order to measure the discharge current of the triggered lightning, current sensors are installed at the rocket launching site which has been known to be struck by conventional triggered lightning. Generally, the current signals are transmitted through a fiber-optic link system to a control room (tens or hundreds of meters away) for data recording. Instruments for detecting the EM fields of the triggered lightning can be installed at different determined distances from the rocket launcher. The optical observations, by streak camera in the early years or by high speed video camera in recent years, are used to observe the evolution of the lightning luminous channel. Additionally, some particular observations can also be made using specially designed instruments, such as the so-called Pockels sensor for detecting the electric field very close to the lightning channel [20]. Overall, benefiting from the certainty of the occurrence of triggered lightning both in time and space, synthesized observation by different means can be designed and conducted, while it is not feasible for natural lightning.

Processes of the triggered lightning

The polarity of the triggered lightning is dependent on the charged cloud overhead at the time the rocket is ignited, both negative and positive lightning could be successfully triggered under suitable conditions. Generally, it is much easier to trigger negative lightning than positive, with the triggering success ratio being much higher when the cloud overhead is negatively charged [22]; [7]. Exceptions have occurred in Japan (during a winter thunderstorm) and in northeastern China, where the triggered events were always reported to be positive and contained just the initial continuing current stage when the cloud overhead was positively charged [14]; [23];[10].

The electric field at ground level is usually used as a reference to launch a rocket for triggering lightning, although the electric field at altitude is more indicative [24] but difficult to measure. The surface electric field is usually 5-10 kV/m when lightning is triggered successfully. Figure 3 shows two photographs of the triggered lightning using the conventional technique (with the wire grounded) and the altitude technique (with the wire ungrounded), respectively. The luminosity of the channels is due to the discharge process and the vertical straight portion corresponded to the wire-vaporized channel. Figure 4 shows the sketch processes of the triggered lightning from the ascent of the rockets under negative charged clouds, for the conventional triggering technique and the altitude triggering technique, respectively.

For conventional triggering, the wire tip reaches an altitude of 200-400 m 1-2 seconds after ignition of the rocket. A positive leader forms under the enhanced ambient electric field. This positive leader breaks down the virgin air and propagates toward the cloud, yielding an initial continuous current (ICC) which vaporizes the triggering wire. The natural channel established by the upward positive leader and the wire trace channel together build up the whole discharge channel between the cloud and the ground, and the discharge current can be measured at the channel bottom. The ICC lasts around several hundreds of milliseconds, on which some current pulses (referred as ICC pulses) may be superimposed. There is a no-current stage after the initial continuous current. Then one or more dart leader-return strokes will occur, generally traversing the original channel. The leader-return stroke sequences in triggered lightning is considered to be very similar to the dart leader-subsequent return stroke sequences in natural downward lightning [25]; [21]. Interstroke processes, such as continuous current and M component, can also be observed after the return stroke, or between adjacent return strokes. Triggered lightning using the conventional technique has contributed to most of the findings of the triggering lightning experiment, and more detailed information about it will be given in the following section.

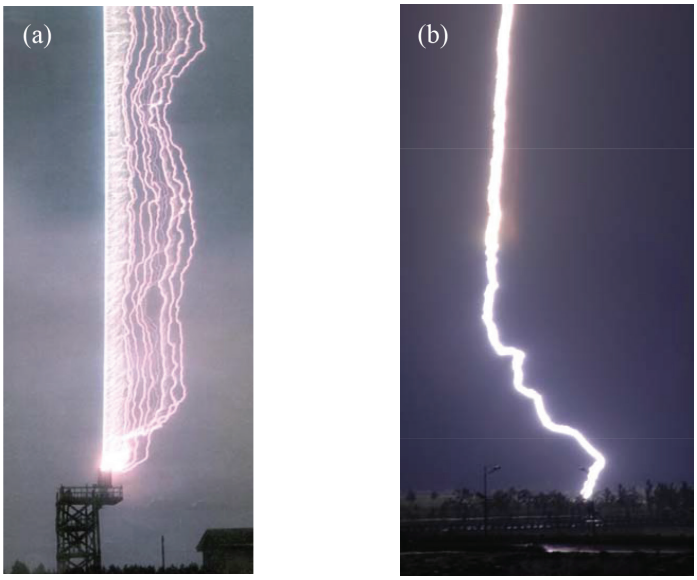

Figure 3 - Photographs of rocket-triggered lightning flashes. (a) with conventional technique, in ICLRT, Florida America, [7], (b) with altitude technique, in SHATLE, Shandong China, [11].

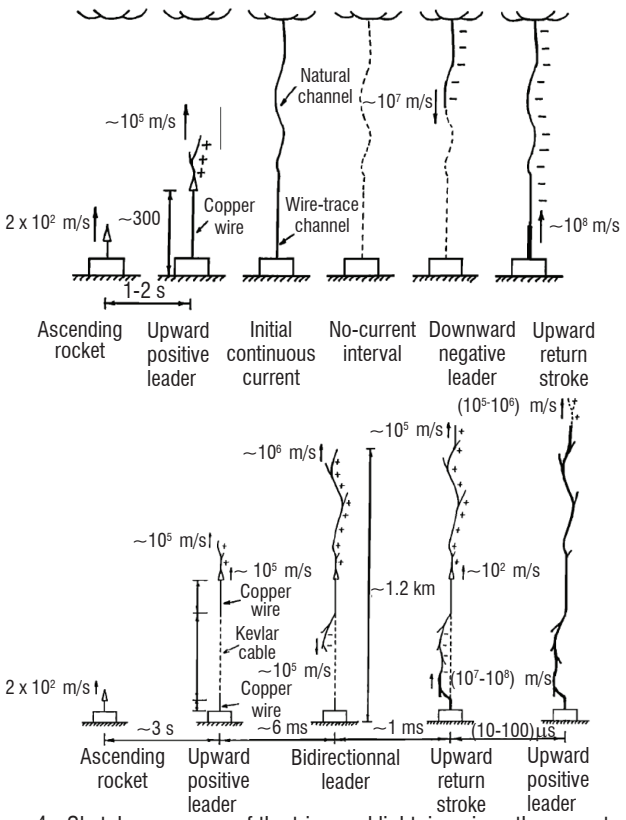

Figure 4 - Sketch processes of the triggered lightning since the ascent of the rockets, under negative charged clouds. (a) conventional triggering technique, (b) altitude triggering technique. [18]

For altitude triggering, the initial processes are different. A bi-directional leader process, which involves a primary upward positive leader at the wire tip and a following downward negative leader at the wire bottom with a lag time of a few milliseconds, occurs as the wire ascends to several hundred meters high. When the downward negative leader approaches the ground, a positive connecting leader initiates from the ground (sometimes from the triggering facilities or a short grounded wire connected to the bottom of the Kevlar cable), and the attachment of these two leaders results in a mini-return stroke or first return stroke. Because of its short discharge distance and different charge source, this return stroke is usually weaker than the normal strokes. The mini-return stroke or first return stroke quickly catches up and leads to an intensification of the upward positive leader. Then, the following processes are considered analogous to those in conventional triggered lightning. Triggered lightning by means of the altitude technique have provided clear optical evidence of the bi-directional leader development [26]; [27]; [28]. The developments of the upward leader and the downward leader (after emerging from the upper and lower extremities of the elevated wire, respectively) are coordinated in phase with each other. Generally, it is hard to measure the current of the altitude triggered lightning due to the indeterminacy of its grounding point. In this case, magnetic field measurement at close range would provide a good approach to current retrieval [29].

Initial stage and upward positive leader

Initial continuous current and ICC pulses

The upward positive leader and the initial continuous current (including the relevant ICC pulses) as a whole, are defined as the initial stage (IS) of a conventional triggered lightning. The initial stage is also present in structure-initiated lightning while absent in natural downward lightning. Wang et al., [30] have analyzed the current recordings of 37 negative triggered lightning flashes in Alabama and Florida. They found that the duration of the initial stage involved a geometric mean (GM) value of 279 ms and, correspondingly, the charge transferred by the ICC was 27 C. Based on charge transfer and duration of the initial stage, the average current was estimated to be 96 A with a minimum of 27 A and a maximum of 316 A. Miki et al [31], by using the data of 45 triggered lightning occurrences in Florida, found the GM values of the duration, charge transfer and average current to be 305 ms, 30 C, and 100 A, respectively. Yang et al. [32] have analyzed the IS in two SHATLE triggered flashes and found quite short durations of about 20 ms.

As for those pulses superimposed on the ICC, referred to as ICC pulses, Wang et al., [30] firstly pointed out that their current waveforms were similar to that of M components superimposed on the continuous current following the return strokes in triggered lightning and, reasonably, both the ICC pulses and the M component (which will be illustrated in detail in the following section) were associated with the same physical process or the same mode of charge transfer from cloud to ground. Qie et al., [33] have analyzed the simultaneous current and electric field of the so-called large ICC pulse (with the current peak up to several kilo amperes, as shown in figure 5) and confirmed this similarity. The dashed line in figure 5 indicated the times of the current starting, the peak of the electric field, and the peak of current. It is clear that the electric field waveform was recorded earlier than the current waveform at the channel bottom.

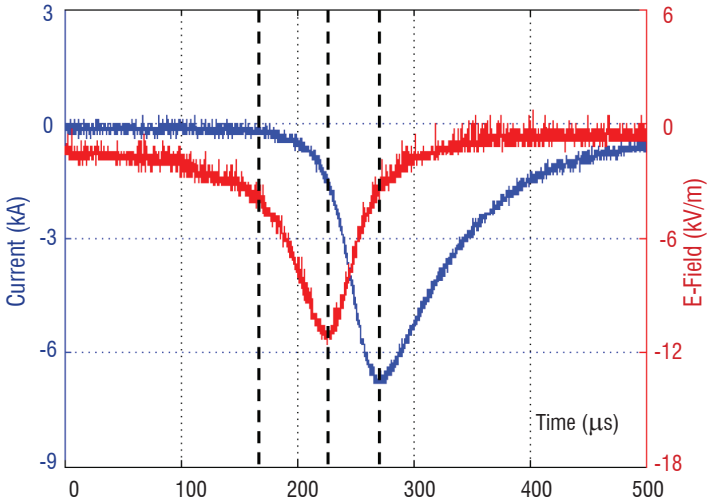

Figure 5 - Simultaneous current and electric field (at 30 m) waveforms of an ICC pulse with the current magnitude up to several kilo amperes. [33].

Upward positive leader

The formation and sustained development of an upward positive leader from the upper extremity of the ascending wire (when the cloud overhead is negatively charged) is the prerequisite to successfully triggering a negative lightning. Since the distance between the sensor and the launcher is exactly known it is possible to obtain the 2-D speed (by optical measurement) or even the 3-D speed (by VHF source imaging) of the leader with reasonable accuracy. Generally, the extending speed of the upward positive leader is between $\sim 10^4$ m/s - $\sim 10^5$ m/s at the initial stage after it emerges from the wire-tip, exhibiting an obvious acceleration tendency afterwards [22]; [8]; [34]; [35]. The speed value can increase to $\sim 10^6$ m/s as the leader reaches up to several kilometers high [36]. Table 1 shows the propagating speed results of UPLs observed during different lightning-triggering experiments.

The wire bottom current associated with UPLs generally starts as a cluster of pulses, which is followed by a steady current that increases gradually in magnitude, as shown in figure 6. The waveform of these current pulses are similar to those so called precursors [37] which are related to the inception attempt of the leader (non-sustained) during the ascent of the triggering wire. The starting of the stable upward positive leader was confirmed to take place at time t=0, in figure 6, making it easy to infer that the damped oscillating current pulses were attributed to the stepped development of the leader [38]; [39]. The electric field measurements associated with UPLs in other triggered lightning further supported such an inference [86]. Recently, similar impulsive currents of an UPL were observed to be coordinated with discrete steps in the initial development, distinguished by high speed video images [40]; [35]. It is reasonable that a leader step process would cause an injection of the positive charge to the leader tip, yielding an abrupt discharge which may physically be unipolar. Since the current signals were detected in the wire bottom, the oscillating behavior of the current pulses were probably caused by the current reflections occurring both at the wire tip and the ground. However, some observations of the UPLs did show the unipolar current pulses that are associated with leader steps [41]. Nevertheless, it is worth noting that the distinct confirmation of the stepped propagation associated with upward positive leaders is only possible with certainty during the very initial stage of their developments, after which they could propagate either continuously or intermittently.

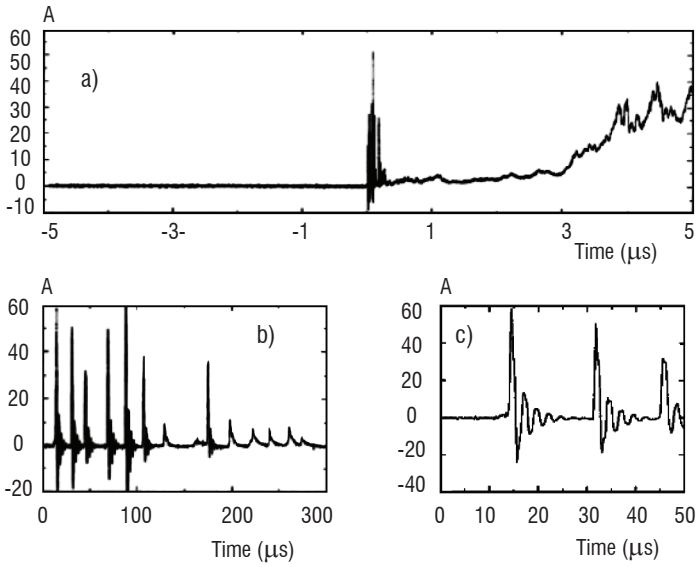

Figure 6 - Wire bottom current for an upward positive leader. [38]

Selected references	Measurement	2-D/3D	Brief notes on leader speed
[Fieux et al., 1978] [22]	Streak camera	2-D	2×10^4 to 1×10^5 m/s in the view range of the camera
[Laroche et al., 1985] [8]	Streak camera	2-D	$\sim 10^4$ m/s at the initial stage
[Y. Kito et al., 1985] [82]	Streak camera	2-D	Started at around 0.1×10^5 m/s with some branches, the final speed accelerated to 5 to 10 times faster.
[Idone, 1992] [83]	Streak camera	2-D	Flash 8827: 1.2×10^5 m/s to 6.5×10^5 m/s, Flash 8911: 2.7×10^5 m/s to 9.4×105 m/s
[Baigi et al., 2009] [34]	High speed camera	2-D	Stepped, a constant speed of 5.6×10^4 m/s over its initial 100 m.
[Yoshida et al., 2010] [36]	VHF	3-D	2 UPLs with average speeds of the order of 10^6 m/s at altitudes of 2.4 km and 3.7 km respectively
[Jiang et al., 2012] [41]	High speed camera	2-D	130-730 m above ground, average speed: 1.0×10^5 m/s, partial speeds: 2.0×10^4 m/s to 1.8×10^5 m/s.

Table 1 - Propagating speeds of upward positive leaders in triggered lightning.

Stepping evidence of negative leaders and the lightning attachment process

Evidence of the stepping mechanism in negative leaders

It is well known that the developments of negative leaders breaking down virgin air are step-wise, and those leaders propagating through the former channel are always continuous, referred to as dart leader. In some instances, the dart-stepped negative leader (also through former channel) may occur as an intermediate pattern, whether in natural lightning or in triggered lightning [42]. On the basis of the laboratory gap spark experiments, the stepped propagation of the negative leader has been attributed to the "space stem" development ahead of the leader tip. The connection of such space stem to the primary streamer channel was considered to result in a step [43]; [18]. This mechanism was presumed to be suitable for interpreting the step-wise development of negative leader occurring in the atmosphere. However, such an analogy is not very solid because the scales of discharge current, length, and duration of the leaders in the laboratory and in the atmosphere are really quite different. To clarify the above presumption, lightning-related observation facts are needed.

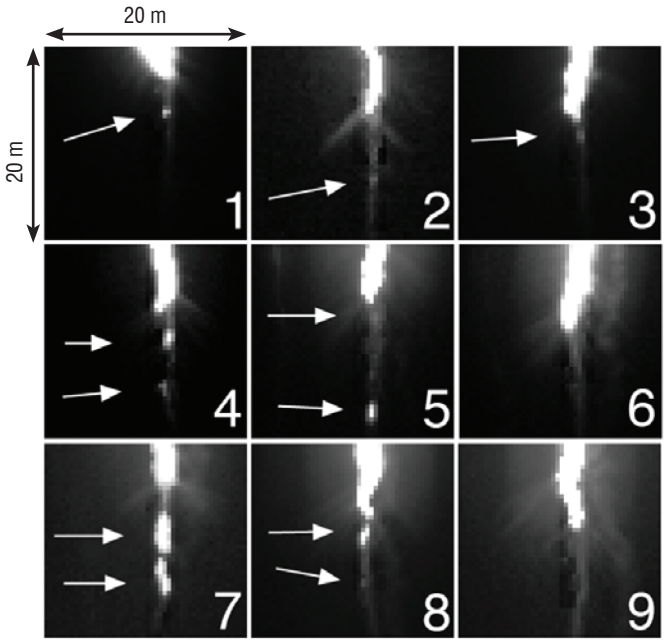

Figure 7 - Expanded images for channel tips (at different heights) of a downward dart-stepped negative leader in a triggered lightning in ICLRT, Florida. The images were taken by a high speed video camera operated at 240 kfps. [44]

Triggered lightning has, for the first time, provided evidence of "space stem" development in atmospheric negative leader [34], [44]. Figure 7 shows the expanded images for channel tips (at different heights) of a downward dart-stepped negative leader in a triggered lightning flash. The arrows indicate the separated luminous segments ahead of the channel, which were quite possibly associated with the "space stem" development. The lengths of these channel segments were found to be 1-4 m, and that of the dark gaps between the segments and the primary channel were 1-10 m. The occurrence of the space stems was reinforced by the leader-related dE/dt pulses, which exhibited 1-3 secondary peaks prior to or following the main peak [44].

Lightning attachment process

The attachment process of the downward leader and the upward connecting leader with different polarities (the upward one occurs in response to the approaching downward one) is an important issue in the study of lightning physics. Understanding of this process helps to reveal the transition between the leader stage and the return stroke stage of lightning, which is fundamental to the design of lightning protection. Based on triggered lightning, data has been obtained for investigating the attachment process [45]; [46];[47]; [34]. [46] observed two dart leader-return stroke sequences in conventional negative triggered lightning by using a digital optical system of ALPS. Figure 8a shows the diagrammatic sketch of the attachment process according to the observation results of one event. The upward connecting leader exhibited lower luminous intensity than the downward dart leader, with a propagating speed of about 2×10^7 m/s. The junction point was 7-11 m above ground (4-7 m for another event), and the duration of the upward connecting leader was several hundred nanoseconds. It was confirmed that the return stroke process starts with a bidirectional development that originates at the junction point. Figure 8b shows the image of a downward negative leader and the responsive connecting positive leader before the occurrence of a subsequent return stroke in triggered lightning, which also illustrates the weaker intensity of the upward connecting discharge [34]. The so-called streamer zones, composed of filamentary corona streamers with even lower luminous intensity, were found to appear in front of the downward negative leader while not evident ahead of the upward connecting leader. Nevertheless, we need to recognize the limitation of the above results for revealing the attachment process in virgin air, since the dart leader-return stroke sequences occur in the remnant of the former channel. So further observations on the attachment process of altitude triggered lightning are needed, though an analysis had been briefly conducted by P. Lalande et al. [38] based on the data of channel base current and electric field.

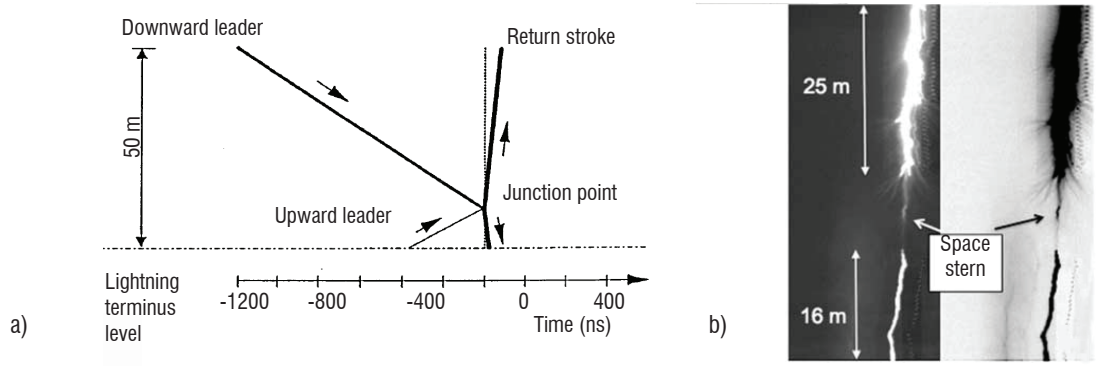

Figure 8 - Observation facts of the attachment process in triggered lightning. a) Diagrammatic sketch of the attachment process according to ALPS observation [46]. b) Image of a downward negative leader and the responsive connecting positive leader, just before the return stroke [34].

Channel base current and close EM field of return stroke

Current waveform parameters

The return stroke is always considered as the key issue in lightning physics since it is the strongest discharge process and results in the severest effects of lightning on ground objectives. An accurate understanding of the return stroke properties, especially the discharge current, is essential for the design of effective protection against lightning. It has been confirmed from different aspects that the return strokes in triggered lightning are similar to the subsequent return strokes in natural downward lightning. Hence, accumulation of the current records for the triggered lightning provides a good opportunity to obtain statistical characterization of return stroke current.

There are several statistical researches on the current waveform parameters based on triggered lightning [25]; [48]; [49]; [21]; [50]; [51]. Figure 9 shows the current waveform (the blue curve) of a return stroke in triggered lightning 0901 in SHATLE. The peak current of this return stroke was 11.7 kA, with the risetime from 10% to 90% peak (in the leading edge of the waveform) being 1.0 μs and the half peak width (the time interval between 50% values of the peak in the leading edge and the trailing edge of the waveform) being 20.9 μs. By calculating the time integral of the current waveform, the charge transferred (or neutralized) by this return stroke was 0.5 C. Since the duration of individual return stroke can not be easily differentiated when it is followed by continuous currents, the parameter of charge transfer is usually defined as a numerical integral of current to within 1 ms [11], although sometimes a duration of several hundred microseconds or even less than 100 μs have also been used [52]; [53].

Table 2 gives the statistical results of the current waveform parameters of return stroke, obtained by different experiments. As shown in the table, the statistics of the return stoke currents from different areas are generally consistent with each other. The GM values of the peak current are around 12 kA, though the result in Guangdong, China (GCOELD) is a bit larger, with the value of 16.1 kA. Shœne et al. [21] used the largest sample size and the GM value of the peak current was 12.2 kA, with a logarithmic standard deviation of 0.22. Some return stokes may involve the peak current up to more than 40 kA and, as in the table, Depasse et al. [48] have reported a peak value of 49.9 kA. At Camp Blanding, a peak current of 56 kA was measured during summer 2000 [54]. The largest peak current in triggered lightning was reported by Leteinturier et al. [55], with the maximum value exceeding the saturation current of 60 kA (estimated as 76 kA by $\int dI/dt$). Saba et al. [16] once reported an altitude triggered lightning of which the currents were obtained. Among the 7 return strokes, the most intense exhibited a peak current of 44 kA. The risetime from 10% to 90% peak by different authors are within the order of magnitude of a microsecond, with the usual GM values of no more than 1 μs, though the corresponding result from the SHATLE experiment was reported to be 1.9 μs, probably owing to the relatively low upper-frequency-limit of the current measuring system used in the first few years of the experiment [56]. Besides the above results, other parameters such as steepness from 10% to 90% peak, and the action integral ($\int i^2 dt$) have also been used by different authors when analyzing the current waveforms of return strokes. Fisher et al. [25] reported the GM values of 28 kA/μs and 3.5×10^3 A^2•s, for the parameters of steepness and action integral, respectively.

Close electric field changes for leader-return stroke sequences

The certainty of the strike point of the triggered lightning using the conventional technique facilitates the measurements of EM field at close ranges. Figure 9 shows the electric field waveform coordinated in time with the current measurement. The E-field sensor was located 30 m away from the lightning channel. The leading edge of electric field waveform was due to the approaching of the dart leader, which propagated from cloud to ground. The bottom of the asymmetric V-shaped electric field waveform corresponded to the instant when the leader reached to the ground and, consequently, the transition from leader to return stroke [57];[58]; [59].

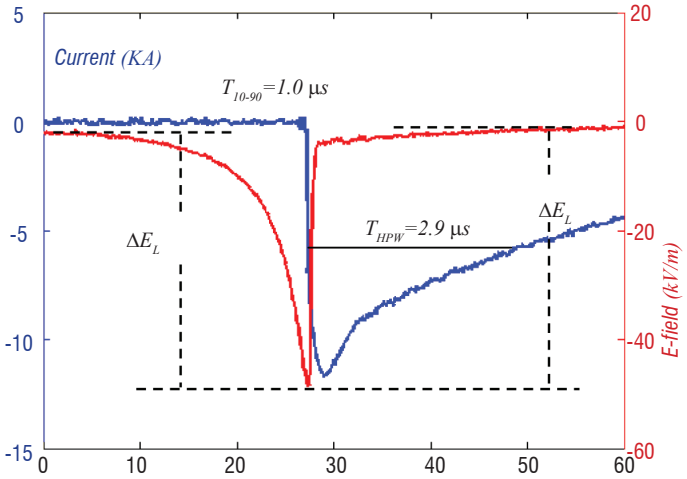

Figure 9 - Simultaneous current and electric field (at 30 m) waveforms of a return stroke in triggered lightning 0901, SHATLE.

It has been possible to obtain statistics on distance dependence of electric fields due to the leader-return strokes from multiple-station measurements in triggered lightning. By analyzing the fields measured at different distances from the lightning channel, Crawford et al. [57]. and Zhang et al. [59] have concluded that the distance dependence of leader electric field change (ΔE_L) was inversely proportional, or somewhat slower than that. Generally, the electric field change of return stroke (ΔE_{RS}) differed not very much from leader field change (ΔE_L), although some records involved a so-called residual electric field, with the ΔE_{RS} being appreciably smaller than the ΔE_L [58]. On the basis of the measurements for 86 return strokes during ICRLT 1999-2000, Shœne et al. [60] studied the statistical characteristics of ΔE_{RS} at 15 m and 30 m, of which the GM values were 96 kV/m and 55.3 kV/m, respectively.

M components superimposed on the continuous current after return strokes

The concept of "*M* component" was first proposed by Malan and Colleus [61], based on the temporary luminescence enhancement of lightning channel during the stage of continuing current flowing through the channel. The *M* component often associates a hook-shaped electric field change at the ground. Early researches into M components were mainly based on the optical and *EM* field observation of natural lightning [62]; [63]; [64]; [65], then VHF radiation source imaging of lightning also provided valuable results [87,66]. However, the absence of discharge current information and the uncertainty of the distance between the sensor and the channel hampered further investigation of the nature of *M* components using

Experiment	Sample	Min	Max	Arithmetic Mean	Standard Deviation	Geometric Mean	SD* $\log_{10}(x)$
Peak current (KA)							
KSC, Florida 1990 and Alabama 1991 [Fisher et al., 1993] [25]	45	--	--	--	--	12.0	0.28
Saint-Privat d' Allier 1986, 1990-1991 [Depasse, 1994] [48]	54	4.5	49.9	11.0	5.6	--	--
ICLRT, Florida 1997 [Crawford, 1998][49]	11	5.3	22.6	12.8	5.6	11.7	0.20
ICLRT, Florida 1999-2004 [Schoene et al., 2009] [21]	165	2.8	42.3	13.9	6.9	12.2	0.22
SHATLE 2005-2010 [Qie et al., 2012] [84]	36	4.4	41.6	14.3	9.2	12.1	0.23
GCOELD 2008-2011 [Zheng et al., 2011] [85]	29	6.7	31.9	17.43	6.95	16.1	0.18
Risetime from 10% to 90% of peak current (μs)							
KSC, Florida 1990 and Alabama 1991 [Fisher et al., 1993] [25]	43	--	2.9	--	--	0.37	0.29
Saint-Privat d' Allier 1986, 1990-1991 [Depasse, 1994] [48]	37	0.25	4.9	1.14	1.1	--	--
ICLRT, Florida 1997 [Crawford, 1998][49]	11	0.3	4.0	0.9	1.2	0.6	0.39
ICLRT, Florida 1999-2004 [Schoene et al., 2009] [21]	81	0.2	5.7	1.2	0.8	0.9	0.32
Half peak width (μs)							
KSC, Florida 1990 and Alabama 1991 [Fisher et al., 1993] [25]	41	--	--	--	--	18	0.30
Saint-Privat d' Allier 1986, 1990-1991 [Depasse, 1994] [48]	24	14.7	103.2	49.8	22.4	--	--
ICLRT, Florida 1997 [Crawford, 1998][49]	11	6.5	100	35.7	24.6	29.4	0.29
ICLRT, Florida 1999-2004 [Schoene et al., 2009] [21]	142	4	93	23	17	19	0.30
Charge et transfer within 1ms (C)							
ICLRT, Florida 1999-2004 [Schoene et al., 2009] [21]	151	0.3	8.3	1.4	1.4	1.0	0.35
SHATLE 2005-2010 [Qie et al., 2012] [84]	36	0.18	4.2	1.1	0.76	0.86	0.31
GCOELD 2008-2011 [Zheng et al., 2011] [85]	29	0.44	4.2	1.8	1.24	1.4	0.32

Table 2 - Statistical characteristics of current waveform parameters of return stroke in triggered lightning, obtained from various experimental campaigns.

natural lightning observation. Triggered lightning experiments now open new insight into such an interstroke process.

Based on the directly measured current data, M components register as current pulses superimposed on the continuous current after the return stroke, and the pulse waveforms on expanded timescale are typically more or less symmetrically V-shaped, as illustrated in figure 10 a. For most of the M components the preceding continuous current at the channel bottom was observed to be of the order of 30 A or higher [67]. Fisher et al.[24] firstly pointed out that M components generally involved longer rise time than return stroke current pulses, by 2 or 3 orders of magnitude. The waveform parameters of M component were statistically summarized by Thottappillil et al. [66], according to whom the peak current, 10%-90% rise time, and charge transfer of an M component were 100-200 A, 300-500 μs, and 0.1-0.2 C, respectively. The detailed statistics for each parameter are shown in table 3 and, based on triggered lightning data, the occurrence of M components were found to outnumber that of return strokes by 4:1. Though the majority of M components were observed to have peak current no more than several hundred amperes, there were a few samples with the current magnitude exhibited up to the kilo amperes range [6]; [20]. [68] Qie et al. [33]once found 5 larger-than-usual M components in a triggered lightning, with GM peak current, 10% to 90% rise time and half peak width being 5.1 kA, 34.6 μs, and 73.6 μs, respectively. It appeared that those M components with larger current magnitude may involve shorter time parameters.

Parameter	Sample Size	GM	Case exceeding tabulated value			
			SD $\log_{10}$(x)	95%	50%	5%
Magnitude, A	124	117	0.50	20	121	757
Rise time, μs	124	422	0.42	102	425	1785
Duration, μs	114	2.1	0.37	0.6	2.0	7.6
Half-peak width, μs	113	816	0.41	192	800	3580
Charge, mC	104	129	0.32	33	131	377
CC level, A	140	177	0.45	34	183	991
M interval, ms	107	4.9	0.47	0.8	4.9	23
Elapsed time, ms	158	158	0.73	0.7	7.7	156

Table 3 - Statistics of current parameters of M components in triggered lightning conducted in Florida (1990) and Alabama (1991). [67]

It is widely acknowledged that the M component involves a different mechanism to that of the leader-return stroke sequence; the former propagates in an already existing channel while the latter is usually in a channel with current cutoff. The measurements of discharge current and EM field at known distances for triggered lightning make it possible to verify the physical mechanism of the M component and establish an engineering model for mathematical representation and simulation. Rakov et al. [69] concluded that at a near distance, the magnetic field and current of the M component shared similar waveforms, while the electric field appears to be proportional to their time derivative. As in figure 10, the electric field began its negative directed change ahead of current. The red line in the figure indicates when the electric field reaches its peak, and at the same moment, the channel base current had already emerged from the background level with the value being about 3 kA. The multi-station observation showed that the electric field peak basically follows a logarithmic distance dependence [70]; [71]. On the basis of these concluded features, a "two wave" mechanism has been proposed to explain the developing process of the M component through the channel [69]. According to this mechanism the M component involves two guided waves which propagate in opposite directions and have equal amplitudes. The downward incident wave forms primarily and develops to the ground, and as it reaches the ground, a mirroring (reflected) wave starts to generate and propagate upward. The ground is sensed as a short circuit, with the reflectance for current at the ground being approximately $+1$ while the counterpart for charge density is -1. The two waves have similar contributions to the total outflow of the charge from the lightning channel base at any moment in time. And at any section of the discharge channel, their currents are additive while their charge densities are subtractive. The simulation of EM fields on the basis of a "two wave" theory has shown that such a mechanism is a reasonable explanation of the M component [70]; [71].

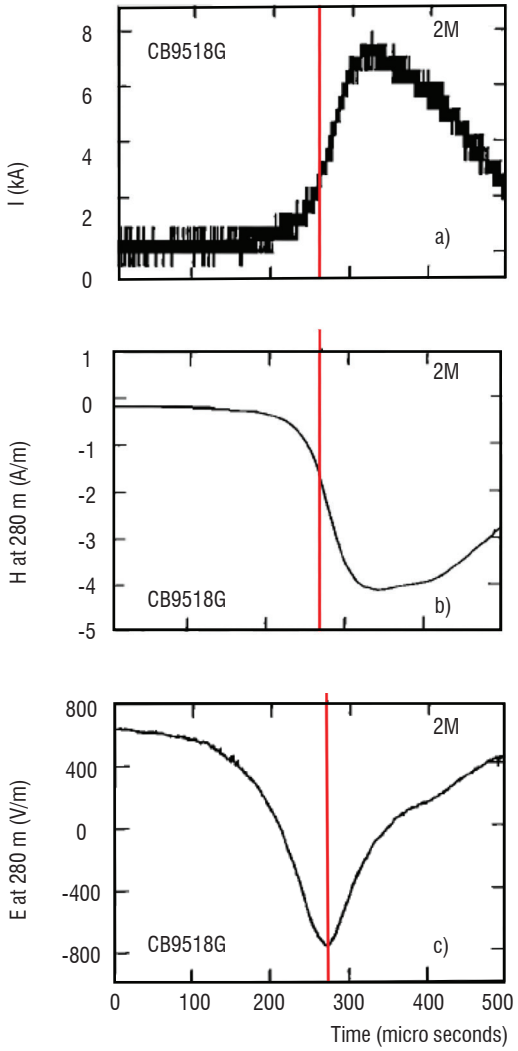

Figure 10 - Synchronous (a) current, (b) magnetic field, and (c) electric field for an M component in triggered lightning flash 9518 (Camp Blanding, Florida). The field sensors were located 280 m away from the launcher. [6]

Energetic radiations from triggered lightning

Early in the 1920s, Wilson [72] suggested that electrons could be accelerated to relativistic energies in electrified thunderstorms with very strong electric fields. Since then, numerous attempts have been made to observe the high-energy electrons or the associated energetic rays under thunderstorm conditions. Credible evidence of energetic radiation from thunderstorms or lightning flashes have been obtained by aircraft-, balloon- and satellite-based observations since the 1980s [73]; [74]; [75]. These findings have pioneered a leading edge field in lightning physics and, consequently, appropriate observations were designed and set up on the basis of the triggering lightning experiment. [76], [77] using NaI(TL) scintillation detectors, discovered marked bursts of energetic radiation which were confirmed to be definitely attributable to the occurrence of the triggered lightning. These energetic radiation events were observed to primarily consist of X-ray emission with the signals being recorded in the form of a pulse cluster, during the leader phases prior to or just at the beginning of the return strokes. The pulse trains of the X-ray emission generally start at ~20 μs (occasionally up to ~100 μs) before the return strokes, with a single burst lasting no more than 1 μs and involving an energy spectrum of 30-250 keV. Figure 11 shows the simultaneous waveforms of current, electric field (at 80 m) and X-ray energy at 3 different distances for a leader-return stroke in triggered lightning. This event exhibited long duration of the X-ray emission during the leader phase. The attenuation of the X-ray intensities with distance is shown in the figure (the peaks of the X-ray pulses indicate the deposited energies of a radiation burst). Also seen in the figure is the gradual increase of the X-ray intensities when the leader approaches the ground, with the largest pulses occurring immediately before the return stroke (see the UPMT curve). It seems that X-ray emission could be detected in most of the leader-return stroke sequences in triggered lightning. Based on the data from 2002 to 2003, [77] concluded that 81% of the leader-return strokes impulsively emitted energetic radiation and have suggested that X-ray emission is a common phenomenon in natural lightning.

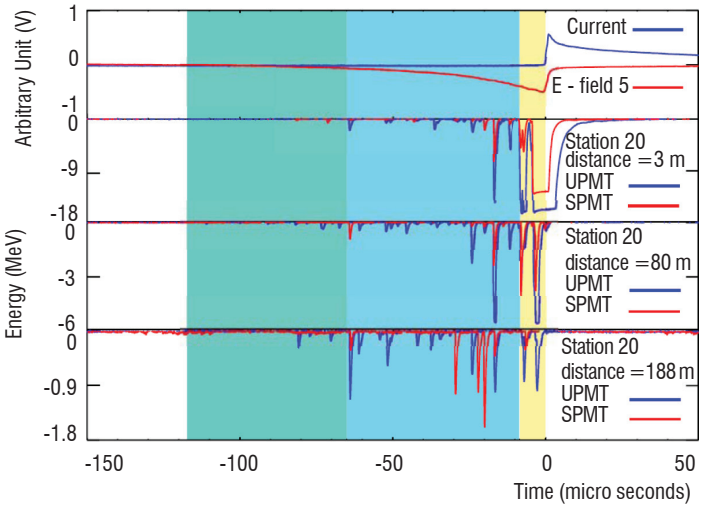

Figure 11 - Simultaneous waveforms of current at the channel bottom, electric field at 80 m, and X-ray energy at different distances (3 m, 80 m, and 188 m, respectively), for a leade r-return stroke in triggered lightning, with the return stroke started at time 0. [86]

It has been well demonstrated that in natural lightning X-ray emission is consistent over time with the leader steps [78]. The synchronous measurements of the current, electric field, and energetic radiation for the dart-stepped leaders in triggered lightning further confirmed such a close relation between the X-ray emission and the step formation [79]; [44]. It is confirmed by the multiple station signals that the X-ray emission and the leader step E-field changes may be derived from the same location, with a temporal deviation of 0.1-1.3 μs and spatial error of less than 50 m [79]. Although most of the observed energetic radiation associated with triggered lightning was in the form of X-rays, [79] once reported an intense gamma-ray burst detected on the ground 650 m away from the triggered-lightning channel, with the energies rising up to more than 10 MeV during a relatively long period of 300 μs. The gamma-ray burst was produced in coincidence with an extremely large current pulse with a peak of 11 kA occurring during the triggered lightning initial stage, that is, before the first dart-leader/return-stroke sequence.

Concluding remarks

The rocket-and-wire technique for artificially triggering lightning has been significantly improved and has become an effective approach to the study of lightning physics. Abundant valuable results have been obtained by the experiments conducted in different countries. These results have provided considerable new insights into lightning properties, many of which are not easily revealed by observation of natural lightning. Due to the length limitation on the manuscript, the review of the results of triggered lightning is very brief in this paper. For more detailed information, the reader may wish to consult the referred articles.

In addition to the investigation of the lightning process, triggered lightning also has wide application. Simultaneous measurements of the discharge current at channel bottom and the *EM* fields at different distances make it feasible to test the validity or applicability of various lightning models. Since the strike point of the triggered lightning is predetermined, observation programs could be designed for investigating the interaction between the lightning and the objects that are struck (or are located very close to the discharge channel), which may help toward better understanding of the mechanism of damage-causing lightning. And also, experiments to evaluate the effectiveness of lightning protection devices could be conducted under real lightning discharge conditions. In addition, the occurrences of triggered lightning, with exact location and time information, provides ground-truth data for the calibration of various lightning location systems [81].

The rocket triggering lightning experiment will be continued in various countries in the coming years. With state-of-the-art experimental and detection technologies it is hoped that new results will be obtained both in researches on lightning physics and applications in the validation of lightning protection and location devices ■

Acknowledgements

This research was supported by National Natural Science Foundation of China (Grant Nos. 41175002, 40930949).

References

[1] K. BERGER - *Novel Observations on Lightning Discharges-Results of Research on Mount San Salvatore.* J. Franklin Inst. 283, 478-525. (1967). doi:10.1016/0016-0032(67)90598-4
[2] M. M. NEWMAN, J. R. STAHMANN, J. D. ROBB, E. A. LEWIS, S. G. MARTIN, and S. V. ZINN - *Triggered Lightning Strokes at Very Close Range*. J. Geophys. Res., 72(18), 4761-4764, (1967). doi:10.1029/JZ072i018p04761
[3] R. FIEUX, C. GARY, and P. HUBERT - *Artificially Triggered Lightning Above Land*. Nature, 257, 212-214, (1975). doi:10.1038/257212a0
[4] P. HUBERT, P. LAROCHE, A. EYBERT - BERARD, and L. BARRET - *Triggered Lightning in New Mexico*. J. Geophys. Res., 89, 2511-2521, (1984).
[5] J. C. WILLETT - *Rocket-Triggered-Lightning Experiments in Florida*. Res. Lett. Atmos. Electr., 12, 37-45, (1992).
[6] V. A. RAKOV, M. A. UMAN, K. J.RAMBO, M. I. FERNANDEZ, R. J. FISHER, G. H. SCHNETZER, R. THOTTAPPILLIL, A. EYBERT-BERARD, J. P. BERLANDIS, P. LALANDE, A. BONAMY, P. LAROCHE, and A. BONDIOU-CLERGERIE - *New Insights into Lightning Processes Gained from Triggered-Lightning Experiments in Florida and Alabama*. J. Geophys. Res. 103, 14117-14130, (1998). doi:10.1029/97JD02149
[7] V. A. RAKOV, M. A. UMAN, and K. J. RAMBO - *A Review of Ten Years of Triggered-Lightning Experiments at Camp Blanding,* Florida. Atmos. Res., 76, 503-517, (2005).
[8] P. LAROCHE, A. EYBERT-BERARD, and L. BARRET - *Triggered Lightning Flash Characteristics*. 10th International Aerospace and Ground Conference on Lightning and Static Electricity, Cent. Natl. de la Rech. Sci., Paris, (1985)
[9] Y. XIA, Q. XIAO, and Y. LU - *The Experimental Study of the Artificial Triggering of Lightning.* Chinese Journal of Atmospheric Sciences (in Chinese), 3(1), 94-97, (1979)
[10] X. LIU, C. WANG, Y. ZHANG, Q. XIAO, D. WANG, Z. ZHOU, and C. GUO - *Experiment of Artificially Triggered Lightning in China*. J. Geophys. Res., 99, 10727-10731, (1994)
[11] X. QIE, Q. ZHANG, Y. ZHOU, G. FENG, T. ZHANG, J. YANG, X. KONG, Q. XIAO, and S. WU - *Artificially Triggered Lightning and its Characteristic Discharge Parameters in Two Severe Thunderstorms.* Sci. China, Ser. D Earth Sci., 50(8), 1241-1250, (2007)
[12] X. QIE, Y. ZHAO, Q. ZHANG, J. YANG, G. FENG, X. KONG, Y. ZHOU, T. ZHANG, G. ZHANG, T. ZHANG, D. WANG, H. CUI, Z. ZHAO, and S. WU - *Characteristics of Triggered Lightning During Shandong Artificially Triggered Lightning Experiment (SHATLE)*, Atmos. Res., 91:310-315, (2009)
[13] K. HORII - *Experiment of Artificial Lightning Triggered With Rocket*. Mem. Fac. Eng. Nagoya Univ., 34, 77-112, (1982)
[14] Y. KITO, K. HORII, Y. HIGASHIYAMA, and K. NAKAMURA - *Optical Aspects of Winter Lightning Discharges Triggered by The Rocket-Wire Technique in Hokuriku District of Japan*. J. Geophys. Res., 90(D4), 6147-6157, (1985)
[15] K. NAKAMURA, K. HORII, M. NAKANO, and S. SUMI - *Experiments on Rocket Triggered Lightning.* Res. Lett. Atmos. Electr., 12, 29-35, (1992)
[16] M. M. F. SABA, O. PINTO Jr., A.EYBERT-BERARD - *Lightning Current Observation of an Altitude-Triggered Flash*. Atmos. Res., 76, 402-411, (2005)
[17] O. PINTO Jr., I. R. C. A. PINTO, M. M. F. SABA, N. N. SOLORZANO, and D. GUEDES - *Return Stroke Peak Current Observations of Negative Natural and Triggered Lightning in Brazi*l. Atmos. Res., 76, 493-502, (2005). doi: 10.1016/j.atmosres. 2004.11.015
[18] V. A RAKOV, and M.A. UMAN - *Lightning: Physics and Effects*. Cambridge University Press, 687pp, (2003)
[19] X. QIE, J. YANG, R. JIANG, J. WANG, D. LIU, C. WANG, Y. XUAN - *A New-Model Rocket for Artificially Triggering Lightning and its First Triggering Lightning Experiment.* Chinese Journal of Atmospheric Sciences (in Chinese), 34(5):937-946, (2010).
[20] M. MIKI, V. A. RAKOV, K. J. RAMBO, G. H. SCHNETZER, and M. A. UMAN - *Electric Fields Near Triggered Lightning Channels Measured with Pockels Sensors*. J. Geophys. Res., 107, 4277, (2002). doi:10.1029/2001JD001087
[21] J. SCHOENE, M. A. UMAN, V. A. RAKOV, K. J. RAMBO, J. JERAULD, C. T. MATA, A. G. MATA, D. M. JORDAN, and G. H. SCHNETZER - *Characterization of Return-Stroke Currents in Rocket-Triggered Lightning*. J. Geophys. Res., 114, D03106, (2009). doi: 10.1029/2008JD009873.
[22] R. P. FIEUX, C. H. GARY, B. P. HUTZLER, A. R. EYBERT-BERARD, P. L. HUBERT, A. C. MEESTERS, P. H. PERROUD, J. H. HAMELIN, and J. M. PERSON - Research on Artificially Triggered Lightning in France. IEEE Trans. Pow. Appar. Syst., PAS-97, 725-733, (1978).
[23] Z.-I. KAWASAKI, and V. MAZUR - Common Physical Processes in Natural and Triggered Lightning in Winter Storms in Japan. J. Geophys. Res., 97(D12), 12,935-12,945, (1992). doi:10.1029/92JD01255.
[24] X. QIE, S. SOULA and S. CHAUZY - *Influence of Ion Attachment on Vertical Distribution of Electric Field and Charge Density Under Thunderstorm*. Annales Geophysicae, 12, 1218-1228, (1994), DOI: 10.1007/s005850050143.
[25] R. J. FISHER, G. H. SCHNETZER, R. THOTTAPPILLIL, V. A. RAKOV, M. A. UMAN, and J. D. GOLDBERG - *Parameters of Triggered-Lightning Flashes in Florida and Alabama*. J. Geophys. Res., 98(D12), 22,887-22,902, (1993). doi:10.1029/93JD02293
[26] M. CHEN, N. TAKAGI, T. WATANABE, D. WANG, Z. KAWASAKI, T. USHIO, M. NAKANO, K. NAKAMURA, S. SUMI, C. WANG, X. LIU, X. QIE, and C. GUO - *Leader Properties and Attachment Process in Positive Triggered Lightning Flashes*. J. Atmos. Electr., 19, 45-59, (1999).
[27] M. CHEN, T. WATANABE, N. TAKAGI, Y. DU, D. WANG, X. LIU - *Simultaneous Observation Of Optical And Electrical Signals In Altitude-Triggered Negative Lightning Flashes*. J. Geophys. Res., 108, 4240, (2003). doi:10.1029/2002JD002676
[28] W. LU, Y. ZHANG, X. ZHOU, X. QIE, D. ZHENG, Q. MENG, M. MA, S. CHEN, F. WANG, AND X. KONG - *Simultaneous Optical and Electrical Observations on the Initial Processes of Altitude-Triggered Negative Lightning*. Atmos. Res., 91, 353-359, (2009). doi: 10.1016/j.atmosres.2008.01.011
[29] J. YANG, X. QIE, G. ZHANG, and H. WANG - *Magnetic Field Measuring System and Current Retrieval in Artificially Triggering Lightning Experiment*. Radio Sci, 43(RS2011), (2008), doi: doi:10.1029/2007RS003753.
[30] D. WANG, V. A. RAKOV, M. A. UMAN, M. I. FERNANDEZ, K. J. RAMBO, G. H. SCHNETZER, and R. J. FISHER - Characterization of the Initial Stage of Negative Rocket-Triggered Lightning. J. Geophys. Res., 104, 4213-4222, (1999). doi: 10.1029/1998JD200087
[31] M. MIKI, V. A. RAKOV, T. SHINDO, G. DIENDORFER, M. MAIR, F. HEIDLER, W. ZISCHANK, M. A. UMAN, R. THOTTAPPILLIL, and D. WANG - *Initial Stage in Lightning Initiated from Tall Objects and in Rocket-Triggered Lightning.* J. Geophys. Res., 110, D02109, (2005). doi:10.1029/2003JD004474.
[32] J. YANG, X. QIE, Q. ZHANG, Y. ZHAO, G. FENG, T. ZHANG, AND G. ZHANG - *Comparative Analysis of The Initial Stage in two Artificially-Triggered Lightning Flashes*. Atmos. Res., 9, 393–398, (2009)
[33] X. QIE, R. JIANG, C. WANG, J. YANG, J. WANG, and D. LIU - *Simultaneously Measured Current, Luminosity, and Electric Field Pulses in a Rocket-Triggered Lightning Flash*. J. Geophys. Res., 116, D10102, (2011). doi:10.1029/2010JD015331
[34] C. J. BIAGI, D. M. JORDAN, M. A. UMAN, J. D. HILL, W. H. BEASLEY, and J. HOWARD - *High-Speed Video Observations of Rocket-and-Wire Initiated Lightning.* Geophys. Res. Lett., 36, L15801, (2009). doi:10.1029/2009GL038525

[35] C. X. WANG, X. S. QIE, R. B. JIANG, and J. YANG - *Propagating Properties of an Upward Positive Leader in a Negative Triggered Lightning*. Acta Physica Sinica, 61(3): 039203, (2012).
[36] S. YOSHIDA, C. J. BIAGI, V. A. RAKOV, J. D. HILL, M. V. STAPLETON, D. M. JORDAN, M. A. UMAN, T. MORIMOTO, T. USHIO AND Z.-I. KAWASAKI - *Three-Dimensional Imaging of Upward Positive Leaders in Triggered Lightning Using Vhf Broadband Digital Interferometers*. Geophys. Res. Lett., 37, L05805, (2010). doi:10.1029/2009GL042065
[37] J. C. WILLETT, D. A. DAVIS, and P. LAROCHE - *An Experimental Study of Positive Leaders Initiating Rocket-Triggered Lightning*. Atmos. Res., 51, 189-219, (1999). doi: 10.1016/S0169-8095(99)00008-3
[38] P. LALANDE, A. BONDIOU-CLERGERIE, P. LAROCHE, A. EYBERT-BERARD, J.-P. BERLANDIS, B. BADOR, A. BONAMY, M. A. UMAN, and V. A. RAKOV - *Leader Properties Determined With Triggered Lightning Techniques*. J. Geophys. Res., 103(D12), 14,109-14,115, (1998). doi:10.1029/97JD02492
[39] P. LALANDE, A. BONDIOU-CLERGERIE, G. BACCHIEGA, I. GALLIMBERTI - *Observations and modeling of lightning leaders*, C. R. Phys., 3, 1375-1392, (2002). doi: 10.1016/S1631-0705(02)01413-5
[40] C. J. BIAGI, M. A. UMAN, J. D. HILL, D. M. JORDAN - *Observations of the Initial, Upward-Propagating, Positive Leader Steps in a Rocket-and-Wire Triggered Lightning Discharge*. Geophys. Res. Lett., 38, L24809, (2011). doi:10.1029/2011GL049944
[41] R. JIANG, X. QIE, C. WANG, J. YANG - *Propagating Features of Upward Positive Leaders in the Initial Stage of Rocket-Triggered Lightning*. Atmos. Res., (2012) doi:10.1016/j.atmosres.2012.09.005. in press
[42] D. WANG, N. T. TAKAGI, V. WATANABE, A. RAKOV and M. A. UMAN - *Observed Leader and Return-Stroke Propagation Characteristics in the Bottom 400 m of a Rocket-Triggered Lightning Channel.* J. Geophys. Res., 104, 14 369-14 376, (1999b). doi: 10.1029/1999JD900201
[43] B. N. GORIN, V. I. LEVITOV, and A. V. SHKILEV - *Some Principles of Leader Discharge of Air Gaps With a Strong Non-Uniform Field*. IEE Conf. Publ., 143, 274-278, (1976).
[44] C. J. BIAGI, M. A. UMAN, J. D. HILL, D. M. JORDAN, V. A. RAKOV, and J. DWYER - *Observations of Stepping Mechanisms in a Rocket-and-Wire Triggered Lightning Flash.* J. Geophys. Res., 115, D23215, (2010). doi:10.1029/2010JD014616
[45] V. P. IDONE, and R. E. ORVILLE - *Three Unusual Strokes in a Triggered Lightning Flash*. J. Geophys. Res., 89(D5), 7311-7316, (1984). doi:10.1029/JD089iD05p07311
[46] D. WANG, V. A. RAKOV, M. A. UMAN, N. TAKAGI, T. WATANABE, D. E. CRAWFORD, K. J. RAMBO, G. H. SCHNETZER, R. J. FISHER, and Z. I. KAWASAKI - *Attachment Process in Rocket-Triggered Lightning Strokes*. J. Geophys. Res., 104(D2), 2143-2150, (1999c). doi:10.1029/1998JD200070
[47] J. SCHOENE, M. A. UMAN, and V. A. RAKOV - *Return Stroke Peak Current vs. Charge Transfer in Rocket-Triggered Lightning*. J. Geophys. Res., 115, D12107, (2010). doi: 10.1029/2009JD013066
[48] P. DEPASSE - *Statistics on Artificially Triggered Lightning*. J. Geophys. Res.2, 99(D9), 18,515-18,522, (1994). doi: 10.1029/94JD00912
[49] D. E. CRAWFORD - Multiple-Station Measurements of Triggered Lightning Electric and Magnetic Fields. Master's thesis, Univ. of Fla., Gainesville, Fla., (1998).
[50] Q. ZHANG, X. QIE, Z. WANG, T. ZHANG, Y. ZHAO, J. YANG, and X. KONG - *Characteristics and Simulation of Lightning Current Waveforms During one Artificially Triggered Lightning.* Atmos. Res., 91(1-4), 387–392, (2009).
[51] Y. ZHAO, X. S. QIE, X. Z. KONG, G. S. ZHANG, T. ZHANG, J. YANG, G. L. FENG, Q. L. ZHANG, and D.F. WANG - *Analysis of The Parameters of the Current Waveforms of Triggered Lightning (In Chinese)*. Acta Physica Sinica, 58(9), 6616–6625, (2009).
[52] V. COORAY, V. A. RAKOV, N. THEETHAYI - *The Lightning Striking Distance-Revisited.* J. Electrostatics, 65, 296-306, (2007). doi:10.1016/j.elstat.2006.09.008
[53] J. SCHOENE, M. A. UMAN, and V. A. RAKOV - *Return Stroke Peak Current vs. Charge Transfer in Rocket-Triggered Lightning*. J. Geophys. Res., 115, D12107, (2010). doi: 10.1029/2009JD013066
[54] C.T. MATA, V. A. RAKOV, K. J. RAMBO, P. DIAZ, R. REY, and M.A.UMAN - *Measurement of the Division of Lightning Return Stroke Current Among the Multiple Arresters and Grounds of a Power Distribution Line.* IEEE Trans. on Power Delivery, 18, 1203-1208, (2003). Doi:10.1109/TPWRD.2003.817541
[55] C. LETEINTURIER, J. H. HEMELIN, A. EYBERT-BERARD - *Submicrosecond Characteristics of Lightning Return-Stroke Currents*. IEEE Trans. Electromagn. Compat. 33, 351-357, (1991).
[56] J. YANG, X. QIE, G. ZHANG, Q. ZHANG, G. FENG, Y. ZHAO, and R. JIANG - *Characteristics of Channel Base Currents and Close Magnetic Fields in Triggered Flashes in SHATLE*. J. Geophys. Res., 115, D23102, (2010). doi:10.1029/2010JD014420
[57] D. E. CRAWFORD, V. A. RAKOV, M. A. UMAN, G. H. SCHNETZER, K. J. RAMBO, M. V. STAPLETON, R. J. FISHER - *The close Lightning Electromagnetic Environment: Dart-Leader Electric Field Change Versus distance.* J. Geophys. Res., 106, 14909-14917, (2001).
[58] V. A. RAKOV, KODALI, D. E. CRAWFORD, J. SCHOENE, M. A. UMAN, K. J. RAMBO, and G. H. SCHNETZER - *Close Electric Field Signatures of Dart Leader/Return Stroke Sequences in Rocket - Triggered lightning showing residual fields*. J. Geophys. Res., 110, D07205, (2005b). doi:10.1029/2004JD005417.
[59] Q. ZHANG, X. QIE, Z. WANG, T. ZHANG, and J. YANG - *Simultaneous Observation on Electric Field Changes at 60 m and 550 m from Altitude-Triggered Lightning Flashes*. Radio Science, 44, RS1011, doi:10.1029/2008RS003866, (2009)
[60] J. SCHOENE, M. A. UMAN, V. A. RAKOV, K. J. RAMBO, J. JERAULD, C. T. MATA, A. G. MATA, D. M. JORDAN, and G. H. SCHNETZER - *Characterization of Return-Stroke Currents in Rocket-Triggered Lightning*. J. Geophys. Res., 114, D03106, (2009). doi: 10.1029/2008JD009873.
[61] D. J. MALAN, and H. COLLENS - *Progressive lightning. III. The fine structure of return lightning strokes*. Proc. R. Soc. London, Ser. A, 162, 175-203, (1937). doi:10.1098/rspa.1937.0175
[62] D. J MALAN, AND B. F. J. SCHONLAND - *Progressive Lightning. VII. Directly Correlated Photographic and Electrical Studies of Lightning from Near Thunderstorms.* Proc. R. Soc. London, Dec. A, 191, 485-503, (1947). doi:10.1098/rspa.1947.0129
[63] R. THOTTAPPILLIL, V. A. RAKOV, and M. A. UMAN - *K And M Changes in Close Lightning Ground Flashes in Florida*. J. Geophys. Res., 95(D11), 18,631-18,640, (1990).
[64] V. A. RAKOV, R. THOTTAPPILLIL, and M. A. UMAN - *Electric Field Pulses in K and M Changes of Lightning Ground Flashes*. J. Geophys. Res., 97(D9), 9935-9950, (1992). doi:10.1029/92JD00797
[65] D. M. JORDAN, V. P. IDONE, R. E. ORVILLE, V. A. RAKOV, and M. A. UMAN - *Luminosity Characteristics of Lightning M Components*. J. Geophys. Res., 100(D12), 25,695-25,700, (1995). doi:10.1029/95JD01362
[66] V. MAZUR, P. R. KREHBIEL, and X.-M. SHAO - *Correlated High-Speed Video and Radio Interferometric Observations of a Cloud-to-Ground Lightning Flash.* J. Geophys. Res., 100(D12), 25,731-25,753, (1995). doi:10.1029/95JD02364
[67] R., J THOTTAPPILLIL, D. GOLDBERG, V. A. RAKOV, M. A. UMAN, R. J. FISHER, and G. H. SCHNETZER - *Properties of M Components from Currents Measured at Triggered Lightning Channel Base.* J. Geophys. Res. 100, 25711-25720, (1995).
[68] R. JIANG, X. QIE, C. WANG, J. YANG, Q. ZHANG, M. LIU, J. WANG, D. LIU, L. PAN - *Lightning M-Components with Peak Currents of Kilo Amperes and Their Mechanism*. ACTA Physica Sinica (in Chinese), 60, 079201, 1-8, (2011).

[69] V. A. RAKOV, R. THOTTAPPILLIL, M. A. UMAN and P. P. BARKER - *Mechanism of the Lighting M Component.* J. Geophys. Res., 100, 25,701-25,710, (1995)
[70] V. A. RAKOV, D. E. CRAWFORD, K. J. RAMBO, G. H. SCHNETZER, M. A. UMAN, and R. THOTTAPPILLIL - *M-Component Mode of Charge Transfer to Ground in Lightning Discharges.* J. Geophys. Res., 106, 22,817-22,831, (2001).
[71] Q. ZHANG, J. YANG, M. LIU, and Z. WANG - *Measurements and Simulation of the M-Component Current and Simultaneous Electromagnetic Fields at 60 m and 550 m.* Atmos. Res., 99, 537-545, (2011).
[72] C. T. R. Wilson - *The Acceleration of β-Particles in Strong Electric Fields Such as Those of Thunderclouds.* Proc Cambridge Philos Soc, 22(4): 534-538, (1925).[73] Parks, G. K., B. H. Mauk, R. Spiger, and J. Chin - X-ray enhancements detected during thunderstorm and lightning activities. Geophys. Res. Lett., 8(11), 1176-1179, (1981). doi:10.1029/GL008i011p01176
[74] G. J. FISHMAN, P. N. BHAT, R. MALLOZZI, J. M. HORACK, T. KOSHUT, C. KOUVELIOTOU, G. N. PENDLETON, C. A. MEEGAN, R. B. WILSON, W. S. PACIESAS, S. J. GOODMAN, H. J. CHRISTIAN - *Discovery of Intense Gamma-Ray Flashes of Atmospheric Origin*. Science, 264, 1313-1316, (1994). doi: 10.1126/science. 264.5163.1313
[75] K. B. EACK, W. H. BEASLEY, W. D. RUST, T. C. MARSHALL, and M. STOLZENBURG - *Initial Results from Simultaneous Observation of X Rays and Electric Fields in a Thunderstorm.* J. Geophys. Res., 101(D23), 29,637-29,640, (1996). doi:10.1029/96JD01705
[76] J. R. DWYER, M. A. UMAN, H. K. RASSOUL, M. AL-DAYEH, L. CARAWAY, J. JERAULD, V. A. RAKOV, D. M. JORDAN, K. J. RAMBO, V. CORBIN, B. WRIGHT - *Energetic Radiation Produced During Rocket Triggered Lightning.* Science, 299, 694-697, (2003). doi: 10.1126/science.1078940.
[77] J. R. DWYER, H. K. RASSOUL, M. AL-DAYEH, L. CARAWAY, B. WRIGHT, A. CHREST, M. A. UMAN, V. A. RAKOV, K. J. RAMBO, D. M. JORDAN, J. JERAULD, and C. SMYTH - *Measurements of x-ray Emission from Rocket-Triggered Lightning.* Geophys. Res. Lett., 31, L05118, (2004a). doi: 10.1029/2003GL018770
[78] J. R. DWYER, H. K. RASSOUL, M. AL-DAYEH, L. CARAWAY, A. CHREST, B. WRIGHT, E. KOZAK, J. JERAULD, M. A. UMAN, V. A. RAKOV, D. M. JORDAN, and K. J. RAMBO - *X-ray Bursts Associated With Leader Steps in Cloud-to-Ground Lightning*. Geophys. Res. Lett., 32, L01803, (2005). doi:10.1029/2004GL021782
[79] J. HOWARD, M. A. UMAN, J. R. DWYER, D. HILL, C. BIAGI, Z. SALEH, J. JERAULD, and H. K. RASSOUL - *Co-location of Lightning Leader x-Ray and Electric Field Change Sources.* Geophys. Res. Lett., 35, L13817, (2008). doi:10.1029/2008GL034134
[80] J. R. DWYER, H. K. RASSOUL, M. AL-DAYEH, L. CARAWAY, B. WRIGHT, AND A. CHRES, M. A. UMAN, V. A. RAKOV, K. J. RAMBO, D. M. JORDAN, J. JERAULD, and C. SMYTH - *A Ground Level Gamma-Ray Burst Observed in Association with Rocket-Triggered Lightning*. Geophys. Res. Lett., 31, L05119, (2004b). doi:10.1029/2003GL018771
[81] J. JERAULD, V. A. RAKOV, M. A. UMAN, K. J. RAMBO, D. M. JORDAN, K. L. CUMMINS, and J. A. CRAMER - *An Evaluation of the Performance Characteristics of the U.S. National Lightning Detection Network in Florida Using Rocket-Triggered Lightning.* J. Geophys. Res., 110, D19106, (2005). doi:10.1029/2005JD005924
[82] Y. KITO, Y., K. HORII, Y. HIGASHIYAMA, and K. NAKAMURA - *Optical Aspects of Winter Lightning Discharges Triggered by the Rocket-Wire Technique in Hokuriku District of Japan.* J. Geophys. Res., 90(D4), 6147–6157, (1985) doi:10.1029/JD090iD04p06147
[83] V. P. IDONE, - *The Luminous Development of Florida Triggered Lightning*. Res. Lett. Atmos. Electr., 12, 23-28, (1992).
[84] X. QIE, J. YANG, R. JIANG, R. JIANG, C. WANG, G. FENG, S. WU, G. ZHANG – *Shandong Artificially Triggered Lightning Experiment and Current Characterization of Return Stroke.* Chinese Journal of Atmospheric Sciences (in Chinese), 36(1): 77-88, (2012).
[85] D. ZHENG, Y. ZHANG, W. LU, Y. ZHANG, W. DONG, S. CHEN, J. DAN - *Return Stroke Currents of Triggered Lightning in Guangdong, China*. 7th Asia-Pacific International Conference on Lightning, 231-234, (2011).

Acronyms

IS (Initial Stage)
ICC (Initial Continuous Current)
VHF (Very High Frequency)
UPLs (Upward Positive Leaders)
ALPS (Automatic Lightning Processing Feature Observation System)
UPMT (Unshielded/Unattenuated Photomultiplier Tube)
RS (Return Stroke)
SHATLE (Shandong Artificially Triggered Lightning Experiment)
ICLRT (International Center for Lightning Research and Testing)

AUTHORS

Xiushu Qie holds a Ph.D. in Atmospheric Physics. She became a professor in 1996. Her fields of interests include lightning physics and effects, lightning and severe thunderstorm, and thunderstorm electricity. She is the author or co-author of more than 160 papers and one book. She serves as an associate editor or co-editor for 6 Journals. She is a member of International Commission on Atmospheric Electricity, and served as Chairperson of the 13th International Conference on Atmospheric Electricity in Beijing in 2007.

Rubing Jiang is a Ph.D student at the Key Laboratory of Middle Atmosphere and Global Environment Observation, Institute of Atmosphere Physics, Chinese Academy of Science. His study work for a doctorate mainly concerns the characteristics and mechanism of physical processes in triggered lightning.

Pierre Laroche received his engineering degree from the Institut Polytechnique de Grenoble in 1971. He joined The French Aerospace Lab the same year and became involved in triggered lightning experiments in France and the United States of America. His background is in the physics of lightning and Atmospheric Electricity. He is author or co-author of more than 100 papers and one book and has served as co-editor for 2 journals. He was President of the International Commission on Atmospheric Electricity (IUGG/IAMAS) from 1999 to 2007.

P. Laroche, P. Blanchet,
A. Delannoy †, F. Issac
(Onera)

E-mail: pierre.laroche@onera.fr

Experimental Studies of Lightning Strikes to Aircraft

Civil aviation transportation has been growing since the early forties and has become today a massive and unique transport system for people across continents and large countries. First age propeller airliners flew at low altitude and were often subjected to dangerous atmospheric and cloud hazards. Low visibility, heavy precipitation, severe turbulence, wind shear, icing and lightning are common weather hazards that are a challenge for flight safety. Among those weather hazards, lightning was the most unrecognized and misunderstood. Damages to aircraft due to lightning strike were frequently noticed; they range from arc spots on metal to centimeter-size holes in the fuselage, and dielectric radome and antenna destruction. Some cases of catastrophic events are directly attributed to lightning [1], [2]. Experimental in-situ studies were initiated no later than the early sixties [3], but the main in-flight research efforts were undertaken at the beginning of the eighties, when the perspective of a massive use of composite material in aviation was identified for a near future. Three major in-flight test programs were initiated in the USA and Europe by NASA, the Air Force, the FAA and the French Civil and Military Aviation Authorities, associated with Research Organizations. This paper is a review of the in-flight lightning strike experiments performed during that period. Information on aircraft missions, performances and instrumentation is given. Available results and proposed interpretations are presented. The main outcomes of those experiments are emphasized and knowledge gaps and missing information are mentioned.

Lightning strike to civil and military aircraft

Despite the fact that civil and military aircraft avoid flying in thunderstorms because of the severity of the weather hazards encountered, such as hail, heavy precipitation, turbulence and wind shear, noticeable, serious or catastrophic accidents are reported to be due to lightning strike as a primary cause [4], [1]. For civilian aircraft, a catastrophic accident in the USA on a Pan Am Boeing 707 in 1963 was reported by the civil aviation investigation board to be due to induced electromagnetic effects in the fuel tank [2], [http://en.wikipedia.org/wiki/Pan_Am_Flight_214].

In 1976, an Iran Air Boeing 747 crashed before landing in Madrid, just after being struck by lightning. The investigation board concluded that the probable primary cause of the catastrophe was arcing in the fuel tank, induced by a direct lightning strike [1]. A report on an accident ending with the loss of an F4 air fighter clearly established a problem of a fuel tank explosion due to a lightning strike.

Detailed data on lightning strikes to military and civil aircraft are based on crew and maintenance team reports. Data for the 1950-1974 period has been reported for the USA [5] and Japan [6], [7] where winter storms bring peculiar lightning configurations [8], and for South Africa [9]. Combining propeller and jet airliner data, a mean rate of one event per year, or per 3000 h of flight, is reported. Similar data analyses were done for the UK, France and Germany, for military and civil aircraft [10].

In any case, lightning strike to airliners is common enough to be observed and documented when it happens near an airport [11]. Figure 1 shows 3 cases of lightning strike on different airliners flying at low altitude. It must be noticed that, for the 3 cases, the aircraft is at the center of the lightning flash and pictures show evidence of upward and downward branching of the lightning channel from the aircraft.

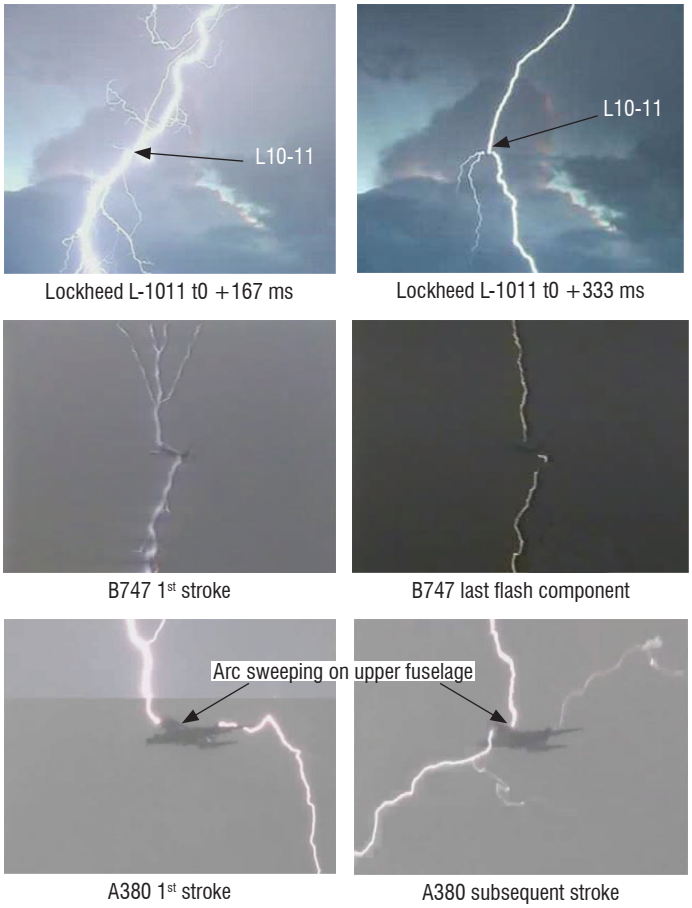

Lockheed L-1011 t0 +167 ms | Lockheed L-1011 t0 +333 ms

B747 1st stroke | B747 last flash component

A380 1st stroke | A380 subsequent stroke

Figure 1 – In-flight lightning strikes to airliners

Aircraft instrumentation for in-flight lightning strike studies

Four aircraft were instrumented to observe and analyze the processes involved in the initiation phase of a lightning strike. They were different in size, flight domain and mission. F100 and F106 are fighters with a capacity of Mach 2 up to 50 000 ft. Convair CV580 is a low wing bi-turboprop 50 seat commuter. Transall C160 is an upper wing bi-turboprop large military transport aircraft similar in size to the four engine Hercules C130 aircraft. Other aircraft were instrumented to remotely observe electrical activity inside a thunderstorm. Occasionally, during their observing mission, they were struck by lightning and despite the fact that their instrumentation was not designed for analyzing a direct strike, they gathered interesting information.

In situ measurement of the atmospheric electrical field

The magnitude and orientation of the atmospheric electrostatic field is an important local physical parameter in the processes of lightning interaction with aircraft. Such in situ measurement on aircraft is done with field meters of the field mill type, implemented at different locations on the aircraft wings and fuselage. The aircraft surface is conducting enough to locally distort the electrical field and the measurement of the undisturbed field consists in a computed evaluation based on the Uniform Field Concept: the space charges creating the local electrical field are far enough from the aircraft to make valid the hypothesis that the aircraft is flying in an area where the electrical field is uniform. Consequently, the magnitude of the electrostatic field at any location on the aircraft surface is a linear function of the three atmospheric field components and of the aircraft net charge, or net electrical potential.

To measure the atmospheric electrical field, at least four independent measurements of the electrostatic field on the aircraft are necessary. To validate the concept, or evaluate the quality of each sensor, more than 4 measurements are needed. If n measurements are available, M being the matrix of the local sensor factor expressing the n measurements versus the matrix E, the 3 components of the field and the aircraft net potential, the least square expression of E is [12]:

$$E = (M^T.M)^{-1}.M^T.S$$

where S is the matrix of the n measurements. The theoretical and practical calibration process of this type of measurement has been extensively analyzed [13], [14], [15]. Commonly, 4 to 8 field mill sensors are implemented on aircraft to measure the atmospheric field [16],[17], [18], [19], [20]. Figure 2 shows the implementation of field mills on a Convair CV 580 and a Transall C160.

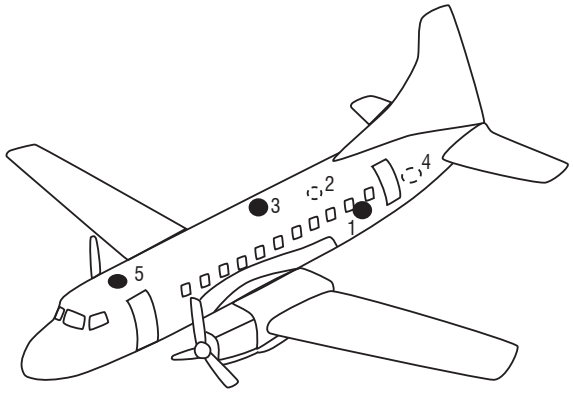

Convair CV580

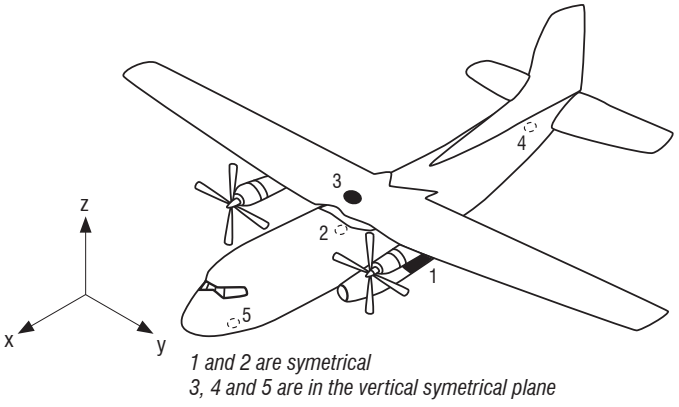

Transall C160

Figure 2 – Field mill sensor implementation on the CV580 and C160 aircraft. These sensors measure the electrostatic field on the surface of the aircraft

Observation of distant activity

NASA Ames Learjet 705

The Learjet is a small business bi-turbojet aircraft (10.8 m span, 13.2 m length and 3.8 m height). The model instrumented by NASA was operated in 1976 within the framework of an international experimental program TRIP 76 [16]. The concern was already with the frequency spectrum of the lightning signal and how it interferes with on board electronic devices, by electromagnetic coupling through apertures and non-shielded composite structures. The objective was not to obtain direct strikes on the aircraft, but

rather to measure the electromagnetic effect of nearby lightning flashes. The aircraft was instrumented to measure the electric atmospheric field near thunderstorms and to record the HF transient signal produced on test equipment inside and outside the aircraft. Narrow band measurements were made on 5 frequencies: 10 kHz, 1 MHz, 3 MHz, 10 MHz and 30 MHz. This rather low frequency coverage includes most of the spectrum of a return stroke component, of a Cloud-to-Ground flash.

Hercules C130 aircraft

In 1981, a C130 Aircraft, instrumented by NOAA, was flown in the vicinity of thunderstorms, in order to gather measurements on the electromagnetic effects of distant flashes on an aircraft. This aircraft had been directly struck by lightning twice [21]. The Hercules C130 is a four engine turboprop Military transport aircraft with a 40.4 m span, 29.8 m length and 11.6 m height; its speed is 150 m/s and its service ceiling is 33 000 ft. The NOAA aircraft was equipped with dE/dt, dH/dt and dI/dt sensors with ranges set for a large lightning flash at a distance of 35 km. The environment of the aircraft was surveyed with a digital onboard weather radar and an onboard lightning detector.

Aircraft instrumentation for direct lightning strike studies

Four aircraft have been instrumented specifically for direct lightning strike studies.

F-100F aircraft

The North American Super Sabre F-100F aircraft was a two seat military trainer single engine jet fighter (14 m length + 2.8 m pitot, 11.8 m span, 4.95 m height). From 1964 to 1966, an aircraft of this type was instrumented with electric current measuring boom, electrostatic field measurements and video camera to obtain data on direct lightning strikes [3]. For the experiment conducted by the Air Force Cambridge Research Laboratory, the aircraft was flown in thunderstorms over Florida, USA, and was struck by lightning 33 times during the 1965 experiment. Simultaneously, atmospheric electric field measurements were preformed around and above the storms by a C130 and U2 instrumented aircraft. Data acquisitions were performed with the 60's state of the art recording devices and quantitative information on direct lightning current is not available in the literature.

F-106B Delta Dart aircraft

The Convair F-106 B is a two seat military jet fighter aircraft, operated by NASA Langley Research Center (figure 3) between 1980 and 1986. It is longer than the F100F aircraft, but much smaller than the two instrumented transport aircraft described below: wing span 11.7 m, length 21.6 m and height 6.2 m. It had a service ceiling of 17 km (52 700 ft). The aircraft was modified for the purpose of the lightning experiment. One significant modification was the replacement of the composite nose radome by a metallic radome. The maximum speed of the F-106 is Mach 2.3. During the lightning experiment it was flown at a subsonic speed; cloud penetration was performed at 300 kt (about 150 to 170 m/s from 14 000 ft to 20 000 ft). Air speed is a significant parameter to interpret the timing of the interaction of the aircraft with a lightning flash. The F106 was equipped with optical sensors (video camera and light detector). Electromagnetic instrumentation consisted in B-dot, D-dot sensors and current measurement with resistive shunt. Data acquisition was performed with the 1980's state of the art digital waveform recorders: 10 ns sample interval and 6 bit resolution, allowing a continuous record of 1.3 ms. Permanent record of the entire duration of a lightning event was provided, with analogue tape recorder, on which the time derivative of the current between the nose boom and fuselage, and the time derivative of magnetic and electric flux measured in six different place on the aircraft (see figure 4 from [22]) were recorded. The measuring range of the sensors was adapted to the signal observed during the flight research program, from 1980 up to 1986.

Figure 3 – NASA F-106 B research aircraft. [Photo NASA]. The aircraft was devoted to the NASA Langley Research Center from 1979 to 1991. Modified for in flight lightning experiments in 1979, it was used by NASA for in-flight lightning experiments from 1980 to 1986

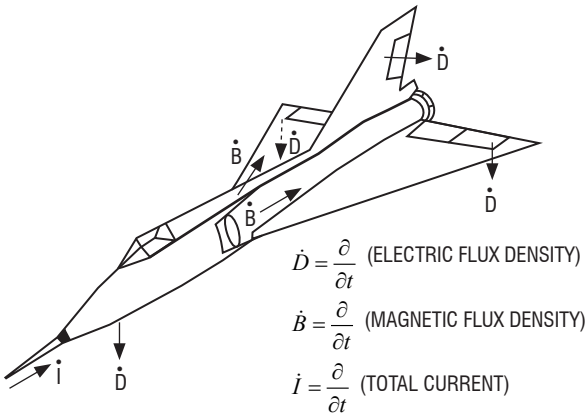

Figure 4 – Electromagnetic sensors on the F-106 B aircraft (from [22]). A boom is connected to the aircraft nose, with a dI/dt sensor. dE/dt and dB/dt sensors are mounted on the aircraft fuselage

Convair CV-580 aircraft

The CV 580 aircraft is a two engine turboprop 50 seat commuter that was extensively used for medium hauls by several US airliners between the 60 s and the 80 s. The Federal Aviation Administration operated such an aircraft in 1984 and 1987 to conduct a lightning research program with Air Force Wright Aeronautical Laboratories [23], [24]. The aircraft length and span were, respectively, 24.8 m and 32.1 m. The standard speed for the experiment was between 80 m/s and 140 m/s.

The aircraft, identified as N49, was instrumented to measure the electrical parameters of the interaction between the lightning flash and the aircraft. Direct current flowing through the wings and the tail of the

aircraft is measured by 4 resistive shunts (5 mΩ). The time derivative of the current flowing through the aircraft fuselage is measured at 5 different locations. The time derivative of the displacement current is delivered by 5 flush sensors, providing the electric field variations at each measuring site. All of these measurements are organized to make possible the description of the phenomenology of a lightning strike and to produce a quantitative evaluation of the threat.

The general objective of the experiment was to gather data on the high frequency variation of the electromagnetic fields produced by direct lighting strikes to aircraft and to compare those values with the magnitude applied by standard procedures in aircraft certification processes. The CV580 was flown in 1984 and 1985 close by and inside Florida thunderstorms with a particular effort to undergo lightning strike at a low level (between 2 000 and 4 000 ft AMSL), with the purpose of having the aircraft involved in a Cloud-to-Ground lightning flash, which are the type known to provide the largest current threat. The aircraft was not modified for the experiment, but extensive inspection and ground lightning tests were conducted, for safety purposes. A less volatile fuel, the JP-5, was used for the flight to minimize the risk of fire and explosion.

Determination of the electrostatic configuration of aircraft lightning strikes was possible, with the installation of a DC field meter of the field mill type. 4 sensors were installed by NRL and 5 by Onera.

Transall C160 aircraft

A Transall C160 aircraft was instrumented in the early 1980s to observe and analyze direct lightning strikes. The C160 is a bi-turboprop military carrier, with a typical airspeed of 140 m/s and an effective operating ceiling of 26 000 ft . The overall dimension of the standard aircraft is 40 m span, 32.4 m length and 11.78 m height. The actual length of the Transall, equipped with nose and tail current measuring boom, was 42.4 m. Two major field experiments were conducted in 1984 and 1988, for which measurements were available to characterize the lightning parameter and the storm environment. 32 direct lightning strikes were observed during the two campaigns.

Instrumentation for lightning characterization

Direct current measurements were performed with two 5 m booms connected to the fuselage by a 5 mΩ resistive shunt. Two 1.5 m length booms were installed on the left and right wing tips, and connected to the structure with a 5 mΩ shunt. The measuring range was ± 100 kA (bandwidth 10 MHz). Current derivative sensors were installed in the middle of the nose and tail boom; the measuring signal was transmitted with a fiber optic link; the measuring range was 10^9 to 10^{11} A/s.

Fast electric and magnetic field variations produced by a direct lightning strike were measured at 7 locations on the aircraft (figure 5), in order to obtain a comprehensive interpretation of the current flow and field variation on the surface of the aircraft. The electric field variation was delivered by an FPD sensor (Flush Plate Dipole) whose signal was recorded in 3 separate ranges: E from 10^3 to 10^5 V/m and dE/dt from 10^{10} to 10^{12} V/m.s (frequency range 200 MHz) and EBF from 10^4 to 10^6 V/m (frequency range 5 Hz - 5 MHz).

7 video cameras running at 200 fps provided the general visual aspect of the lightning channels attached to the aircraft.

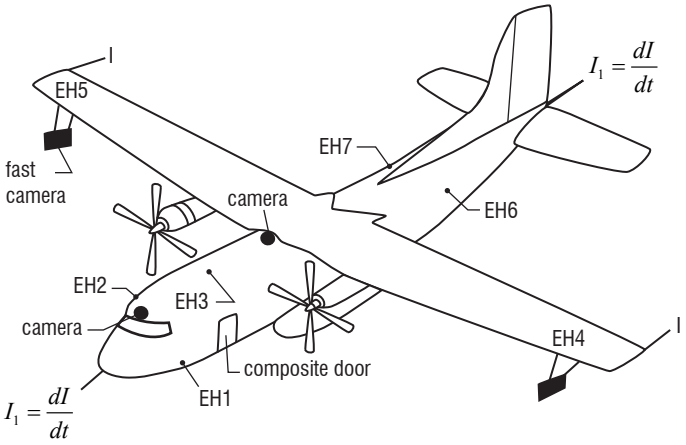

Figure 5 – General instrumentation of the C160 aircraft. EH1-EH7 are fast capacitive antennas, I and dI/dt are the shunt and current derivative sensor installed on current measuring booms (from figure 1 of [39])

Electrical environment of a direct lightning strike.

Onboard electrical measurements provided information on the electrical conditions in which the aircraft had been struck by lightning. The aircraft potential and atmospheric electric field were derived from a DC field meter of the "field mill" type, installed flush at 5 different locations on the fuselage (figure 2); the measuring range of each sensor was +/- 1 MV/m and the rise time of the sensor was 15 ms.

The triboelectrical current was evaluated with an electrode deposited on the leading edge of a pod installed under the wing, carrying various particle measuring devices. The effective surface of the probe was 0.24 m² and the measuring range was +/- 100 μA (figure 6).

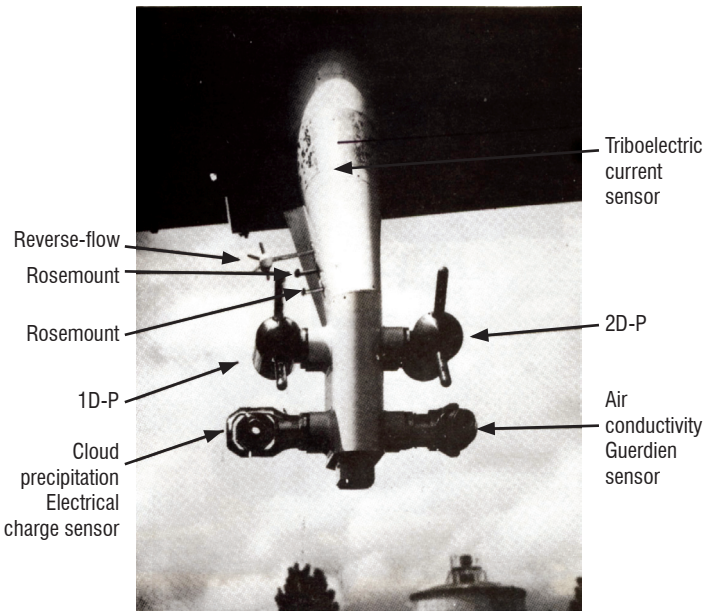

Figure 6 – Cloud parameter measuring pod installed under the C160 aircraft wing

The electrical ionic conductivity of the air was provided by a Guerdien type sensor. The electrical charge of water drops and ice particles was measured by an electrical induction cylinder [25], [26]. Particle Measuring Sensors provided data on the size and shape of cloud particles. With these measurements, it is possible to determine whether the aircraft was flying in cloudy or clear air.

Several passive dischargers were instrumented to measure the corona current emitted by these devices in storm cloud conditions.

General results

Distant and close lightning observations

The NASA Learjet performed 29 flights, during which 300 passes were made near thunderstorm cells. During one flight, the aircraft was struck by lightning. The magnitude of the ambient electric field was 68 kV/m just prior to the lightning strike [16]. The altitude was 11.2 km, the top of the cells was 13.1 km and the authors assumed that the field magnitude was large enough in relation to the aircraft dimension for it to trigger a lightning flash (1 MV of potential drop along the aircraft dimension).

The C130 was struck by lightning twice. The two events were obtained at the -0.7 °C and -5 °C level over Florida, USA. Instrumentation provided information on a low level signal for the initiation phase and during the entire duration of the event. The authors claimed to have indications of leader emission from the aircraft, triggering a cloud-to-aircraft lightning flash.

Direct lightning strike observations

Between 1980 and 1986. NASA conducted extensive in-flight lightning strike experiments with an instrumented F106 aircraft. This aircraft penetrated thunderstorms about 1500 times and was struck by 714 lightning flashes [27],[21].

During the two year campaign of 1986 and 1987 [23], [24], [28] [29], the CV580 aircraft was struck by lightning 52 times. Five lightning strikes occurred at low altitude, below 4 000 ft. The other events were observed above 14 000 ft. The trajectory of the aircraft was chosen to approach thunderstorm cells at a given altitude, staying outside of a precipitation echo larger than 40 dBz, as indicated by the onboard weather radar. 47 events were observed between 14 000 ft and 19 000 ft, with the local temperature depending on the situation and varying from +5 °C to – 9 °C. The results of this lightning strike chasing are illustrated in Table 1 below, from [24]. No lightning strike was obtained between 6 000 ft and 14 000 ft; events below 4 000 feet were difficult to obtain.

Altitude (ft)	Flying time (h)	N° of events
17 000 and above	*12.0*	*16*
15 000 – 17 000	*7.0*	*7*
13 000 – 15 000	*18.0*	*24*
11 000 – 13 000	*2.4*	*0*
9 000 – 11 000	*2.3*	*0*
7 000 – 9 000	*2.3*	*0*
5 000 – 7 000	*12.0*	*0*
3 000 – 5 000	*5.0*	*2*
BELOW 3 000	*17.0*	*3*

Table 1 – CV580 lightning campaign: Number of strikes versus hours flown at a given altitude (From TABLE 4 of [24])

Direct lighting strike observations on the C160 Transall aircraft were obtained during the 1984 and 1988 campaigns [30], [31]. The flight pattern followed by the aircraft to be struck by lightning consisted in successive level explorations, from 10 000 ft to 20 000 ft. The aircraft flew out of the 40 dBz echo to avoid hail and heavy turbulence. The first campaign was held in the South West of France and was associated to the LANDES 84 experiment, which contributed the support of ground atmospheric measurements from a Doppler weather radar. 18 lightning strikes were observed during 7 different storms in June 1984, between 0 °C and - 8 °C. The mean duration of the flashes was 300 ms (maximum 800 ms, minimum 80 ms). The electromagnetic signals measured consist in bursts of pulses with a duration of a few ms and a repetition rate of a few hundred μs, and of isolated pulses with a rise time of about 100 ns and a typical rate of a few ms.

The experiment was reproduced in 1988 without the ground weather radar support. 17 lightning strikes were obtained between 10 000 ft and 20 000 ft. Table 2 below shows the number of events versus the altitude and the local temperature.

N° of flashes	Temperature	Altitude
1	*-4°C*	*10 000 ft*
5	*-5°C*	*14 000 ft*
4	*-10°C*	*14 000 ft*
3	*0°C*	*15 000 ft*
1	*-10°C*	*19 000 ft*
3	*-12 °C*	*20 000 ft*

Table 2 – C160 aircraft 1988 campaign. Number of flashes versus altitude and temperature

Phenomenology of lightning strikes to aircraft

Initiation of a lightning strike

The description of the physical processes involved in the first phase of the initiation of a lightning strike is an important step in the understanding of the phenomenology of the event. The design of the instrumentation of the experimental aircraft was oriented toward the observation of large magnitude electromagnetic signals and bright optical phenomena. Low currents associated with the onset of discharge were not easily detected. Also, the faint luminosity of the streamer and leader approaching to, or merging from the aircraft cannot be detected by the video camera installed onboard. The most sensitive parameter available for the observation of the initiation of a lighting strike is the electric field variation (or its time derivative), measured over the aircraft surface.

The fast electric field variation on the surface is produced either by the fast charging of the aircraft, or by displacement of conductive elements from, or close to the aircraft, in the ambient atmospheric electrical field. A similarity was observed between the signals measured on the CV580, C160 and F106B. The interpretation of these measurements in terms of lightning phenomenology referred to lightning flashes “triggered” by the aircraft or “interception” by the aircraft of a natural lightning flash channel.

Atmospheric field and aircraft net charge prior to the initiation of the flash

Analyses of the DC field measurements are presented in documents [20] for the campaigns performed on the C160 and CV580. The atmospheric field is obtained before and after the lightning strike, because the

uniform field concept is not valid when the aircraft is connected to lightning channels. It is shown that the transversal, longitudinal or vertical components of the atmospheric field may or may not be permanently affected by the lightning strike, depending on the position of the aircraft versus the electric structure of the charged cloud inside which the lightning flash propagates. When an aircraft is submitted to a high electrostatic field, its net charge is determined by the value and orientation of the field and by the shape of the aircraft surface, from which corona discharges are emitted. This behavior is evidenced in [20], by considering the variation of the aircraft net potential produced by the large permanent field variation due to a nearby natural lightning flash.

The aircraft net charge is found to be negative prior to lightning ignition. The mean net charge before a lightning strike was respectively -0.64 mC and -1.2 mC on the CV580 and C160. This is consistent with a scenario of initial positive corona or leader emission. This observed negative net charge is not necessarily an obstacle to the ignition of positive discharge from the aircraft. It can be interpreted as an initial process of the positive corona emission, which may be followed by the full development of a positive leader. It is not clear whether this net charge can facilitate the lightning strike occurrence or not, but it is worth considering that the electrical energy made available by the net charge is small, 276 J and 720 J respectively, on the CV580 and C160, keeping in mind that 500 J is the electrostatic energy of a 50 m^3 area where a 30 kV/m uniform atmospheric field is applied. Table 3 from [32] shows the mean electrostatic configuration before a lightning strike.

CV580				
	Average	Standard deviation	min	max
Q (mC)	*-0.66*	*± 0.25*	*-1.11*	*-0.23*
Es (kV/m)	*51*	*± 19*	*25*	*87*
Es/p (kV/m/bar)	*92*	*± 39*	*32*	*172*
C160				
	Average	Standard deviation	min	max
Q (mC)	*-1.2*	*± 0.75*	*-1.94*	*-0.84*
Es (kV/m)	*59*	*± 11*	*44*	*75*
Es/p (kV/m/bar)	*104*	*± 19*	*77*	*131*

Table 3 – Ambient field and aircraft net charge just before a lightning strike to an aircraft - from [30]

The average mean field magnitude is similar for the two aircraft. Es/p is the ratio of the Atmospheric field over the local pressure. This parameter determines the behavior of the discharge propagating from an aircraft [32], [33], [34]. The reduced field in the aircraft vicinity at the onset of the lightning strike is close to 100 kV/m/bar; this corresponds to an atmospheric field of 100 kV/m close to the ground and close to 48 kV/m at an altitude of 6 000 m (~20 000 ft). The atmospheric field magnitude close to, or exceeding, 50 kV/m is commonly observed in the vicinity of, or inside, mature storm clouds [35], [36],[37], [38].

The aircraft triggering process

As mentioned above, the ignition processes are identified by the signature of the first fast E field signals measured on the aircraft. Two classes of signature have been observed. The first one consists in a fast and continuous decrease of the electric field at the aircraft surface, lasting a few milliseconds. In [39] [40], such a signature was reported as the first signals observed during a lightning flash ignition on the C160 aircraft. In figure 7a from [39], similar field excursions are recorded at five different locations on the aircraft. The magnitude of the field increases during about 2.5ms, before a sharper decrease and inversion. In figure 7b from [39], the detailed evolution of a field variation of the same event compared to the current collected at the C160 nose boom shows that the decrease in the field excursion starts simultaneously with the onset of the first pulses of current. An inversion of the electric field excursion occurs when the stepping current is no longer visible and a continuous current of a few hundred amps in magnitude is established.

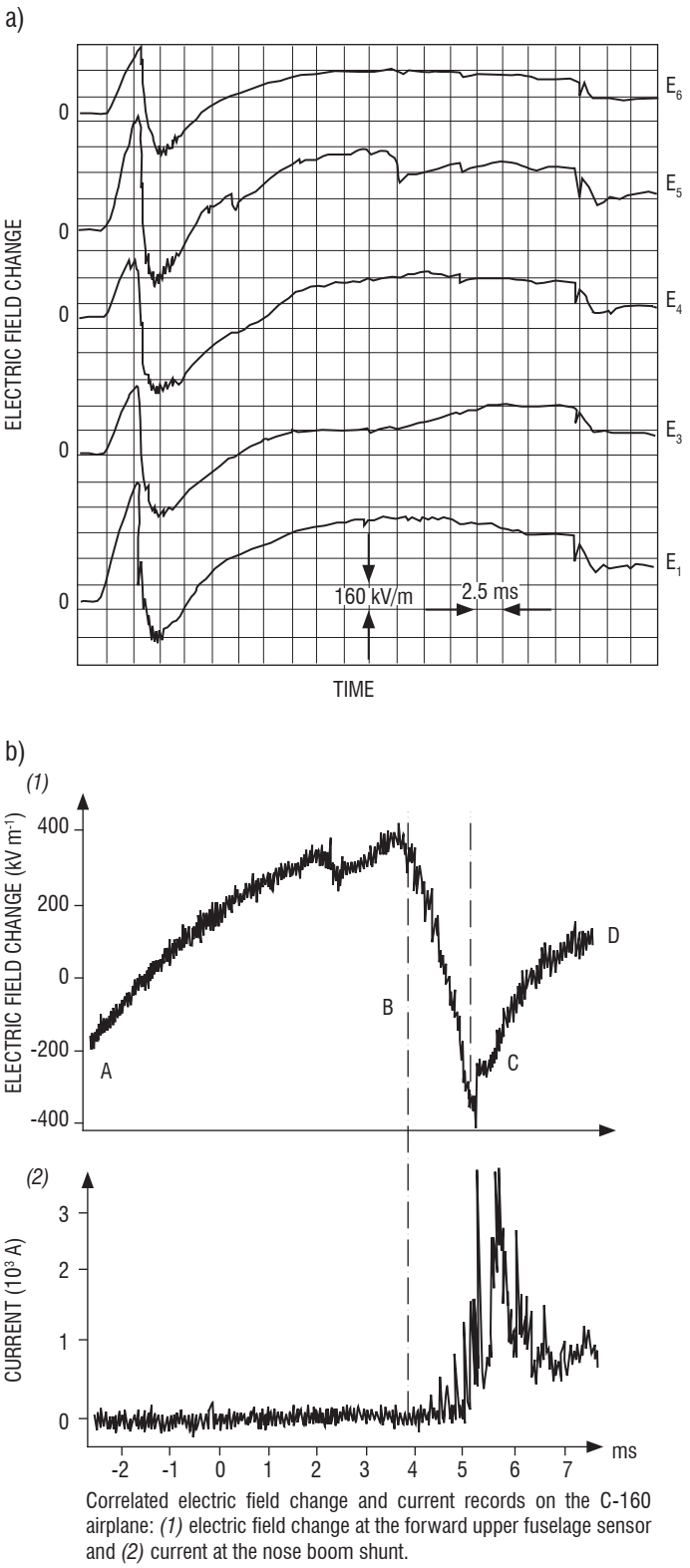

Correlated electric field change and current records on the C-160 airplane: *(1)* electric field change at the forward upper fuselage sensor and *(2)* current at the nose boom shunt.

Figure 7 – Lightning initiation - Typical 1st large E field signal on the C160 aircraft -from [39]

Similar surface E field variations are observed on the CV580 aircraft during the initiation phase of a lightning strike. The electric field waveforms observed on the Convair aircraft are presented and described in [29] and [24]. Figure 8 from [29] shows such a field variation. If we compare this signal with the signals recorded on the Transall aircraft (figure 7), it appears that not only the waveforms are similar but both the duration to peak and magnitude are comparable (3 to 5 ms and few hundred kV/m). For the F106 Aircraft. which is quite a different type of aircraft, similarity with the initial E field variation are pointed out in [40]. In figure 9 from [40], it is explained that an initial positive variation of the field would be due to the onset of a negative corona, which would be faint enough to produce low current pulses not detectable by the measuring shunt or the I dot sensor. This first signal is followed by a negative variation of the field, lasting about 0.5 ms. The signal on the F106B is, since this phase, similar to the first E field variation recorded for the CV580 (figure 8) and for the C160 (figure 7). The third step of this initiation phase is also similar for the 3 aircraft and corresponds to the occurrence of current pulses in bright channels. According to [40] the few hundred amp pulses are emitted by a negative stepped leader merging from a high negative field area of the aircraft; this negative current produces a continuous positive variation of the electric field on the aircraft, which is explained by the author as corresponding to a variation of the potential (modification of the net charge of the aircraft).

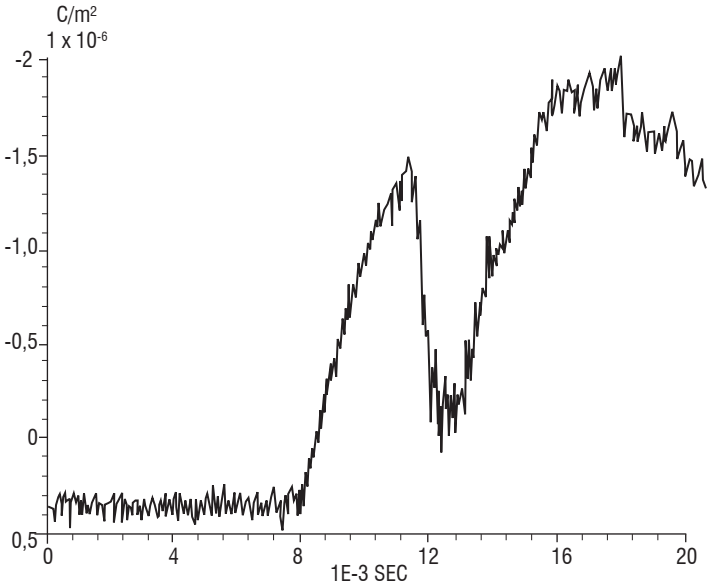

Figure 8 – Lightning initiation. Typical 1st large E field signal on the CV580 aircraft - from [29]

Interpretation of measurements on the three instrumented aircraft lead to the same description of the phenomenology of lightning strike ignition. When the atmospheric electric field is large enough, a positive leader merges from the aircraft. A negative charge is induced on the aircraft, so that the entire system – the aircraft and the positive leader – remains electrically neutral. Increasing the aircraft negative charge makes possible the onset from the aircraft of a negative stepped leader, propagating from the aircraft in the opposite direction. The observations are consistent with the physical differences in the behavior of the positive leader and negative leader [33], [34]. Positive leader propagation initiates at a speed of a few 10^4 m/s and involves a typical current of few amps; the propagation is continuous and becomes pulsed when the leader accelerates to a speed of a few 10^5 m/s. The negative leader is highly stepped and exhibits isolated pulses of a few hundred amps at an initial rate of a few hundred μs. This scenario, which corresponds to about 90 % of the observations made on the CV580 and C160, is illustrated in figure 10. It consists in the development of a bileader discharge, propagating freely from the aircraft in an area where a high electrical atmospheric field is present, inside or outside of a storm cloud.

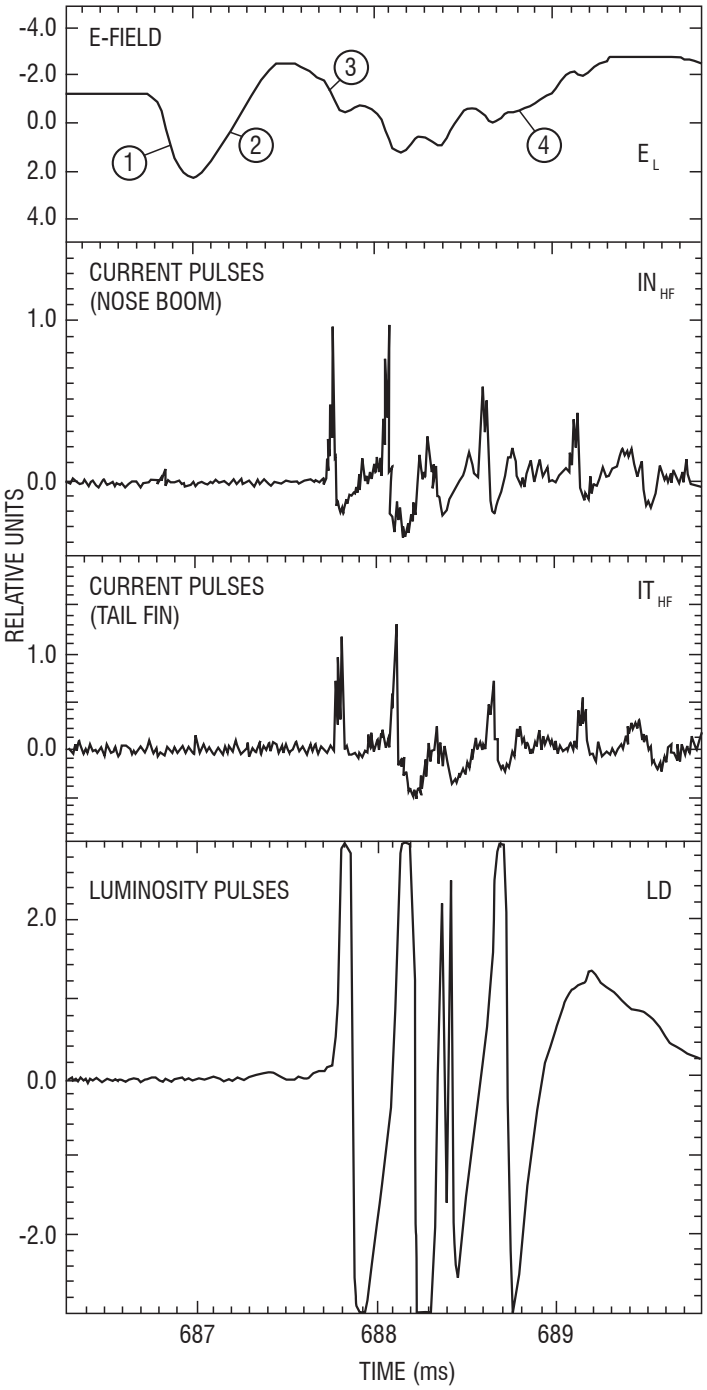

Figure 9 – Initial lightning strike signal on the F106B - Fast field mill measurement - from figure 7 of [40]

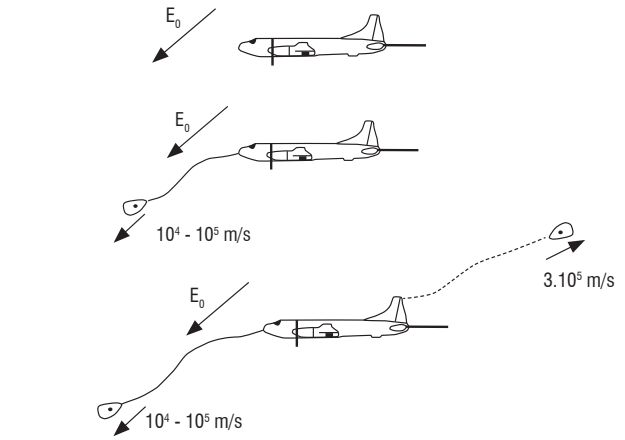

Figure 10 – Lightning triggering scenario. E_0 is the ambient atmospheric electric field. A positive leader merges from the front part of the aircraft and propagates in the direction of the atmospheric field. It induces a negative charge on the aircraft, increasing the local field on the rear part of the aircraft, from which a negative leader starts its propagation. The total charge of the positive leader, the negative leader and the aircraft is neutral.

This scenario, assuming an early emission of a positive leader from the aircraft, had been successfully confirmed by a numerical simulation applied to the data of an actual lightning strike to the Transall aircraft [41]. Computation performed on a 3D mesh of the aircraft and of the lightning channel showed a good correspondence between the E field measurement at 8 locations on the aircraft and the simulation results (figure 11).

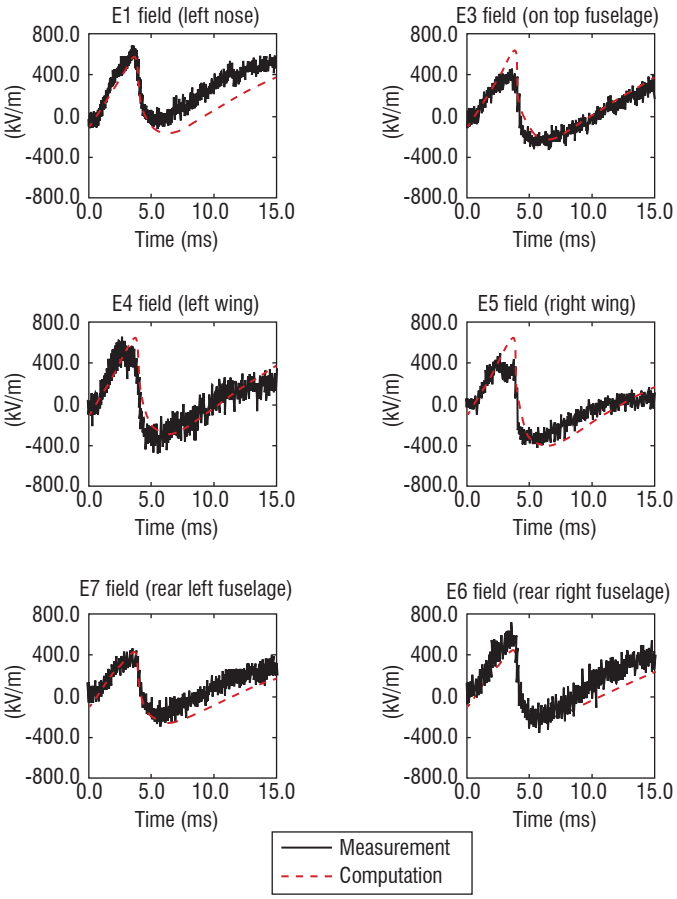

Figure 11 – Lightning initiation on the Transall aircraft: comparison between computation and measurement for the electric field variation at each measuring site on the C160 aircraft. The measurement is shown in black and the computation is in red. E1 to E6 refer to the measuring sites (see figure 5) - from [41]

The lightning channel connection process

The second type of waveform signature of the first large field variation on an aircraft struck by lightning observed on the C160 and CV580 was reported in [24] and [39]. These waveforms are commonly referred to as the "lightning interception" signature. In figure 12 from [24], an example is given of four categories of this type of waveform observed on the forward part of the CV580 fuselage. Differences with the first type of waveform discussed in the preceding chapter are evidenced in the very first part of the four signals, by the continuous increase of the field on the aircraft, which may be attributed to the approach of a negatively charged channel. The continuous evolutions are interrupted by a sharp field variation, which may be produced by a connecting breakdown discharge. The magnitude of the three signals is similar. By a detailed analysis of the available signal, the authors of Article [24] were able to convincingly describe the phenomenology as corresponding with the interception of an approaching negative leader. Similar waveforms were observed on the C160 aircraft. In figure 13 from [39], which shows two fast electric field variations measured on the forward and rear part of the Transall fuselage, it appears even more clearly that the field variation on the aircraft corresponds to an electrical polarization produced by an approaching lightning channel. The scenario is illustrated in figure 14; it involves a bileader propagation from the aircraft, triggered by an approaching lightning channel that becomes connected to the aircraft at the end of this initial process.

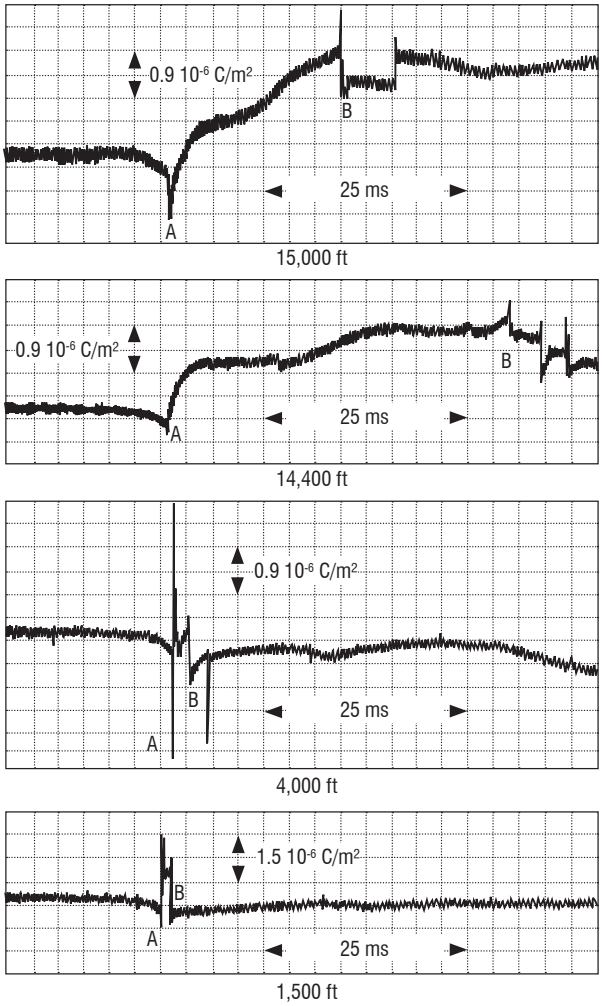

Figure 12 – Electric induction signal (proportional to the electric field) measured on the front part of the CV580 fuselage for the 4 observed categories of lightning interception by aircraft (from figure 13 of [24])

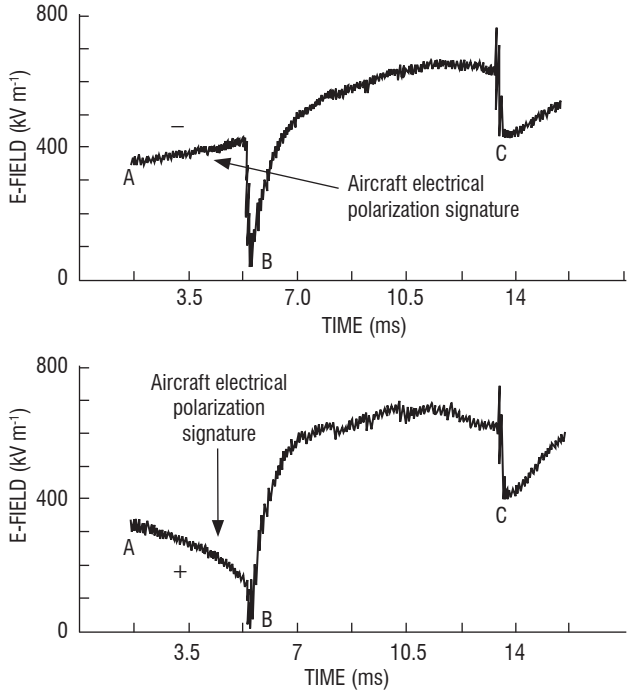

Figure 13 – Interception of a lightning flash channel by the C160 aircraft (from figure 13 of [39])

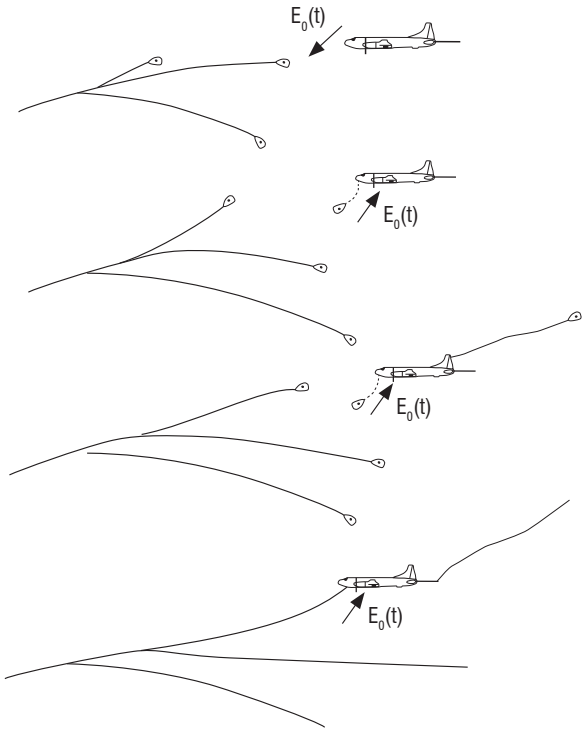

Figure 14 – Scenario of the "interception" of a lightning positive leader by the aircraft

Development of the lightning flash

After the initiation phase, the development of the entire lightning flash continues. The aircraft is connected to a kilometer long lightning channel, as illustrated in the actual airliner lightning strike of figure 1. It is highly probable that the behavior of the lightning flash is no longer influenced by the aircraft itself, but is rather determined by the storm cloud characteristics. Either "triggered" or "intercepted", the flash behaves as a natural flash. Two main phases can be observed on the aircraft.

The sweeping process consists in the displacement of the root of a lightning channel over the aircraft surface, produced by a combined effect of the aerodynamic forces due to the aircraft displacement and the electrodynamic behavior of the lightning channel. Figure 15 shows the sweeping of the lightning channel from the nose boom to the rear boom of the Transall aircraft. It has been observed that the mean speed of the sweeping process is close to the aircraft airspeed but the sweeping process is not always continuous; depending on the nature of the material and the state of the surface, the arc channel stays attached and propagates by step as a result of the combined effect of the aerodynamics and of the occurrence of the electrical breakdown between the arc and the aircraft surfaces. This dwelling effect is indicated by the traces left on the aircraft surface, the spatial period of the stepping on the aircraft being of a few tens of centimeters. The sweeping process occurs during the continuous current process of the lightning flash; it consists in the flow of a continuous current of few hundred amps in the lightning channel connected to the aircraft. An analysis of the C160 and CV 580 direct lightning strike data give a mean continuous current of 330A (σ 285 A, min 100 A, max 1.2 kA) for a mean duration of 188ms (σ 156 ms, min 34 ms, max 510 ms) [32]. The magnitude and duration of this continuous current phase is similar to that observed for natural lightning.

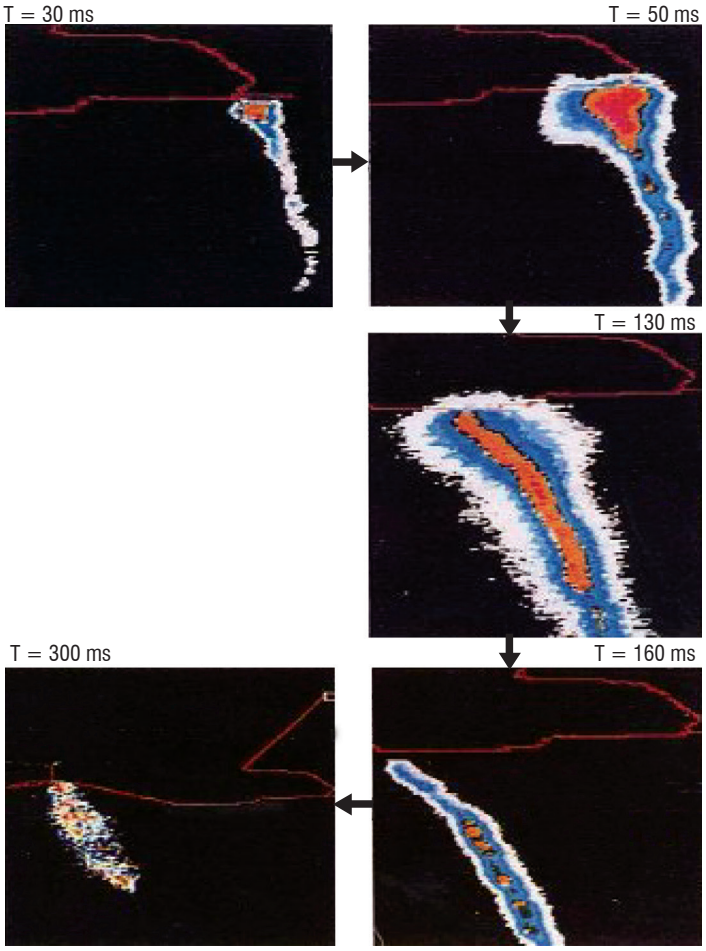

Figure 15 – Lightning channel sweeping from nose to tail on the C160 aircraft. Relative light intensity is color coded

Recoil processes occur during the continuous current process and may continue after the continuous current cutoff. They consist of a fast recoil process (a few 10^7 m/s) propagating within the traces of the lightning flash leaders and connecting directly to the aircraft or, more commonly, connecting to the continuous current channel and propagating through

this highly conductive arc channel toward the aircraft. Referred to the general phenomenology of a natural lightning flash, these recoil processes are subsequent or first return stroke propagating down to the ground, dart leader, recoil streamer or M change process (connection to an active lightning channel) [43]. When the connection is established, a large current pulse is injected into the aircraft. The place of the impact depends on the progression of the sweeping process. Consequently, direct measurement of this current pulse on the instrumented aircraft is often not possible because it occurs when the lightning arc has already swept away from the measuring boom. In any case, the evaluation of the magnitude of the pulse is possible through the magnetic field variation produced at the various measuring sites on the fuselage.

Several lightning strikes on the CV580 aircraft were produced by lightning flashes observed with a ground measuring network [24]. It was therefore possible to identify which flash component produced what current pulse on the aircraft. In figure 16 from [24] two current pulses produced by a first return stroke of a negative cloud-to-ground flash are shown. The rise time is few hundred ns and the wave shape and the decay time is typical of a 1st return stroke, but the magnitude measured at the tail boom was only 3 kA. In figure 17 from [24], current pulses attributed to the dart leader and subsequent return stroke during the same event are shown. The rise time of the subsequent stroke is of a few μs, much longer than the typical initial rise time for such an event. Apparently, the fastest current signal recorded on the aircraft may be produced by a local breakdown process and not by a propagating current wave. In [32], analyses of 43 events on the CV580 and C160 indicate that the mean number of high current pulses per event was 15 and the maximum directly measured current is 20 kA. The time interval between pulses ranges from 10 ms to 300 ms. These values are typical of the interstroke interval for natural lightning.

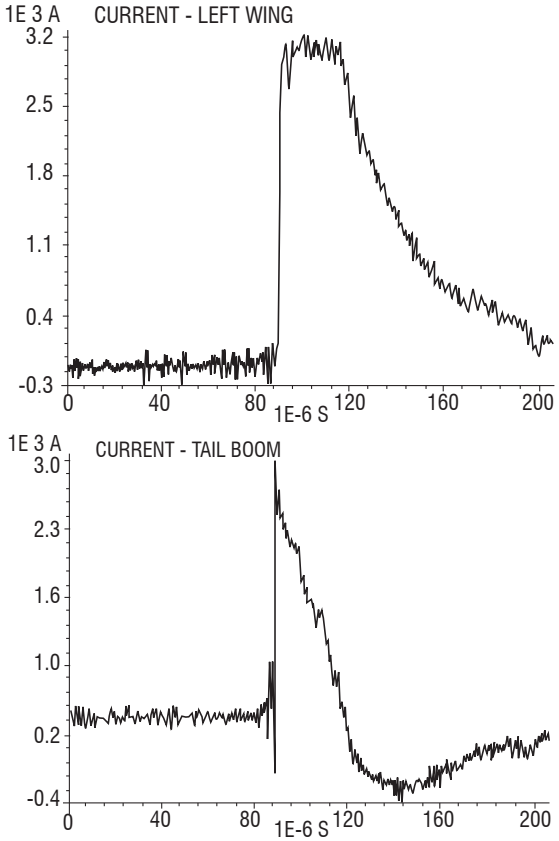

Figure 16 – 1st return stroke connection on the CV580 from [24]. The current signal on the left wing sensor is saturated

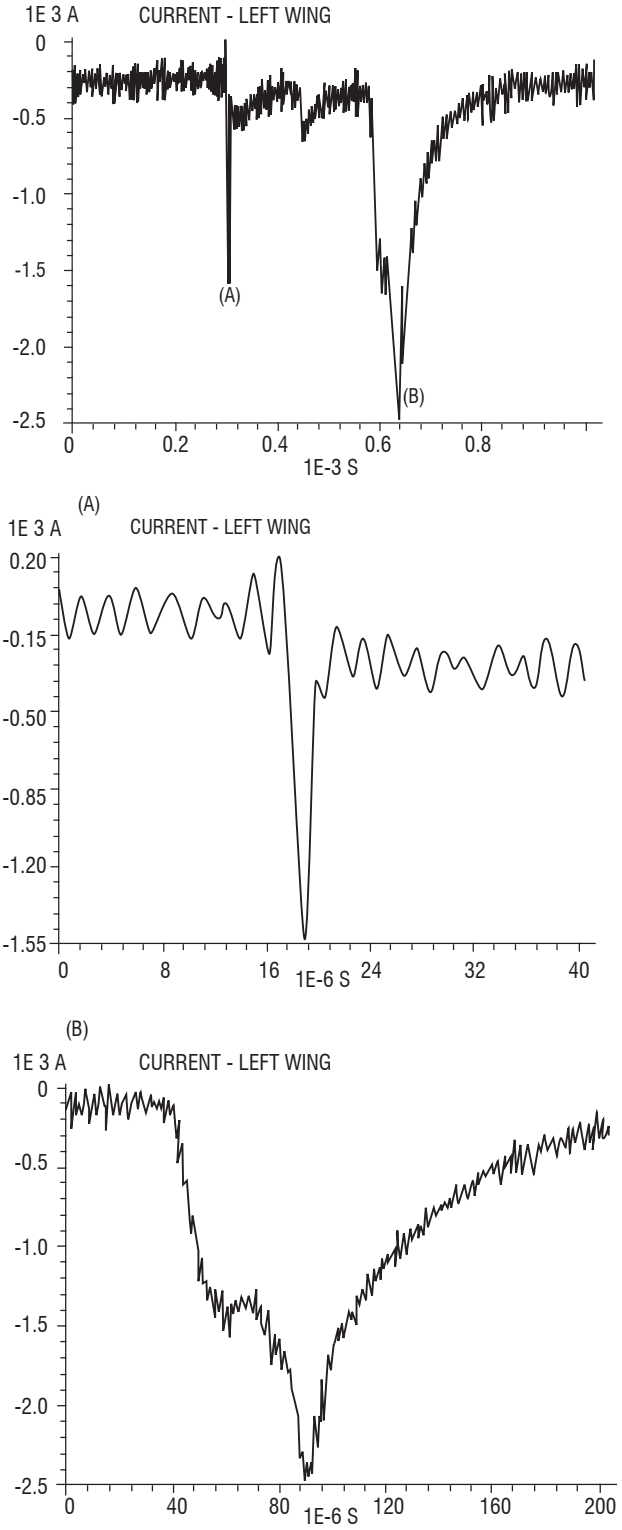

Figure 17 – Dart leader (A) and subsequent stroke (B) connection on the CV580 aircraft (from [24])

Typical profile of a lightning strike to aircraft

The data collected during the experiments conducted with the three instrumented aircraft make possible the definition of an "identikit picture" of the lightning threat to aircraft (figure 18 from [32]). The typical sequence is the following:

- a continuous current of about 1 A lasting a few ms, produced by a merging positive leader;

• a train of 10 pulses lasting 3 ms at a repetition rate of 250 μs and with a peak amplitude of 850 A, produced by a merging negative stepped leader;

• a continuous current sequence lasting 200 ms and with 330 A magnitude;

• a train of 15 large current pulses occurring during or after the continuous current, with a repetition rate of a few tens of ms.

The greatest threat to aircraft comes from the continuous current sequence and from a large current pulse train. Because of the limited amount of data available, a statistically representative distribution of the magnitude of large current pulses cannot be derived from the in-flight direct lightning experiment.

Summary

Three major in-flight lightning strike experiments were conducted during the same period (1980-1986) in the USA and Europe with three different aircraft. These campaigns engaged important efforts in logistics and state of the art instrumentation. Significant ground measurements were gathered to support and document the data collected on board. The motivation for these experiments was similar. It was mainly with the concern of using new technologies, such as the extensive use of composite material on aircraft fuselage and wings and the setting up of “fly by wire” technologies. The justification of the high level of threat imposed by the Standard and Certification process was also a concern. A database of actual in-flight lightning strike parameters was also needed. In particular, the effort in the CV580 campaign was to obtain information on the interaction between the aircraft and the largest component of a Cloud-to-Ground Flash. However, despite many attempts to be struck at low level, at or below 4 000 ft AMSL, no direct interaction with a large Return Stroke process was obtained. The largest recorded current was 24 kA for a lightning event that occurred above 14 000 ft. The electromagnetic threat imposed by the lightning flash was in the limited frequency range of the lightning phenomena, from a few kHz up to a few tens of MHz. No high level very high frequency threat was encountered during the in-flight experiment. The important outcome of these lightning flight experiments is a detailed and comprehensive demonstration of the process of initiation of a lightning flash on an aircraft. In a large majority of the events observed on the instrumented aircraft, the aircraft itself triggers the lightning flash when flying in a high atmospheric electrostatic field area (50 kV/m and above) by initiating the propagation of a bi-directional positive and negative discharge (about 90 % of the cases).

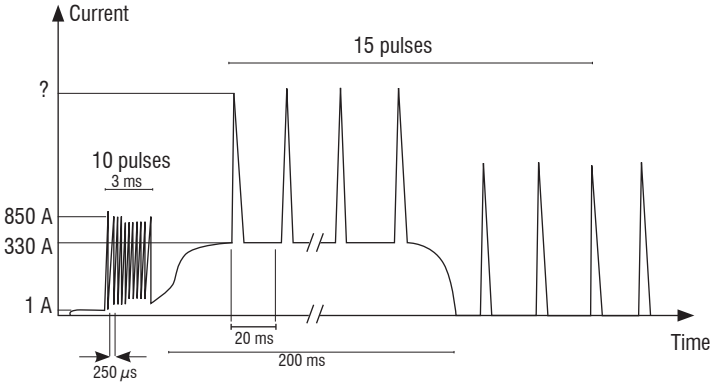

Figure 18 – Typical average current waveform deduced from the in-flight experiments conducted on the CV580 and C160 aircraft - from figure 1 of [32]

Large current threats were not observed in flight. In any case, real life experiences have shown that aircraft can be struck by large first return stroke current pulses when taxiing, or during takeoff and landing [42].

In-flight lightning experiments were performed close to 30 years ago, on vintage turboprop aircraft. Modern jet airliners are extensively made of Carbon Fiber Composite material and their electrical design is totally different. Certification rules again lightning threats are basically identical to those applied in the 1980s. Experiments on modern jet airliners would certainly contribute new information on the effect of high current return stroke and recoil leader processes on composite aircraft ■

References

[1] *Wing Failure of Boeing 747-131 Near Madrid Spain May 9, 1976.* Report n° NTSB-AAR-78-12.
[2] *Aircraft Accident Report, Boeing 707-12, N709PA Pan American World Airways, Inc, Near Elkton, Maryland, Dec. 8, 1963*. Civil Aeronautic Board File n° 1-0015, http://en.wikipedia.org/wiki/Pan_Am_Flight_214, 1965.
[3] D. R. FITZGERALD – *Probable Aircraft "Triggering" of Lightning in Certain Thunderstorms.* Monthly Weather Review, vol. 95, n° 12, pp. 935-842, 1967.
[4] D.W. CLIFFORD – *Aircraft Mishap Experience from Atmospheric Electricity Hazards.* In NATO AGARD Lecture Series, n°110, paper n°2, 1980.
[5] F. A. FISHER, A. PLUMER and R. PERALA – *Lightning Protection of Aircraft.* Lightning Technologies Inc. Second Printing, 1999.
[6] Y. MUROOKA – *A Survey of Lighting Interaction with Aircraft in Japan.* Res Lett Atmos Electricity, 1992.
[7] K. MICHIMOTO – *Statistics of Lightning Strikes to Aircraft in Winter around Komatsu Airbase, Japan*. Journal of Atmospheric Electricity, vol. 13, pp.47-58, 1993.
[8] T. SUZUKI, Y. MATSUDO, T. ASANO, M. HAYAKAWA and K. MICHIMOTO – *Meteorological and Electrical Aspects of Several Winter Thunderstorms with Sprites in the Hokuriku Area of Japan*. JGR, vol. 116, 2011.
[9] R. ANDERSON and H. KRONINGER – *Lightning Phenomena in the Aerospace Environment .Part II: Lightning Strikes to Aircraft.* Transaction of South Africa Institute of Electrical Engineering, n° 66, pp. 166-175, 1975.
[10] M. R. VILE and C. C. R. JONES – *Fulmen Analysis of Experimental Data and Models for Upgraded Lightning Protection Requirements: Lightning Ground Strikes, in-Service Strikes to Aircraft and Induced Pulse Threats Databases.* Report AI-95-SC.204/RE-101-BAe European Transport R&T DGVII, 1997.
[11] K. FUMIAKI, S. TAKATSUGU and M. KAZUTOSHI – *Aircraft Triggered Lightning Caused by Winter Thunderclouds in the Hokuriku Coast, Japan – A case Study of a Lightning Strike to Aircraft below the Cloud Base*. SOLA, vol. 3, pp. 109-112, 2007.
[12] P. LAROCHE – *Airborne Measurements of Electrical Atmospheric Field Produced by Convective Clouds.* Revue de Physique Appliquée, n° 21, pp. 809-815, 1986.
[13] D. M. MACH and W. J.K OSHAK – *General Matrix Inversion Technique for the Calibration of Electric Field Sensor Arrays on Aircraft Platforms.* J. of Atmospheric and Oceanic Technology, vol. 24, pp. 1576-1587, 2007.
[14] W. J. KOSHAK – *Retrieving Storm Electric Fields from Aircraft Field Mill Data. Part I:Theory.* J. of Atmospheric and Oceanic Technology, vol. 23, pp. 1289-1302, 2006.
[15] W. J. KOSHAK, D. M. MACH, H. J.CHRISTIAN, M. F. STEWART and M. G. BATEMAN – *Retrieving Storm Electric Fields from Aircraft Field Mill Data. Part II: Applications*. J. of Atmospheric and Oceanic Technology, vol. 23, pp. 1303-1322, 2006.
[16] J. E. NANEVICZ, R. C. ADAMO and R. T. BLY Jr. – *Airborne Measurement of Electromagnetic Environment near Thunderstorm Cells (TRIP 76).* SRI Report, 1977.
[17] R. V. ANDERSON and J. C.BAILEY – *Vector Electric Fields Measured in a Lightning Environment*. NRL Memorandum Report 5899, 1987.
[18] J. E. DYE, M. G. BATEMAN, H. J. CHRISTIAN, E. DEFER, C. A. GRAINGER, W. D. HALL, E. P. KRIDER, S. A. LEWIS, D. M. MACH, F. J. MERCERET, J. C. WILLETT and P. T. WILLIS – *Electric Fields, Cloud Microphysics, and Reflectivity in Anvils of Florida Thunderstorms.* JGR, vol. 112, D11215, 2007.
[19] K. L.GIORI and J. E. NANEVICZ – *Airborne Observations of Electric Fields Around Growing and Decaying Cumulus Clouds.* ICOLSE NASA Conf Pub 3106, vol. 1, pp. 19-1,19-10, 1991.
[20] P. LAROCHE, A. DELANNOY and H. LE COURT DE BERU – *Electrostatic Field Conditions on an Aircraft Striken by Lightning*. Int Conf On Lightning and Static electricity, Onera TP n° 1989-148, 1989.
[21] F. L. PITTS, G. B. FINELLI, R. A. PERALA and T. H.RUDOLPH – *F-106 Data Summary and Model Results Relative to Threat Criteria and Protection Design Analysis,* ICOLSE, pp. 5-1,5-20, 1986.
[22] F. L. PITTS – *Electromagnetic Measurement of Lightning Strikes to Aircraft.* J. Aircraft, vol. 19, n° 3, 1981.
[23] P. L. RUSTAN Jr. – *The Lightning Threat to Aerospace Vehicles.* J. Aircraft, vol. 23, n°1, pp. 62-67, 1986.
[24] H. D. BURKET, L. C. WALKO, J. REAZER, A. SERRANO – *In-Flight Lightning Characterization Program on a CV-580 Aircraft*. AFWAL-TR-88-3024, 1988.
[25] P. GONDOT, A. DELANNOY and P. BLANCHET – *In-Flight Conductivity Measurements in Convective Clouds Onera.* ICOLSE TP n° 1988-63, 1988.
[26] P. GONDOT – *Definition et exploitation de capteurs adaptés à la mesure de la conductivité électrique dans les nuages d'orage*. Thesis Paris 6 University, 1985.
[27] V. MAZUR, B. D. FISHER and J. C. GERLACH – *Lightning Strikes to a NASA Airplane Penetrating Thunderstorms at Low Altitudes.* J. Aircraft, vol. 23, n° 6 pp. 499-505, 1986.
[28] P. L. RUSTAN, B. KUHLMAN, J. SHOVALTER and J. REAZER – *Electromagnetic Measurements of Lightning Attachment to Aircraft.* ICOLSE DOT/FAA/CT-83/25, pp. 45-1, 45-8, 1983.
[29] J. S. REAZER, A. V. SERRANO, L. C. WALKO and H. D. BURKET – *Analysis of Correlated Electromagnetic Fields and Current Pulses During Airborne Lightning Attachments.* Electromagnetics, n° 7, pp. 209-539, 1987.
[30] P. LAROCHE, M. DILL, J. F. GAYET and M. FRIEDLANDER – *In Flight Thunderstorm Environmental Measurement during the LANDES 84 Campaign.* 10th ICOLSE, pp 59-66, 1985.
[31] J. P. MOREAU and J. C. ALLIOT – *E and H Field Measurement on the Transall C160 Aircraft during Lightning Flashes.* 10th ICOLSE, pp 281-287, 1985.
[32] P. LALANDE, A. BONDIOU-CLERGERIE and P. LAROCHE – *Analysis of Available In-Flight Measurements of Lightning Strikes To Aircraft.* ICOLSE Toulouse, 1999.
[33] P. LALANDE and V. MAZUR – *A Physical Model of Branching in Upward Leader.* Aerospace Lab Issue 5, December 2012.
[34] P. LALANDE, A. BONDIOU-CLERGERIE, G. BACCHIEGA and I. GALLIMBERTI – *Observations and Modelling of Lightning Leaders*. CR Physique, vol. 3, n° 10, pp. 1375-1392, 2002.
[35] W. P. WINN and C. B. MOORE – *Electric Field Measurements in Thunderclouds Using Instrumented Rockets.* JGR, vol. 76, n° D21, pp. 5003-5017, 1971.
[36] M. STOLZENBURG and T. MARSHALL – *Serial Soundings of Electric Field Through a Mesoscale Convective System*. JGR, vol. 106, n° D12, pp. 12371-12380, 2001.
[37] T. MARSHALL and M. STOLZENBURG – *Voltages inside and just above Thunderstorms.* JGR, vol. 106, n° D5, pp. 4757-4768, 2001.
[38] R. GUNN – *Electric Field Intensity Inside of Natural Clouds.* Journal of Applied Physics, vol. 19, pp. 481-484, 1948.
[39] J. P. MOREAU, J. C. ALLIOT and V. MAZUR – *Aircraft Lightning Initiation and Interception from in situ Electric Measurements and Fast Video Observations.* JGR, vol. 97, n° D14, pp. 15903-15912, 1992.
[40] V. MAZUR – *A physical Model of Lightning Initiation on Aircraft in thunderstorms.* JGR, vol. 94, n° D3, pp. 3326-3340, 1989.
[41] A. BONDIOU-CLERGERIE et P. LALANDE – *Modélisation de l'initiation d'un éclair sur un avion en vol*. SEE, 1997.
[42] B. VONNEGUT – *Effects of a Lightning Discharge on an Aeroplane.* Weather Review, vol. 21, pp. 277-279, 1966.
[43] V. A. RAKOV, R. THOTTAPPILLIL, M. A. UMAN and P. P. BARKER – *Mechanism of the Lightning M Component.* JGR, vol. 100, n° D12, pp. 25701-25710, 1995.

Acronyms

Air Force (US Air Force, USA)
AMSL (Above Mean Sea Level)
DC (Direct Current)
FAA (Federal Aviation Administration, USA)
HF (High Frequency)
NASA (National Aeronautics and Space Administration, USA)
NOAA (National Oceanic and Atmospheric Administration, USA)
NRL (Naval Research Laboratory)
TRIP 76 (Thunderstorm Research International Program)
UK (United Kingdom)

AUTHORS

Pierre Laroche received his engineering degree from the Institut Polytechnique de Grenoble in 1971. He joined The French Aerospace Lab the same year and became involved in triggered lightning experiments in France and the United States of America. His background is in the physics of lightning and atmospheric electricity. He is the author or co-author of more than 100 papers and one book, and has served as co-editor for 2 journals. He was the President of the International Commission on Atmospheric Electricity (IUGG/IAMAS) from 1999 to 2007.

Patrice Blanchet graduated in Physics instrumentation and sensing in 1984. He participates in experimental studies of lightning strike to aircraft, large field experiments with lightning mapper, radar… and experiments to measure the atmospheric electric field with an instrumented rocket. He is also involved in the development of electrostatic sensor for rockets, development of lightning mapper of the electrical activity of the storms based on the detection and the location of the VHF-UHF emission radiated by flashes. Recently a large part of his activity has been the development of electric field sensors of field mill type to instrument an aircraft.

Alain Delannoy † (1951 - 2012) received a PhD in Atmospheric Physic from University PARIS 6 in 1979. He joined Onera in 1980 and was engaged in research on Atmospheric Electricity, Cloud microphysic and Physic of Lightning. His interest focused on in situ electrical measurements in cloud for what he setup specific instrumentations. He was engaged in lightning strike experiment on aircraft. Alain Delannoy was author and co-author of numerous articles and reports on Atmospheric Electricity and Lightning.

François Issac obtained his Technical University Degree (DUT) in physics measurement in 1982, in Montpellier, France. He began working at Ecopol from 1983 to 1986 on lightning effects and he joined the Office National d'Etudes et de Recherches Aérospatiales (Onera) where he became involved in numerous large scale EMC experiments (in-flight lightning tests on a Transall aircraft in 1987-1990; EMPTAC tests on EM Topology, 1993-1996; joint cooperation on mode stirred chambers with DERA, 1999-2000). Nowadays, his field of interest covers a large area, from low frequency to high frequency, mainly from an experimental point of view. He is co-author of numerous papers dealing with EM measurement validations carried out at Onera.

P. Lalande
(Onera)
V. Mazur
(National Severe Storms Laboratory)

E-mail: philippe.lalande@onera.fr

A Physical Model of Branching in Upward Leaders

The physical processes leading to branching and physical factors affecting branching features are poorly understood. We are applying the tested physical model of axisymmetrical leader development following the streamer-leader transition to a 3-dimensional propagation of the leader with branching. The propagation of the leader is driven by the potential drop at the leader tip. The branching occurs when the drop potential at the leader tip reaches a threshold. The space charge around the leaders self regulates the total number of active branches by reducing the available potential for the propagation. The model has been applied to simulate the time evolution of an upward leader started from a tall ground structure and developing in an electric field produced by a mature thunderstorm. We are satisfied with the fact that the results of computer simulation of branching leader closely resemble branching of upward positive leaders triggered by tall structures depicted in high-speed video images.

Introduction

The physical processes that lead to branching, and the physical factors that affect branching features remain among several unresolved issues in our understanding of lightning development. The questions, such as: Under what conditions does the leader start branching? How does the branching form? And how do the neighboring branches interact, and does this interaction lead to the arrest of the propagation of some branches, while others continue to propagate? All these questions come to the mind of an observer who views and analyzes the fascinating high-speed video images of branched leaders.

Some laboratory experiments and field observations have exposed features of branching processes. For example, we know, from studies of discharges developing within a layer charge inserted in plastics [1] that branching channels prefer space charge regions and avoid regions that are free of space charge. A similar conclusion can be drawn from the analysis of maps of lightning radiation sources, obtained with the time-of-arrival technique, that have their highest density within the charge layers of a thundercloud.

Computer models of lightning development that considered induced charges on a leader channel have produced only single, vertical channels of intracloud and negative cloud-to-ground flashes [2], [3]. Lightning branching was introduced in the numerical models of a thunderstorm based on the stochastic dielectric breakdown concept [4], [5]. These fractal models, although applying the equipotential hypothesis by Kasemir [6] to floating leaders, simulated macroscopic behavior of leaders without addressing the internal physical processes involved in leader development. Also, a large space resolution of storm models cannot reproduce the actual sizes of leader cross-sections and the dimensions of leader branching.

The objective of this study is to address the processes of branching first for a unidirectional positive leader, as a less complex type of leader development. We are applying the tested physical model of axisymmetrical leader development following streamer-leader transition to a 3-dimensional propagation of a leader with branching. In the course of creation of the model of a branched leader we define the model's variables and range of those variables that could be confirmed by field observations or measurements. For the computer simulation of the branching leader, we used a simplified model of thunderstorm charges, in order to determine the sensitivity of the branching model to various parameters of the model.

Principles of modeling a straight-propagating upward leader

In modeling the propagation of upward leaders, we applied the principles used in modeling the development of a straight leader, as a non-time-dependent extension of the already-existing leader channel by the streamer-leader transition process, regardless of the mechanism of leader initiation [7]. During the streamer-leader transition, cold streamers, which fan like a cone ahead of the leader tip, produce, in the course of leader extension, a space charge in the form of a cylindrically shaped envelope surrounding the hot plasma channel of the leader. This space charge is stationary, and remains so for a period of time much longer than the lifetime of a lightning flash.

The variables that describe the electrical conditions governing development of the leader, some of which are a function of an altitude, z, are:

- $U_{atm}(z)$ - ambient potential, assumed to be distributed linearly.
- $U_{extr}(z)$ - potential at the leader tip.
- $U_{ce}(z)$ - potential produced by a space charge of corona streamers.
- ΔU_T - potential difference ahead of the tip of the leader, also called "potential drop".
- E_0 - ambient electric field, constant for linear potential distribution.
- E_{int} - internal electric field in a leader channel due to its finite resistivity.
- E_{stab} - stability field, which is an electric field inside the streamer zone, assumed to be 400 kV m^{-1} and 800 kV m^{-1}, for positive [8][9][10] and negative streamers [11], respectively.
- q_{ce} – space charge per unit length generated by the streamer-leader transition (C m^{-1}).

The variables that describe the physical dimensions of the leader are:

- H - height of the structure, from which leader is initiated.
- L - length of the developing leader.
- L_C - length of the streamer zone ahead of the leader.
- a_{ce} - a radius of a space charge envelope surrounding the leader.

The variables that describe the atmospheric conditions along the leader path, and a function of altitude, z, are:

- $P(z)$ - ambient pressure, P_0 is the atmospheric pressure at the ground level.
- $T(z)$ - ambient temperature, T_0=300 K is a normal temperature.
- $\rho(z)$ - air density, $\rho(z) = [P(z)\ T_0] / [P_0\ T(z)]$.

The potential distribution along and immediately ahead of the developing leader is depicted in figure 1. This potential distribution is affected by the presence of the space charge envelope. The magenta line indicates the potential distribution due to the ambient field E_o. The tall structure, from which leader initiates is assumed to be a perfect conductor, and thus on a zero ground potential. The leader is resistive, so its current produces a potential gradient of E_{int}, assumed to be constant. The space charge region ahead of the leader affects longitudinal propagation of the leader, by reducing the electric field at the leader tip. The dotted curve ahead of the leader tip depicts the variation of the potential distribution from the leader tip to the ambient electric field. The potential difference available to sustain the leader propagation is the potential drop ΔU_T at the leader tip, and is expressed by equations 1- 4:

$$\Delta U_T = U_{extr}(H+L) - \left[U_{atm}(H+L) + U_{ce}(H+L)\right] \tag{1}$$

where

$$U_{atm}(H+L) = -E_o(H+L) \tag{2}$$

$$U_{extr}(H+L) = -E_{\text{int}} L \tag{3}$$

$$U_{ce}(H+L) = U_{ce1}(H+L) + U_{ce2}(H+L) \tag{4}$$

U_{ce1} is the potential on the axis due to the space charge, and U_{ce2} is the component due to the image on the ground.

In our simplified model, the space charge is in form of a cylinder of radius ace and of length $L+L_c$, with a uniform charge of linear density q_{ce} and a total charge of $q_{ce}L$. With these assumptions, the two components of the potential due to the space charge have the following expression:

$$U_{ce1} = \frac{q_{ce}L}{4\pi\varepsilon_o a_{ce}^2 (L+L_c)} \times \left[-\left(L^2 + L_c^2\right) + a_{ce}^2 \ln\left[\frac{\sqrt{a_{ce}^2 + L_c^2} + L_c}{\sqrt{a_{ce}^2 + L^2} - L}\right] + L\sqrt{a_{ce}^2 + L^2} + L_c\sqrt{a_{ce}^2 + L_c^2} \right] \tag{5}$$

$$U_{ce2} = -\frac{q_{ce}L}{4\pi\varepsilon_o a_{ce}^2 (L+L_c)} \times \left[(2H+L)^2 - (2H+2L+L_c)^2 + a_{ce}^2 \ln\left[\frac{\sqrt{a_{ce}^2 + (2H+L)^2} - (2H+L)}{\sqrt{a_{ce}^2 + (2H+2L+L_c)^2} - (2H+2L+L_c)}\right] + (2H+2L+L_c)\sqrt{a_{ce}^2 + (2H+2L+L_c)^2} - (2H+L)\sqrt{a_{ce}^2 + (2H+L)^2} \right] \tag{6}$$

The linear charge density of ~50 μC m^{-1} and ~145 μC m^{-1} for a positive and a negative leader, respectively, were derived from laboratory measurements [12][13]. Lalande et al. [7] assumed the value of the radius a_{ce} of the space charge envelope as 0.5 m for leaders of both polarities. In a simplified and consistent physical model [7][12], this value fits the measurements of Willet et al. [14] for a case of a rocket-triggered lightning. The corona length L_c is inferred from the stability field E_{stab} and ΔU_T by the (7):

$$L_c = \frac{\Delta U_T}{E_{STAB}} \tag{7}$$

Electrical discharges are sensitive to air density variation, such as described by Paschen's Law. Lalande [15] shows that, for lightning leaders, the ambient field $E_o(z)$ has to be corrected by the factor , $1/\rho(z)$ in order to take into account the air density variation with altitude.

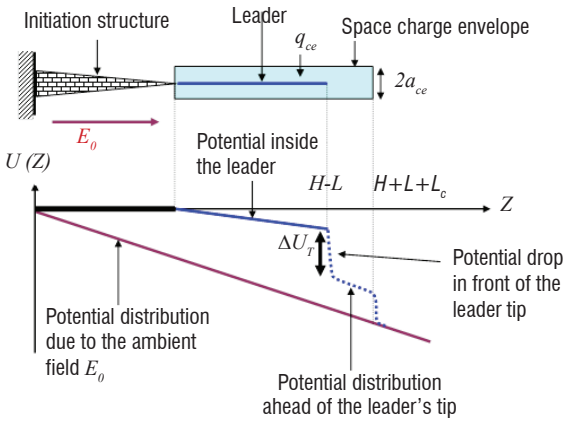

Figure 1 - Longitudinal potential distribution along the path of an upward positive leader developing from a ground structure

Modeling the 3-D propagation of the straight leader in a thunderstorm

For computer simulation of the 3-D leader propagation, we used the electrostatic model of a mature storm [3]. This storm model is represented by four charged cylinders with a constant charge density (figure 2). The vertical potential profile from ground to 1500 m altitude, computed for this model, is in close agreement with the potential profile measured by Willet et al [14] during a rocket-triggered lightning experiment.

Figure 3 depicts the concept of 3-D propagation of a leader segment that is assumed in our model. A new direction of propagation of the leader tip is chosen at each time step, and a new segment of the leader and its associated space charge is added to the preceding segment. In adaptation of the axisymetrical model of the leader to the 3-D development, we replaced the space charge envelopes of the leader segments with the sets of equivalent charge lines. Their effects on the electrical potential are similar to those produced by the space charge envelopes. We use the Boundary Element Method (BEM) that is based on the solving of integral equations to compute the new electrostatic setup and the resulting voltage drop at the leader tip at each time step.

The direction $\overrightarrow{d_{max}}$ is towards the maximum potential drop, which is computed at a distance $2L_C$ from the tip on a sphere centered at the

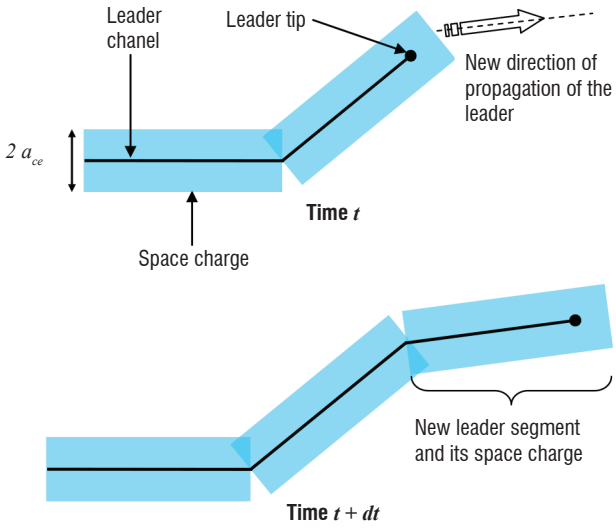

Figure 3 - Depiction of the 3-D propagation of a leader filament in time steps

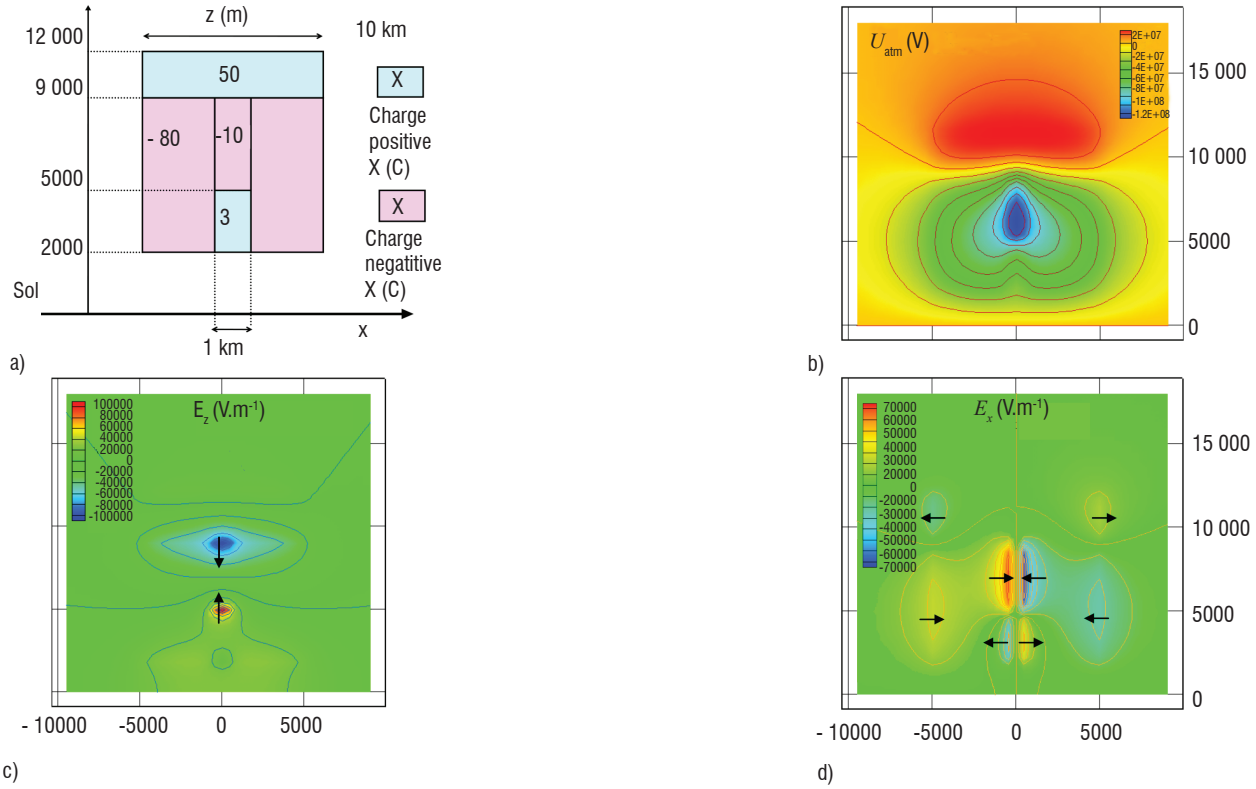

Figure 2 - Vertical slides *(x, y=0, z)* of (a) electric charge distribution inside a mature thundercloud [3], (b) atmospheric potential UATM, (c) vertical component of the atmospheric field *Ez*. and (d) horizontal component of the atmospheric field *Ex*. The black arrows show the direction where the *E*-field intensifies.

leader tip. The computation is not performed at L_c where the effects of both leader and space charge are maximal, but slightly ahead of it, to make it more sensitive to the cloud potential. In choosing the direction of propagation the model takes into account the stochastic character of leader's motion. We assume that the final direction $\vec{d}$ of leader propagation for the angle θ is determined by a Gaussian distribution centered on 0°, with a standard deviation of 45°, and for the angle φ by uniform distribution from 0 to 360° (figure 4).

Leader branching criterion

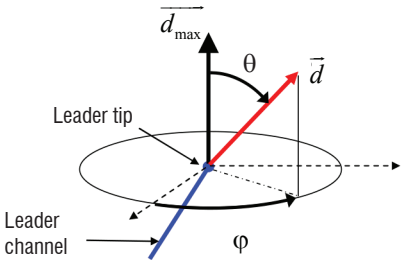

Figure 4 - Choosing the direction of leader propagation $\vec{d}$ at each time step (angles θ, φ). $\vec{d}_{max}$ is the direction where the potential drop between the leader tip and a point at $2L_c$ ahead of the leader is at its maximum.

The most challenging task in modeling branching leaders is to determine the electrostatic criteria for branching. Here is what we learned from studying upward positive leaders starting from tall towers [16]: single-channel upward leaders are triggered either by (1) passing-by negative leaders of intracloud flashes, or (2) by return strokes of positive CG flashes. In the first case, these upward leaders start branching when they approach the cloud base above. It is known that the potential drop ahead of the ascending upward leader is greater near the cloud base than at the ground level. In the second case, the upward leaders branching occurs right from the start (the top of the tall structure), triggered by return strokes of nearby positive CG flashes. Our explanation of the noticed difference in when and where the leader branching starts is as follows: The impact of the electric field change produced by return strokes of $+CG$ flash on the triggering of an upward leader is much greater than that of the intracloud negative leader passing by, due to its much higher current and speed. We interpret the high-speed video observations of branching in positive upward leaders from tall towers referred to here as indicating that branching occurs at rather high electric field changes, and therefore, at the potential drops values that are greater than those needed for development of a single, non-branched leader channel.

We also recognize that branching of the leader may affect the speed of leader propagation, in comparison with that of a non-branching leader, and make such assumption in our model. An empirical formula (8) expresses the relationship between the leader's velocity and the potential drop ahead of the leader ΔU_T, which is the driving force of the leader progression, in relationship to the variable ΔU_B that represents the potential drop required to start branching.

$$V_L = V_{LR\max}\left(1 - e^{\frac{-2|\Delta U_T|}{\Delta U_B}}\right) \quad (8)$$

The variation of the leader's velocity as a function of the potential drop ΔU_T, with ΔU_B being constant, is depicted in figure 5 for different values of V_{LRmax} and ΔU_B.

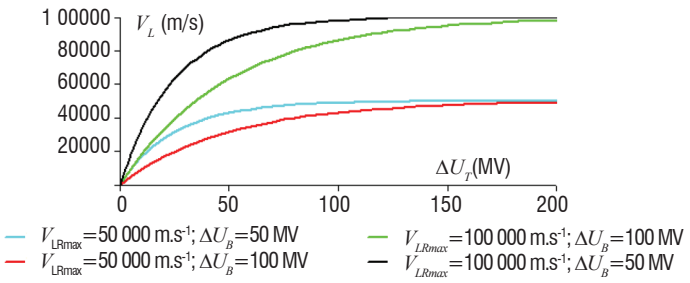

Figure 5 - Evolution of the leader velocity as a function of the potential drop at the leader tip ΔU_T for different values of V_{LRmax} and ΔU_B.

The dynamics of branching for a natural upward leader is seen in figure 6a, for an upward positive leader started from a tall tower. In this example and in numerous others obtained with a high-speed video system, the characteristic feature of branching is the splitting of a single channel into two branches [13]. There is also indication of a prevalent angle between two new branches, the value of which is hard to obtain from the two-dimensional images. In our model, branching also always occurs as the splitting of a single channel into two, after ΔU_T reaches or exceeds ΔU_B (figure 6b). After that, each part of the branch develops as a single channel, with its own velocity, and the possibility of further branching, depending upon the potential drop ΔU_T at its tip .

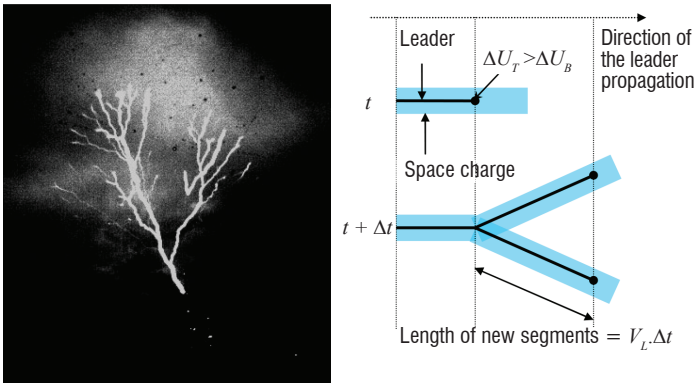

Figure 6 - (a) Composite image of an upward branching leader (courtesy of Tom Warner) and (b) depiction of the branching concept model.

The range of values of the branching criterion ΔU_B is determined from the comparison of 3-dimensional lightning mapping observations, obtained with the Lightning Mapping Array (LMA), with the electric potential profile inferred from balloon soundings of the electric fields in New Mexico mountain thunderstorms [17]. The altitude histogram of the flash radiation sources in figure 7 shows two maxima of radiation source density: at the band of 6 - 7 km, and at the band of 9 - 11 km. These are two bands where leaders propagate horizontally and also branch within. Negative leaders produce much stronger VHF radiation than positive ones. This strong radiation identifies the altitudes of 9-11 km as associated with a negative leader development zone and the altitudes of 6-7 km as associated with positive leader propagations. The bidirectional leader originates at the altitude of ~8 km, and propagates vertically until its upper and lower tips reach 9 and 7 km altitudes, respectively. During its vertical development phase, the leader is in electrostatic equilibrium with the ambient potential

profile (marked by the blue line in figure 7). Assuming that the positive leader starts branching only after reaching the 6 -7 km band, we infer, from the potential profile in figure 7, the corresponding values of the branching potential drop ΔU_B to be in the range of 20 to 50 MV. Adjusted for the air density at these altitudes, the values for ΔU_B at mean sea level would be from 35 MV to 105 MV.

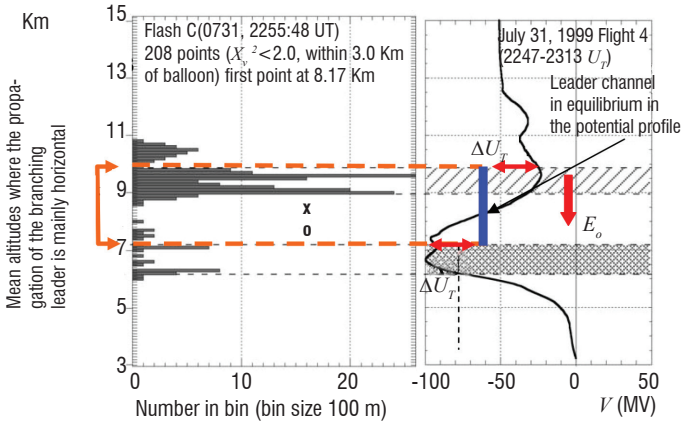

Figure 7 - (a) Altitude histogram of lightning radiation sources. The cross marks the altitude of the first LMA source and the likely location of flash initiation. (b) The vertical potential profile inferred from balloon soundings of the electric field in New Mexico mountain thunderstorms. The circle indicates the altitude of the balloon at the time of the flash [17].

The dotted lines and cross-hatching in the histogram identify the boundaries of the regions with most radiation sources. The upper region is associated with negative polarity leaders and the lower region with positive polarity leaders. The blue vertical line corresponds to the potential of the vertical part of the bidirectional leader channel before it propagates horizontally and branches. The red horizontal bidirectional arrows correspond to the potential drop available at each extremity of the bidirectional leader before the branching process occurs.

Computer simulation of branching in upward leader

Computer simulation of branching was performed for an upward positive leader that started from a tall grounded structure during a mature thunderstorm (see model in figure 2), the vertical potential profile of which is presented in figure 2b. In a thunderstorm with this ambient potential profile, the leader can propagate to a maximum altitude that is slightly below 10 km. However, when conditions for branching exist, the duration of a time step affects the computer simulation of the branching structure. Without branching, there is no influence of the time step on the results of simulation.

With the drop potential ΔU_T equal to or above the branching criteria ΔU_B, the leader splits into two branches. The distance d_{bb} between the two new segments, measured horizontally between tips of branches, depends on the time step, as shown in the following expression:

$$d_{bb} = 2V_L \Delta t \sin\alpha \qquad (9)$$

where α is the angle between the two new segments with a mean value of 45°. The smaller the time step, the smaller the distance d_{bb}. The number of active leader tips (N_{al}) increases following the mathematical law $N_{al} = 2^{\frac{t}{\Delta t}}$, where t is the period of time since the first branching occurs.

When there is no physical limitation in the branching process, the branching structure calculated for three time steps (Δt=0.5 ms, Δt=1 ms, Δt=2 ms) is as shown in figure 9.

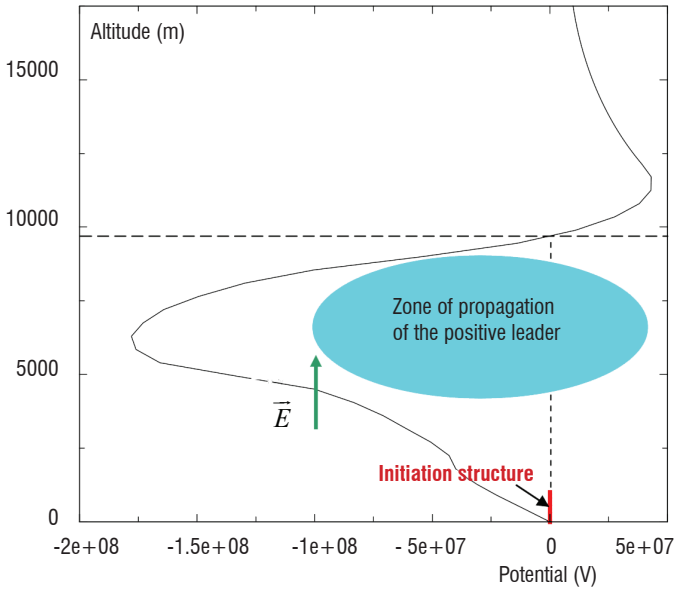

Figure 8 - Vertical ambient potential profile of the mature thunderstorm structure shown in figure 2. The vertical red bar identifies the tall structure from which a positive upward leader develops. The horizontal dashed line indicates the maximum altitude for the positive leader propagation.

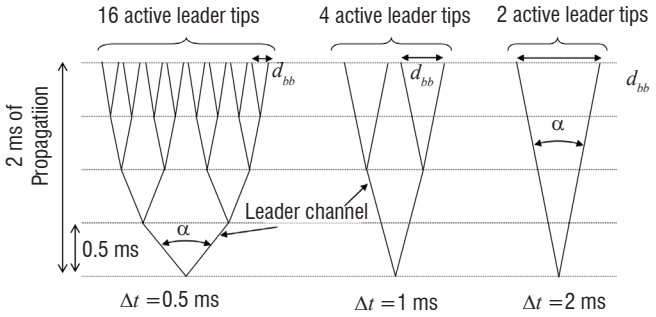

Figure 9 - Depiction of the unrestricted development of branches for three time steps (Δt=0.5 ms, Δt=1 ms, Δt=2 ms) for a 2 ms-long propagation. In this conceptual figure, and also in figure 10, the angle α between branches in all figures is the same, and is shown as different for the illustration purpose only.

In our model, the distance between branches plays a significant role in the leader propagation because of the presence of a space charge envelope of the same polarity on each branch. The drop potential of a neighboring branch may be drastically reduced by the close proximity of the space charge envelope, which may arrest the development of a new branch. The smaller this distance, the greater the screening effects of the space charge of one branch on the potential drop ΔU_T of the other branch. When two new branches are created at each time step, and the distance between the two new leader tips is big enough, both branches can propagate; otherwise one of them stops. In the example shown in figure 10, only two active leader tips remain at the end of 2 ms-long propagation, regardless of the choice of time step. It is also apparent that the larger the space charge per unit length (q_{ce}), the smaller the number of branches produced. Thus, the electrostatic interaction between leader's parts limits the development of new branches in our model.

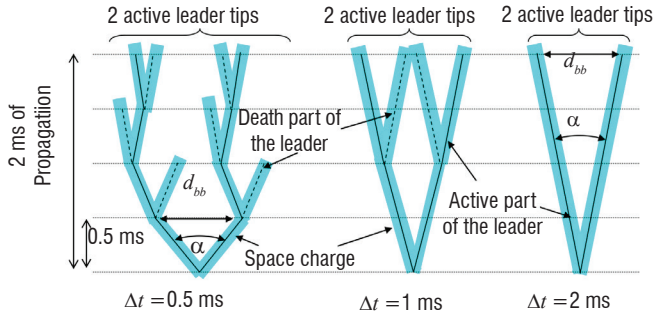

Figure 10 - Depiction of the development of a branching upward leader as a function of the time step when the effect of space charge envelopes is considered. The blue zone identifies the space charge envelope of the branch. The full line is associated with an active part of the leader channel. The dashed line is a branch, which stopped propagating. d_{bb} is the distance between the two new leader tips.

We calculate the branching characteristics of an upward leader with the space charge-per-unit length (q_{ce}) of 100 μCm^{-1}, which develops with time steps of Δt=0.5 ms, Δt=1 ms, and Δt=2 ms (figure 11). The branching criterion ΔU_B is set at 30 MV. The mean vertical velocity of the branched leader is 6.4 x 10^4 m s^{-1}. The final altitude reached by the branched leader is 8000 m, which is 2000 m lower than the maximum theoretical altitude shown in figure 8. As seen in the plot in figure 11a, there is a weak dependency of the final altitude on the duration of the time step. Figure11b shows the time evolution of the total number of branches, as well as of the total number of arrested branches. The difference between these two numbers gives the number of active branches. Both the number of branches and the number of arrested branches depend on the duration of the time step. As figure 11b shows, these two numbers are not so different.

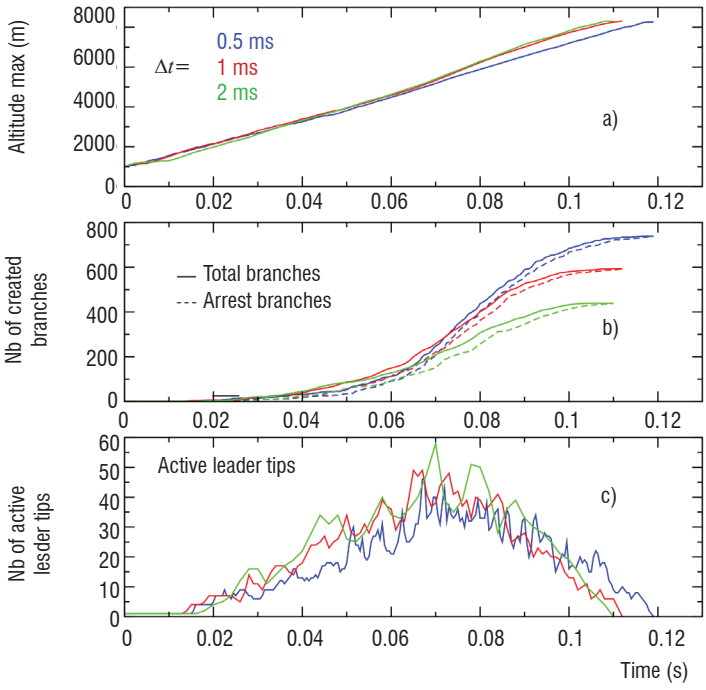

Figure 11 - Effect of the time step duration Δt on branching characteristics of upward leader. (a) Maximal vertical extension of the upward leader. (b) The total number of branches created at a given time and the total number of arrest branches. (c) The total number of active branches. Parameters of computation ΔU_B = 30 MV, q_{CE} = 100 μC m^{-1}, Δt=0.5 ms, 1 ms and 2 ms.

The figure 11c depicts the number of active leader tips as a function of time. The branching starts at altitude of 2000 m. The number of active leader tips increases up to an altitude of 5000 m where the maximum potential values are found, and then decreases at higher altitudes. It is clearly seen in figure 11c that the number of active leader tips is mostly independent of the time step duration. The upward leader propagates longer than 100 ms before it stops, which is within the range of durations commonly observed in nature for upward positive leaders.

For the same three values of the time step duration, we have plotted all leader branches created at the end of the upward leader propagation (figure 12). The results show that the total horizontal extension of the discharge is larger for larger time steps. This is due to a few branches that have a mostly horizontal propagation during a few steps and then stop, while the majority of active branches continue their propagation in the region of high ambient potential. At the end of the propagation, the zones where the majority of branches are located are quite similar and independent of the time step duration.

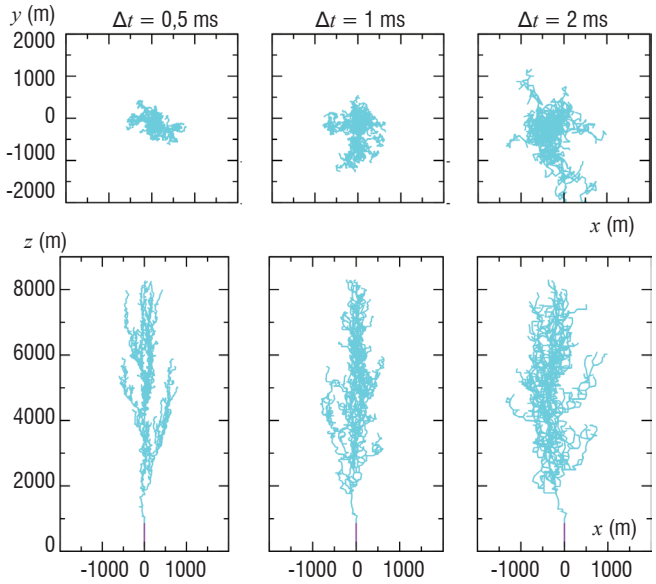

Figure 12 - Effect of the time step on the total leader branches at the end of the discharge propagation. q_{ce}=100 μC m^{-1} et ΔU_B=30 MV.

Conclusion

The modeling of the three-dimensional propagation of a branching leader has been based on an electrostatic model, the parameters of which have been inferred from physical models and validated by observations. The propagation of the leader is driven by the potential drop at the leader tip, which differs from most previous fractal models of branching that used the electric field as a propagation criterion. Branching, by splitting a branch into two new branches, occurs when the drop potential at the leader tip reaches a threshold, which we inferred from LMA observations and the ambient electric field measurements in a thunderstorm. In the model, the space charge around the leaders regulates the total number of active branches by reducing the available potential for their propagation. The model has been applied to simulate the time evolution of an upward leader developing from the tall ground structure. We are satisfied with the fact that the results of computer simulation of a branching leader resemble the branching structures in high-speed video images of upward positive leaders triggered by tall structures. One may expect the results of branching simulation to differ for different storm stages, and thus, the different potential profiles ■

Acknowledgements

The authors wish to thank Isabelle L'Helgoualc'h for her major contribution to this work.

References

[1] E. R. WILLIAMS, C. M. COOKE, ET K. A. WRIGHT - *Electrical Discharge Propagation in and Around Space Charge Clouds*. Journal of Geophysical Research, vol. 90, n°. D4, pp. 6059-6070, 1985
[2] R. SOLOMON, M. BAKER - *A One-Dimensional Lightning Parameterization.* Journal of Geophysical Research, vol. 101, n °. D10, pp. 14,983-14,990, June 1996
[3] V. MAZUR et L. H. RUHNKE - *Model of Electric Charges in Thunderstorms and Associated Lightning*. Journal of Geophysical Research, vol. 103, n°. D18, pp. 23,299-23,308, 1998
[4] E. R. MANSELL, D. R. MACGORMAN, C. L. ZIEGLER, J. M. STRAKA - *Simulated Three-Dimensional Branched Lightning in a Numerical Thunderstorm Model*. J. Geophys. Res., vol. 107, pp. 12, May 2002
[5] J. A. RIOUSSET, V. P. PASKO, P. R. KREHBIEL, R. J. THOMAS, W. RISON - *Three-Dimensional Fractal Modeling of Intracloud Lightning Discharge in a New Mexico Thunderstorm and Comparison with Lightning Mapping Observations*. Journal of Geophysical Research, vol. 112, n°. D15, August 2007
[6] H. W. KASEMIR - *A Contribution to the Electrostatic Theory of a Lightning Discharge*. Journal of Geophysical Research, vol. 65, n°. 7, pp. 1873-1878, 1960
[7] P. LALANDE, A. BONDIOU-CLERGERIE, G. BACCHIEGA, I. GALLIMBERTI - *Observations and Modeling of Lightning Leaders*. Comptes Rendus Physique, vol. 3, n°. 10, pp. 1375-1392, December 2002.
[8] C. T. PHELPS - *Field-Enhanced Propagation of Corona Streamers*. Journal of Geophysical Research, vol. 76, n°. 24, pp. 5799-5806, 1971
[9] R. F. GRIFFITHS, C. T. PHELPS - *The Effects of Air Pressure and Water Vapour Content on the Propagation of Positive Corona Streamers, and Their Implications to Lightning Initiation*. Quarterly Journal of the Royal Meteorological Society, vol. 102, n°. 432, pp. 419-426, April 1976
[10] R. F. GRIFFITHS, C. T. PHELPS - *Positive Streamer System Intensification and its Possible Role in Lightning Initiation*. Journal of Atmospheric and Terrestrial Physics, vol. 36, n°. 1, pp. 103-111, january 1974.
[11] Groupe des Renardières - *Negative Discharges in Long Air Gaps at Les Renardières, 1978 Results*. ELECTRA, 1981
[12] A. BONDIOU, I. GALLIMBERTI - *Theoretical Modelling of the Development of the Positive Spark in Long Gaps*. Journal of Physics D: Applied Physics, vol. 27, n°. 6, pp. 1252-1266, june 1994
[13] I. GALLIMBERTI, G. BACCHIEGA, A. BONDIOU-CLERGERIE, P. LALANDE - *Fundamental Processes in Long Air Gap Discharges*. Comptes Rendus Physique, vol. 3, n°. 10, pp. 1335-1359, December 2002
[14] J. WILLETT, D. DAVIS, P. LAROCHE - *An Experimental Study of Positive Leaders Initiating Rocket-Triggered Lightning*. Atmospheric Research, vol. 51, n°. 3-4, pp. 189-219, July 1999
[15] P. LALANDE - *Etude des conditions de foudroiement d'une structure au sol*. Université Paris XI Orsay, 1996. Ph. D. Thesis.
[16] T. WARNER - *Personal Communication*
[17] L. M. COLEMAN, T. C. MARSHALL, M. STOLZENBURG, T. HAMLIN, P. R. KREHBIEL, W. RISON, R. J. THOMAS - *Effects of Charge and Electrostatic Potential on Lightning Propagation*. J. Geophys. Res., vol. 108, pp. 27 , May 2003

Acronyms

BEM (Boundary Element Method)
LMA (Lightning Mapping Array)

AUTHORS

Philippe Lalande graduated from the "Ecole Supérieure de Physique Chimie de Paris" Paris (1992) and received a PhD degree in Plasma Physics from University Paris XI (1996). He joined Onera in 1996 where he has been involved both in the modelling of lightning interaction with aircraft and in the development of onboard atmospheric sensors. He is the head of the lightning and plasmas Research Unit at Onera Chatillon.

Vladislas Mazur was educated in Russia, and emigrated to the United States in 1978. He received his Ph.D. in Electrical Engineering from the University of Oklahoma, in 1981. He has worked at the National Severe Storms Laboratory in Norman, Oklahoma, since 1984 as a Physicist. He has a long history of scientific collaboration with scientists at Onera in lightning–aircraft interaction studies, and his main interests are physics of lightning processes and its application to lightning protection.

P. Lalande, A. Delannoy †
(Onera)

E-mail: philippe.lalande@onera.fr

Numerical Methods for Zoning Computation

Zoning consists in establishing lightning strike zones to locate and classify surfaces on an aircraft which are exposed to a part of the lightning current components. The current standard used to certify aircraft is empirical and qualitative, and fails to predict certain features, such as lightning attachment on the middle of the wing. Furthermore, the standard will be difficult to apply to the next generation of aircraft having geometry, engines and fuselage material that will be very different from current designs. Two approaches have been developed to elaborate a zoning around an aircraft. An empirical developed by BAe is based on the rolling sphere model. The input parameter is the radius of the sphere which is evaluated by service lightning strike experience for a given aircraft. The second approach is based on the physical description of the lightning strike on an aircraft. From the physical modelling of lightning discharge, Onera has developed a general method to compute a probabilistic zoning. This method takes into account the fundamental processes occurring during a lightning strike on an aircraft. The attachment process is computed from the aircraft geometry and the atmospheric electric field direction leading to the lightning inception. The results of this computation give the initial points on the fuselage where a lightning can develop and their probability of inception as a function of the skin geometry and the field direction. These inputs are used in a swept model to compute, for each attachment point, the lightning attachment point displacement due to the aircraft motion, the airflow and the lightning channel geometry. The model is based, for computing power purposes, on a macroscopic description of the lightning channel during the continuous current phase. For a given single aisle aircraft, we compute and record in a database several million cases of lightning strikes. By using the distribution of lightning stroke arrival times, the probability that a specific zone of this aircraft will be struck by a stroke is computed.

Introduction

A single-aisle aircraft is usually struck by lightning once a year. This event is unpredictable and unavoidable and can cause major safety issues if a specific protection design is not applied to the aircraft. This is why aircraft manufacturers have to demonstrate that their aircrafts are adequately protected from both the direct and indirect effects of lightning. The demonstration uses regulatory documents, such as Aerospace Recommended Practice (ARP) edited by the SAE international group, which explains how to proceed for the lightning certification. In the ARP 5412A [1], the lightning current waveforms are simplified by an idealised environment composed of a set of current waveforms A, B, C and D (figure 1). These waveforms are not intended to copy a specific lightning event but to reproduce the same effects on the aircraft as those expected from natural lightning. The current waveforms A and B represent the effect of a first return stroke and the waveform D, the effect of a subsequent return stroke. The waveform C simulates the effect of continuing lightning current.

During a lightning strike on an aircraft not all of these current components enter and exit an aircraft at the same spot. The lightning channel can remain stuck to certain zones, like the wingtips, while the attachment point remains only for a limited time on other parts of the aircraft. The purpose of establishing lightning strike zones (Zoning computation) is to locate and classify surfaces on an aircraft which are exposed to a part of these four composite current components.

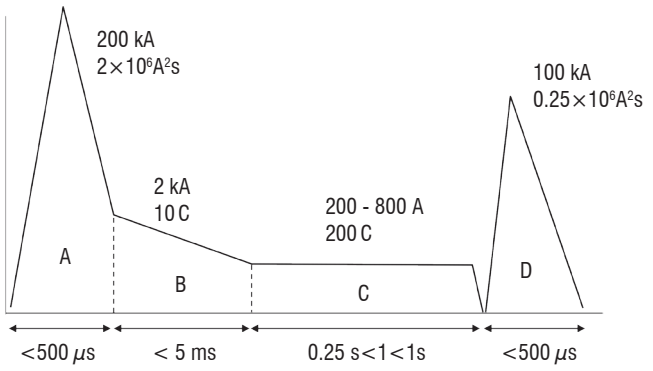

Figure 1 - Current components A, B, C, D for direct effects testing recommended in the ARP 5412A [1]

The zoning is the first step in protection design and the guidance for its implementation are described in the ARP5414A [2]. In the regulatory guide [2] the surface of the aircraft is divided into a set of regions called lightning strike zones. Three main zones, index 1, 2 and 3, are defined depending on whether the zone can experience a direct attachment of a lightning attachment point and whether the current flowing in the attachment point is due to a first or a subsequent return stroke. The previous zones are subdivided, A, B and C, to take account of duration while the attachment point remains hanging on to the zone. In the ARP5414A the six following zones are specified and the current threat associated with each zone is presented Table 1:

- zone 1A: First Return Stroke Zone with small Hang-On of the lightning attachment point
- zone 1B: First Return Stroke Zone with Long Hang-On of the lightning attachment point
- zone 1C: Transition Zone for the First Return Stroke with small Hang-On of the lightning attachment point
- zone 2A: Subsequent stroke with small Hang-On of the lightning attachment point
- zone 2B: Subsequent stroke with long Hang-On of the lightning attachment point.
- zone 3: Zone with no direct attachment of the attachment point on the zone and only subject to current conduction.

Zone	1	2
A	200 kA 2×10⁶A²s A+B	D
B	A+B+C+D	D+C
C	100 kA 0.8×10⁶A²s Ah+B	

Table 1 : Part of the lightning current waveforms set to each zone. For the zone C, a waveform A_h, between waveforms A and D, has been added.

The guidance in the ARP 5414 for the zoning of a new aircraft is neither based on mathematical rules nor physical methods but only on qualitative observations. An example of the zoning for transport aircraft, proposed by the ARP 5414A, is presented in figure 2. It is based on the similarity method. If a new aircraft has no significant differences compared to a previously certified aircraft the zoning of which has been validated by service lightning strike experience, then the same zoning can be used for both aircraft. No significant differences means no significant change in the electrical conductivity of the aircraft surface, no significant differences in the geometry, no significant changes in the flight characteristics (speed and altitude envelope). At the end of the zoning process, the zoning is reviewed with the certifying authority to obtain its concurrence.

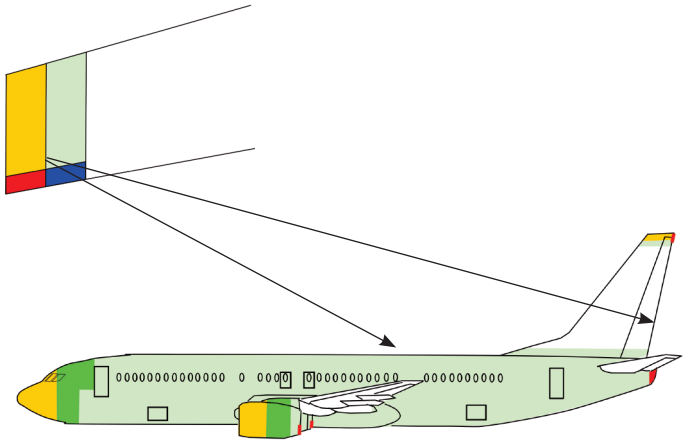

Figure 2 - Example of Lightning Strike Zone Details for Transport Aircraft [2]. The color scale is associated with the definition of zones 1 and 2. Zone 3 is white.

This approach, giving qualitative results, fails to predict damage due to lightning strikes at the middle of the wing such as observed in figure 3. No information is available on the type of lightning stroke (first or subsequent return stroke) associated with this damage. The zone surrounded by the black circle is usually considered in the ARP 5414A as a zone 3 where direct strikes of a lightning could not occur. Moreover, the guidance will be difficult to apply to the next generation of aircraft (figure 4) with both non conventional geometry and fuselage materials very different from aircraft currently in service.

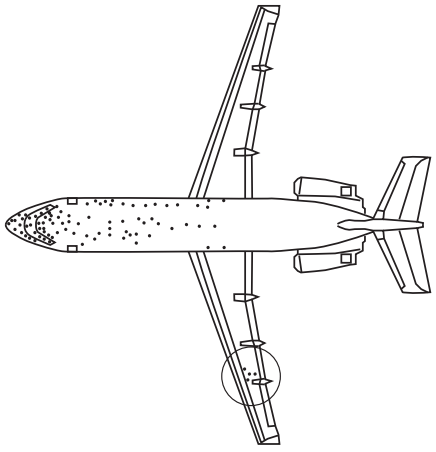

Figure 3 - Data collected by BAe in the framework of the European FULMEN project. The black dots on the fuselage show the lightning strikes to the aircraft. The circle surrounds the lightning strikes on the wing.

Figure 4 - A30X Concept for single-aisle aircraft [3]

The purpose of this paper is to review the numerical methods available for the zoning. Firstly, we review the different physical processes occurring during a lightning strike to aircraft. Secondly, we present and analyze the rolling sphere model used by British Aerospace (BAe) for the zoning [4]. Lastly, we present a new physical model for probabilistic zoning.

Description of a lightning strike on an aircraft

In-flight lightning campaigns, detailed in Laroche et al. [5], have shown that in the majority of events it is the aircraft that triggered the lightning strike. The development of a lightning strike can be split into two elementary time sequences. The first, which lasts a few milliseconds, is associated with the inception and the development of the positive and the negative lightning leaders from the aircraft. The initiation points associated with the positive leaders are called entry points and exit points for the negative leaders. It determines the initial lightning attachment points. The process is so fast that the displacement of the aircraft can be ignored. The governing parameters for the location of the initial attachment points are the aircraft geometry, the fuselage materials and the electric field generated by the thundercloud. The second time sequence lasts several hundreds of milliseconds during which the lightning strokes strike the aircraft. The motion of the aircraft leads to the displacement of the two lightning attachment points on the fuselage, depending on their initial location. This phenomenon is called sweeping. It depends on the skin properties (paint thickness, rivets, junction, etc.), the aerodynamic flow profile, lightning channel characteristics and the initial location and orientation of the lightning channels connected to the fuselage.

The rolling sphere model for the zoning

At the beginning of the twentieth-century, with the development of electricity, several research programs were run to reduce the effect of lightning on power transmission lines. By the 50's these studies had provided a rough mathematical description of the interaction between lightning and a grounded structure. This empirical model, called the electro-geometrical model [6], allows determination of the striking points (or attachment points). It only simulates the connection between a downward negative leader and a grounded structure. It should be remembered that the striking process results from the connection of the approaching negative leader and a positive upward "connecting leader" developing from the grounded structure. This positive leader initiates when the electric field due to the coming negative leader reaches a minimum threshold. In this model the structure does not move so no sweeping is taken into account. It follows that the lightning channel remains hanging at the same spot during the lightning strike. In this case the initial attachment points and the striking points are the same which is not the case during lightning strikes on aircraft.

The determination of the attachment point (i.e. the point of inception of the positive connecting leader) is as follows:

- a sphere of radius Ra is placed at the negative leader tip;
- the attachment point corresponds to the first point of the structure or of the ground which touches this sphere;
- the sphere, which is assimilated into "the attraction" zone of the negative leader, is rolled on all the structure surfaces (figure 5); all the points touched by the sphere can be struck by lightning.

We can see that the results depend to a great extent on the radius of the sphere Ra. It is generally expressed, as a function of the peak current I of the first return stroke, by the following expression:

$$R_\alpha = aI^b \qquad (1)$$

Where a, b are some coefficients which are respectively in a range of [1-20] and [0.2-1], depending of the model used for the downward negative leader, and the inception threshold for the upward positive connecting leader [7].

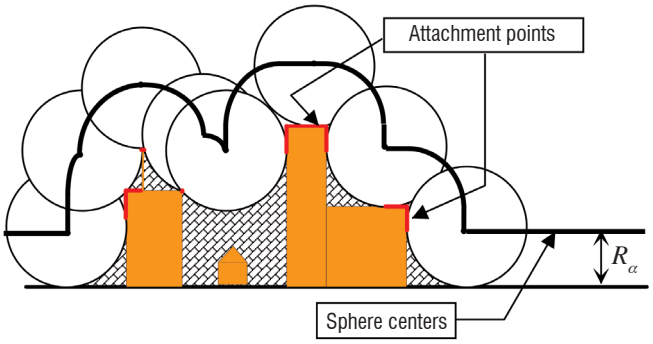

Figure 5 - Description of the rolling sphere method. The orange color represents buildings. The red lines represent the zones on the buildings which can be struck by lightning. The spheres are associated with the attraction zone of the negative downward leaders. The thick black line is associated with the sphere centers located at a distance R_α from the ground or building surface. The crosshatched pattern is the zone where a lightning strike cannot occur.

BAe has applied the rolling sphere model to the case of a lightning strike on an aircraft to compute the initial attachment zones of the lightning [4] even if this model assumes that the aircraft intercepts natural lightning which is not consistent with in-flight observations showing that it is the aircraft which triggers the lightning strike.

The attachment points are computed by rolling the sphere on the aircraft surface (figure 6). The points touched by the sphere correspond to entry points. From the external surface generated by the sphere centers, the probability that an elementary surface of the aircraft may be struck can be inferred. For instance, in figure 6, the attractive zone of dS_1 is the external surface S_1 because all the negative leaders which enter the surface S_1 are at the critical distance R_α from $dS1$. Then, all these leaders connect dS_1. The probability P_1 associated with dS_1 can be expressed as follows:

$$P = \frac{S_1}{S_{tot}} \qquad (2)$$

where S_{tot} is the total external surface generated by the sphere centers.

This model always computes higher probability at the sharp extremity of the aircraft such as dS_1 than at flat parts of the fuselage such as the surface at dS_2.

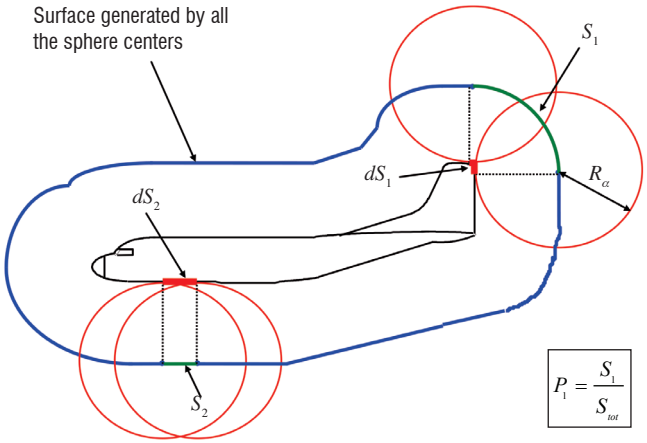

Figure 6 : Rolling sphere method applied to an aircraft.

The advantage of this model is to directly associate with a given area of the aircraft a probability of being struck by lightning. However, we have to remember that this method is based on an empirical model. It is consistent with one of the lightning strike processes which is the least probable in the case of aircraft. Moreover, the results greatly depend on the choice of the radius. It has been set by BAe in order that results are consistent with service lightning strike experience for a given aircraft. For a new aircraft, where the similitude approach could not be used, it will be difficult to determine the value of this parameter. Finally, the computation gives the initial attachment points and not the striking points where the damage is located. The sweeping process occurs between them and this is not taken into account in this model.

Description of the physical approach for zoning design

Within the framework of European programs (FULMEN and EM-HAZ), Onera has adapted its physical models [8][9][10] simulating the development of lightning leaders to the processes occurring during a lightning strike on aircraft. Two models have been developed to be consistent with the observations [5]. The first, called the “attachment model”, simulates the initial phase of a lightning strike on an aircraft. The second, called the “sweeping model”, computes the displacement of the two lightning attachment points on the aircraft surface.

In this part, we present the main principles of these models, which are detailed in references [8][9][10][11][12][13][14], and we explain how they can be used and completed for a zoning approach.

Attachment model

The attachment model is based on the electrostatic time-independent model described in [10], which is a simplification of the physical models [8][9]. The lightning leader is simulated by a space charge surrounding the hot conductive plasma channel. Figure 7b illustrates this modeling in the case of an upward leader initiating from a grounded structure. The lightning leader can propagate until the potential drop ΔU_T in front of the leader tip remains higher than 250 kV (figure 7a). The input parameters of this model are:

- the background atmospheric field E_o. It is assumed to be constant around and above the initiation structure;
- the space charge envelope radius a_{ce};
- the charge per unit of leader length q_{ce}.

Lalande et al. [10] set the parameters of q_{ce} to 50 μC/m and a_{ce} to 0.5 m for a positive leader and to 140 μC/m and 0.5 m for a negative leader in order that the results fit the ones derived from the physical models of Gallimberti et al. [9] and Bondiou et al. [8]. The physical models show that in order to take into account the effect of air density (altitude) on the leader development, the background electric field has to be divided by the reduced air density ($\delta = P/P_o.T_o/T$ where P and T, P_o and T_o are the ambient air pressure and temperature and the standard pressure and temperature at Mean Sea Level, respectively). It means that a leader can develop in a lower atmospheric field at higher altitude than at mean sea level.

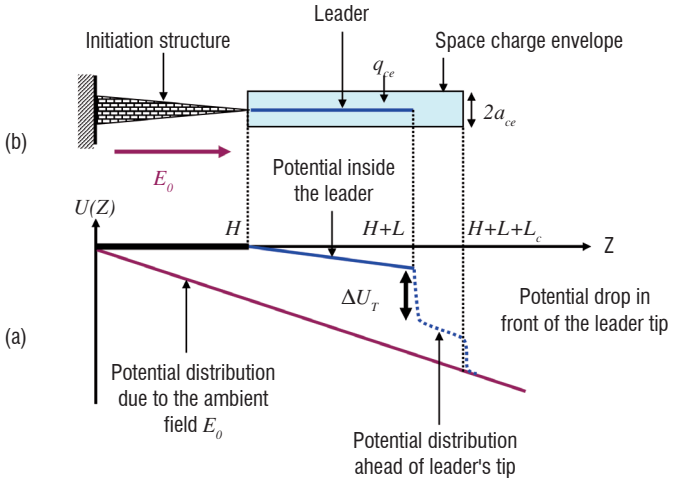

Figure 7 - Longitudinal potential distribution (a) along the path of an upward leader (b) developing from a ground structure.

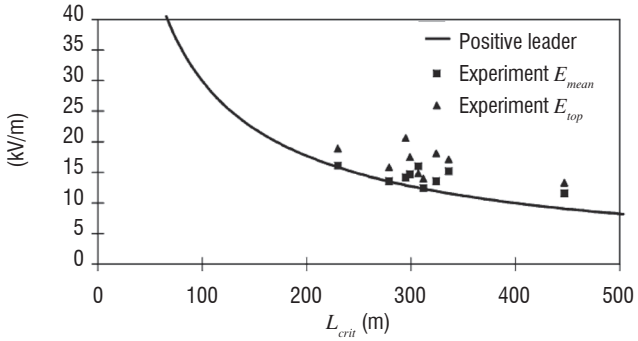

Figure 8 - Comparison between the computed stabilization field of a positive lightning leader (black line) and the measured mean atmospheric field E_{mean} (mean value of the atmospheric field along the rocket trajectory) just before the lightning is triggered[15]. E_{top} is the atmospheric electric field at the altitude of the rocket tip (black triangle). L_{crit} is the length of spooled copper wire to trigger the lightning. It is similar to H in figure 7.

For a given geometry, we are able to compute from these models the minimum atmospheric field E_o, called the stabilization field, leading to a sustained propagation of the lightning leader from a structure. These

stabilization fields have been compared to the measurements of Willet et al. [15] in a case of rocket triggered lightning (figure 8). The good agreement between the measurements and the computation means we can apply this model to lightning strikes on aircraft.

In-flight lightning campaigns have shown that lightning strike starts from the development of a positive leader from the aircraft. The electrostatic set-up is the aircraft geometry and the direction of the background atmospheric electric field, generated by the thunderstorm. Electrostatic computations are made using a boundary element method (BEM, based on the solving of integral equations). From only one point "P", to minimize processing time, we compute, with the model described previously, the value of the stabilization E_{omin} (figure 9). We assume that points around the point *"P"* can also lead to lightning leader if the electric field on the aircraft skin is higher than the stability field inside a corona. For a positive corona, it is equal to 0.5 MV/m [16][17]. We prefer to use this rather than the air breakdown field (3 MV/m) because we are not able to take into account in the aircraft mesh all the sharp points due to dust, rivets, junctions, etc. which strongly enhance the surface electric field on the aircraft up to the air breakdown field (3 MV/m). At the end of this computation we shall have, for a given atmospheric field direction:

- the stabilization field E_{omin};
- an area where positive lightning leaders can develop.

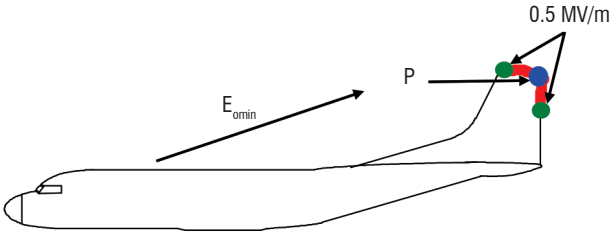

Figure 9 - Determination of the area of entry points (positive leader inception point) for a given direction of the ambient field.

The elongation of the positive leader from the aircraft increases the electric field at the opposite extremity of the aircraft. We compute for which positive leader length L_{min} a negative leader incepts from the point P' of the aircraft (figure 10). This length depends on the electric field E_{omin} and the aircraft size. We use the stability field of a negative corona (1 MV/m[18]) to define the area where a lightning negative leader can develop. Note that at this step the electric field on the fuselage is different to that of the previous step because of the presence of the positive leader.

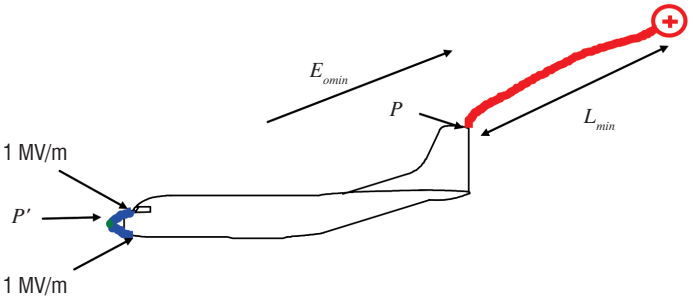

Figure 10 - Determination of the area of the exit points (negative leader inception point) for a given direction of the ambient field and length of the positive discharge.

From this model, two parameters have been computed for comparison to the in-flight lightning measurements taken with a Transall (C160) [19].

The first one is the stabilization field E_{omin}. The computed values, from 95 to 130 kV/m.Atm (depending on the angle between the atmospheric field direction and the fuselage), are in good agreement with the measured values which are in the range 84 to 124 kV/m.Atm. The second parameter available from the measurements is the time inception difference dTab between the positive and negative leaders. This parameter cannot be directly computed from the model which is a time independent model. We have only access to L_{min}. The mean value of L_{min} is 100 m. On the assumption that the positive leader velocity is between 10^4 and 10^5 m/s, $dTab$ is in the range of 1 to 10 ms, which includes the measurements (table 2).

	Mesurements	Computation
E_{omin} (kV/m/Atm)	104±20	95 to 130
$dTab$ (ms)	4.3 ± 2.7	1 to 10 ms

Table 2: - Comparison between the measured and computed values of the stabilization field Eomin and the time inception difference between the positive and negative leaders.

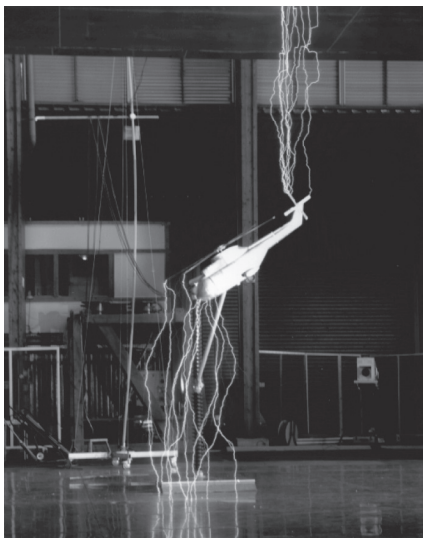

Figure 11 - Still photograph, taken at DGA-TA [20], of ten lightning strikes on a helicopter mock-up. The mock-up is electrically isolated from the ground and high voltage. It is placed inside a high voltage gap of 5 m composed of a planar electrode of 5x10 m above the ground.

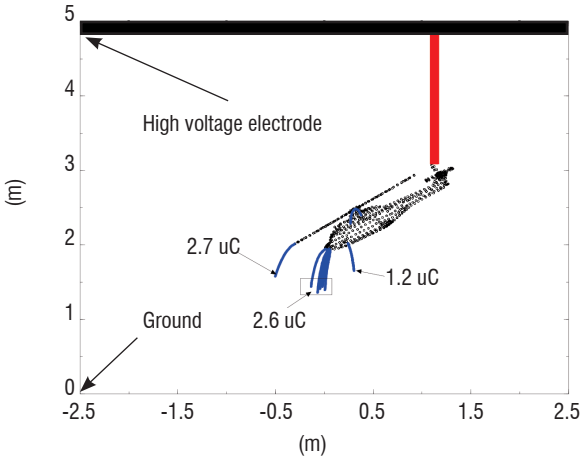

Figure 12 - Computation of the corona charge at some attachment points of the negative leaders for the test set-up of figure 11. The red line is associated with the positive leader and the blue lines the negative leaders. The electrostatic computation has been performed when the positive leader is connected the high voltage electrode.

At this step of the computation we have two zones associated with both leaders for a given atmospheric field direction and aircraft geometry. Inside a zone, the location the most probable for the leader inception is unknown. As part of the European FULMEN project, laboratory tests were performed at the DGA-TA test center [20] to simulate the inception of leaders from a mock-up [14]. The mock-up was placed above the ground and under a high voltage plane electrode. The mock-up was electrically isolated from the ground and the high voltage electrode. Figure 11 shows a still photograph of ten lightning strikes on a helicopter mock-up. We can see that, for a given set-up, multi-leader inception points are possible. An advanced analysis of these results has shown that the value of the corona charge, computed with the model of Goelian el al. [12], can be associated with the probability of a strike inside a given zone (figure 12). Where the charge is larger the probability of leader inception is higher.

On the aircraft surface mesh, the probability P_i that a positive leader initiates from the cell "i" of surface S_i is given by the following expression:

$$P_i = \frac{Q_i S_i}{\sum_{n=1}^{N} Q_n S_n} \qquad (3)$$

where Q_j is the corona charge computed at the cell "i" and N is the total number of cells of the surface mesh.

We see that P_i varies with the direction of the background field.

Sweeping model

The second model, called the Sweeping model, simulates the displacement of the lightning attachment point due to the motion of the aircraft. This model is described in detail in the articles of Larsson et al.[21][22]. Only the main principles are described here.

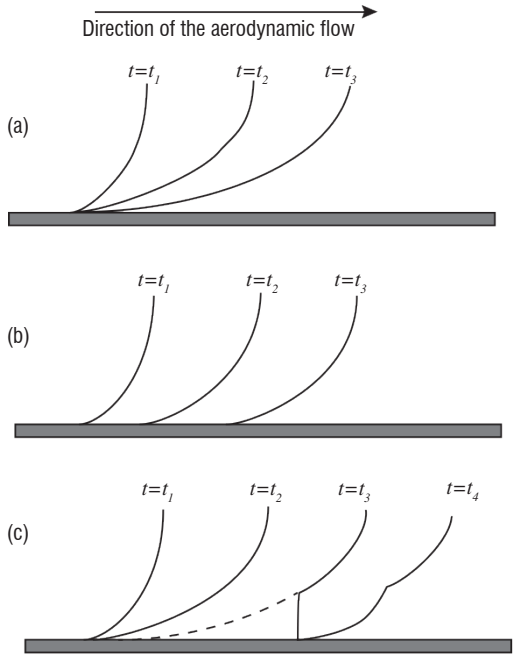

Figure 13 - Illustrations of three different swept-stroke phenomena. The lines represent the position of the lightning channel. (a) The attachment point remains at the same spot, (b) the attachment point sweeps continuously along the surface and (c) a breakdown occurs between the channel and the surface (at $t=t_3$) and the attachment point makes a jump (a reattachment). The broken curve shows the short-circuited part of the channel [21].

Two phenomena may occur at the attachment point. Firstly, the attachment point may continuously sweep along the surface (figure 13b). Secondly, the attachment point may remain at the same spot (figure 13a) and thus follow the aircraft as it moves through the air. This results in a large deformation of the lightning channel until a reattachment (or re-connection) occurs (figure 13c).

A lightning channel has a more complex geometry and cannot be described by a simple line. The channel distortion is driven by magneto hydrodynamic forces which lead to a tortuous geometry of the channel and to its chaotic motion inside a tube of 10 to 15 cm of radius, as observed by Tanaka et al in the case of a long free burning arc [23] and Airbus France during lightning strikes on aircraft (figure 14).

In the model, the lightning channel is described by an equivalent tube of 30cm diameter that is drifted and distorted by the air flow. Larsson et al.[22] obtained consistent results with this model for the cases filmed during the in-flight lightning Transall Campaign.

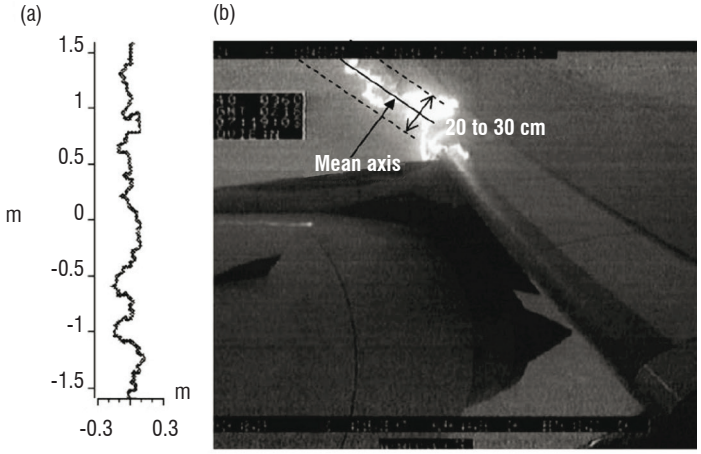

Figure 14 - Examples of a long free burning arc, (a) from Tanaka et al. [23], (b) from a lightning strike on an airliner (Photograph by Airbus France).

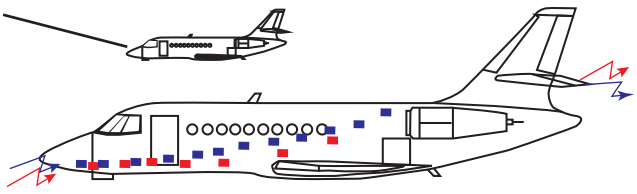

Figure 15 - Location of the lightning traces observed on the fuselage after two lightning strikes on a Falcon 2000; (blue dash) and (red dash). The grey line in front of the small aircraft shows the lightning channel location at the beginning of the sweeping.

Others comparisons have been performed by Broc et al. [24] with typical lightning strikes, collected by Dassault Aviation, on the Falcon Family. In a conventional case (figure 15), the lightning is initiated from the nose to the tail. The attachment points associated with the tail remain hanging on while the attachment points from the nose sweep along the fuselage following the stream lines of the air flow. The sweeping model has been applied to a Falcon 900 with an air flow configuration associated with an approach. In this configuration, the stream lines of air flow move back up along the fuselage. Only the lightning channel from the nose is considered. At the beginning of the computation it is assumed to be a straight line. The figure shows that the sweeping, assumed to be continuous, follows the stream lines

and the attachment point moves back up until a part of the lightning channel intercepts a stabilizer and jumps onto it.

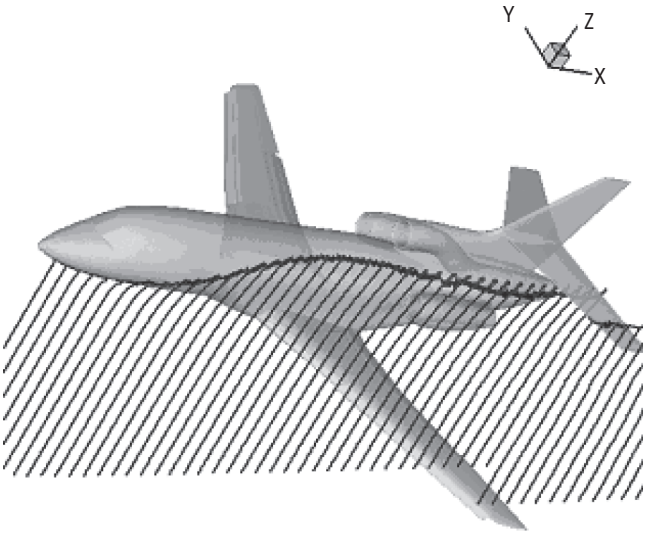

Figure 16 - Simulation of the sweeping of the lightning channels of the events shown in figure 15. The trace on the fuselage is the location of the attachment point. Each line corresponds to the lightning channel location at a given moment in time. In this case the air flow configuration is associated with an approach configuration (1000 ft, $V = 130$ Kts, 9.8° angle of attack, flaps extended).

Description of the probabilistic approach to zoning

From the both models previously described, we are able to build, for a given aircraft, a database of:

- for each thunderstorm field direction, the initial attachment points;
- for each attachment point, the sweeping trace on the fuselage and the location of the attachment point for a given moment in time.

Figure 17 presents data from the database for the case of a generic single-aisle aircraft. It is associated with a field direction Eo along the fuselage. The aircraft skin is assumed to be metallic with no paint layer leading to a continuous sweeping. The lightning channel (black line) is derived from the electric stream line from one of the initial attachment points. The sweeping model computes the time location of the attachment point from the initial attachment point. In this case, the attachment point sweeps from the nose to the wing root until the lightning channel intercepts the leading edge and the engine nacelle. Finally, the attachment point sweeps over the nacelle and remains hanging on at its extremity.

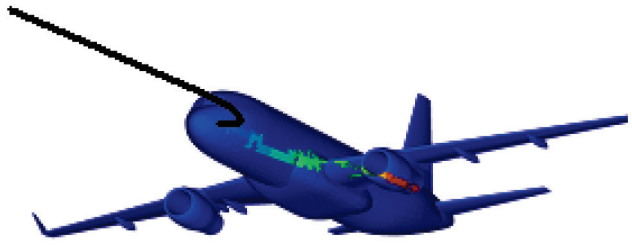

Figure 17 - Result of a sweeping starting from the initial attachment point and sweeping along the fuselage. The color scale represents the location in time of the attachment point on the fuselage. The computation has been performed on a generic single-aisle aircraft in cruise flight at a velocity of 250 m/s.

This approach has to be completed in order to determine all the locations of the damage associated with the lightning stroke components. The location of the damage will depend on the times of arrival of the lightning strokes. The figure 18 shows a typical lightning current composed of a continuing current on which three stroke currents, numbered 1, 2 and 3, have been superimposed. The location of the stroke damage on the aircraft (full white circles) are computed by using the time location of the attachment point (figure 17) and the time of arrival of each stroke.

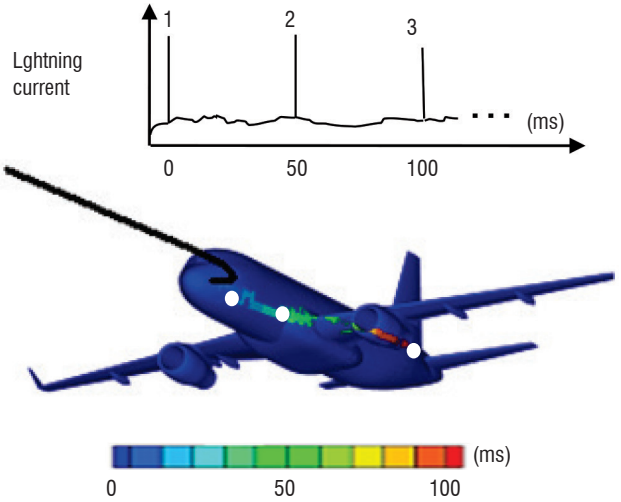

Figure 18 - Schematic figure of a typical lightning current composed of a continuing current on which three lightning strokes are superimposed. The full white circles show the lightning strikes due to the three strokes.

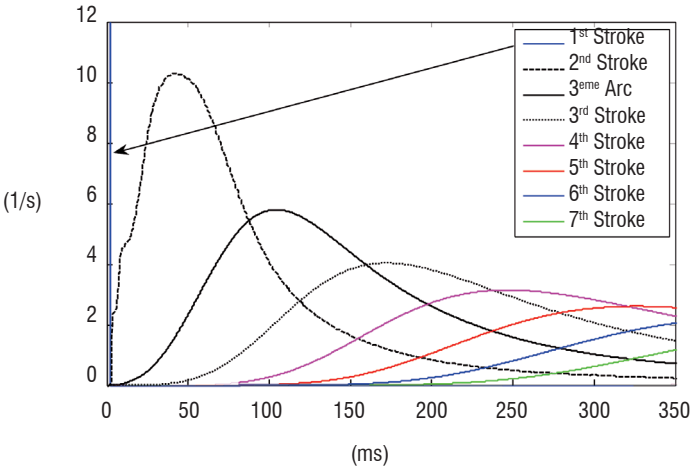

Figure 19 - Distributions of the time of arrival of strokes for a lightning strike on an aircraft at an altitude of 500 m. The distribution for the first stroke is not resolved in this figure. It is similar to a sharp peak.

The time of arrival of each lightning stroke is not determinist. For each stroke (first, second, third, …), the time of its arrival can be described by a statistic distribution that has been derived from both in-flight measurements and ground lightning network. It means, for instance, for the first stroke that the associated damages will not be located in a single point but distributed along the sweeping trace of figure 17 as a function of the time distribution of the first stroke arrival. At low flight altitude, the lightning strikes are due to cloud to ground lightning. Then, the time of arrival of the first stroke is the time for the lightning discharge to reach the ground (few milliseconds depending on the altitude). For the others strokes, the time of arrival is driven by the statistic distribution of the time between two strokes derived from observations. In figure 19, the

distribution of the time of arrival of the strokes has been plotted for a lightning strike on an aircraft at an altitude of 500 m.

The probabilistic approach of the zoning has to be completed by taking into account the distribution of the ambient field orientations experienced by the aircraft. In this article, an equi-distribution of the directions of thunderstorm fields is assumed.

The probabilistic zoning (figure 20) results in the combination of:

- The attachment/sweeping database which depends on the aircraft geometry and the flight parameters.
- The distribution of the time of arrival of lightning strikes.
- the distribution of the direction of the background atmospheric electric field associated with the thunderstorm.

Results and discussion

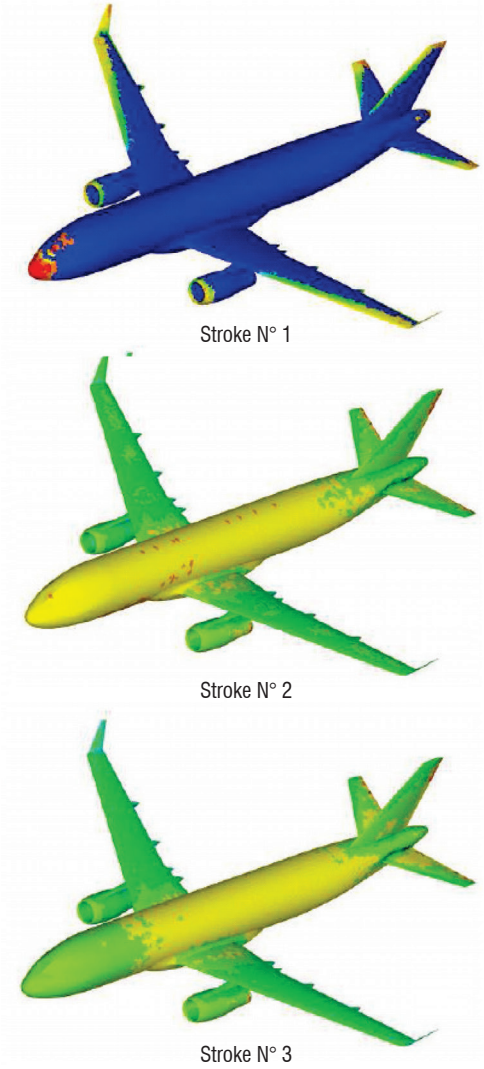

Figure 20 - Generic single-aisle aircraft flying at an altitude of 500m and a velocity of 250 m/s. The color scale is associated with probability value that a lightning stroke strikes a zone of the aircraft. It is a log scale probability from 10-3 (red color) to 10-10 (blue color).

Figure 20 shows a result of the probabilistic zoning associated with the geometry of a generic single-aisle aircraft flying at an altitude of 500 m and a velocity of 250 m/s. The surface mesh is composed of 150,000 nodes and 300,000 triangles. 1800 field directions have been considered. For each direction, a mean value of 10,000 initial attachment points has been computed. All the results, corresponding to 18 million lightning strikes to this aircraft, have been stored in a dedicated database for this aircraft. Probabilistic zoning computes from this database the probabilities on this aircraft that a lightning strike hits a zone of the aircraft. In this figure, only the three first strokes have been presented. The color is on a log scale probability from 10^{-3} (red) to 10^{-10} (blue). Yellow is one decade higher than green. The first stroke is located near the initial points of attachment because the time for the lightning to reach the ground is 0.5 ms for an altitude of 500 m. The nose, the winglets and the extremity of the vertical stab are the zones where the probabilities are the highest. The probabilities are not zero on the leading edge but they are very small and strongly decreasing from the wing extremity to the wing root. The second stroke may occur between 1 ms to 150 ms (figure 19). During this period, the lightning attachment point has swept over the aircraft. The probabilities, mainly concentrated at the nose for the first stroke, spread over the fuselage, the wing and the nacelle for the second stroke. At the extremities of the stabs and trailing edge the probabilities increase due to the lightning attachment points which remain hung on. For the third stroke, the probability decreases at the front of the aircraft and increases at the rear because most of the attachment points have enough time to move from the front to the rear.

The probabilistic zoning is quite different from that derived from the ARP 5414A. Lightning strikes on the upper part of the wing are possible even if the probability is low. These lightning strikes are only due to subsequent strokes. This model based on lightning physics can be applied to any geometry (aircraft, launcher, helicopter, etc.) and could be introduced into a standard document to have a physical computation of the zoning.

Conclusion

A new approach to zoning has been developed by Onera. It is based on two physical models. One simulates the lightning attachment processes on the aircraft. It computes the initial points of attachment of both lightning leaders (positive and negative). The second model simulates the sweeping processes of the lightning attachment point on the fuselage, from the initial attachment points until the attachment point remains hung on the fuselage. The output of this model is the time location of the attachment point on the fuselage which depends on the aircraft geometry, the air flow distribution and the lightning channel orientation. Both models are used to produce a database associated with a specific aircraft, holding all the possible points of initial lightning attachment and for each lightning attachment the associated sweeping points. From in-flight measurements and lightning ground networks, the statistic distribution of the time of arrival of each stroke has been determined. The probabilistic zoning is computed by combining the statistic distributions of time of arrival of each stroke with the background atmospherics field direction of the previous database. The results are probability values, on the aircraft surface, of being struck by one of the strokes. This new approach can be applied to the next generation of aircraft even if their geometry may be non conventional. Investigations shall have to be made to link this probabilistic zoning to standard zoning ■

References

[1] *Aircraft Lightning Environment and Related Test Waveforms*. ARP 5412A, 2005.
[2] *Aircraft Lightning Zoning*. SAE ARP 5414A, 2005.
[3] *Airbus' Global Market Forecast P82*. GMF, 2099.
[4] C. C. R. JONES - *The Rolling Sphere as a Maximum Stress Predictor for Lightning Attachment and Current Transfer.* International Aerospace and Ground Conference on lightning and statis electricity, Bath, 26-sept-1989.
[5] P. LAROCHE, P. BLANCHET, A. DELANNOY, F. ISSAC - *Experimental Studies of Lightning Strike to Aircraft.* Aerospace Lab, 2012.
[6] R. H. LEE - *Protection Zone for Buildings Against Lightning Strokes Using Transmission Line Protection Practice.* IEEE Transactions on Industry Applications, déc-1978.
[7] R. H. GOLDE - *Lightning Volume 2 : Lightning Protection*. Academic Press. 1977.
[8] A. BONDIOU, I. GALLIMBERTI - *Theoretical Modelling of the Development of the Positive Spark in Long Gaps.* Journal of Physics D: Applied Physics, vol. 27, no. 6, p. 1252-1266, juin 1994.
[9] I. GALLIMBERTI, G. BACCHIEGA, A. BONDIOU-CLERGERIE, P. LALANDE - *Fundamental Processes in Long Air Gap Discharges.* Comptes Rendus Physique, vol. 3, no. 10, p. 1335-1359, déc. 2002.
[10] P. LALANDE, A. BONDIOU-CLERGERIE, G. BACCHIEGA, I. GALLIMBERTI - *Observations and Modeling of Lightning Leaders.* Comptes Rendus Physique, vol. 3, no. 10, p. 1375-1392, déc. 2002.
[11] A. DELANNOY, P. LALANDE, E. MONTREUIL, A. BROC, P. LAROCHE, F. UHLIG, V. SRITHAMMAVANH, S. ZEHAR, C. PROVENCHÈRE, H. ANDREU, C. ANDRÉ, H. W. ZAGLAUER, N. PEGG - *ATLAS: a Zoning Tool for Aircraft.* presented at the ICOLSE, 2003.
[12] N. GOELIAN, P. LALANDE, A. BONDIOU-CLERGERIE, G. L. BACCHIEGA, A. GAZZANI, I. GALLIMBERTI - *A Simplified Model for the Simulation of Positive-Spark Development in Long Air Gaps.* Journal of Physics D: Applied Physics, vol. 30, no. 17, p. 2441-2452, sept. 1997.
[13] P. LALANDE, A. BONDIOU-CLERGERIE, P. LAROCHE - *Computations of the Initial Discharge Initiation Zones on Aircraft and Helicopter.* presented at the ICOLSE, Toulouse, 1999.
[14] P. LALANDE, A. BONDIOU-CLERGERIE, P. LARCOHE, A. ULMANN, P. DIMNET, J.-F. BOURILLON, L. TAMIN, A. DOUAY, F. UHLIG, P. GONDOT - *Determination in Laboratory of Zone of Initial Lightning Attachment on Aircraft and Helicopter.* presented at the ICOLSE, Toulouse, 1999.
[15] J. . WILLETT, D. . DAVIS, P. LAROCHE - *An Experimental Study of Positive Leaders Initiating Rocket-Triggered Lightning.* Atmospheric Research, vol. 51, no. 3-4, p. 189-219, juill. 1999.
[16] C. T. PHELPS - *Field-Enhanced Propagation of Corona Streamers.* J. Geophys. Res., vol. 76, no. 24, p. PP. 5799-5806.
[17] R. F. GRIFFITHS, C. T. PHELPS - *Positive Streamer System Intensification and its Possible Role in Lightning Initiation*. Journal of Atmospheric and Terrestrial Physics, vol. 36, no. 1, p. 103-111, janv. 1974.
[18] *Negative Discharges in Long Air Gaps at Les Renardières, 1978 Results.* ELECTRA, 1981.
[19] P. LALANDE, A. BONDIOU-CLERGERIE, P. LAROCHE - *Analysis of Available in-Flight Measurements of Lightning Strikes to Aircraft*. presented at the ICOLSE, Toulouse, 1999.
[20] *DGA Techniques aéronautiques.* [Online]. Available: http://www.defense.gouv.fr/dga/la-dga2/expertise-et-essais/dga-techniques-aeronautiques. [Accessed: 29-mai-2012].
[21] A. LARSSON, P. LALANDE, A. BONDIOU-CLERGERIE, A. DELANNOY - *The Lightning Swept Stroke Along an Aircraft in Flight. Part I: Thermodynamic and Electric Properties of Lightning Arc Channels.* J. Phys. D: Appl. Phys., vol. 33, no. 15, p. 1866-1875, août 2000.
[22] A. LARSSON, P. LALANDE, A. BONDIOU-CLERGERIE - *The Lightning Swept Stroke Along an Aircraft in Flight. Part II: Numerical Simulations of the Complete Process.* J. Phys. D: Appl. Phys., vol. 33, no. 15, p. 1876-1883, août 2000.
[23] S. TANAKA, S. KIN'YA, G. YUTAKA - *Three Dimensional Analysis of DC Free Arc Behaviour by Image Processing Technique.* Construction of Estimation Method of Column Path and Analysis of Long Gap Horizontal Free Arc Beaviour. Denryoku Chuo Kenkyujo Yokosuka Kenkyujo Hokoku, 1999.
[24] A. BROC, P. LALANDE, E. MONTREUIL, J.-P. MOREAU, A. DELANNOY, A. LARSSON, P. LAROCHE - A *Lightning Swept Stroke Model: A Valuable Tool to Investigate the Lightning Strike to Aircraft.* Aerospace Science and Technology, vol. 10, no. 8, p. 700-708, déc. 2006.

AUTHORS

Philippe Lalande graduated from the "Ecole Supérieure de Physique Chimie de Paris" Paris (1992) and received a PhD degree in Plasma Physics from University Paris XI (1996). He joined Onera in 1996 where he has been involved both in the modelling of lightning interaction with aircraft and in the development of onboard atmospheric sensors. He is the Head of the lightning and plasmas Research Unit at Onera Chatillon.

Alain Delannoy † (1951-2012) received a PhD in Atmospheric Physic from University PARIS 6 in 1979. He joined Onera in 1980 and was engaged in research on Atmospheric Electricity, Cloud microphysic and Physic of Lightning. His interest focused on in situ electrical measurements in cloud for what he setup specific instrumentations. He was engaged in lightning strike experiment on aircraft. Alain Delannoy was author and co-author of numerous articles and reports on Atmospheric Electricity and Lightning.

L. Chemartin, P. Lalande,
B. Peyrou, A. Chazottes,
P.Q. Elias
(Onera)
C. Delalondre
(EDF)
B.G. Cheron
(Cnrs)
F. Lago
(DGA)

E-mail: laurent.chemartin@onera.fr

Direct Effects of Lightning on Aircraft Structure: Analysis of the Thermal, Electrical and Mechanical Constraints

This paper deals with the direct effects of lightning strike on aircraft structures. In a first part, the phenomenology of lightning arc attachment on aircraft is introduced. Some specific features of lightning arcs observed in flight or created in the laboratory are presented. Some recent developments and results from numerical simulations are shown. The shapes, the behaviors and other specific points are compared with experiments, in order to bring to light some explanations on the complex features of lightning arcs. The second section presents the direct effects of lightning on aircraft skins. Both thermal and mechanical constraints are introduced and illustrated with experimental and numerical results. The negative effects of the paint layer on the damaging of composite and metallic materials are illustrated. The last section is focused on the direct effects of lightning on fasteners. The main mechanisms occurring during sparking phenomena are presented.

Introduction

Lightning strike to aircraft represents a possible safety hazard. The goal of lightning protection is to prevent accidents and increase the reliability of aircraft. The protection of aircraft is based on standards and certification steps [3]. The first step of the certification process, called “zoning”, consists in highlighting the most probable locations of attachment and sweeping zones on the aircraft [31]. Those zones are associated with specific lightning currents. In a second step, structures are tested in the laboratory, under controlled lightning conditions. The physical damages occurring at the attachment point of the lightning arc and, more generally, the damages caused by the conduction of the current into the structure are called “direct effects of lightning”. They can be ascribed either to lightning arcs or to sparks at the surface. The aim of this paper is to investigate the direct effects of lightning arcs on aircraft. The numerical and experimental approaches relevant to this research domain are presented in § "Simulation of lightning arcs". The direct effects on the aircraft skin (wings and fuselage), and on fasteners and assemblies, are respectively presented in § "Lightning direct effects on aircraft skin" and "The direct effects of lightning on fasteners in composites".

Simulation of lightning arcs

Introduction

Industrial and laboratory high power arcs essentially differ from natural lightning ones by their ignition paths. In the former case, the ignition is generally switched on by electric contact (copper wire, mobile electrodes), or by using a high voltage source. In the latter one, high electric strengths in storm clouds lead to the formation and development of streamers, which trigger off the passage to arcs. Another specific feature of lightning arcs concerns the current waveform that travels along them: typically, it consists of a long continuing current on which multiple peaks of current with different amplitudes and shapes are superimposed [1]. A standardized form [2] has been adopted, which involves a sequence of four main current components, called A, B, C and D-waveforms (see figure 1).

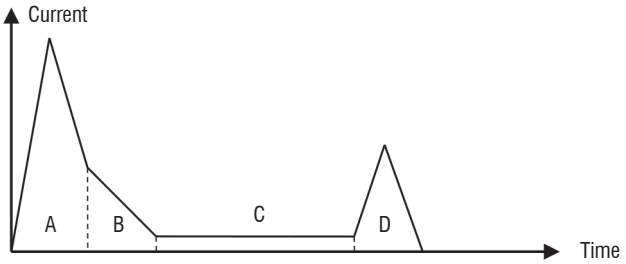

Figure 1 - Standardized lightning current waveforms for lightning direct effect tests (ARP 5412, 2)

These components are related to measured natural lightning currents. The C-waveform is a continuous component. It is associated with the propagation of the lightning discharge in the atmosphere [5]. It can reach hundreds of Amperes with duration of hundreds of milliseconds. The standardized waveform requires a charge transfer of 200 C with current intensities ranging between 200 A and 800 A.

The component A is a high intensity peak. It is followed by an intermediate intensity peak (B). These components are associated with the return stroke phenomena. A-waveform reaches 200 kA with a rise time of a few microseconds and a growth rate of 140 kA/μs. The subsequent stroke (D-waveform) reaches 100 kA with the same rate of rise. A simple bi-exponential formulation is proposed for current components A, B and D [3]:

$$I(t)=I_0\,[e^{-at}-e^{-bt}]$$

This pulse waveform is encountered in RLC electric circuits; it may be used to simulate laboratory capacitive discharge current lightning peaks. Contrary to the evolution described by this equation, measured lightning currents at the ground show a current rate close to zero at the triggering of a return stroke. This data is taken into account by the Heidler waveform [4]. For the sake of comparison, both waveforms are presented in figure 2, together with their rates of rise.

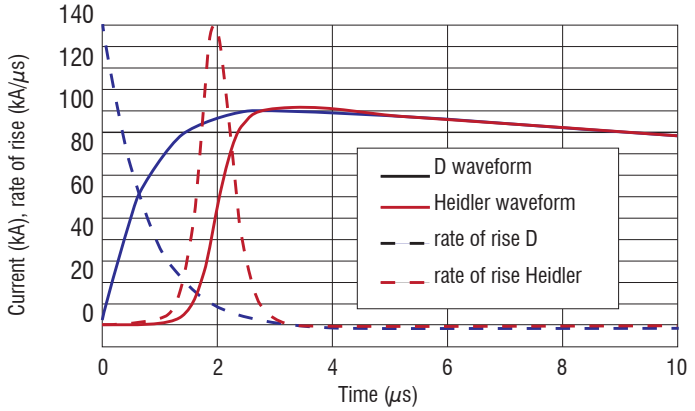

Figure 2 - Comparison of D waveform and Heidler waveform, with their respective rates of rise

International Standard IEC 62305 / European Standard EN 62305 defined return stroke currents with similar shapes. Future lightning waveforms advised in ED-84 [32] documents will take into account this feature.

Transition to thermal arc

The first phase of a lightning strike to an aircraft is associated with the development of a bi-directional leader, which creates the conductive channels. The theoretical analysis of the plasma created by these discharges shows a significant discrepancy between the electron temperature and the heavy particle temperature, due to the high intensity of the electric field necessary for the propagation of the corona [6]. However, once the electric field has decreased enough, elastic collision processes quickly (few microseconds) equilibrate the plasma phases to the same temperature. This transition to LTE (Local Thermodynamical Equilibrium) is an important path in the formation of lightning arcs. The temperature and the electron density in the plasma may be derived from spectroscopic diagnostics by using equilibrium relations (Boltzmann and Saha) and the thermodynamic and transport properties resulting from LTE calculations [7] may be inserted in the set of equations describing the dynamics of the lightning arcs.

Numerical model of lightning arcs

The magneto-hydrodynamic approach (MHD) is one of the ways to simulate the complex dynamics of unsteady electric arcs [8]. In this theoretical frame, the determination of the plasma characteristics requires a set of coupled non-linear equations describing the dynamics of the plasma (Navier-Stokes equations) and the electromagnetic source distributions (Maxwell equations) to be solved. The conservation laws of mass, momentum and total energy of a compressible fluid can be written as:

$$\frac{\partial \rho}{\partial t}+\vec{\nabla}.(\rho\vec{v})=0 \quad (1)$$

$$\frac{\partial \rho\vec{v}}{\partial t}+\vec{\nabla}.(\rho\vec{v}\otimes\vec{v})=-\vec{\nabla}p+\vec{\nabla}.\vec{\tau}+\vec{J}\times\vec{B} \quad (2)$$

$$\frac{\partial \rho e}{\partial t}+\vec{\nabla}\cdot\left((\rho e+p)\vec{v}\right)=\vec{\nabla}.\left(\vec{\tau}\cdot\vec{v}\right)+\vec{J}.\vec{E}-S_{rad} \quad (3)$$

In the above expressions, p, $\vec{v}$, ρ, e and $\vec{\tau}$ are the pressure (Pa), the velocity vector (m/s), the density (kg/m3), the energy per unit mass (J/kg) and the shear stress tensor (Pa) respectively. The momentum $J\times B$ source term is the magnetic force (or Laplace force, N/m3) due to the electric current density J (A/m²) flowing within the lightning channel and inducing a magnetic field $B(T)$. The Joule effect J.E (W/m3) is associated with the heating of the plasma by the current. Ohm's law provides the relationship between the current density J and the electric field E (V/m):

$$\vec{J}=\sigma.\vec{E} \quad (4)$$

Under LTE hypothesis, the electrical conductivity σ (S/m) only depends on the temperature and pressure. The electric field is assumed to play a negligible role in producing free electrons. In the lightning arc and in the aircraft structure, the current distribution satisfies the current conservation equation:

$$\vec{\nabla}\cdot\vec{J}=0 \quad (5)$$

The magnetic field is derived from the Maxwell-Ampere law:

$$\vec{\nabla}\times\vec{B}=\mu_0.\vec{J} \quad (6)$$

In equation 3, S_{rad} (W/m3) is the volumetric radiative power. The accurate calculation of the radiative transfers is a challenging task, due to the spectral, spatial directional and time dependence of the radiation field. Radiative transfers play an important role in high temperature arcs. The volumetric radiative power S_{rad} (W/m3) may be greater than the Joule heating in the constricted regions of the lightning arc and in high intensity pulsed arcs [9], [10]. Several methods have been proposed to calculate this source term. The simplest one is the Net Emission Coefficient, which can be simply tabulated versus temperature. This method quite accurately predicts the temperature level in the hottest part of the plasma, but fails to describe the coldest ones where absorption dominates. Some authors use geometrical methods for accurate calculation of the radiative transfer distribution in the arc (Ray Tracing, P1, Discrete Ordinate Method, etc.). The calculation generally requires a set of spectral bands with averaged absorption coefficients to be selected, in order to avoid huge calculation cost [11].

Simulation of lightning arcs in the laboratory

The direct effects of the lightning arcs are evaluated in the laboratory, using a test set-up advised in the SAE ARP 5416 document [12]. The arc is generated between an electrode and an object under test: generally, a sample of fuselage or wing material (skin) or an assembly. The current generator delivers a specific current waveform associated to the zoning of the structure under test. In the case of a sample associated to fuselage (2A zone), it may be subjected to swept stroke [3]. Thus, the current is composed of D, B and C waveforms. The arc ignition is performed with a thin conductive wire that helps the breakdown in the air gap between the wire and the sample. This electrode is generally a tungsten rod ending in a jet diverter made with a sphere of insulating material. The sphere avoids the test set-up to cause unnatural damages on the surface under test for two main reasons. First, the shock wave associated with current surge is not directed toward the surface. Figure 3 shows indeed the propagation of the pressure wave in the gap between the electrode and the sample 23 μs after ignition. The electrode is above the sample under test. The reflected shockwave close to the sphere is directed towards the sample, but it is relatively low and its intensity decreases with time.

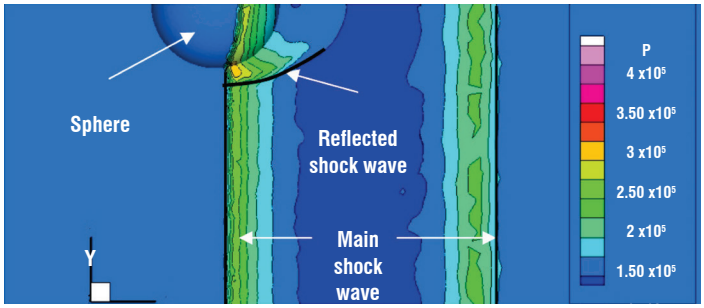

Figure 3 - Formation of shock waves 23μs after ignition with the test set-up advised in the SAE ARP 5416 document

Moreover, the sphere avoids the formation of a jet of plasma directed form the electrode to the sample, as encountered in welding or cutting arcs. Figure 4 shows two laboratory lightning arcs. The electrode is above the test object. The picture on the left was captured by a high speed video camera, 20 ms after the ignition. The current is continuous and its intensity is 800A. The interaction of the plasma jets originating from both electrodes produces instabilities and fluctuations of the arc [13]. The picture on the right was taken with a low shutter speed. The arc is crossed by a surge current of 20 kA. No plasma jet is observed on either of the metallic surfaces due to short time duration of the current pulse. The emissive zone of the arc seems to be more homogenous.

Figure 4 - Left: arc with continuing current of 800A (unpainted aluminum panel, picture DGA-Ta); Right: arc with current surge of 20 kA on copper rod (Onera)

The observation by high speed video cameras helps to understand the complex behaviour of the arc (column and root) during the tests performed with a continuous current wave. One of the most important results derived from video captures is the natural production of a plasma jet on the tested object.

The fluctuations originating from the interaction of the plasma jets during the C-waveform period can be numerically simulated from MHD modeling. Figure 5 shows the results of such calculations for a current intensity set at 800 A, 10 ms after the ignition. The formation of separate plasma jets associated with the highest temperature zones is clearly shown in the picture on the left. These jets result from the strong enhancement of the current density at the electrode interfaces. This constriction of the current streamlines is shown in the picture on the right.

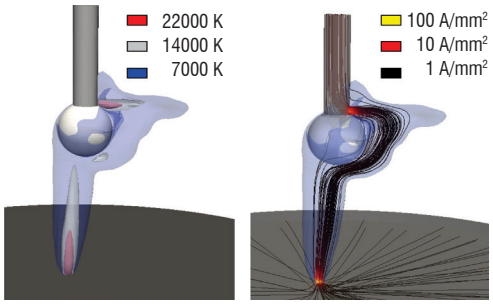

Figure 5 - Left: Calculated isothermal surfaces of an 800 A arc; Right: Calculated current streamlines of an 800 A arc (Onera)

At first, this jet seems to be stable and steady. Then, it is perturbed by the other plasma jet originating from the other electrode. At the panel surface, in the hottest regions, the arc appears to exhibit an axisymmetric brightness profile shape (figure 6, left). In this zone, the numerical simulation highlights a significant increase in the Laplace force resulting from the pinching of the current streamlines, which increases the local pressure and accelerates the plasma outwards. The plasma velocity may reach more than 1000 m/s. We will come back, in the following sections, to the consequences of this high jet constriction on the lightning direct effects on the structure.

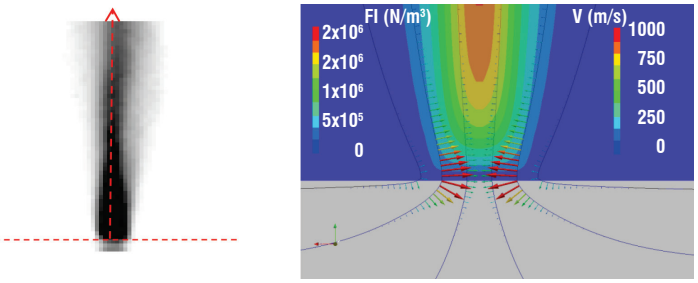

Figure 6 - Left: Picture of the plasma jet at the panel attachment point (DGA-TA) Right, Velocity and Laplace force distributions at the attachment point (Onera)

While the typical radius of an arc attachment with continuing current never exceeds 7mm, numerical investigations on return stroke arcs clearly indicate that this radius continuously expands during the first 100 μs and may reach more than 5 cm for current peaks greater than 100 kA. Since the current density rapidly increases inside the arc (up to 10^9 A/m^2), the temperature quickly increases and reaches 35000 K after a few microseconds. At the same time, the induced Laplace force gives rise to a magnetic pressure with a parabolic shape. This overpressure plays an important role on the dynamics of the arc and on the velocity of the shock wave generated by the return stroke.

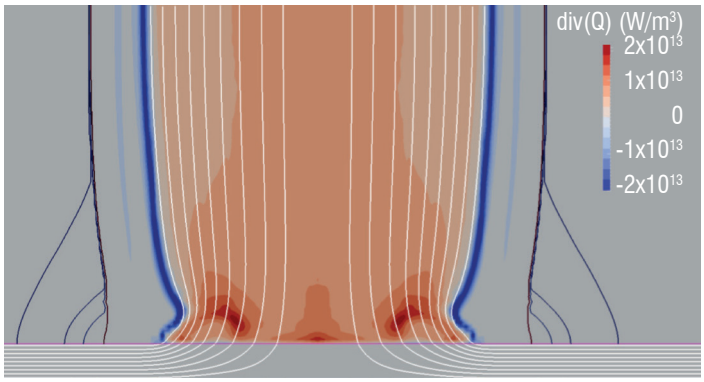

Figure.7 - Color: divergence of the radiative flux (W/m3); White lines: electric current streamlines; Black lines: isobars. (Arc subjected to A/2 waveform at t=10μs on unpainted aluminum panel, Onera)

This overpressure also leads to a significant increase in the radiative emission, which limits the temperature and pressure increase in the core of the arc. On the other hand, the strong energy absorption occurring at the same time in the peripheral regions (blue zones in figure 7) heats the boundary of the arc, the plasma becomes conductive and current flows in this region. Energy absorption is one of the most important mechanisms in the expansion of the arc.

Simulation of lightning strikes in flight

When the lightning strikes happen in flight, the arc is generally more unstable as a result of the aerodynamic flow. A phenomenological description of the swept stroke has been proposed by Larsson et al. [14]. According to this description, the arc root may either dwell at the same spot and follow the fuselage displacement in the air, or continuously sweep the fuselage over small distances. In both cases, the result is a large deformation of the lightning channel and an increase in the electric field in the air gap between the channel and the fuselage (red arrow in figure 8). This electric field is approximately proportional to the length of the channel. When the electric field reaches the critical electric field E_c of the air (about 1 to 3 kV/mm), a dielectric breakdown may happen in the gap. In that case, the arc root jumps from a spot location to a new one. The increase of electric field may be also caused by the natural fluctuation of the arc column, as shown in figure 8.

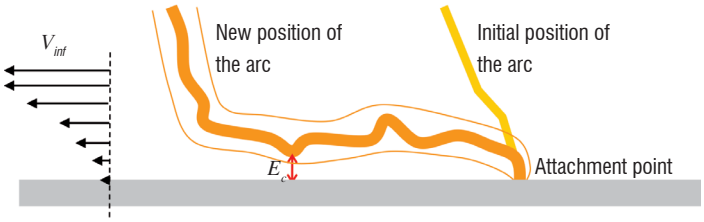

Figure 8 - Schematic drawing of the swept stroke

The objective of the studies dedicated to swept strokes is to characterize the process and to evaluate a dwell time, which is an important parameter for the waveform definition to be applied on the swept zones of aircraft (2 A zone for example). The thermal constraint on the aircraft skin increases as the arc root stays longer at the same point. Some authors have studied the behaviour of the arc sweeping over a structure, using magnetic deflection, wind tunnels [15] or moving structures [16]. They all report a dwell time of a few milliseconds, depending on the fuselage material and on the method used to simulate the swept stroke. These experiments are extremely complicated and they unfortunately do not provide a sufficient collection of data for the engineering.

Such a phenomenon can be simulated by resolving the set of MHD equations presented above. Three important features must be taken into account in the calculation of a swept stroke:

- The natural chaotic behaviour of its long column
- The formation of the plasma jets at the attachment points
- The flow profile along the fuselage, in relation with the aircraft displacement.

Two parameters of the long arc columns greatly influence the reattachment and sweeping processes: the intensity of the internal electric field (or voltage gradient) and the scale of the arc fluctuations. Tanaka et al. [17] have characterized the natural fluctuations of long arc columns by using a high speed imaging technique associated with a reconstruction algorithm. Two values of DC currents were tested: 100 A and 2000 A, with two gap lengths: 1.6 and 3.2 m. These experiments have shown that the motion of the arc columns does not depend on the gap length. Therefore, the role of the electrodes may be neglected in the simulation of such long arcs. Two geometric parameters mainly quantify the tortuosity of the arc: the “expansion radius”, which is the maximum distance from the gap axis reached by the channel, and the “normalized length”, which is the ratio between the effective channel length and the gap value.

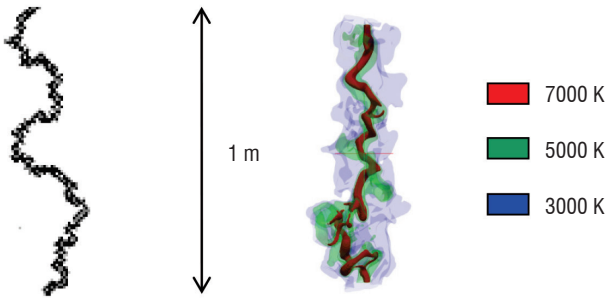

Figure 9 - Behavior of long continuing current arc. Left, picture from Tanaka et al. [17], right simulation [8].

Experiments carried out on long arcs lead to a mean expansion radius of about 10cm for a current of 100 A, with an internal voltage gradient ranging between 500 and 1000 V/m. The normalized length ranges from 1.2 to 1.5. Numerical results [8] quite agree with this experimental data, which validates the use of an electric arc model to simulate the swept stroke. A comparison of the observed and simulated shapes is presented in figure 9

The description by Larson et al. of the sweeping of a lightning stroke was numerically simulated along a simple unpainted panel with a displacement velocity magnitude of 100m/s. Initially, the boundary layer velocity distribution between the panel and the free atmosphere is approximated by means of a Blasius profile extending over 10 to 20 mm. The time of the simulation is 25 ms, corresponding to a panel displacement of 2.5 m. The current is set to 400A. More than 50 reattachments are observed with an expansion radius of about 3 cm around the mean axis of the arc. Figure 10 illustrates a reattachment during the sweeping process. At the time t=11.3 ms, (picture 1), the arc column is slightly extended by the displacement of the skin. The deformation of the column increases with time (picture 2, t=11.85 ms) and the electric field increases between the arc and the panel. This local increase is displayed in picture 10: the blue volume corresponds

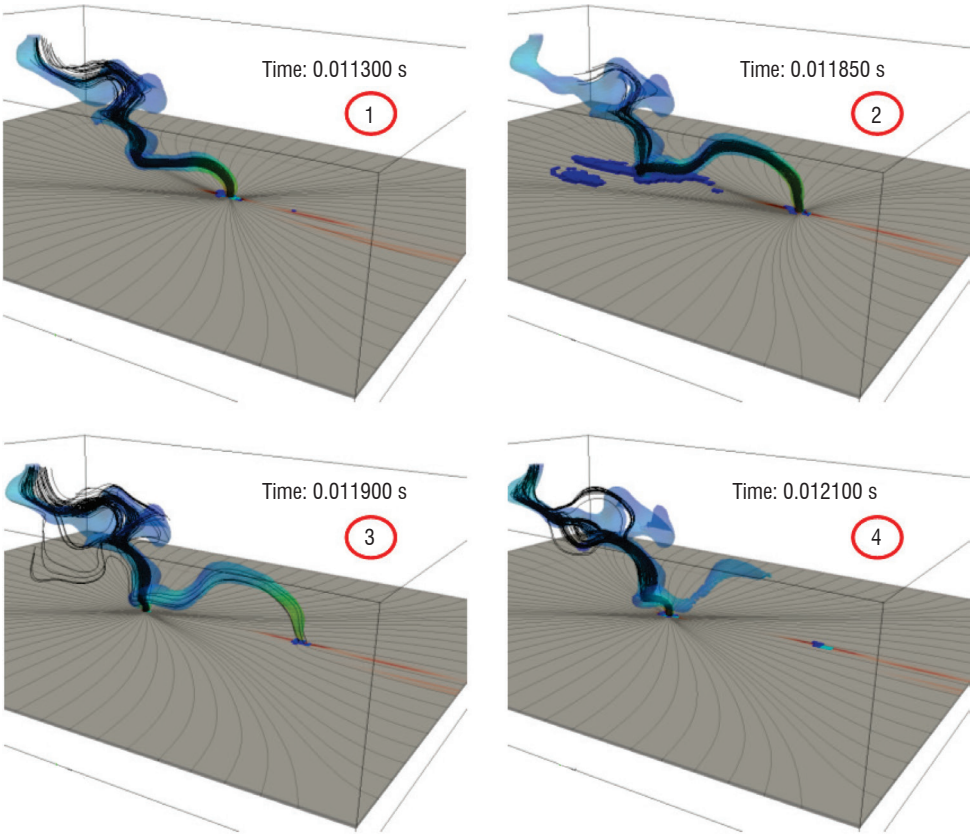

Figure 10 - Simulation of reattachment during the sweeping of a lightning strike along a panel

to a zone in which the electric field amplitude is greater than 0.1 kV/mm. A dielectric breakdown occurs at t=11.9 ms (picture 3) and the arc reattaches in another spot on the panel.

The calculated mean dwell time increases between 0.5 and 3 ms during the sweeping of the arc due to the continuous growth of the boundary layer. These reattachments are associated with quick variations of the voltage, as illustrated in figure 11: four reattachments, with a voltage drop of about 200 V, occur within a 1.5 ms time interval.

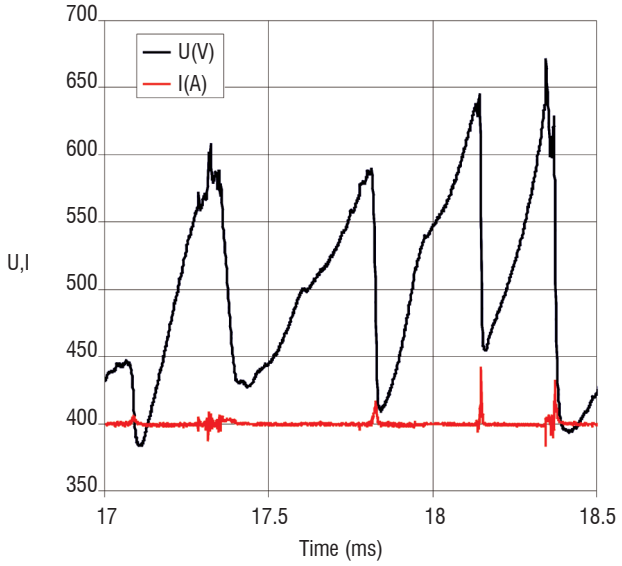

Figure 11 - Evolution of the voltage across the arc during a swept stroke

This evolution of voltage is similar to the voltage measurements of Dobbing & Hanson [16]. It is also similar to the voltage in an argon DC plasma torch in restrike mode [33]. The voltage continuously increases during the lengthening of the arc column and steeply drops at each reattachment. The comparison between a sweeping stroke and a laboratory stationary arc shows that the thermal flux is slightly higher in the former case, while the root radii are in the same order of magnitude. Dobbing & Hanson [16] reported similar conclusions and concluded that laboratory testing with a stationary arc is quite representative of the lightning strike in flight.

Lightning direct effects on aircraft skin

The effects of a lightning strike on aircraft are classified into two main categories: while direct effects are associated with physical damages occurring at the attachment point and in equipment, the indirect effects concern the interferences due to the electromagnetic coupling with the systems and the cabling. This section deals with the direct effects, which are nowadays of primary concern because of the massive use of composite material in the aircraft structure. In a first part, the different mechanisms of damaging are presented. The second part introduces the main physical characteristics of the arc root, and provides the orders of magnitude that define the lightning constraints at the attachment point. The third part presents calculations and measurements of the behaviour of materials struck by the different components of the lightning.

Introduction

The constraints related to direct lightning effects can be divided into two main categories:

The thermal constraints, which are particularly important during the continuing current stage, generate a fast increase in the temperature of the material. They may cause melting or puncture. Some authors have reported empirical linear relationships that give the size of the hole as a function of the total charge transfer and panel thickness [18]. The main energy sources are the direct plasma heat flux (conduction, electronic or ionic recombination and radiation flux) and the Joule heating within the material. In the case of a metal structure, the latter source is negligible due to the high electric conductivity. However, Joule heating may be as important as the flux originating from the plasma in the case of a composite material. Obviously, this difference results from the weak value of the electric conductivity (1000 times lower), but it also comes from the laminate structure of the composite material, which prevents the diffusion of the current through the panel.

The mechanical constraints, which can lead to breaking, delaminating and puncture, are particularly important during the current peaks. The first component of these constraints is the overpressure due to the explosion of the lightning channel, which gives rise to the propagation of a strong shock wave in the radial direction of the arc. The explosion comes from the fast increase in the arc temperature in the channel, up to 30000 K within a time interval of a few microseconds. The magnetic force induced by the current circulation also makes a significant contribution to the mechanical constraint in the arc column and in the material. First of all, the internal pressure of the arc column is reinforced by the concentric magnetic force ("magnetic pinch"): the pressure may reach more than 50 bars within a few microseconds. Furthermore, the current flowing in the structure directly acts as an additional mechanical constraint on the skin ("magnetic pressure"). Finally, the expansion resulting from the very fast increase in temperature of the material yields an additional contribution to the mechanical stress.

Notice that the composite materials are also constrained by the electric field, which can cause internal arcing inside the material and between plies, and lead to the weakening or delaminating of the structure.

The different constraints that occur at the attachment point are shown in figure 12. Different levels of yellows are used in order to feature the arc at different times.

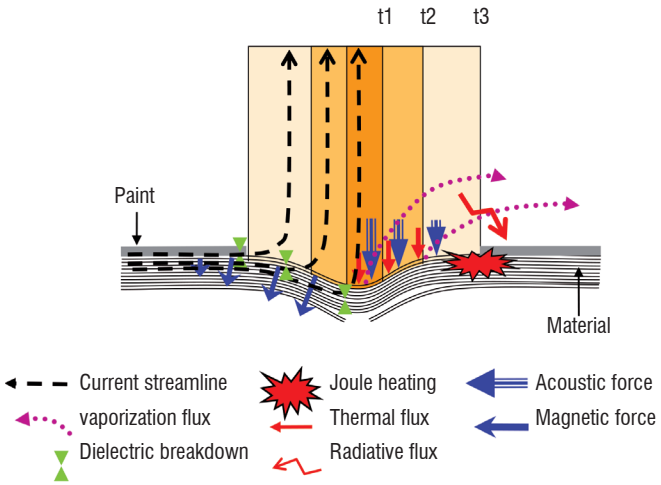

Figure 12 - Illustration of the various direct constraints at the attachment point

The increase in the arc root radius during the lightning stroke highly depends on the surface characteristics of the panel, particularly in the case of paint layers. In the next part, we present various relationships that enable us to assess the various components of the lightning constraints as functions of the arc root radius. These relationships highlight the importance of the radius for the damages. A brief description of various techniques developed to minimize these damages in composite materials is also presented.

Thermal fluxes on arc attachment

The interaction of an arc with an electrode has been widely studied for many years in the context of arc engineering (welding, switching, coating processes, etc.). In the case of lightning strike to aircraft, we can show that the main component of thermal flux is associated with the conduction of the current from the plasma to the structure. The fluxes associated with the vaporizing of the material or radiative emissions are negligible. The physical process involved in the thermal flux depends on the polarity of the material. In the case of an anode, the flux of electrons is directed towards the material, and their acceleration takes place in a thin layer of thickness approximately equal to the mean free path of the electrons (a few μm). The flux component associated with this acceleration is the product of the total current J (A/m²) and an anodic voltage drop noted as U_a (V). When the electrons enter the material, they release some energy and the flux associated with this process is the product of the work function of the material Φ_{Mat} (V) by the total current J. Finally, the conductive flux due to the interaction of neutral particles with the material depends on the plasma temperature T_p and the material temperature T_W. The anodic flux Q_A (W/m²) is generally written as [19]:

$$Q_A = J\left(U_a + \Phi_{Mat} + \frac{5k_b}{2e}\left(T_P - T_W\right)\right)$$

where k_b is the Boltzmann constant and e is the electron electrical charge. The conductive flux is negligible in the case of high current arcs. It is generally considered that both the anodic voltage drop and the material work function are about 4 to 5 V. Thus, a simple relationship of the anodic thermal flux is:

$$Q_A \approx 10\,J \approx 10\,I/\pi R_{c^2}$$

The interaction with a cathode is more complicated because of the thermo-electronic process. When the temperature of the material reaches hundreds of Kelvin, the thermo-electronic emission becomes the main source for the production of electrons. A simple description of the thermal flux between an arc and a cathode consists in considering only thermo-electronic and ionic currents in a mono-atomic and simply ionized plasma layer. With these assumptions, the thermal flux on a cathode Q_K is a function of the thermo-electronic current J_{em} and ionic current J_i :

$$Q_K = -J_{em}\left(\frac{2k_b}{e}T_W + \Phi_{Mat}\right) + J_i\left(\frac{5k_b}{2e}T_W + U_k + \Phi_i\right)$$

Where U_k is the cathode voltage drop (about 10 V), ΦMat is the work function (V) and Φ_i is the ionization potential (13.6 V). The thermo-electronic current is calculated with the Richardson – Dushman formula. An upper bound of the thermal flux on a cathode is:

$$Q_K \approx 24\,J \approx 24\,I/\pi R_{c^2}$$

Thus, it may be considered that the thermal fluxes on both cathode and anode are of the same order of magnitude. While thermal flux relationships with the current density J are linear, the Joule heating depends on the square of the current density (J^2/σ) and the power of

4 of the inverse of the arc root radius. As a conclusion, the thermal constraints highly depend on the radius of the arc root.

Mechanical constraint on arc attachments

The mechanical constraint may be evaluated by the calculation of the magnetic contributions as a function of the radius of the arc attachment. The channel overpressure due to magnetic pinch may be estimated with Newton's first law.

$$\vec{\nabla} p \approx \vec{J} \times \vec{B}$$

The plasma acceleration is neglected and we assume a constant distribution of the current in the arc column of radius R_C. The integration of the pressure along the radius of the channel gives:

$$p_{arc} = \frac{\mu_0 i^2}{4\pi^2 R_C^2}\left[1 - \left(\frac{r}{R_C}\right)^2\right]$$

The contribution of the magnetic force associated with the current drained in the panel may also be decomposed into two contributions. The first contribution is associated with the distribution of the force below the arc root. This force is mainly distributed toward the center (see the right part of figure 6), and the resulting force is necessarily lower than the magnetic pressure of the arc that acts on the panel. This contribution is generally neglected. The second contribution is associated with the outer regions of the arc root [20], [21]. If we consider the same assumptions as before (constant current in the panel and static law), the magnetic pressure is written, for $r > R_C$, as:

$$P_{panel} = \mu_0 i^2 / (4\pi^2 r^2)$$

The sum of both contributions gives the total magnetic pressure acting on the structure, as illustrated in figure 13, for a total current of 100 kA.

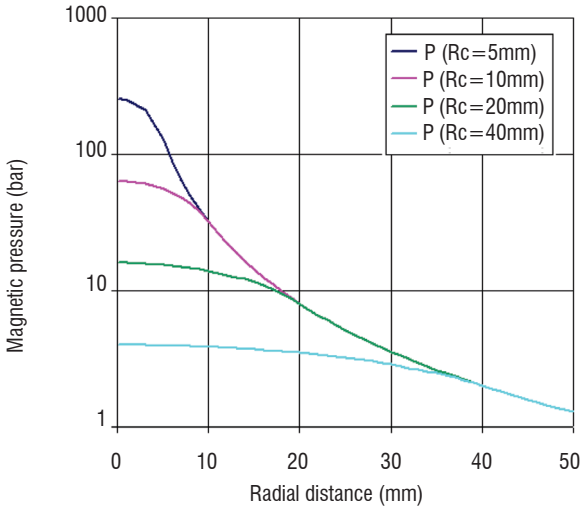

Figure 13 - Distribution of the magnetic pressure at the attachment point for a 100 kA arc

We can see that the maximum pressure reached at the center of the arc column also depends on the inverse of the square of the arc root, as was concluded for the thermal flux.

The acoustic component of the overpressure is due to the fast deposit of energy during the ignition stage of the arc. Some works [22] give some relationships to evaluate the main characteristics of the shock wave after an instantaneous and punctual energy deposit in the case of a perfect gas. The calculation of the fluid flow in the case of a lineic energy deposit indicates that the cylindrical shock position expands with time as a square root law $(R \sim k\sqrt{t})$. This law is proportional to a constant k that takes into account the equivalent energy deposit. The accurate calculation of this energy remains an important issue for the evaluation of the shock wave characteristics with this analytic approach. Numerical modeling and experimental measurements are probably more suitable for the accurate calculation of this component. Such a calculation is presented in the next part, taking into account a more realistic deposit of energy.

Some authors [20], [23] have mentioned the explosion of surface protection as an important contribution to the mechanical stress. This explosion is caused by the strong energy deposit by Joule heating into the thin metal wires of the protection. According to Lepetit et al. [23], the resulting overpressure may reach more than 50 bars.

Characteristics of the arc root

The electric arc model presented in the first section of this paper allows accurate calculations of the characteristics of the arc attachment for the two lightning current components. In the case of the continuing current stage, the goal is to estimate the radius reached at the attachment point. In the case of the current impulses, the model may be used to calculate the evolutions of the arc root radius and total overpressure on the skin.

Characteristics of the arc root during C-waveform

During continuing current tests, observations with high speed video cameras and numerical simulations (figure 6) show that the arc reaches a quasi-steady state shape. Numerical simulations show that the current density profile at the interface with the material reaches a Gaussian like shape (see figure 14). In this condition, it is possible to evaluate a radius R_C into which a given part of the total current flows, for example 99% of the current.

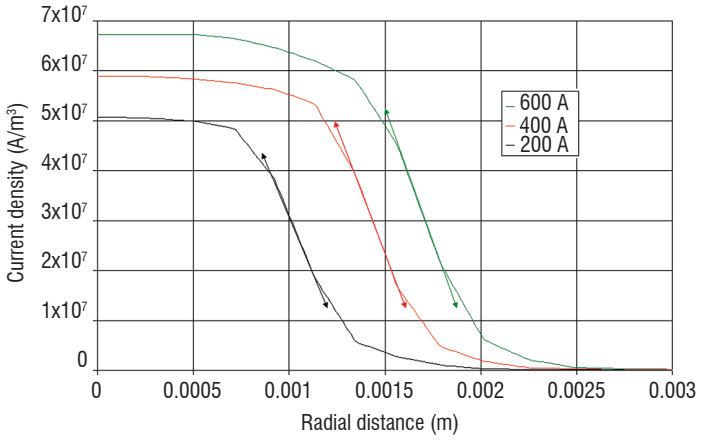

Figure 14 - Calculated distributions of the current at the attachment point during the C waveform

With this assumption, numerical simulations give an equivalent radius of about 1.6 mm for a 200 A arc, 1.8 mm for a 400 A arc and 2.5 mm for an 800 A arc. Thus, the arc root radius depends on the total current that flows into the arc. These values seem to be lower than the

size of the melted zones observed after the tests on material and also the apparent radius evaluated with the analysis of arc pictures. This difference may be explained by the thermal diffusion in the material (see § "Thermal Damaging") which extends the melted zones.

Simulations also indicate that the size of the arc root depends on the presence of a paint layer only during the first 10 milliseconds. After that time, there is no correlation between the presence of the paint layer and the arc root radius. Indeed, the material located around the arc root reaches a temperature above the boiling point in a few milliseconds, while the total duration of the C-waveform is greater than 250 ms. Thus, the paint layer is either vaporized, or carried away by the metal drop (see § "Thermal Damaging").

Characteristics of the arc root during A or D waveforms

While the presence of a paint layer does not affect the arc root radius during the C-waveform, observations of panels after A or D-waveform indicate that the arc root size highly depends on the presence of a paint layer. In the case of an unpainted aluminum panel, the radius of the damaged zone reaches more than 2 cm, while painted panel arc root radii do not exceed 0.5 cm. This feature is illustrated in figure 15, in which the left picture shows the damaged zone of an unpainted aluminum panel tested with a 100 kA arc and the right one shows a painted panel tested under the same conditions.

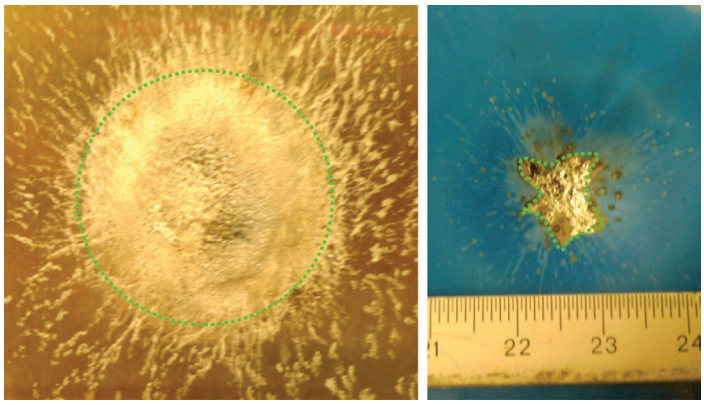

Figure 15 - Pictures of the damaged areas on an aluminum panel after a 100kA lightning test: left on unpainted panel and right with painted panel (same scale).

We can also notice that the damaged area is roughly circular on the unpainted panel, while the shape of the damaged zone on the painted panel is more irregular. A similar analysis of the carbon composite panel may be done, but the action of the protection on the surface is also an important parameter that changes the shape and the size of the damaged zone. Thus, the thermal and mechanical constraints on the panel may be increased by a factor of 10 just because of the presence of a thin paint layer.

Numerical simulations of the arc attachment during the high current stage on unpainted metallic panels show that the arc root continuously expands in the radial direction. This expansion comes from the fluid flows associated with the explosion of the arc and the radiative transfers that heat the surrounding zones of the arc core (see figure 7). During the first 100μs, the arc root characteristics on unpainted aluminum skins are similar to the characteristics of free exploding arcs in air, particularly the temperature and pressure. The results presented in figure 16 concern free exploding arcs in air and provide a good order of magnitude for the interaction of a pulsed arc with an aluminum panel. The current density rapidly increases inside the arc (up to 10^9 A/m^2) and the temperature increases and reaches more than 30000 K within the first microseconds (see figure 16). This deposit of energy leads to the detachment of a shockwave soon after, at about 0.3μs after the arc ignition. This shockwave is associated with an important drop in the pressure, similar to a discontinuity. At the same time, the magnetic force induced by this current density and the magnetic field gives rise to a magnetic pressure with a parabolic shape, as was explained in § "Mechanical constraint on arc attachments". The sum of both contributions gives this typical pressure profile that constrains the skin. The shockwave expansion is faster than the expansion of the conductive zone. However, since the channel radius is expanding and the current starts to decay after 5 μs, the Laplace force and the Joule heating decrease because of the decrease in both the current density and the magnetic field. After 100 μs, the pressure inside the channel is no longer affected by the momentum generated by the Laplace Force.

From this calculation, it is possible to evaluate the expansion of the conductive zone of the arc root, which determines most of the constraints applied on the material. The criterion that defines the equivalent radius of the channel may be defined according to the position of the peak value of the magnetic field in the arc. This criterion gives similar radii to the criteria based on the current content used for continuing current. The evolution over time of this radius R_C is presented in figure 17, with three fit functions associated with three temporal ranges. We can notice that the conducting

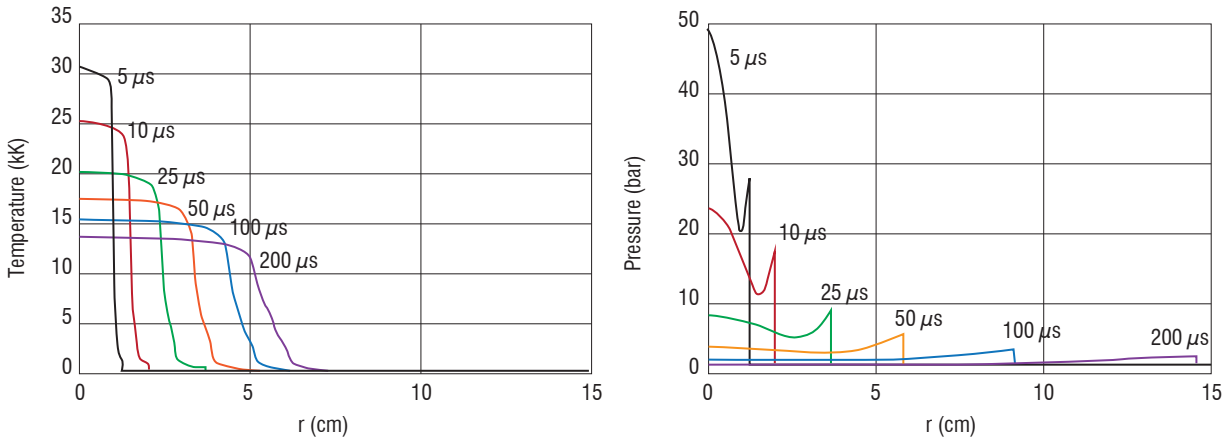

Figure 16 - Distribution of the temperature and pressure at the attachment point during the A/2 waveform

core of the arc expands faster than a pure cylindrical shock wave during the first 20 μs: the fit function during the first tens of μs is a power of 0.57 while the shock radius in a perfect gas expands as a square root. After 50 μs, the conducting core expansion is slower than the pure cylindrical shock (a power of 0.39). This feature may be explained by the fast cooling of the core that increases the density of the plasma and slows down the fluid flow. The effect of the current peak value on the evolution is close to linear. However, as we can observe in figure 17, the expansion velocity decreases with time for all values of the current. The analyses show that the expansion velocity decreases more rapidly when the current is lower. This feature may be explained by the action of the radiative transfers, which plays a very important role in the channel expansion when the current is significant.

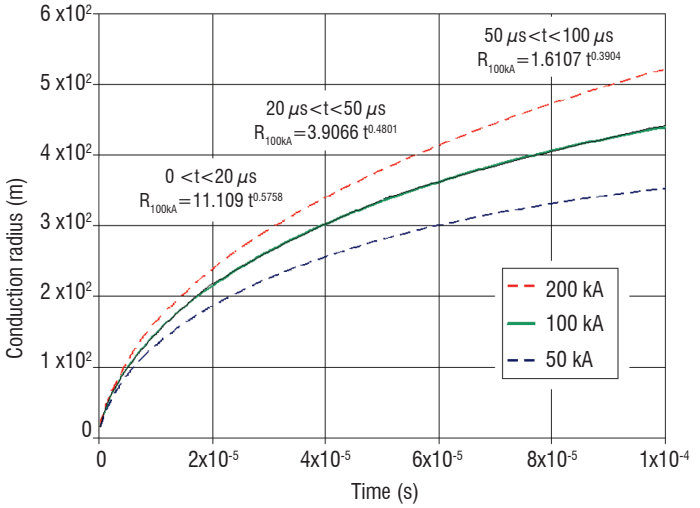

Figure 17 - Evolution of the conductive radius during A/4, A/2 and A waveforms (Onera)

Thermal damaging of aluminum panels during the C-waveform

Observations of continuing arc spots after tests indicate that the areas of melted metal increase with the current value for a same charge transfer [23]. They also indicate that the areas and the depth of the melted zones are more important for cathode polarity [16]. After the test, the spot presents a kind of swelling with a volume greater than the initial state, as illustrated in the two pictures of figure 18 with green dashed lines. This swelling is due to the formation of a molten pool at the arc spot, with air bubbles trapped within. The arc seems to attach onto the top of this swelling and it modifies the shape, as illustrated with red arrows.

Figure 18 - Picture on the left, section through the center of the cathode spot (Dobbing & Hanson, 1978). Picture on the right, view of a cathode spot for an 800A, 200C arc on an aluminum panel (DGA-TA). The drop of metal is deformed by gravity.

This feature highly depends on the metal melting and boiling phenomena and the numerous physical processes involved: metal vapor contamination, surface tension on the molten pool, formation of internal bubbles, etc. Numerical simulations of the arc attachment on such structures are extremely complicated, but some models dedicated to welding engineering give good agreements with observations of arc spots and molten pool formation [24].

Damaging of a carbon composite panel during A or D waveforms

The attachment of the arc on composite panels highly depends on the characteristics of the paint layer and the protection layer. The lightning protection systems are used to prevent composite damage from lightning. These protection subsystems are generally performed with a thin layer of metal located between the ply and the paint layer. A large variety of surface metallization shapes can be used, including expanded copper or aluminum foils (respectively ECF and EAF), solid foil, or bronze mesh (BM). Figure 19 shows two examples of protection used for composites: the left picture is a bronze mesh and the right is an expanded copper foil.

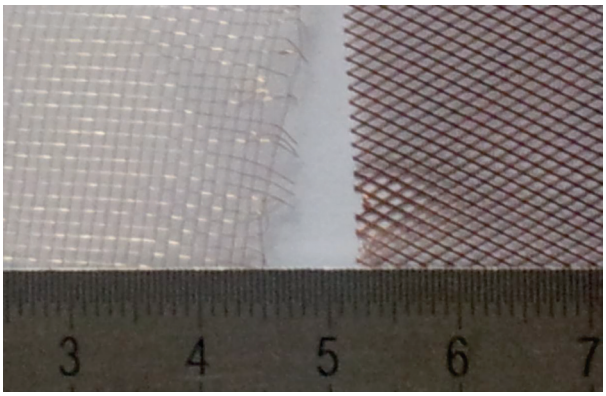

Figure 19 - Left: bronze mesh (BM), right: expanded copper foil (ECF)

This strong interaction between the arc attachment and the surface characteristics (paint and protection system) leads to different types of damaging. The examination of damages after lightning tests indeed shows a large variety of shapes, areas and numbers of damaged plies (see [21]). Areas of damaged protection reported by these authors are greater than 30000 mm² (17 cm wide) on painted panels subjected to an A-waveform (200 kA). They also report areas in which the first ply is seriously damaged with surface damages greater than 3000 mm² (5 cm). Some authors also estimated the delamination area in the composite material using ultrasonic C scan [25] or X ray analysis [26] and they reported a damaged area of thousands of mm². Examples of typical shapes of damaged zones after tests are presented in figure 20, for two types of protection [21]. In these examples, the lightning protection systems are different, but the current component (D) and the paint thicknesses (about 100 μm) are the same for the two panels. In the picture on the left, the protection used is a 65 g/m² Bronze Mesh (BM), while the panel in the picture on the right is protected with a 90 g/m² Expanded Aluminium Foil (EAF).

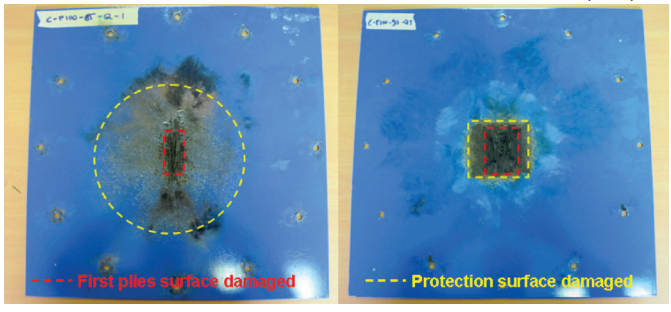

Figure 20 - Picture of the damaged surfaces evaluated for a painted panel protected with BM 65 g/m² (left) and with EAF 90 g/m² (right).(Lago et al. [21])

The EAF 90 g/m² protection seems to be more efficient than the BM 65 g/m² protection in terms of the protection surface damaged. On the other hand, the BM 65 g/m² protection is more efficient than the EAF 90 g/m² if we consider the area in which the first ply is damaged. Experiments show that such a conclusion changes if the waveform, the paint thickness or characteristics of the composite panel change. Thus, it is very difficult to provide a general behavioral law of the arc-panel interaction. Some authors [27] have proposed a classification of the damages as a function of two main types of protection, the paint thickness and the current peak value. For a given paint thickness and a given peak value, the "arc root dispersion" protections (BM 65g/m² for example) give wide and superficial damages while "current conduction" protections (e.g. EAF) are associated with deeper damages over smaller areas.

Numerical simulation may help in the understanding of direct effects of lightning on composite panels. To achieve this goal, all of the processes involved in the damaging must be taken into account. It is also necessary to calculate the distribution of the electric field over the entire integrated panel, in the metallic protection, in the plies, between the plies, and in the paint layer respectively. The current density must be injected into the structure according to the interaction of the arc root with the temporal evolution the surface roughness (presence of paint, metallic protection, resin or composite). The interaction between the vaporization of the protection and the paint layer must be taken into account to correctly simulate the expansion of the arc root. Finally, the dielectric breakdowns between the plies and the pyrolysis of the matrix must be modeled for the calculation of the current distribution in the structure. Such a numerical model is based on many assumptions and cannot pretend to accurately evaluate the damages of a given structure with a given current waveform. However, it provides a qualitative behaviour of the damaging process of a composite panel. The left hand side of figure 21 shows the surface roughness after a 50 kA waveform on a 0.2 cm×10 cm×10 cm carbon stratified panel with a paint layer of 20 μm. The arc attachment radius was set to 1cm. The damaged area is of about 1000mm² and the first ply is not deeply damaged. The right hand side shows the internal state of the panel at t=5 μs for three different paint thicknesses, for a current D waveform. In these simulations, the arc root expands freely according to surface roughness (presence of paint).

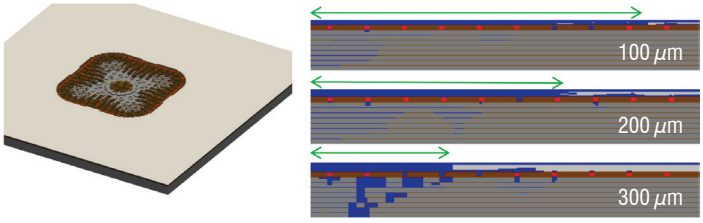

Figure 21 - Left: view of the surface roughness after a 50 kA waveform on a 0.2 cm×10 cm×10 cm carbon stratified panel with a paint layer of 20 μm. Right: cross section of the material at t=5 μs for a D waveform for three different paint thicknesses. (Blue: air plasma, white: paint, red: bronze mesh, brown: resin, grey: ply).

The size of the arc root is visualized with a green arrow on these pictures. We can notice that the arc root radius is greater than 1cm at this time for the 100 μm paint thickness panel while it is about 3.5 mm for the 300 μm paint thickness panel. We can notice that the damages are superficial in the case of the 100 μm paint thickness, while the panel is punctured for a paint thickness of 300 μm. We also notice that several dielectric breakdowns have occurred between the plies (presence of blue layers between the plies). This mechanism is associated with the formation of a conductive path between the plies which gives rise to internal sparking phenomena. Some authors [25] consider that the internal pressure coming from pyrolysis gases accelerates the propagation of the delamination of the stratified material. Internal sparking is an important mechanism in the damaging of composite structure. For the 300 μm paint thickness, the temperature increase in the deep plies is very fast, because the arc root remains small. This leads to a rapid puncture of the panel (t=5 μs). Simulations have shown that foil or expanded metal protections limit the electric field penetration into the material and avoid the breakdowns between deep plies. Moreover, metal meshes involve current reinforcements on each crossing of wires, which give rise to metal vaporization and the rapid decrease in mesh resistance. This mechanism does not exist in metal foil protections because they lead to a continuous current dispersion toward the boundary of the panel.

Mechanical damaging of aluminum and composite panels during stroke

In § "Mechanical constraint on arc attachments" and § "Characteristics of the arc root", the theoretical mechanical force that acts on the panel was presented. The examination of aluminum panels after tests shows a plastic deformation that may reach more than one centimeter. The plastic deformations in composite panels do not appear clearly, probably due to the elastic nature of the composite material. However, the mechanical damage in composite panels is the delaminating phenomena, which require internal analysis (X ray, ultrasonic scan, etc.). Some experimental measurements of the panel displacement during lightning attachment have been performed with various techniques [20], [21] and [28]. They showed transient deflection that evolves as a decaying sine wave, on which some additional modes may be superimposed. Observation of 2D displacements with a digital image correlation technique [21] shows that the deflection of the panel is mainly axisymmetric. These modes are represented in figure 22.

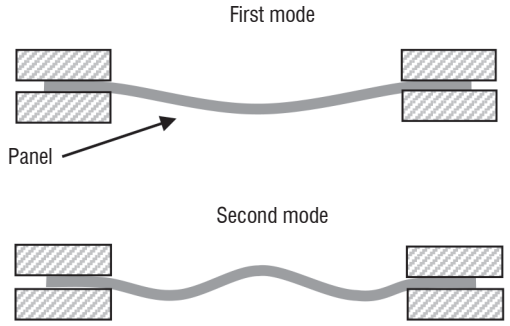

Figure 22 - First and second axisymmetric modes of an embedded panel

Deflection analyses show some important features associated with the mechanical stress that leads to mechanical damage. These have shown that the maximal deflection recorded is proportional to the square root of the action integral. They give some theoretical explanations of this feature, for both aluminum and composite materials. This result allows the correlation of an arc parameter (e.g. the action integral) with the mechanical response (the maximal deflection) of a given sample. Experimental measurements also highlight the fact that the presence of a paint layer increases the deflection of tested panels. For aluminum skins, the paint layer drastically increases the plastic deformation at the attachment point. For composite panels, as is observed for thermal damages, it is more the paint/protection couple

that has an effect on the panel. High current tests (A waveform) with thick painted panel (>300 μm) generally lead to large scale delaminating and mechanical breakdown. It is believed that the mechanical impulse on such panels is the most important constraint.

Simulations of the mechanical response of panels, on which theoretical mechanical stresses evaluated with arc simulations are used, give relatively good agreements with measurements. A transient nonlinear approach is required for this type of simulation. The results indicate that both the magnetic and hydrodynamic pressure must be taken into account to correctly calculate the panel deflection in all types of material, with or without paint. Figure 23 shows a 2D simulation of the deflection of a 2mm thick aluminum panel. The blue zone represents the panel position before the load, and the colored zone represents the panel with lightning load at t=1.4 ms. During this simulation, the maximal deflection is about 1mm. This figure shows the internal Von Mises stress that predicts yielding of materials under the loading condition. We can notice that the stress is maximal at the center of the panel, near the attachment of the arc on both sides of the panel.

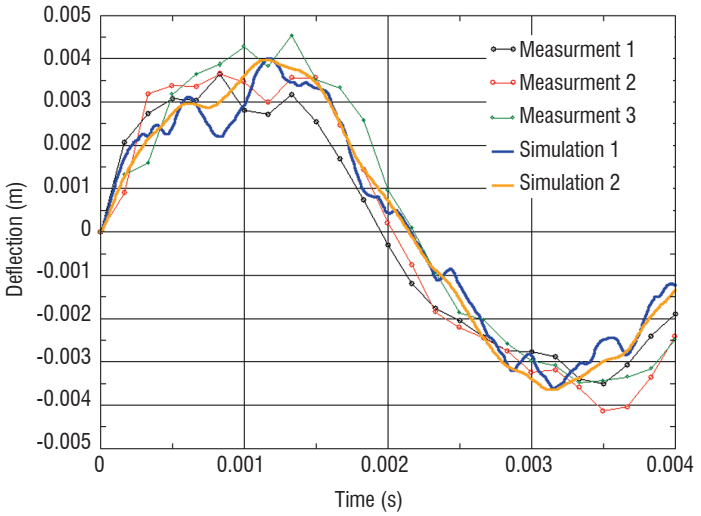

Figure 24 - Evolutions of the measured and simulated deflections of composite panels

Analyses have indicated that the location of the attachment point on the panel does not change either the frequency of the oscillations, or the position of maximal deflection, which is always located at the center of the panel. Moreover, the maximal deflection slightly varies with the location of the attachment point. These conclusions are important because accurate control of the arc root position during testing is not possible. Thus, comparisons of the measured and simulated maximal deflection point on the panel can be performed. Figure 24 shows the changes in the measured deflection at the center of the panel, for three composite panels subjected to a D waveform. The changes in deflection calculated with mechanical software are also plotted with bold continuous lines. The loading associated with this deflection is a sum of the magnetic pressure presented in § "Mechanical constraint on arc attachments" with an analytic model of shock wave propagation. Two values of equivalent radius Rc have been used: the lowest value corresponds to “Simulation 1” and the highest to “Simulation 2”. We can notice a relatively good agreement with measurements on the rise time and the maximum deflection.

More generally, numerical and experimental analyses indicate that the deflection of unpainted panels (composite and aluminum) is mostly due to the acoustic shock wave, while painted panels seem to be more stressed because the magnetic pressure acts as an additional contribution. More specifically, the large plastic deformation in painted aluminum panels cannot be simulated without taking into account the contribution of magnetic pressure over a small area of 8 to 10 mm radius.

The direct effects of lightning on fasteners in composites

Introduction

The massive use of composite materials in modern aircraft requires careful consideration regarding how the lightning strike attaches and how the current flows through the structure. The great difference between the electric conductivity of metallic fasteners and the conductivity of composite materials increases the probability of lightning attachments to fasteners. Moreover, the large number of fasteners used in aircraft

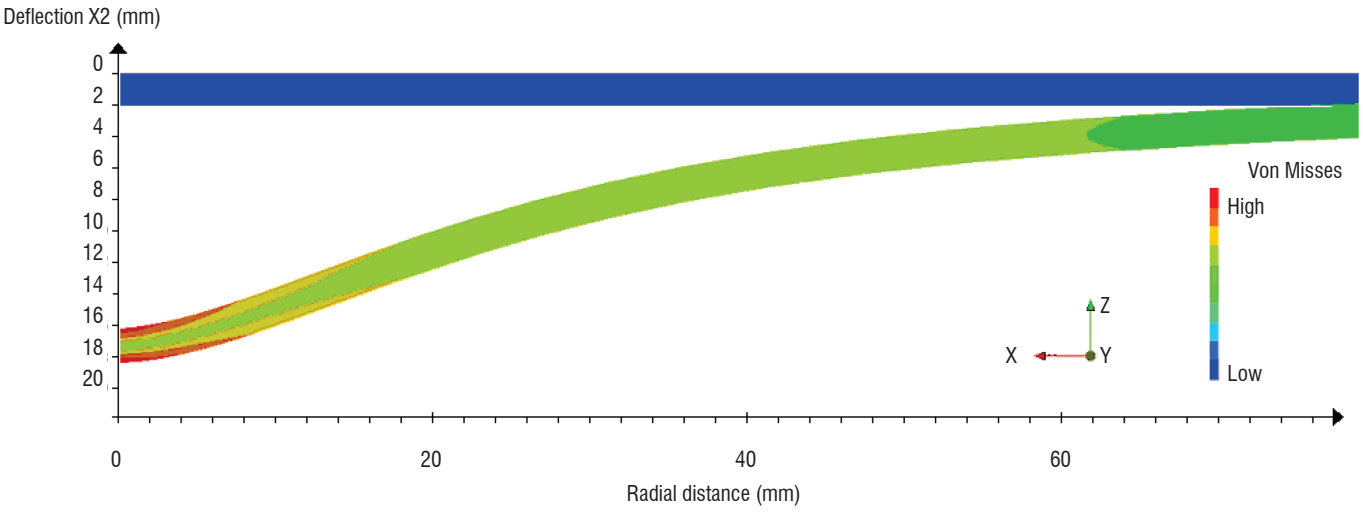

Figure 23 - Deflection of the panel. Color: Von Mises criteria

construction creates conditions for the current to flow through fasteners by conduction in distant zones of attachment. Sparking or arcing phenomena are generally observed on fasteners in which a strong current flows, with likely hazardous effects in the fuel tank area.

Phenomenology

The direct effects of lightning on fasteners and rivets are generally the source of several physical mechanisms. The occurrence of these mechanisms depends on the material used for the assembly (for example, metal rib with carbon composite), the type of electrical threat (attachment or conduction) and the value of the current peak. In the following sketch (figure 25), we present the three main mechanisms that occur on carbon-carbon structure on which a lightning arc is attached.

In that case, the current flows through both the rib and the skin; its typical path is represented with green dashed arrows. The current mainly flows directly in the surface protection, but a significant part of the current may cross the gap between the bolt and the skin or the rib. The intense energy spent in this small resistive gap creates an arc plasma that strongly increases the internal pressure, which blows out in the form of sparks. This mechanism is called "Outgassing" and is considered to be the most important constraint on fasteners. Moreover, in some cases, the electric field may be reinforced between the nut and the rib, and a discharge, called "Thermal spark" may be created. Finally, some discharges may also occur on the edge of composite ribs. This phenomenon, called "Edge Glow" is generally associated with the electric field reinforcement between plies with different orientation.

Sparking simulations

All of the mechanisms associated with sparking phenomena occur during a short time interval ($<1\ \mu s$) and in a small area. Moreover, the sparking location is unpredictable and cannot be accurately determined before the test, as we can see in figure 26. Experiments also bring to light a low repeatability in the results. This could be the reason why advanced characterizations of the plasma associated to sparking phenomena have never been performed or published. The studies are generally based on imaging techniques, electrical characterization and material analyses, which provide some interesting information for the understanding of the sparking phenomena.

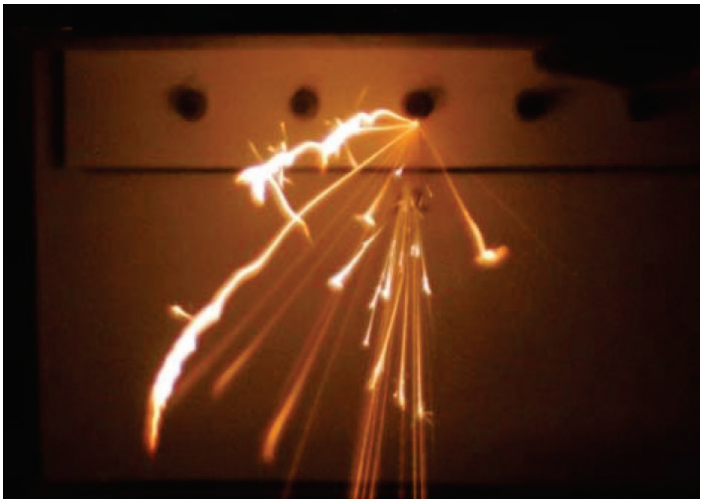

Figure 26 - Picture showing a fastener sparking [30]

Measurements of current distribution into the structures indicate that a significant part of the current may flow into the rib, even if it is initially isolated by insulating layers (sealant or paint) between the skin and the rib, or between the nut and the rib. Rapid breakdowns of dielectric layers may explain the quick transition from insulated to electrically connected rib. Numerical simulations of this mechanism may be performed by taking into account isolating layers and breakdown phenomena (see figure 27).

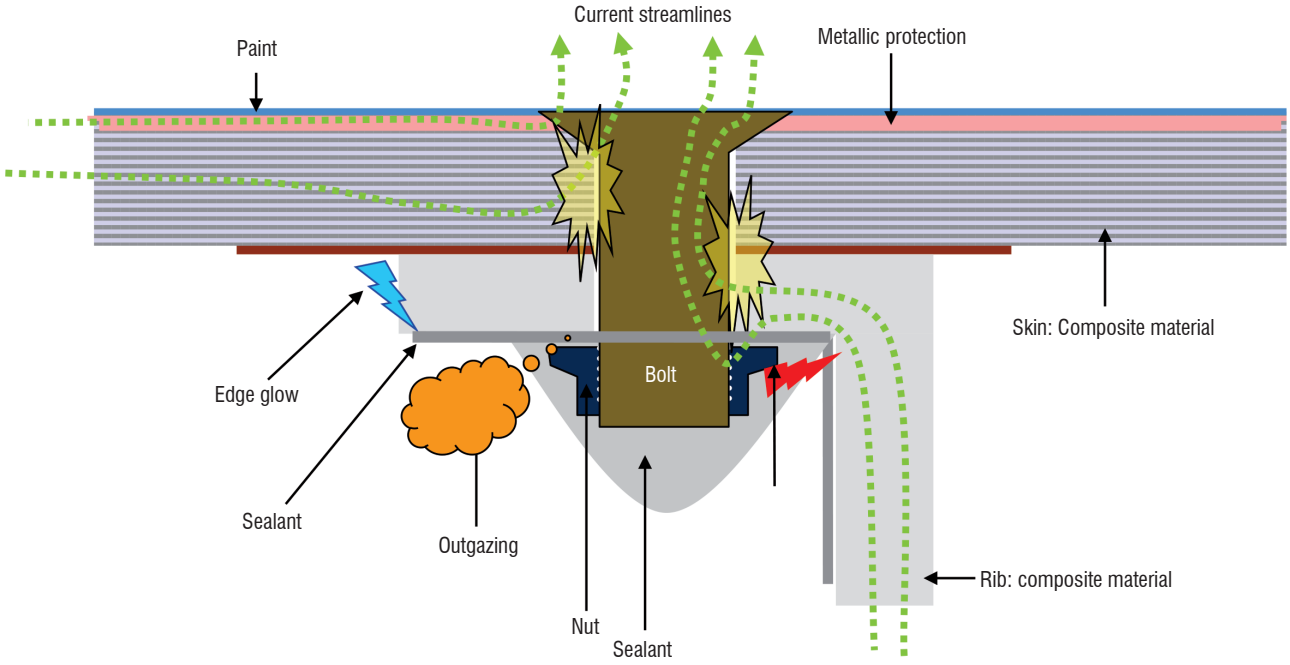

Figure 25 - Schematic drawing of the different mechanisms that occur during sparking phenomenon

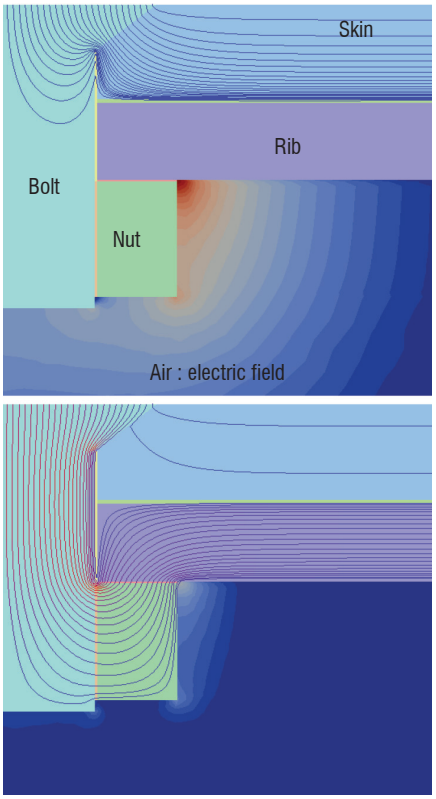

Figure 27 - Current streamlines before and after breakdown of sealant between the nut and the rib. The air zone is colorized with the amplitude of the electric field. The total voltage drop is the same on both situations

On the left hand part of figure 27, the current essentially flows from the head of the bolt to the skin and the resistance between the nut and the rib remains relatively high at this time. We notice an important reinforcement of the electric field close to the nut-rib interface, which leads to a breakdown occurrence. Once this short-circuit has occurred, the current mainly flows through the nut and the rib, and the electric resistance of the assembly decreases. The electric field takes on a relatively low amplitude in relation to the previous state. Some measurements [29] indicate that the presence of metal protection on the surface of the skin is required to restrict most of the current flowing through the rib, by decreasing the skin resistance. Measurements of the resistance of the fasteners before and after a shot indicate significant discrepancies, which may reach a factor of 100. It is generally believed that this changing is associated with melting or welding occurrences in the contact between the different materials.

Arc occurrence in electrical contacts

One of the main physical mechanism involved in the sparking phenomena is associated with the electrical contacts between the different materials used in assemblies. As is shown on the left hand side of figure 28, the real contact area may be very small, because of the surface roughness. Mulazimoglu [30] presented Scanning Electron Microscope (SEM) micrographs showing the micro-structure between a metallic fastener and a carbon fiber composite. Many micro-voids are shown between the metal and the composite structure, which may explain the sparking occurrence during tests. The current density increase may lead to the explosion of the contact spots into the cavity and create important overpressure. Moreover, the electric field in the insulating gaps between the two pieces may give rise to breakdown occurrences of the air or sealant gap, which leads to the fast decrease of the contact resistance in the assembly. Teulet et al. [31] evaluated the internal overpressure due to sealant ablation and arc formation to be about 100 to 450 bars.

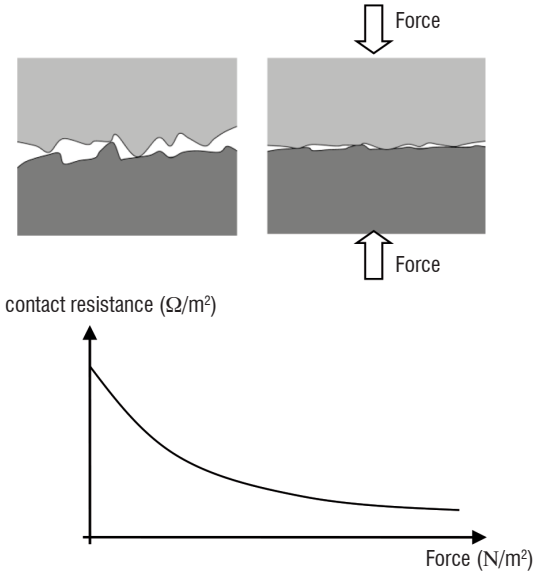

Figure 28 - Schematic drawing of the actual contact area associated with surface irregularities. Right: relationship between contact resistance and the force applied on the contact

One way to reduce the gap and the contact resistance consists in increasing the force into the assembly. The right side of figure 27 shows the typical evolution of the contact resistance between to metallic materials as a function of the pressure. This resistance decreases with pressure, and reaches a minimum value under which the pressure does not act anymore. This feature is quite similar in metal-carbon interfaces. The use of conforming metals that deform into the gap is also a good way to improve contact efficiency. This solution brings the material into intimate electrical contact with the composite structure, which prevents arc and spark formation [30].

Conclusion

The direct lightning effects on aircraft structures are of great importance nowadays, because of the massive use of composite materials in the new generations of aircrafts. In this paper, we have presented the phenomenology of the lightning arc attachment on aircraft. We have shown some differences between lightning arcs observed in flight and those simulated in the laboratory. We have also introduced some recent developments and results from numerical simulations. The shapes, the behaviors and other characteristics are compared with experiments. Discussions on the differences are also presented. In a second section, we have introduced the direct effects of lightning on aircraft skins. Both thermal and mechanical constraints are introduced and illustrated with experimental and numerical results. The negative effects of the paint layer on the damaging of composite and metallic materials have been illustrated. We have finally presented the direct effects of lightning on fasteners in the third section. The main mechanisms that occur during sparking phenomena were presented. Some results available in the literature were also presented and discussed, and we have concluded with the recent solutions to avoid sparking in fasteners and assemblies ■

References

[1] P. LALANDE, A. BONDIOU-CLERGERIE, P. LAROCHE - *Analysis of Available in-Flight Measurements of Lightning Strikes to Aircraft.* Int. Conf. On Lightning and Static Electricity, Toulouse, France (1999)

[2] ARP5412 - *Aircraft Lightning Environment and Related Test Waveforms*. SAE International

[3] F. A. FISHER, J.A. PLUMER, R.A. PERALA - *Lightning Protection of Aircraft*. Lightning Technologies Inc., 1989.

[4] F. HEIDLER, J. M. CVETIC, B. V. STANIC - *Calculation of Lightning Current Parameters.* Power Delivery, IEEE Transactions on, vol. 14, no. 2, pp. 399 –404, Apr. 1999.

[5] V. MAZUR - *Triggered Lightning Strikes to Aircraft and Natural Intracloud Discharges.* Journal of Geophysical Research, Vol 94, N° D3, pp 3311-3325, 1989

[6] I. GALLIMBERTI - *The Mechanism of the Long Spark Formation.* Journal de Physique, Tome 40, 1979.

[7] A. D'ANGOLA, G. COLONNA, C. GORSE, M. CAPITELLI - *Thermodynamic and Transport Properties in Equilibrium Air Plasmas in a Wide Pressure and Temperature Range.* The European Physical Journal D, vol. 46, no. 1, p. 22, 2008.

[8] L. CHEMARTIN, P. LALANDE, E. MONTREUIL, C. DELALONDRE, B. G. CHÉRON, F. LAGO - *Three Dimensional Simulation of a DC Free Burning Arc. Application to Lightning Physics.* Atmospheric Research, vol. 91, pp. 371– 380, Feb. 2009.

[9] M. MODEST - *Radiative Heat Transfer*. Academic Press, 2003.

[10] SIEGEL, HOWELL - *Thermal Radiation Heat Transfer*. 4th ed. Taylor & Francis, 2002

[11] PEYROU, L. CHEMARTIN, P. LALANDE, B.G. CHERON, P. RIVIERE, M.-Y. PERRIN, A. SOUFIANI - *Radiative Properties and Radiative Transfer in High Pressure Thermal Air Plasmas.* J. Phys. D: Appl. Phys. 45 (2012) 000000

[12] SAE ARP 5416, Eurocae ED-105, *Aircraft Lightning Test Methods*, Section 5, 2004

[13] L. CHEMARTIN et al. - *Simulated Lightning Attachment on Unpainted Aluminium Panels During Continuing Current Stage: Effects of the Jet Diverting Electrode.* Pittsfield, Icolse 2009

[14] A. LARSSON, A. BONDIOU-CLERGERIE, P. LALANDE, A. DELANNOY, S. DUPRAZ - *New Methodology for Determining the Extension of Lightning Swept Stroke Zones on Airborne Vehicules.* SAE 2001 transactions, Journal of Aerospace 2001.

[15] A. BIZYAEV et al. - *Investigation of the Sweeping of Lightning in Wind Blown Arc Experiments*. Int. Conf. on Lightning and Static Electricity, Toulouse, 1999

[16] DOBBING, HANSON - *A Swept Stroke Experiment With a Rocket Sled*. Proceeding, International Symposium on electromagnetic Compatibility, Atlanta, 1978

[17] S. TANAKA, K, SUNABE, Y. GODA Y - *Three Dimensional Behaviour Analysis of D.C. Free Arc Column by Image Processing Technique*. XIII Int'l Conf on Gas Discharges and their applications, Glasgow, 2000

[18] HAGENGUTH - *Transactions of the American Institute of Electrical Engineers*, Volume: 68 , Issue: 2, July 1949

[19] A. KADDANI, C. DELALONDRE, O. SIMONIN, H. MINOO - *Thermal and Electrical Coupling of Arc Electrodes*. High Temp. Chem. Processes Vol 3, pp.441,(1994).

[20] S.J. HAIGH - *Impulse Effects during Simulated Lightning Attachments to Lightweight Composite Panels*. International Conference on Lightning and Static Electricity, Paris, 2007

[21] F. LAGO - *Measurements by Stereo Correlation of the Deflexion of Panels Submitted to Lightning Pulse Currents.* International Conference on Lightning and Static Electricity, Oxford, 2011

[22] G. B. WHITHAM - *Linear and Nonlinear Waves* (Pure and Applied Mathematics), 1974

[23] L. CHEMARTIN - PhD, University of Rouen, 2008. http://publications.onera.fr/exl-doc/DOC376449_s1.pdf

[24] A.B. MURPHY - *A Self-Consistent Three-Dimensional Model of the Arc, Electrode and Weld Pool in Gas–Metal Arc Welding.* J. Phys. D: Appl. Phys. 44 (2011) 194009 (11pp)

[25] OGASAWARA et al. - *Coupled Thermal–Electrical Analysis for Carbon Fiber/Epoxy Composites Exposed to Simulated Lightning Current.* Composites Part A 41 (2010) 973–981

[26] P.K. ACKERMAN - *Paint Thickness Comparison Over Composite Lightning Surface Protection Systems and in-Service Ramifications.* Seattle, Icolse 2005

[27] A. Mc KEEMAN BROWN - *Evaluating Surface Protection Systems for Aerospace Composites.* Seattle, Icolse 2005

[28] GINESTE et al. - *Assessment of Lightning Direct Effects Damages by Modelling Techniques*. Pittsfield, Icolse, 2009

[29] REVEL - *Understanding of Sparking Phenomenon in CFRP Assemblies.* Pittsfield, Icolse 2009

[30] MULAZIMOGLU et al. - *Development of Conforming Sleeve Fastener Technology For Lightning Protection of Composite Aircrafts*. Pittsfield, Icolse 2009

[31] TEULET et al. - *Calculation of Pressure Build-up Around Fasteners Due to Sparking*. Oxford, Icolse 2011.

[32] *Aircraft Lightning Environment and Related Test Waveforms Standard.* Issued in August 1997

[33] S. A. WUTZKE, E. PFENDER, E. R. G. ECKERT - *Study of Electric arc Behavior with Superimposed Flow.* AIAA Journal, Vol. 5, No. 4 (1967), pp. 707-713.

AUTHORS

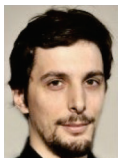

Laurent Chemartin graduated from the Institut National Polythechnique de Grenoble in 2005, and received his Ph.D. degree in 2008 from university of Rouen. His Ph. D. thesis was focused on the modelling and simulation of lighting arc and its interaction with material, in collaboration with EDF and DGA Techniques Aéronautiques. He has been working at Onera as a research engineer since 2009. His main activity is dedicated to the study of direct effects of lighting on aircraft structures. He is currently in charge of the development of a high current generator (GRIFON) for the simulation in laboratory of lighting arcs.

Philippe Lalande graduated from the «Ecole Supérieure de Physique Chimie de Paris" Paris (1992) and received a PhD degree in Plasma Physics from University Paris XI (1996). He joined Onera in 1996 where he has been involved both in the modelling of lightning interaction with aircraft and in the development of onboard atmospheric sensors. He is the Head of the lightning and plasmas Research Unit at Onera Chatillon.

Bruno Peyrou graduated from Ecole Nationale Supérieure d'Ingénieurs de Poitiers in 2008 and received his Ph. D. Degree in 2012 from university of Rouen. His Ph. D. thesis was focused on the development of a lighting arc model dedicated to return stroke. The aim of this work was to simulate the fluid dynamic of arcs subjected to peak of current taking into account the high radiative transfers and the transient electromagnetism phenomenon.

Arnaud Chazottes received an Engineering Diploma from ENSTA in 2005 and a Master degree in Energetic the same year.He joined ONERA in 2007 as icing research scientist in the Physics and Instrumentation department. He has been involved in aircraft and rotorcraft icing for over 4 years, working both on the development and application of several icing codes (2D and 3D). His current activities deal with Atmospheric phenomena modelling and sensor development.

Paul-Quentin Elias graduated from Ecole Centrale Paris in 2003, and hold a Ph. D. from the in Energetics, from the same institution. His main interests are the applications of cold or thermal plasmas to aerospace systems. His current activities involves the development of optical diagnostics for lightning and sliding discharges.

Clarisse Delalondre received the Ph.D. degree in electric arc numerical simulation including non equilibrium sheath modeling from the University of Rouen, France. Since 1990, she has been with Fluid Mechanics, Power Generation and Environment (MFEE) Department, EDF R&D, Chatou, France. She specialized on numerical simulation of electric arc for industrial applications such as welding, arc furnace, plasma torch, circuit breakers, transformer station, and lightning. Her research works focus on nonequilibrium phenomena, unsteady phenomena in electric arc, and developments on electric arc simulations performed in EDF software Code_Saturne®.

Frédéric Lago received his Ph.D. degree in 2004 from the University of Toulouse. His Ph. D. thesis was focused on the modelling of a lighting arc and its interaction with a metallic and composite material, in collaboration with the LAPLACE laboratory and EADS IW. He has been working at DGA Techniques aéronautiques as a lightning expert and test manager since 2007. His main activity is dedicated to the study of direct effects of lighting on aircraft structures. He is in charge of the qualification and certification of aeronautics structure to high current and high voltage directs effects. Frédéric Lago is also a member of the EUROCAE Working Group 31.

Bruno Cheron was born in Rouen on June 16, 1951. He received the degree of Doctor of Physics from the University of Rouen, France in 1979. His thesis was concerned with the Thermodynamic state of an Atmospheric HF Argon Plasma sowed with cadmium. Since 1993, Dr Chéron is Professor of Physics at the University of Rouen. His current research interests include the study of new Plasma Sources, the simulation of Space Shuttle Re-entries, the Treatment of Wastes and the Surface Metrology based on Laser Induced Plasma Spectroscopy.

J.-P. Parmantier, F. Issac,
V. Gobin
(Onera)

E-mail: jean-philippe.parmantier@onera.fr

Indirect Effects of Lightning on Aircraft and Rotorcraft

This article discusses issues related to indirect lightning on aircraft/rotorcraft. The standard waveforms used for qualifying the vulnerability of a system are introduced, with their frequency spectrum. The identification of the elementary EM coupling phenomenon allows the understanding of the key drivers of the current distribution and field scattering on a complex structure. The system level EM coupling analysis starts with examples of cable-measurements on real aircraft/rotorcraft, from which simple models are derived in order to understand the origin of the resulting waveforms. Various ways of protection are then proposed, ranging from passive to active solutions. Finally, despite limitations, 3D EM modeling is presented as an efficient complement to scale-one tests. The article concludes on the validity of current knowledge on indirect lightning for future aircraft designs.

Introduction

When lightning strikes an aircraft/rotorcraft (AC/RC), the system can be described by two conduction lightning channels made up of a positive leader and a negative leader [1]. From an electrical circuit point of view, the positive channel can be seen as the connection injecting charges at an injection point on the AC/RC whereas the negative channel can be seen as the path for evacuating the charges from an exit point of the AC/RC. “Indirect lightning effects” is thereby the dedicated term used to describe the electromagnetic (EM) effects following a “direct lighting” strike. When a direct lightning strike occurs, a large-amplitude current is injected at the point of injection. In addition to the local mechanical-effects and thermal-effects observed at the injection point, the electric current then circulates over all electrically conducting parts of the structure, on its external surfaces and inside the inner parts, including its electrical system, in order to reach the exit point. Such current redistributed over the entire structure is called the “induced” current. This redistribution of the current is a function of the impedances encountered along the various current paths. Since the current waveform is a transient, the impedances are made up of both a DC part (resistance effect) and a time-varying impedance (inductance).

Consequently, we can identify three main effects that are relevant, from the indirect lightning effects:

- Thermal effects: although the most important damages in terms of mechanical and thermal effects are due to the direct effect, indirect lightning can itself produce such effects. Indeed, on its way towards the exit point, the induced current may be obliged to concentrate along some narrow paths and produce heating of the mechanical parts supporting this current concentration.
- Electric discharges: when circulating along resistive and inductive paths, the electric potential varies on all the parts of the system. Large potential differences may be observed between very close paths, thereby resulting in an electric field that is large enough to overcome the electrical breakdown threshold and thereby produce electrical discharges. Such discharges may be observed at rivets or junctions between material parts and are particularly dangerous when they occur in fuel tanks.
- Effects at electronic equipment levels: a potential difference applied on impedant systems acts like source terms, driving induced currents along cables up to the level of the equipment connectors. Such currents may result in mechanical and thermal effects but, more generally, they result in dysfunction of electronic equipment. This explains why such an effect is categorized as an EM effect and why it is a central matter for the discipline of Electromagnetic Compatibility (EMC).

Of course the AC/RC industry has been coping with indirect lightning for a long time, because it addresses safety issues, this is why it is part of lightning certification in aircraft environments [2], [3], either at the equipment level [4], sub-system level or AC/RC level [5]. Over the past twenty years, in parallel to AC/RC development programs, several cooperative research projects have addressed this topic, which shows the concern for such a phenomenon in the aircraft industry. Significant progress has been made on the control of

this phenomenon. Among the various projects, we mention hereafter some projects in which Onera has been involved:

• in the late 80s, Onera took the opportunity of using the in-flight experiment on the C160 Transall Aircraft (see paper [6] in this Aerospace Lab. edition), sponsored by the French Defense Agency ("Délégation Générale pour l'Armement" – DGA), to instrument some EM field surface sensors on the skin of the aircraft and backdoor sensors behind a carbon composite door. At the time, the bidirectional waveforms were found to be very surprising, but they could be explained by current redistributions calculated on a simplified 3D model of the exterior of the aircraft [7]and backdoor electromagnetic EM coupling could be confirmed by the theory of scattering by small loaded apertures [8].

• in the early 90s, the French DGA pushed the aircraft industry, namely Dassault and Airbus, to work on the understanding of indirect lightning effects. Extensive experimentation was then carried out on a Carbon Composite Wing ("Voilure Composite Carbone" in French, VCC). This experiment set the first basis for the understanding of current redistribution on cylindrical-like two-dimensional (2D) structures [9]. The experiment was then followed by several studies extending the 2D approach to the three-dimensional (3D) redistribution effects.

• in the 90s, the European Union (EU) launched two major projects involving Academic, laboratory and industry partners, in which indirect lightning had a significant place. The FULMEN EU project, as part of the framework project 3 (FP3), established the first basis for the 3D modeling of aircraft, as well as its interior [10], [11] including wiring. It was followed by the 5th framework EMHAZ project, which took this analysis a step further by using more complex geometries. After these projects, the 3D modeling of indirect lightning on AC/RC became increasingly usual in AC/RC industry qualification and certification processes.

• from 2005 to 2008, the MOVEA French project, again sponsored by the French DGA, had the ambition of building an AC/RC model to calculate both the EM constraints generated by indirect lightning on an AC/RC, as well as to assess the possible disruptions observed at the level of the equipment [12]. In this project, an extensive analysis of the AC/RC experimental database was carried out, considering the AC/RC wiring as a deployed sensor of indirect current redistribution on AC/RC. Such an analysis investigated and explained in which geometrical configurations, and why, large induced currents could be observed on an AC/RC.

The purpose of this article is to review the fundamental bases, in order to be able to capture the relevant physics of indirect lightning on AC/RC. With this, the reader will understand how indirect lightning becomes a source of induced currents and how those induced currents may be distributed over AC/RC systems. With various types of modeling approaches, it aims at understanding the EM physics that drives indirect lightning induced current waveforms and distribution.

In § "Time domain waveforms and frequency spectrum", we briefly recall the time domain waveforms involved in the indirect lightning process, with their associated frequency spectra. First we introduce the waveforms as they appear in a standard indirect lightning current sequence. Then, we explain the interest in simulating these waveforms as biexponential-like waveforms and how to make this analogy. In § "Elementary EM effects", we present the elementary EM effects that contribute to the overall EM coupling indirect lightning response on a 3D structure. For this, we make the distinction between conduction and scattering effects. Conduction effects are EM effects characterized by the circulation of currents, as a function of the impedance that they encounter: 3 main signatures are considered, DC resistance, frequency varying impedance and current redistribution effects. These signatures are explained with simple analytical calculations and 2D-wire invariant-geometry models. Particularly, current redistribution is demonstrated with a 3D calculation of the surface current on an airplane model and an airplane payload model. A lightning EM scattering related effect is introduced with the problem of small apertures (small compared to the wavelength), for which efficient electric and magnetic dipole models can be derived. This approach logically leads us to the model of loaded apertures, applied in order to describe the field emission produced through materials and at the junction levels. Throughout the chapter, we make a comparison of the influence of the various elementary effects when they happen to be combined.

§ "Indirect lightning EM effects at system level" addresses the problem of effects at the electrical-system level; therefore we introduce here the problem of EM coupling in cables. First, we display some A-waveform induced currents measured on real aircraft and we identify typical frequency variation signatures of the transfer functions between current in wires over total injected currents. Then, in order to analyze the origin of those signatures, we use 2D-invariant models, such as the models considered in § "Time domain waveforms and frequency spectrum". Starting from a simple cylinder shape structure with internal wires, we progressively introduce a more realistic cross-section geometry encountered on a real helicopter. This analysis allows Thevenin-like equivalent source models to be derived, including a voltage generator and associated impedance. The common-mode type of coupling generated by currents flowing over lossy structures is thereby introduced. Finally, we investigate the relevance of the linear approximation by analyzing cable response on a helicopter with different amplitudes of the injected current. A large part of the material in this chapter comes from the MOVEA project previously mentioned [12].

§ "System level indirect lightning protection" introduces the problem of protection against indirect lightning effects. The protection comprises passive protection, which uses the installation of the structure and the system for designing as many shields as possible to decrease the internal EM coupling constraints, and active protection, which acts directly at the level of the equipment parts or electronic systems. The presentation focuses on passive protection concepts and goes through topology-based measures, such as grounding and bounding, cable shielding and cable routing. The shielded-cable part offers the opportunity to introduce the shield transfer impedance concept as a particular application of the EM shielding theory. Active protection mainly considers protection based on equipment inputs, with active non-linear devices triggered by the induced current, which is not considered in this paper because it is very specific to the type of functional signals to be protected. In addition, the specific protection problem of fuel tanks is not addressed in this article, even though its origin is clearly an indirect lightning problem. The reader will find a description of this specific problem [13]. Because of the possible damaging consequences on the mechanical structure, this problem is handled together within the direct lightning effects.

§ "System level numerical simulation" concerns a system level numerical simulation, since we consider that this topic has now become an integral part of any lightning design or analysis process on AC/RC. Based on 3D models capable of solving Maxwell's equations, or some of their approximations, we begin to introduce the specificities related

to indirect lightning and identify real difficulties in building and solving the models. As a demonstration of the progress made on modeling issues, particular emphasis is placed on the recent work by Dassault in the calculation of indirect lightning response, on their F7X airplane, with a degree of complexity that does not seem to have been achieved so far, to our knowledge. The use of stick models is also presented as an old trend recently put again to the fore, with much lighter models than 3D full-wave solvers.

Finally, after a summary of the main lessons of this article, we conclude on the consequence of new system designs, for which it may no longer be possible to separate direct and indirect lightning analysis, as is usually done in current practice.

Time domain waveforms and frequency spectrum

Standard waveforms

The signature of lightning injection current is not reproducible from one event to another, but typical signatures can be observed on all the events. This is why normalization standards have tried to define generic waveforms with which systems must comply [14], [5]. For AC/RC, the RTCA [4] and EUROCAE [15]define the waveform sequences represented in figure 1 and figure 2 ([4], [15]). Figure 1 constitutes the main standardized waveform sequence. The entire waveform is constituted by 4 subsequent elementary waveforms, each having a large action integral. The action integral is defined by the integral of the square of the current waveform; it is thereby related to the energy of the signal. Large action integrals thereby characterize large current amplitudes or long persistence time of their waveform. The 4 elementary waveforms are:

- Waveform A, which is a pulse representing the first arc. It has the largest amplitude of all of the elementary lightning waveforms (200 kA) and a duration of about 500 μs;
- Waveform B is the intermediate pulse current waveform making the slow transition between the waveform A impulse waveform starting from 2 kA and the constant C waveform (figure 1) at a level between 200 and 800 A, on a time scale ranging from 500 μs to 500 ms;
- The C waveform is a constant current representing the persistent current phase (between 200 and 800 A). This phase extends between 500 ms and 1s;
- The waveform D is another impulse waveform representing the second arc with a maximum equal to half of the maximum of the A waveform during 500 μs.

Note that all of the levels defined here correspond to a first arc waveform maximum scaled at 200 kA, which corresponds to the worst case, defined as 1% of all of the current waveforms on aircraft. Usual maximum amplitudes corresponding to 90% of the events have a maximum of the first arc of about 30 kA [16].

In addition to these main waveforms, the RTCA [4] and EUROCAE [15] define repetitive waveforms (the levels defined hereafter are scaled with respect to a 200 kA first arc amplitude waveform). The first type of waveform is the so called “multiburst waveform” (figure 2-a), which corresponds to the phase, in which the lightning channel is not totally established and which occurs before the first arc phase presented in figure 1. The RTCA and EUROCAE waveforms define it as 24 groups of 20 pulses occurring between 10 μs and 200 μs. Each elementary pulse is a called an H waveform, with an amplitude of 10 kA.

A second set of repetitive waveforms correspond to the so-called return stroke phenomenon (figure 2-b). The RTC and EUROCAE standards define it as a series of 24 half-amplitude D waveforms occurring during 2s, every 10-to-200 ms.

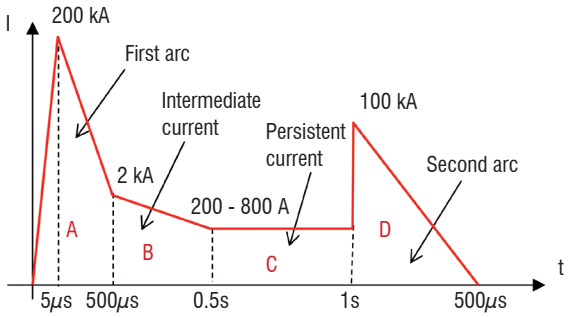

Figure 1 - Typical arc lightning waveform, as defined in the RTCA [4] and EUROCAE [15]

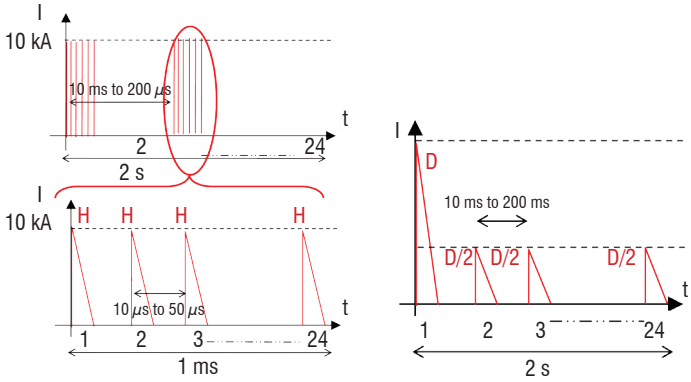

a) Multiple burst waveform (H waveform)

b) Multistroke waveform

Figure 2 - Typical repetitive lightning waveforms, as defined in the RTCA [4] and EUROCAE [15]

Simulation of the standard waveforms

In theory, the standard waveform defined by RTCA and EUROCAE are the ones to be shown by AC/RC airframers. Nevertheless, the test laboratories are not able to generate the set of pulses shown in figure 1 and in figure 2 in sequence. They generally can show, one at a time, some of the elementary waveforms independently and, sometimes, the sequence of two or three of the waveforms, however not necessarily in the right order of occurrence. The main elementary waveforms of lightning current for AC/RC indirect lightning certification are impulse A and H waveforms and, to a smaller extent, D and B waveforms.

Thus, the question is now: how can such pulses be generated with the given rise and decay times and the maximum amplitude? The biexponential waveform provides a very efficient and simple generic mathematical model for all of the elementary waveforms, because they are very close to the waveforms generated by real current sources, generally based on capacitive discharges [17], [18], [15].

The biexponential waveform is defined mathematically by the difference between two decaying exponentials:

$$I(t) = I_o\left(e^{-\alpha.t} - e^{-\beta.t}\right) \quad (1)$$

where α and β are two constant numbers in s^{-1} and I_0 is a constant number in Amperes.

A typical biexponential waveform is represented in figure 3. Its main characteristics are defined as follows:

- Amplitude of the maximum, Imax:

$$I_{max} = I_o\left(K-1\right).K^{\frac{-K}{K-1}} \quad (2)$$

with

$$K = \frac{\beta}{\alpha} \quad (3)$$

note that for $\beta >> \alpha$, $I_{max} = I_0$

- Rise time, T_r, defined as the time difference that exists when the signal rises up from 10% to 90% of its maximum amplitude:

$$T_r = \frac{2.19}{\beta}(s) \quad (4)$$

- Decay time, Δ, defined as the time difference for which the rising waveform and the decaying waveforms are equal to half of the maximum.

$$\Delta = \frac{0.69}{\alpha}(s) \quad (5)$$

Note that the exponential is not the only waveform for approximating the pulse. Especially, the biexponential has a non-zero derivative at time zero which is not physical and may cause problems in models. Other waveforms can be used in order to avoid this drawback [19].

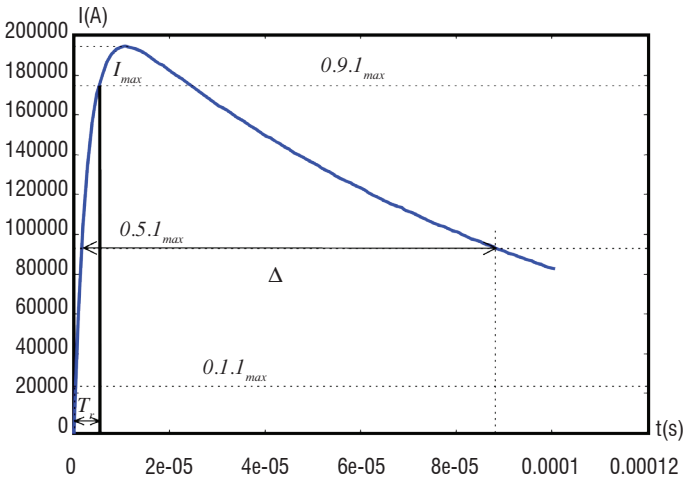

Figure 3 - General biexponential waveform and associated characteristics

Table 1 presents the characteristics of the A, B, D and H waveforms from RTCA and EUROCAE (see Video 1 "Standard lightning waveforms and general lightning current sequence"). Figure 4 zooms in on the first instants of those waveforms, whereas figure 5 displays their frequency spectra. The Fourier transform of the biexponential waveform defined in (1) is equal to:

$$E(f) = \frac{1}{\left(\alpha + j.2\pi f\right).\left(\beta + j.2\pi f\right)} \quad (6)$$

It shows two cut off frequencies f_{c1} and f_{c2} respectively defined by:

$$f_{c1} = \frac{\alpha}{2\pi} \quad (7)$$

and

$$f_{c1} = \frac{\beta}{2\pi} \quad (8)$$

On the one hand, f_{c1} depends on the α coefficient whose inverse defines the decay time, that is to say, the long times of the waveform. On the other hand, f_{c1} depends on the α coefficient whose inverse defines the rise time and is therefore related to the early times of the waveform. Figure 4 and figure 5 clearly show that the B waveform is a slow waveform (frequency content lower than some hundreds of Hz), with a quite large action integral (the integral of the waveform is equal to the Fourier transform at the frequency zero). The A waveform is also a slow waveform with a long rise time and a frequency content lower than some kHz, but with a large energy content (the largest of the 4 waveforms). Waveform D is very similar to waveform A for late times, with an amplitude divided by two. However, the rise time is somewhat larger than the rise time of the A waveform (see also the second cut-off frequency, which is larger than the second cut-off frequency for the waveform A). Finally, the H waveform is the least energetic waveform with the largest frequency content, with a first cut-off frequency of about 100 kHz.

Finally, compared to the usual waveforms considered in EM environments, such as Electromagnetic Pulse (EMP) or High Intensity Radiated Fields (HIRF), it appears that lightning is a low frequency phenomenon. Nevertheless, we will see later on in this document that its frequency content applied on large structures is large enough to generate all types of typical induced EM responses, such as inductive effects, field scattering and wave propagation.

	Waveform A	Waveform B	Waveform D	Waveform H
$Io(A)$	218810	11300	109405	10572
$\alpha(s^{-1})$	11354	700	22708	187191
$\beta(s^{-1})$	647265	2000	1294530	19105100
t_m	0,5 ms	10 ms	1 ms	10 μs
$I_{max}(kA)$	200	5	100	10

Table 1 - α and β coefficients and main characteristics of the impulse [4] and [15] biexponential waveforms

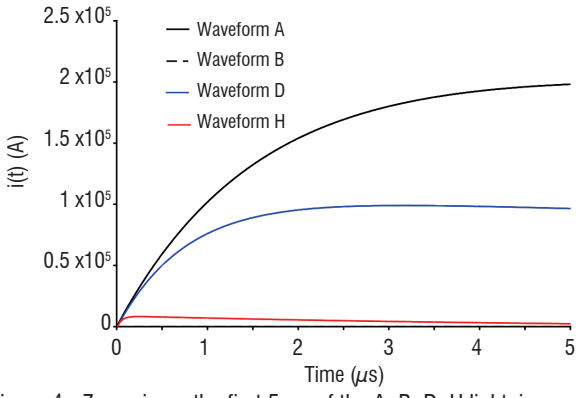

Figure 4 - Zoom-in on the first 5 μs of the A, B, D, H lightning waveforms

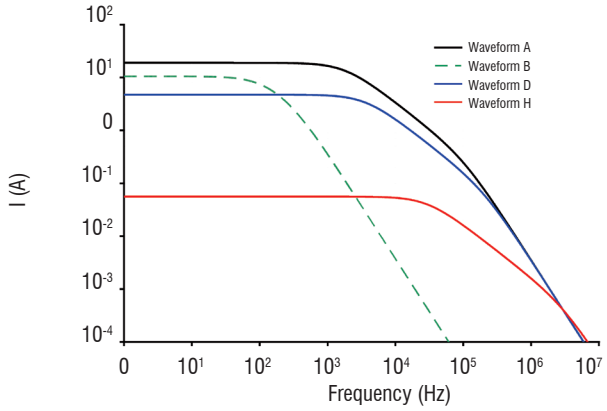

Figure 5 - A, B, D, H lightning waveform frequency spectra

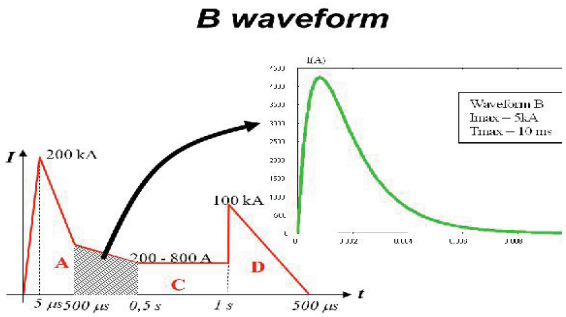

Video 1 - Standard lightning waveforms and general lightning current sequence
http://www.aerospacelab-journal.org/al5/indirect-effects-of-lightning-on-aircraft-and-rotorcraft

Elementary EM effects

We will now concentrate on the EM physics, which characterizes EM coupling on structures likely to be encountered on AC/RC. In particular, we will consider linear effects and assume that the sources triggering those effects do not generate any non-linearity. The physics involves several EM effects of specific nature that we will consider separately, under the name of “elementary effects”. In order to reveal those effects separately we will consider EM coupling situations on generic structures. This simplification restriction will allow us to make the distinction from the so-called “system-level effects”, which will be the subject of the next chapter.

Conduction effect

The conduction effect is related to the injection of an electric current inside the materials that constitute the system. We will distinguish 2 main phenomena:

- the resistance effect, which is a DC or very low frequency phenomenon that only depends on the electric conductivity of materials and therefore on their DC resistance;
- the redistribution effect, which is a dynamic phenomenon involving higher frequencies and depending on the geometry of the structure, and therefore on their frequency-varying impedance.

DC resistance

We will first consider the DC regime, or a regime for which the current can be considered as homogeneous inside a cross-section geometry of a material. With such an approximation, we will see after that we can consider the material as “thin” with respect to so-called “diffusion” effects related to the "skin effect". Let us consider the piece of rectangular material presented in figure 6 (length l, width w and depth d), in which a current I is injected. Assuming a uniform current density in the section of the sample, the resistance is classically given by [20]:

$$R = \frac{\ell}{\sigma S} = \frac{\ell}{\sigma w d} \qquad (9)$$

where σ is the electric conductivity and S is the section of the material at the current injection point, d being the thickness and w the width.

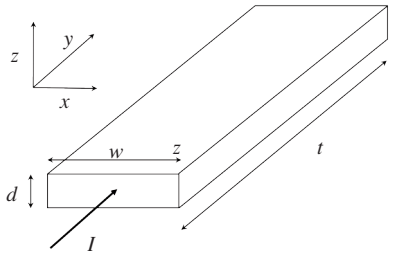

Figure 6: Rectangular material used to demonstrate resistance effects

This resistance concept, well known in electrical circuit theory, can also be derived from EM considerations involving the total tangential electric field Et on the material [8]. Indeed, the surface impedance of a material is defined as the ratio between Et and the homogeneous surface current density of the surface, J_s:

$$Z_s = \frac{E_t}{J_s} = \frac{1}{\sigma . d} \qquad (10)$$

We see that the surface impedance can be also evaluated as the resistance of a square material $(w=l)$. Whereas the resistance definition depends on the size of the material, the surface impedance is characteristic of the material with a given depth, whatever its surface dimensions are. This definition only assumes the homogeneity of the currents in the depth of material (no "skin effect").

Table 2 gives typical values of materials encountered on aircraft. The reference value is the value of the aluminum sheet for which we have a Z_s value calculated from (10) with the theoretical conductivity and the depth. For carbon materials, an equivalent conductivity is obtained from (10). For the two proposed materials used for direct lightning effect protection (copper foil and bronze mesh), only the measured Z_s value is available. In the case of application of those protections on carbon composite materials, the two Z_s values will act in parallel and will of course significantly improve the Z_s.

Type of material	Depth	Conductivity $(\Omega.m)^{-1}$	$Zs(m\ \Omega)$
Aluminum sheet	$10\ \mu m$	$37.6\ 10^{+6}$	2.7 *
Carbon panel (fabric 3 folds)	$900\ \mu m$	$1.5\ 10^{+4}$ *	72
Carbon panel	3 mm	$3.0\ 10^{+4}$ *	11
Expanded copper foil			2
Bronze mesh			6

Table 2 - Typical surface impedance materials (*Calculated)

Box 1 - The Z_s probe: an efficient non-intrusive device for in-situ Z_s measurement of materials

A direct evaluation of the surface impedance with an impedance-meter presents several practical drawbacks:

- This method necessarily adds parasitic junction resistances to the sample under test. They can be due to the additional metal pieces that must be used in order to control the flux of the injected currents;
- It is not compatible with aeronautical in-situ measurements, the material under test being generally not isolated from other parts of the structure and also covered with protection paint, for example.

A "Z_s probe" has been designed at Onera [8] to overcome these restrictions. The main idea is to create no-contact "Foucault currents" inside the material by an illuminating source, these induced currents being related to the impedance of the material (the higher the resistance, the smaller the currents). The completion of the injection probe with a reception probe can give access to the value of the Zs surface impedance.

An appropriate application of this principle is obtained with 2 parallel circular emitting and receiving loops. After a calibration of the coupling, in free space and for a selected band of frequencies, a sample is introduced between the loops (figure B1-1a); the circular induced current being negligible at low frequency and of increasing magnitude for higher frequencies (see numerical simulation in figure B1-1b), the variation of the coupling, in the same frequency band happens to be quite well approximated by a first order filter function for optimized geometrical parameters of the device (figure B1-1c).

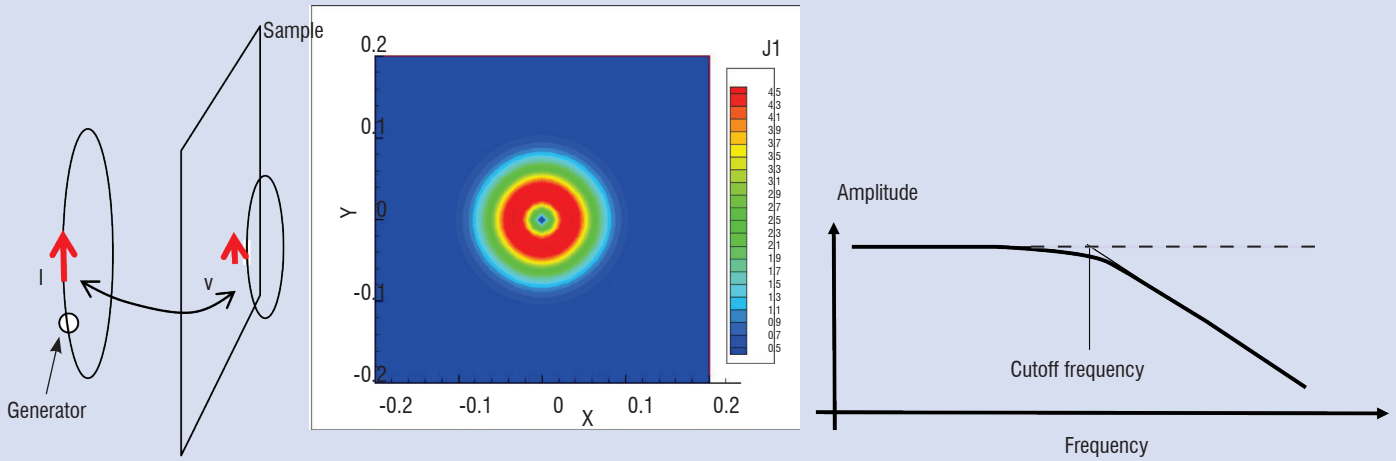

a) Measurement Principle b) Currents developed on the sample c) Transfer function between the two loops (log-log scale)

Figure B1 - 1: Zs probe main features

The measured cut-off frequency is proportional to the impedance of the sample if the material is isotropic and homogenous (typically on a 20 cm x 20 cm surface). Impedances of between a few mOhms to a few Ohms are within the application scope of the technique. The method appears to be efficient to characterize thin metal materials or carbon fiber composite materials, if the fibers are oriented in enough directions (giving rise to an almost planar isotropy).

A variation of the method, with both loops on the same side of the sample, is applicable for material covered by a thin layer of paint and allows application of the technique as a non-intrusive probe directly applicable in-situ.

Frequency varying material resistance

Now, let us consider some higher frequencies, which give rise to another type of EM physics called the “skin effect” [20]. When a material is illuminated by an EM wave, the EM fields penetrate the material; this phenomenon is known by the term “diffusion”; the skin effect is the phenomenon that tends to concentrate the currents on the illuminated side of the material. The distribution of the current density J being exponential in the material, $J=J_s e^{-d/\delta}$, the skin depth is defined as the depth δ for which the surface current density at the surface J_s is divided by e. δ is therefore the depth at which approximately 63% of the current is concentrated. It is defined as:

$$\delta = \frac{1}{\sqrt{\mu\pi\sigma f}} \qquad (11)$$

where μ is the magnetic permeability of the material.

The more the frequency increases, the more δ decreases and the more the resistance increases.

From an EM point of view, the skin effect, by participating in the attenuation of the current inside the material, contributes therefore to the shielding of the magnetic field. It is also at the origin of the frequency

variation of the transfer impedance of shielded cables (see § "Protection with shielded cables").

Current redistribution

At high frequencies current lines tend to repel each other, due to inductive effects. Therefore, the more the frequency increases, the more the current will distribute over the far dimensions of the object, that is to say, the edges and the corners of the structures. This phenomenon thereby depends on the geometry of the structure, unlike the resistance effects seen before, which only depended on the nature of the material.

The skin effect can be seen as a particular case of the current redistribution. In this case, the current is redistributed in the depth of the material. If the material is a plate, as described in the box 2, the current will concentrate on both sides of the material. If the material is part of a closet or a structural metallic surface, the current will concentrate on the external surface of the material.

Box 2 - Current redistribution on a plate

A simple way to describe the current lines is to use a thin wire approximation. This type of approximation will be more extensively used in the following sections (see § "Indirect lightning EM effects at system level").

In figure B2-1a we present the problem of lossy conductive plate on which a current Itot is injected, according to the medium axis of symmetry of the plate. In our case, we are more interested in the distribution of the currents at the center, Icen, and on the edges, I_{ext}. In figure B2-1b we present a rough (but convenient) thin wire approximation of the problem. The 3 currents, Icen and Iext are supported by 3 thin wires connected together at the ends.

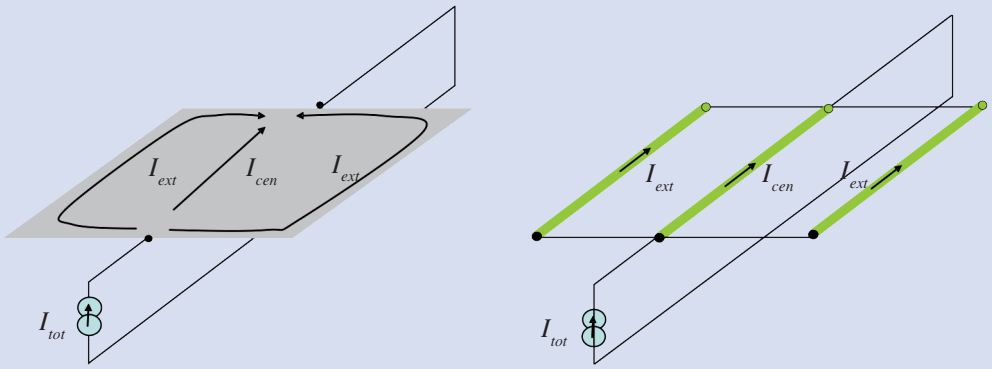

a) Problem to solve b) Thin wire model

Figure B2-1: Thin wire modeling of a metallic plate on which a current is injected

The analytical resolution of such a problem can be performed by solving the equivalent electrical circuit. As for every thin wire model approximation, the equivalent circuit can be described in a matrix form relating the various currents to the voltage drop V between the two sides of the plates. The relation between the currents on the wires and V is provided by an impedance matrix that includes the following terms:

- the resistances of each wire equal to R because the 3 wires are identical (the 3 wire resistances in parallel must be equal to the DC resistance of the plate);
- the self-inductances of each wire. Because our 3 wires are chosen to be identical, the 3 inductances are equal to L;
- the mutual inductances between the wires. Those mutual inductances depend on the geometry of the wires and the distance between them. Because of the symmetry of the problem, two types of mutual inductances must be distinguished:
  - M, the 2 mutual inductances between the center conductor and the 2 edge conductors
  - m, the mutual inductance between the two edge conductors

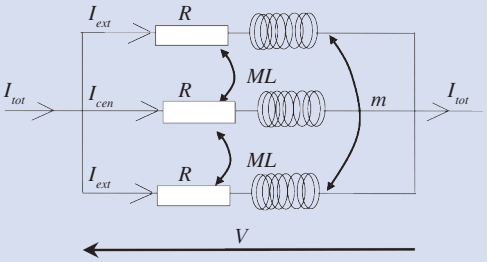

Figure B2-2: Equivalent circuit of the 3-thin-wire conducting plate model in figure B2-1

Finally, the three equations of the matrix equation can be simplified to the following 2 equations:

$$\begin{cases} V = \left[R + j\left(M + m\right).\omega \right].I_{ext} + jM\omega.I_{cen} \\ V = 2\,jM\omega.I_{ext} + \left(R + jL\omega\right).I_{cen} \end{cases} \quad (12)$$

with:

$$I_{tot} = 2.I_{ext} + I_{cen} \quad (13)$$

The resolution of (12) with (13) gives:

$$I_{cen} = \left(1 - \frac{j\omega\left(M - m\right)}{R + j\omega\left(L - M\right)} \right).I_{ext} \quad (14)$$

with $M > m$.

The analysis of (14) gives the following information:

1. At DC ($\omega = 0$), $I_{cen} = I_{ext}$, The current is uniformly distributed
2. At high frequencies (when imaginary parts become much larger than real parts):

$$I_{cen} = \left(1 - \frac{\left(M - m\right)}{L - M} \right).I_{ext} \quad (15)$$

which implies that $I_{cen} < I_{ext}$. The current is lower at the center than on the edges. Of course, as indicated before, this result is a rough approximation, because the model is limited to 3 wires. The model becomes much more precise when the number of wires increases and the model allows the progressive decrease of the currents in the wires from the edges to the center to be shown.

Video 2-a, Video 2-b and Video 2-c illustrate the redistribution effect on a 3D generic structure. Here, the example is a model of a Transall aircraft in various configurations of injection and output points of the current. Those injection and output points are defined from a zoning analysis, as described in [21], [22]. The calculation has been made with the ALICE Finite Difference Time Domain (FDTD) code from Onera. The model is very simple and its only intent is to visualize how the currents will circulate on the 3D surface. Several important elementary effects previously described must be noticed on these animations:

• The redistribution effect, which concentrates the currents on the edges. This effect occurs in the early time of the current injection because the frequency content is maximum. On the wings or on the tail for example, the current is distributed on the edges, whereas on the fuselage, which is close to a circle, the current is almost equally distributed. After the occurrence of the maximum of the current, the current vanishes uniformly on the surface between the injection and the exit points.

• The search for an exit point. The current flows along the minimum impedance path. In the early time, this impedance is mainly inductive. This is why the current may flow in parts of the 3D geometry that are not in the direct path between the injection and the exit point. The phenomenon looks as though the current were seeking its path, from the injection point to the exit point.

• The absence of resonance effects. The size of the aircraft and the frequency content of the A waveform are too small to excite resonances that would appear as currents bouncing back and forth between two geometrical points. On such an object, resonances would be of $l = \lambda/2$, where l is a characteristic dimension of the object (fuselage length or distance between wings, for example) and λ is the smallest frequency of the frequency spectrum. Such resonances are unlikely to occur on usual commercial aircraft in operation at this time, except perhaps for H waveforms on large AC such as Boeing 747 or A380.

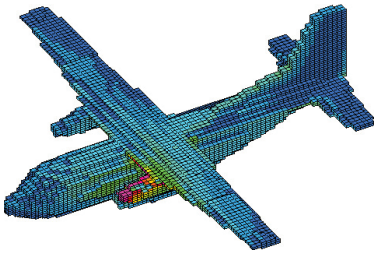

a) Configuration “Engine to tail”

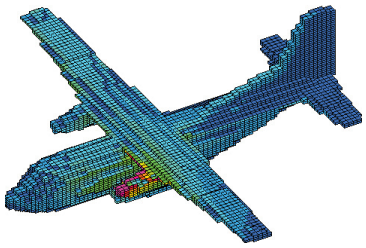

b) Configuration “Engine to Wing”

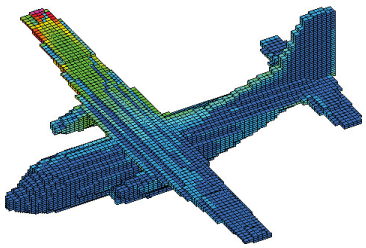

c) Configuration “Wing to Tail”

Video 2 - A waveform lightning injection on a Transall Aircraft
http://www.aerospacelab-journal.org/al5/indirect-effects-of-lightning-on-aircraft-and-rotorcraft

Video 3 presents another animated picture, still calculated with ALICE's FDTD computer code from Onera. It concerns the A waveform lightning injection on the AASM guided bomb developed by SAGEM defense (SAFRAN group) [23]. The first configuration in video 3 a presents the "free-flight" configuration, for which the current enters the bomb at the level of its "guiding kit" in front and exits at the level of its "propulsion kit" at the rear (the animation does not show the damping times but stops at the time of the maximum current). Due to the cylindrical shape of the bomb, the redistribution effect only occurs at the levels of the winglets. Note also some points of intensification of the currents. which consist in obliged paths of circulation of currents at the level of peripheral screws between the guiding kit and the bomb core. Video 3 b consists in an injection on the guiding kit of the bomb and an exit point on the wing of the aircraft. The movie clearly shows the redistribution of the currents on the edges of the wing. Finally, video 3 c shows an injection exit point configuration similar to the "free flight" configuration, but when the bomb is attached to the wing. This time, we see the low impedance path-search phenomenon for which the current flows to the wing before coming back to the exit point, which is at the rear of the AASM. Such a phenomenon gives rise to bipolar time domain surface current signatures, for which the currents flow in two directions at a given observation point on the surface of the object.

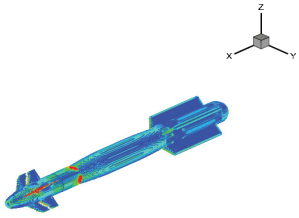

a) Configuration "AASM – AASM" in free flight

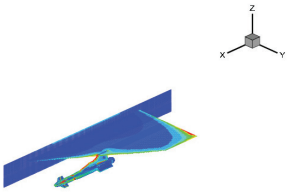

b) Configuration "AASM – wing"

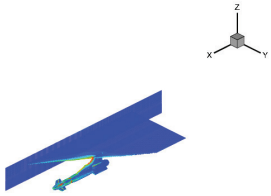

c) Configuration "AASM – AASM"

Video 3 - A lightning waveform injection on the AASM system – Courtesy SAGEM defense
http://www.aerospacelab-journal.org/al5/indirect-effects-of-lightning-on-aircraft-and-rotorcraft

EM scattering effect

In EM coupling theory, "scattering" is the term reserved for the generation of EM fields due to an obstacle in the path of the current on a structure. This is typical physics used on purpose for building antennas. As far as EM coupling is concerned, the radiation of the EM fields is not intentional: EM field scattering is mainly due to the presence of windows or doors, which behave as "apertures". Some of those apertures may be transparent from and EM point of view; they are called "free" apertures. Some are closed with non-transparent materials; they are called "loaded" apertures. This is typically the case of bay-doors on AC/RC.

Besides, we have seen that lightning is a low frequency phenomenon. If we consider 1 MHz as the very maximum frequency of any type of lightning waveform, the wavelength is equal to 30m, which makes any type of aperture encountered on an aircraft behave as a so-called "small aperture". Indeed, the small aperture theory is particularly well suited for lightning waveforms.

Free small apertures

The theory of small apertures allows a very convenient approximation. When an aperture is illuminated by an incident field (this incident field having been produced by a current injection on the structure, for example), it can be shown [24] that the radiation of the field due to the aperture is equivalent to the combined radiation of a magnetic dipole of moment, $\vec{P}_m$, and an electric dipole of moment, $\vec{P}_e$:

$$\overrightarrow{P_e} = \varepsilon_o \alpha_e \overrightarrow{E_{se}} \tag{16}$$

and

$$\overrightarrow{P_m} = [\alpha_m].\overrightarrow{H_{cc}} \tag{17}$$

It can be shown that this approximation is valid for a calculation of the fields at a distance larger than the largest dimension of the aperture. The two dipoles depend on two quantities:

• The geometry of the aperture with two quantities called "electric polarizability"α_e (a scalar) and "magnetic polarizability" $[\alpha_m]$ (a 2x2 diagonal tensor). Table 3 gives practical formulas for several shapes of apertures [25]. The circular aperture formulas generally give a good approximation for any shape of apertures, such as windows, whereas the elliptic apertures give good approximation of one-direction extended apertures such as slots;

Shape	α_e	α_{mxx}	α_{myy}
Circle of radius α	$4\frac{\alpha^3}{3}$	$4\frac{\alpha^3}{3}$	$8\frac{\alpha^3}{3}$
Ellipse	$\frac{\pi}{12}\frac{w^2 l}{G(e)}$	$\frac{\pi}{12}\frac{l^3 e^2}{F(e)-G(e)}$	$\frac{\pi}{12}\frac{l^3 e^2}{(l/w)^2 F(e)-G(e)}$
Narrow ellipse	$\frac{\pi}{12}w^2 l$	$\frac{\pi}{12}\frac{l^3}{Ln(4l/w)-1}$	$\frac{\pi}{12}w^2 l$

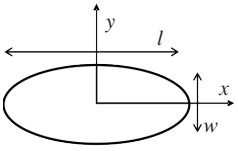

Ellipse dimensions

Table 3 - Polarizabilities of typical apertures (from [25])

with:

$$e = \sqrt{1\left(\frac{w}{l}\right)^2}$$

$$F(e) = \int_0^{\frac{\pi}{2}} \frac{1}{\sqrt{1-e^2\sin^2\theta}} d\theta$$

$$G(e) = \int_0^{\frac{\pi}{2}} \sqrt{1-e^2\sin^2\theta}\, d\theta$$

• The short-circuited incident magnetic fields $\overrightarrow{H_{sc}}$ and electric fields $\overrightarrow{H_{sc}}$ on the aperture, that is to say, the fields that would have been obtained if the aperture were closed by a perfectly conducting material. In [26], it is shown that those surface fields can be measured close to the aperture surface of a 3D structure (they are not significantly modified by the presence of the aperture) and used as source terms for calculating equivalent sources inside a 3D structure. Such short-circuited fields combined to polarizabilities can also be used to directly calculate voltage and current sources induced at the level of a cable running underneath [25]. Note that polarizabilities roughly vary as the cube of the main dimension, which means that the scattered field also follows this cubic variation.

Loaded small apertures

When a small aperture is loaded by a material characterized by its Zs surface impedance, the model of two equivalent magnetic and electric dipoles is still valid, but a frequency variation must be applied on the two free aperture dipoles moments $\overrightarrow{P_{m_o}}$ and $\overrightarrow{P_{e_o}}$ [27], [28]. We have:

$$\overrightarrow{P_m} = \frac{\overrightarrow{P_{m_o}}}{\left(1 + j.\frac{f}{f_m}\right)} \quad (18)$$

with:

$$f_m = \frac{3Z_s}{8\mu_o\alpha} \quad (19)$$

and

$$\overrightarrow{P_e} = \overrightarrow{P_{e_o}}.j.\frac{f}{f_e} \quad (20)$$

with

$$f_e = \frac{1}{16\varepsilon_o Z_s \alpha} \quad (21)$$

Figure 7 shows the electric and magnetic field attenuations for a circular aperture loaded with a $Z_s = 1\Omega$ material (this value is a bad conductivity for usual Carbon Fiber Composite (CFC) materials but is convenient for the normalization of our results). This attenuation is defined as the ratio of the field in the presence of the material over the field without the material. These curves are directly obtained by the ratio between the equivalent dipoles defined in (18) and (20). The electric field attenuation decreases linearly with the frequency. However, for the frequencies concerned by lightning we observe that this attenuation is quite large (more than 80 dBs). On the contrary, we observe that the attenuation of the magnetic field is almost equal to zero up to the f_m cut-off frequency. It is only after this frequency that the attenuation begins. This is a very usual behavior of magnetic fields, which cannot be stopped at low frequencies due to the finite conductivity of materials. This is why, in the continuation of this article, our main concern will be for the penetration of the magnetic field. Nevertheless, the reader must keep in mind that this does not mean that there is no electric field behind the aperture. Because of Faraday's law, the flux of the magnetic field in a closed contour is thereby related to the circulation of the electric field on this contour [29].

Note that the higher importance of the magnetic transfer function vs. the electric transfer function for shields is directly observed for cable shields: to characterize shielded-cables, the transfer impedance of the cable (related to magnetic coupling) is the relevant parameter in general and is available in the data sheets for commercial cables. The transfer admittance (related to electric coupling) is generally neglected and often not mentioned (see box 5).

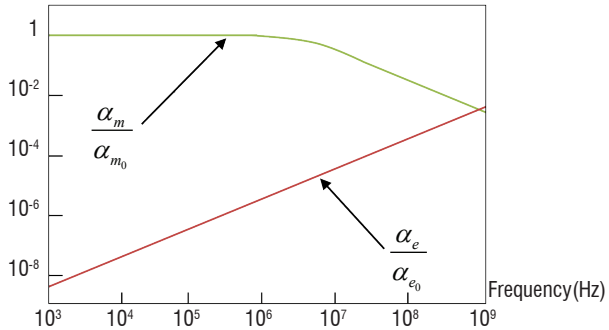

Figure 7 - Electric and magnetic field attenuation for a circular aperture of radius a, loaded by a $Z_s = 1\Omega$ material

Figure 8 shows a shielding effect calculated on a loaded square aperture when a current is injected in the metallic plate supporting the loaded aperture. The calculation is made with an Electric Field Integral Equation (EFIE) solver in the frequency domain. The straight segments represent the flow of the surface current. Their length is proportional to the amplitude of the current. For frequencies lower than f_m, we see that the current flows around the aperture, as if the aperture were free (the currents flow along the minimum resistance path). This deviation of the currents creates the radiation of the EM field. When the frequency is equal to f_m, we see that some part of the current is flowing through the loading material. When the frequency becomes larger than f_m more current is flowing straight across the loading material, thereby providing shielding of the magnetic field.

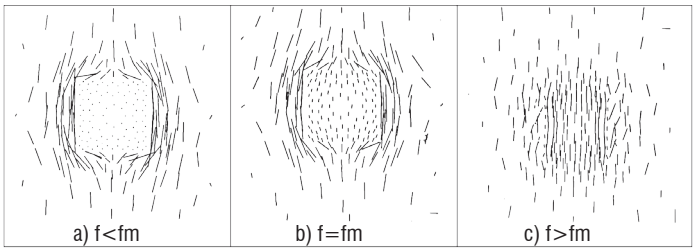

Figure 8 - Magnetic shielding effect on a square loaded aperture (from [8])

The first order filter behavior of the magnetic shielding effect is the universal magnetic shielding rule, which requires current to circulate on a material in order to produce the shielding effect. As a demonstration, table 4 shows that the magnetic cut-off frequencies for geometrical shapes made of a material with a surface impedance Zs_0. f_m is always proportional to Zs_0 and to the inverse of the characteristic dimension of the geometry ("α" in table 4).

Box 3 - EM Scattering versus skin effect

As seen before and related to the skin effect phenomenon, when a volume is closed and lossy with a surface impedance equal to Zs, the EM field enters the cavity by penetrating through the constitutive materials. This diffusion effect produces long time domain waveforms inside the volumes. We can thereby ask ourselves which effect dominates when scattering and diffusion are in competition.
Let us consider a lossy material of depth "e". On the one hand, we can calculate the frequency f_δ for which the skin depth is equal to half of the depth of the material. We find:

$$f_\delta = \frac{4Z_s}{\pi\mu e} \tag{22}$$

(μ is the magnetic permeability of the material). On the other hand, we consider the magnetic cut-off frequency, which characterizes the penetration of the magnetic field through a loaded aperture with the same Zs and diameter D:

$$f_c = \frac{3.Z_s}{8.\mu}.\frac{2}{D} \tag{23}$$

The ratio between these two frequencies gives [30]:

$$\frac{f_\delta}{f_c} = \frac{16}{3\mu} \approx 1,7.\frac{D}{e} \tag{24}$$

This means that, even if the diameter of the aperture becomes equal to the depth of the material, the frequency for which the skin effect begins to be relevant is almost 2 times larger than the frequency after which the magnetic field is attenuated by a loaded aperture. For other shapes of apertures, it can be shown that:

$$\frac{f_\delta}{f_{cs}} = C.\frac{D}{e} \tag{25}$$

with $1<C<2$. This means that as far as $D>e$, small holes in closed volumes will always dominate the skin effect through materials and will allow scattering of H fields in the volumes.

Geometry	Sphere of radius α	Cylinder of radius α	Circular aperture of radius α
Cut-off frequency	$f_m = \frac{3}{2\pi}\frac{Z_{s0}}{\mu_0\alpha}$	$f_m = \frac{3}{\pi}\frac{Z_{s0}}{\mu_0\alpha}$	$f_m = \frac{3}{8}\frac{Z_{s0}}{\mu_0\alpha}$

Table 4: Magnetic cut-off frequencies for different geometries with the a Z_{s0} surface impedance

Influence of contacts

The previous analysis of loaded apertures supposed a perfect contact of the aperture material with the structure. However, this contact is not always perfect. Figure 9-a shows a calculation of the effect of a non-uniform connection of a CFC panel on a square aperture (only two contacts between the two sides of the apertures) and a uniform connection perfect peripheral contact. This calculation has been made with Onera's EFIE computer tool. Figure 9-b shows several measurements of the shielding effectiveness of a panel in a TEM cell when the connection is progressively improved from badly connected (C9) to perfectly connected (C4). The effect of an imperfect connection clearly limits the shielding effectiveness.

It can also be shown that, even if uniform, the contact resistance of a lossy panel on an aperture will modify the f_m (19) and f_e (21) frequencies (f_m increases which reduces the shielding effectiveness).

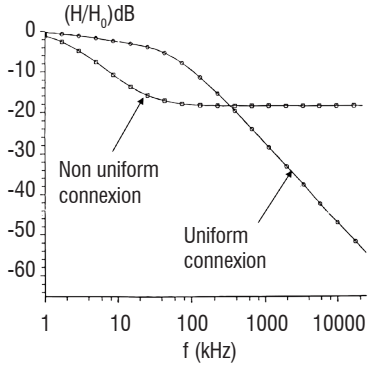

a) Magnetic field shielding effectiveness calculation

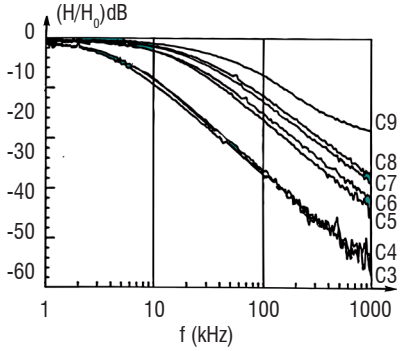

b) Magnetic field shielding effectiveness measurements

Figure 9 - Magnetic shielding effect for different types of connections of materials on an aperture (from [8])

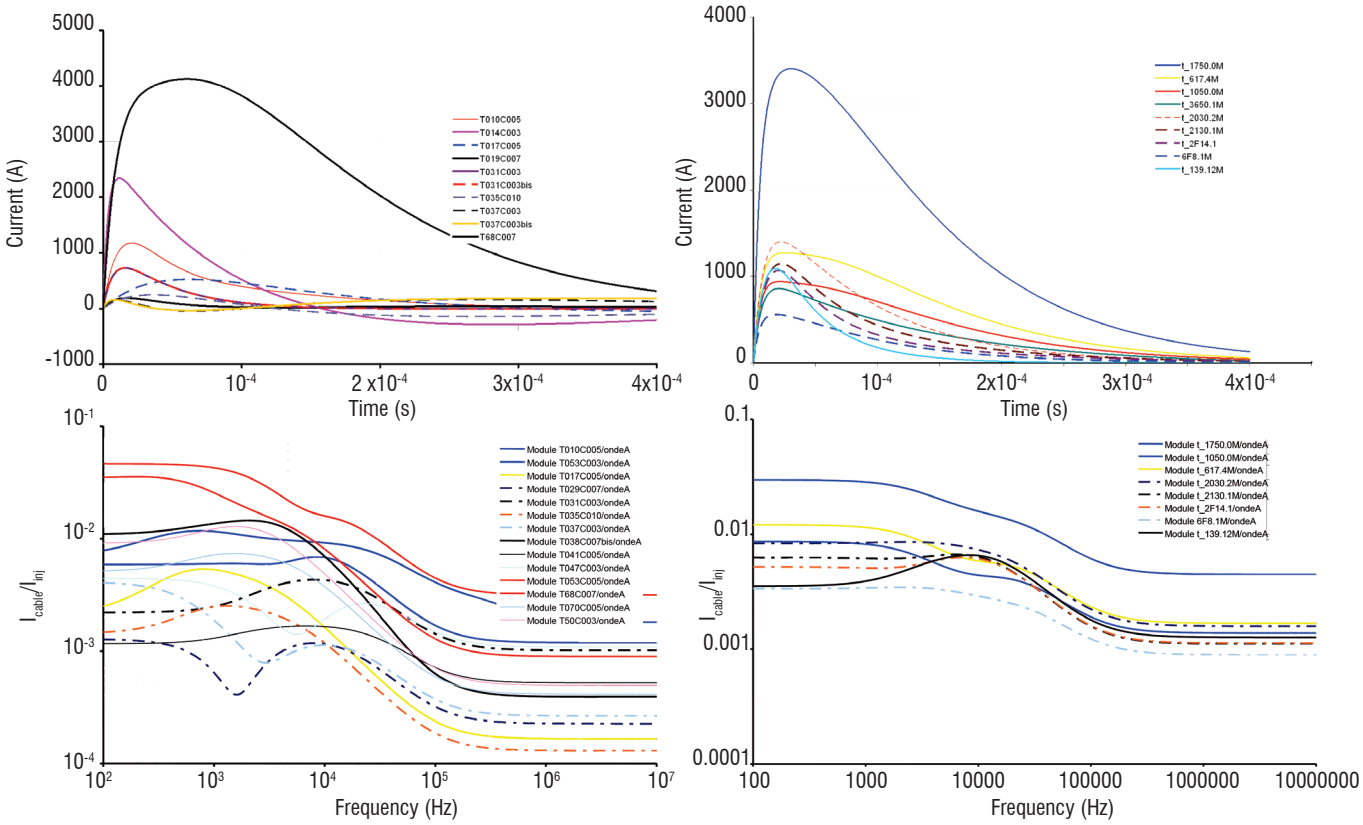

a) NH90 rotorcraft

b) Rafale fighter aircraft

Figure 10 - Low impedance cable currents on two AC/RC (time domain) and frequency spectrum of the Icable/Iinjected transfer function

Indirect lightning EM effects at system level

As far as system level is concerned, the emphasis must be put on cables, since cables are the major vectors of communication of electric and electronic equipment. When indirect lightning occurs on an AC/RC, cables behave as sensors, which capture some portion of the injected current and are thereby likely to transport currents that may be understood as useful electrical signals by electronic equipment. This is why, in this section, we try to analyze typical signatures of cables and we try to introduce main types of protection techniques, either at the level of cables or at the level of equipment inputs.

Typical responses of cables on AC/RC

EM coupling on cables is a particular case of the conduction effect. Figure 10 gives several examples of currents measured on low-impedance cables of the NH90 rotorcraft and the Rafale Fighter Aircraft for an A lightning waveform injected on the two AC/RC [32] in a coaxial-return test configuration [17], [18], [15]. The time domain and frequency spectrum responses of both AC/RC are very similar. The time domain responses show a distribution of maximums ranging between 3 and 4 kA and average maximums of about 1 kA. Almost all frequency spectrums of the Icable/Iinjected transfer function show a first low-pass filter cut-off frequency and most of the time a high frequency stabilized to a constant value.

Cables inside a cylinder

In order to explain the behaviors observed on AC/RC, we will first use a simple 2D model in which the 2D sections can be approached by a set of parallel wires supposed to be short-circuited at their ends. The box 2 shows a 2D invariant geometry of a plane approximated with 3 wires. The model allows the derivation of analytical formulas and shows the current redistribution trend. Such approximations can be generalized to more complex shapes and the formalism can be applied to all types of invariant 2D sections. This is an easy model to estimate the current redistribution for complex shapes and particularly the influence of cables, but this is also an efficient model to explain measurements. In such a model, low impedance cables are also described as thin wires short-circuited to the structure surface.

For the demonstration, let us first consider a 2 m-diameter cylinder (0.53 mΩ/m), with two 6mm-diameter inner wires (60 mΩ/m), one in the center and one close to the surface (10 cm) (figure 11-a). Figure 11-b gives the wire cross-section model of the cylinder with 80 elementary wires.

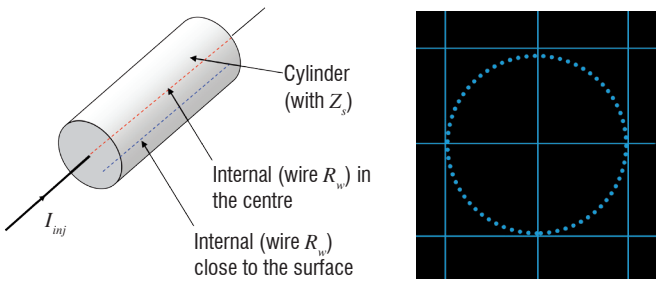

a) One wire in the center and one wire close to the surface

b) 2D wire model of the cylinder (the two inner wires are not represented)

Figure 11 - Cylinder with two inner wires

Figure 12 presents the frequency response of the two wires inside the cylinder. The Icable/Iinjected transfer function presents the same low frequency plateau and a quite similar cut-off frequency. It can be shown that the wire response transfer function (Iwire/Iinj) obeys the following low-pass filter law which gives a good approximation of the real responses observed on AC/RC (figure 10):

$$\frac{I_{wire}}{I_{inj}} == \frac{R_{structure}}{R_{\text{int}}}\left(\frac{1}{1+j\dfrac{f}{f_c}}\right) \quad (26)$$

with

$$f_c = \frac{R_{\text{int}}}{2\pi L_{\text{int}}} \quad (27)$$

where:

$R_{\text{int}} = R_{structure} + R_{wire}$ (transmission line resistance of the wire) (28)

and

L_{int}: transmission line inductance of the wire [31].

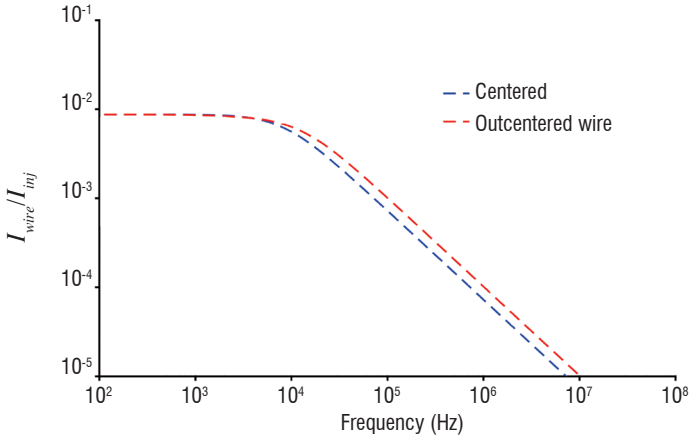

Figure 12 - Cylinder inner wire I_{wire}/I_{inj} transfer function

Cables inside and outside a realistic structure

Let us now consider a more complex 2D cross-section with angles (figure 13). This cross-section geometry is that of a NH90 helicopter [32]. In this case, unlike in the cylinder case, the redistribution effect may occur on the outer surface and has a significant effect on the cable responses, either inside or outside the structure surface. We observe that the inner wire responses all display a curve that is quite similar to a

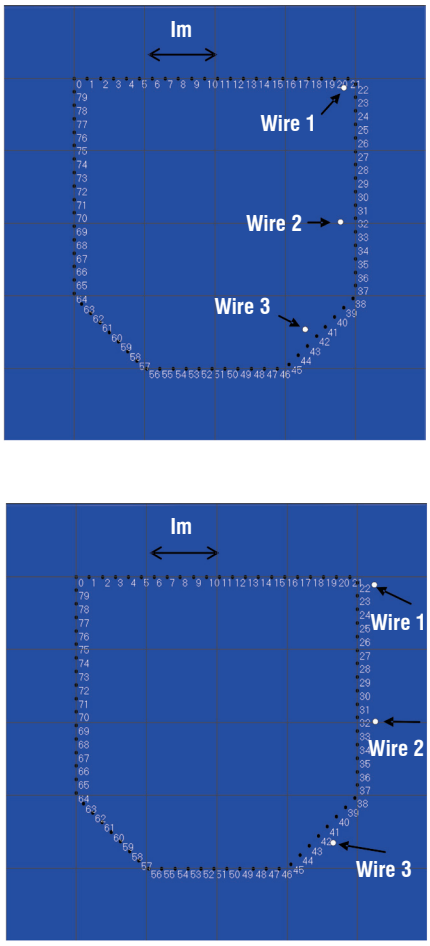

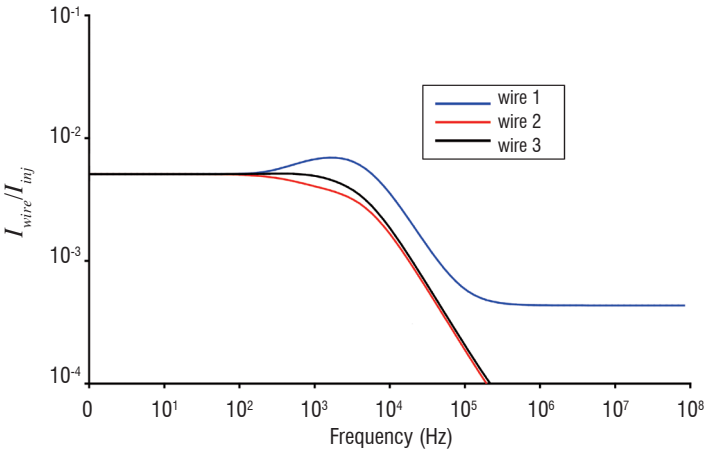

Inner cable response

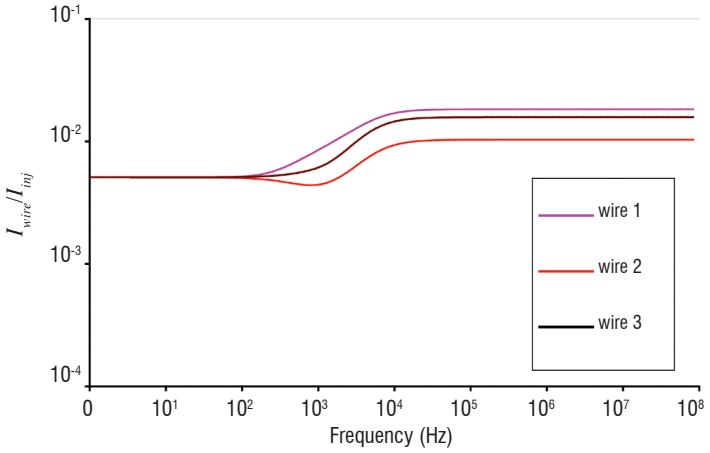

Outer cable response

Figure 13 - Realistic structure inner and outer cable I_{wire}/I_{inj} transfer functions

Box 4 - Thevenin equivalent generator on a cable due to an indirect lightning current injection

Let us consider the electric circuit represented in figure B4-1. In this figure, the ground reference surface is approximated by a single conductor on which a current I_{inj} is injected. Over this ground reference, we consider a cable, short–circuited at one end and in open-circuit at the other end. The cable over the ground conductor constitutes a transmission line characterized by:

- a resistance: $R_{\text{int}}=R_{cable+Rstructure}$
- an inductance: $L_{\text{int}}=L_{structure}+L_{cable}-2M$, where:
  - $L_{structure}$ and L_{cable} are the inductances of the structure and the cable respectively
  - M is the mutual inductance between the ground and the cable conductors.

Figure B4-1a represents the equivalent Thevenin V_{Th} model that must be evaluated.

The measurement of the open-circuit voltage allows the determination of the equivalent Thevenin generator, V_{Th}. The first contributor is due to the so-called "common-mode" voltage developed in the ground, V_{mc}. Since there is no current developed in the cable ($I_{cable}=0$), this common mode voltage entirely appears at the level of V_{oc} (figure B4-1b). The second contributor is due to the flux of the magnetic field in the loop formed by the structure and the cable. This flux is obtained from the mutual inductance between the ground and the cable conductors and the current flowing in the ground. Note that this contribution ends up with a derivative of the injected current (figure B4-1c).

At the end, we can write:

$$V_{Th}=\left(R_{structure}+j\omega M\frac{d}{dt}\right)I_{inj} \tag{29}$$

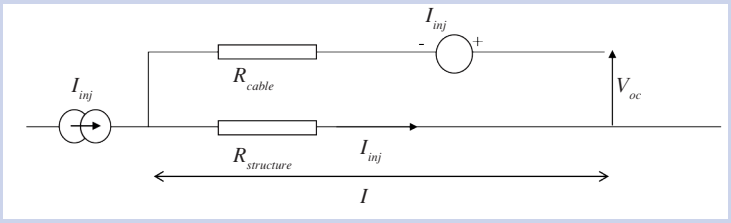

a) Problem to solve

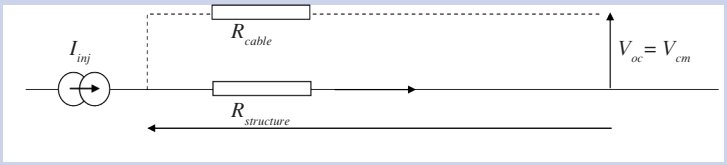

b) Common mode voltage coupling

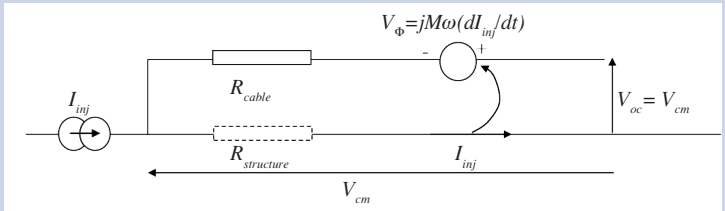

c) Magnetic flux coupling

Figure B4-1- Thevenin generator on an open circuit wire in the case of a lightning injection

low-pass filter, but the cut-off frequency depends on the position of the cables. Particularly, we note that the cable in the upper right corner presents an overshoot before the cut-off frequency. Note that the constant level observed for this wire at high frequency is due to the discretization of the surface in thin wires. With more wires, this level would get lower. In reality, for a full surface, this constant value does not exist and the plot continues on its 20dB/decade decaying slope. Such behaviors are very similar to those observed for the determination of transfer impedance (Z_t) of shielded cables with no circular shields [33].

When the wire is outside the structure, the behavior is quite different since it becomes more like a high pass filter characterized by the fact that the current accumulates in the most exterior parts of the structure, which become the external wires (the flat level at high frequency is due to the thin-wire discretization). Note also here the undershooting phenomenon, which is now occurring on wires parallel to flat parts of the geometry.

Main characteristics of cable responses on AC/RC

Lightning indirect effect coupling on cables is due to the conjunction of two voltage sources (see box 4):

• a common mode coupling, which is due to the development of an electric potential difference on the structure;

• the magnetic field coupling due the magnetic flux inside the loop made by the cable.

For a given injected current, the significant cable currents are scaled by the resistances existing between the connection points of the cables.

In [32] a large investigation has been carried out on two databases of low-impedance cable responses in the Rafale fighter aircraft and in the NH90 helicopter, subjected to an A-lightning waveform injection. This analysis resulted in very significant lessons available for those two types of air vehicles:

• The current on cables is mainly on branches oriented in the direction of the current on the structure. Therefore, if the current is injected longitudinally as for most coaxial-return configurations, the current along branches that are orthogonal to this main direction is low. Along these orthogonal branches, the response is mainly derivative, which means that the coupling is dominated by the coupling due to the scattered field (see Box 4). Such derivative waveforms are also observed for exposed cables, in open areas such as cockpits. Actually, the injection and output points define a transverse variation of the electric potential difference between those two points, which defines at the same time the cable branches supporting the maximum current;

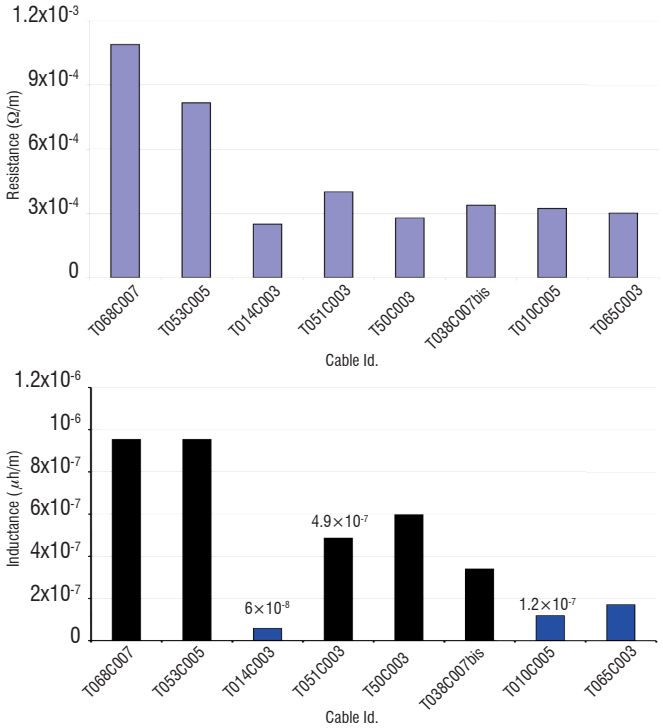

Figure 14 - Low per-unit-length resistance and inductance of low-impedance cables on the NH90 helicopter

• The resistance of the structure can be approximated as a function of the connection points on the aircraft/rotorcraft structure: knowing the height of the cables with respect to the structure, the transmission line inductance L_{int} can be estimated and the analysis of the cut-off frequency of the I_{cable}/I_{inj} transfer function as in (26) thereby allows the identification of the R_{int} (internal resistance) parameter of the low impedance cables (or the parts of the harnesses longitudinal to the current injection into the structure). As an example, this distribution of resistances in Ω/m is reported in figure 14, with a larger distribution for resistances of about 0.3 mΩ/m. From this, if we are able estimate the per-unit-length resistance of the cable shields (an average of 15 mΩ/m is a reasonable approximation), it is possible to estimate the resistance of the structure as a function of the position along the longitudinal current injection axis (figure 15). In this figure, the various straight lines correspond to various longitudinal cable parts having been used to determine the resistance of the rotorcraft between two connection points. The starting coordinate and the end coordinate of those straight lines are referred to a longitudinal position between the two ends of the helicopter in the coaxial return. Of course, the shorter the line, the smaller the impedance. From this figure, looking at the blue and black line, we have an indication that the total resistance of the structure varies between some mΩ and a few tens of mΩ.

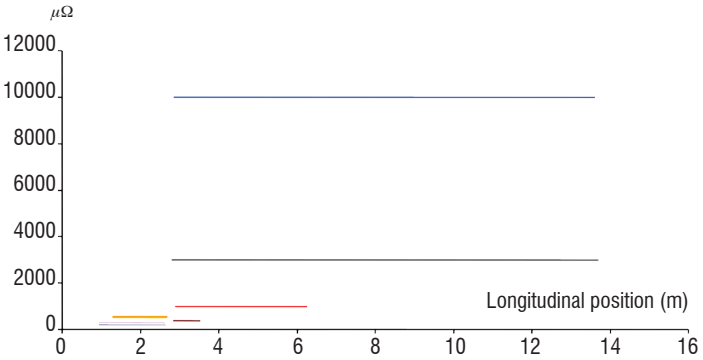

Figure 15 - Resistance of the structure on the NH90 helicopter (each test-line corresponds to a point-to-point longitudinal cable-harness branch)

Justification of the linearity hypothesis

So far, we have made the approximation of linearity of the entire phenomenon. However, lightning is a high level environment constraint and it is important to consider possible non-linear effects. For example, it is known that at the material level, the application of high intensity currents changes the electrical characteristics of the materials, especially their electric conductivity. This is also true for the contact resistances at the level of panel junctions, whose conductivity may also improve when submitted to high level currents. Thus, even if this phenomenon is real, the control of non-linear effects occurring over an entire system becomes very complicated. In the following section, we try to assess to which level the linear approximation remains conservative, in terms of the current level specified at the level of equipment inputs.

Figure 16 shows different Iwire/Iinj transfer functions obtained by different techniques on the same cable in the same system:

• with low-level current injections (with a CW measurement directly made in the frequency domain with a network analyzer and with a low level A waveform injection). This first set of waveforms gives the same transfer functions and testifies that the injected current did not produce any non-linear effects;

• with two medium-level waveforms (some 10 kA) with a high dI/dt derivative (similar to a H waveform). These transfer functions are different from each other, with the previous reference levels, with no non-linear effects;

• with a high level A waveform injection. This transfer function gives another transfer function with the lowest level.

These plots show that the higher the injected current, the lower the transfer function at cable level. This also means that the higher the injected current, the better the shielding brought by the system surface is. This means that the non-linear effects allow better circulation of the currents (less overall resistance).

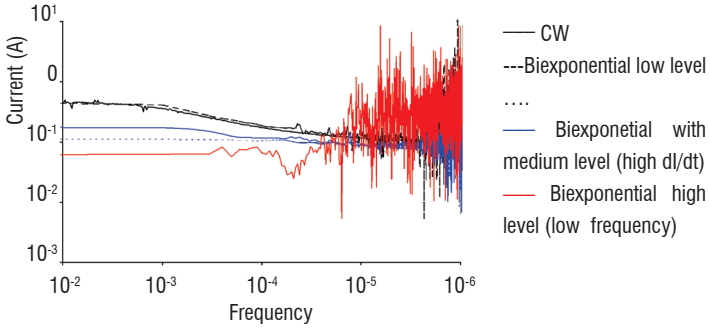

Figure 16 - Measured I_{wire}/I_{inj} transfer functions

In Figure 17, we show the effect of such transfer functions on the time-domain waveforms. Figure 17-a displays two frequency responses for currents measured directly in the frequency domain and obtained on two different cables, as well as the Fourier transform of the injected current (similar to an H waveform). Cable 1 is an open cable, not shielded, whereas cable 2 is a cable inside a shielded cable bundle. Figure 17-b and figure 17-c show the time-domain responses of the two-cables obtained from the transfer functions, compared to the measurement of the current on these cables directly measured in the time domain. Figure 17-b shows that the calculated current for cable 1 must be multiplied by a factor 1.5, in order to find the measured time domain waveform again. Figure 17-c shows that the average level has been well calculated, but the waveform is quite different from the measured level, which clearly shows a waveform signature that we may attribute to a non-linear effect having occurred at the level of the cable or more likely, of its connector.

As a conclusion, non-linear effects clearly occur during indirect lightning current injections, but they are difficult to control. Nevertheless, linear approximation of the phenomenon gives a good estimation for the specification of currents induced at the level of equipment inputs.

System level indirect lightning protection

A straightforward but false idea for lightning environments would be to use installation rules such as to locate sensitive equipment in EM "clean" zones, but this concept cannot work because, as a low frequency phenomenon, lightning conduction is very effective over long distances, especially along cables. Therefore, cables running in EM exposed zones can pick up some interference and drive it up to the level of an equipment box located in a non-exposed zone. Second, cables are organized in cable bundles, which group them all together; clean cables can be spoiled by "dirty" cables. Nevertheless, each aircraft manufacturer applies segregation and installation rules between cable bundles which allow all types of EMC cross-coupling related

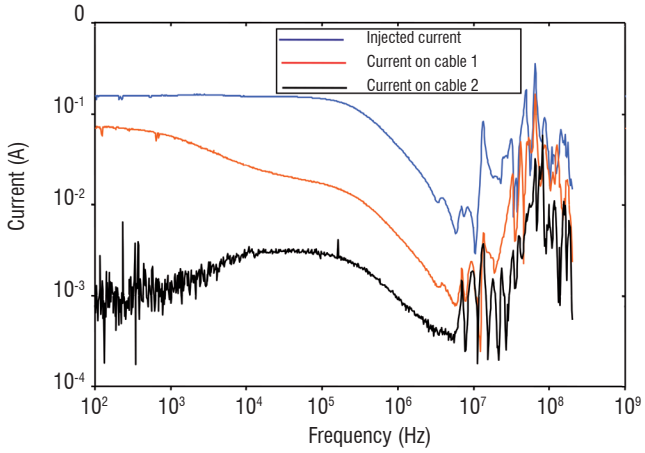

a - Measured transfer functions

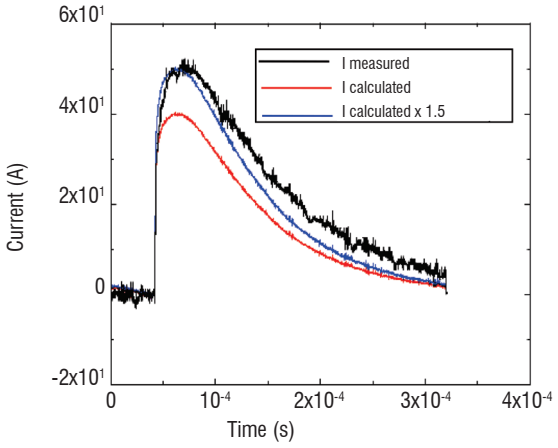

b - Time domain waveforms for cable 1

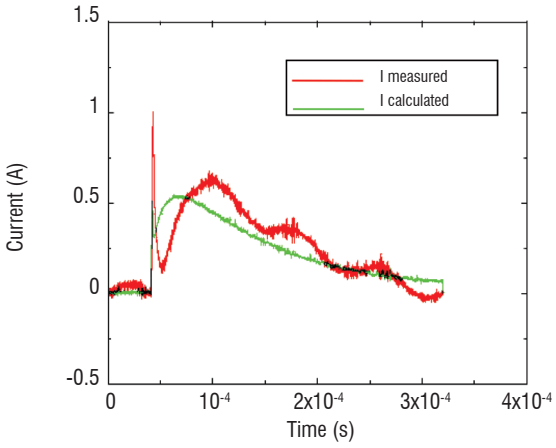

c- Time domain waveforms for cable 2

Figure 17 - I_{wire}/I_{inj} transfer functions generated from measured currents on systems

problems to be sustained. Solutions at use are: separation of cable-bundles with a standardized distance, routes of cable-bundles at specific distances from the mechanical ground.

System level protection against indirect lightning can be seen at three levels: structure level, cable-level and equipment level. As far as system protection against any type of EM effect is concerned, the rule is generally to take advantage as much as possible of the protection that can be naturally provided by the geometry of the structure and the installation of the electric and electronic system. This is why this natural protection is called "passive" protection; it may concern the structure and the cables. Such protection consists in optimizing the shielding effect by maximizing the current that is supposed to circulate on the shields. Such concepts are the ones considered in the theory of EM topology [34], in which design rules are based on the concepts of generalized shields. In this approach, the main rule is that the interacting currents must be concentrated as much as possible on the outside of the structure, using several embedded layers of shields. Even though this design approach cannot be applied as such for indirect lightning, the approach provides very useful guidance rules for designers. Indeed, the more the EM design is controlled and the more the control of possible EM problems will be in the future life of the system.

When all passive shielding protection measures have been applied on the installation, the only solution to improve the protection is to apply the protection directly at the level of the equipment. For this, active non-linear devices are applied on each critical pin, in order to short-circuit unwanted current amplitude to the ground in the event of critical interference. In this paper, oriented on EM aspects and related methods, we will only consider passive protection.

Topology-based protection

Material and structure protection constitutes the first EM shielding volume according to EM topology decomposition. From a practical point of view, the idea is to help the structure act as the best shield possible. For this, depending on the mechanical and budget constraint, several parameters can be optimized for indirect lightning:

- the shape of the structure: we have seen that the closer a cross-section geometry is to a cylinder, the better the current is equally distributed around it. This is the typical case of the fuselage geometry. On the contrary, a current on flat shapes increases the possibility of having current redistribution in the corners and thereby increasing field penetration at this point. From a practical point of view, it is not realistic to think of modifying a shape to make it a cylinder, but it may be clever to take advantage of a cylinder shape and not break its natural symmetry or make its electrical properties dissymmetrical;
- The global conductivity of the structure, in order to drive as much current as possible on this structure. Aircraft manufacturers must comply with specific requirements for the DC resistance of the structure. We have seen that direct lightning metallic grid protections applied on carbon composite materials had a significant impact on the improvement of the Z_s surface impedance and, consequently, of its equivalent electric conductivity. Since the objective of such protections is to facilitate the circulation of the current injected at the lightning striking point, this technique is also well suited to improve the global EM shielding efficiency of the structure, provided that the continuity of the currents is maintained. This typically means that the electric continuity between the panels must be as good as possible. Especially at the design and maintenance phases, efforts must be directed towards achieving the uniformity of the contact, rather than the improvement of the local contacts. Each diversion of a current line or its concentration along a given path is likely to generate EM scattering (see § EM scattering effect);
- In addition to this EM effect, the bad contact or, worse, the isolation between two structural parts supposed to be on the normal evacuation path of the current may lead to an increase in the potential difference between those two parts and may create an electric breakdown between them, as was already mentioned in § Indirect lightning EM model related issues;
- The minimization of the apertures: while efforts have been directed at the geometrical shape and the global conductivity, global EM optimization consists in minimizing the EM scattering effect at openings, such as cabin windows or cockpit canopy: this is done by decreasing their number and their size. If possible (that is to say, if it does not alter visibility), a solution is to use metallic grids, provided that this grid remains in good contact with the structure all around the aperture. The cells of the grid act as small apertures, for which the combined global attenuation is larger than the attenuation of the free aperture [25].

Bounding and Grounding

Bounding and grounding techniques are techniques generally required for electric safety. However, they must be applied properly, in order to be compatible with EM external threats, especially threats such as indirect lightning. Let us also recall that such techniques are effective at low frequencies only. This is why techniques for bounding and grounding always require a short connection and low impedance connections, which leads to the use of large-section conductors or braids.

Bounding consists in connecting all of the conducting parts together, in order to maintain the same electric potential, at least at DC. This action prevents electric breakdown from developing between equipment parts and cables.

Grounding consists in connecting a conducting part to the "ground". For indirect lightning and for all EM threats, the ground to be considered is the "mechanical ground" constituted by the structure surface itself, since this structure is the main contributor to the dissipation of the current.

The development of non-metallic aircraft, such as full composite carbon aircraft, raises the question of the efficiency of grounding and bounding and its compatibility with electric safety rules. Such a concern is very similar to the problem encountered in ground installations (see [35]).

The absence of a structure surface that is conducting enough to be considered as a good mechanical ground makes it necessary to recreate this ground reference by introducing a grounding network, which partly cancels the weight reduction advantage claimed by the use of carbon composite materials. Different techniques may be proposed, from bus-bars to metallic tubes, for building this network. The first one offers simplicity of maintenance on cables and electronic equipment, which is not the case for the second one. However, the second provides efficient cable shielding at the same time as the ground reference. The use of raceways could be a good compromise for the tubes and they may be used in combined configurations with bus-bars.

Box 5 - Transfer impedance of a cable-shield

Even if the shield connection is made at both ends, this does not mean that the shielding attenuation is perfect. As for material, the shield possesses an electrical conductivity, which therefore allows penetration of the magnetic field. In the same way as we have said that materials could be characterized by a Z_s surface impedance quantity, the shielding property of a cable-shield can be characterized with a quantity, homologous to a per-unit-length (p.u.l.) impedance $Z_{t,}$ called the transfer impedance.

Provided that the shield is well connected at both of its ends, the coupling model on the inner wire $V_s(z)$ is obtained by applying a distributed voltage generator of the type:

$$V_s(z)=Z_t.I_s(z) \tag{30}$$

where $I_s(z)$ is the distributed current on the shield and z is the position along the cable.

From a modeling point of view, the Z_t concept therefore allows the decomposition of the problem of EM coupling evaluation along the cable into two independent problems:

- the evaluation of the current on the shield, Is
- the evaluation of the response of the inner-wires. The interest in this part is that the inner-wire geometry is fully appropriate for the application of Multiconductor Cable models, in which the shield is the reference of the transmission lines.

Note that as there is a Z_t parameter relating the shield current to the inner equivalent voltage source; there is also a transfer admittance called Y_t that relates the shield voltage to an inner equivalent current source, due to small holes existing in braided shields, for example (see § Loaded small apertures).

Note also that the Z_t parameter is an integral part of multiconductor p.u.l. electrical impedance matrices, since it describes the relation between the inner and outer transmission line when this model is applicable for the shield with respect to its reference. This parameter therefore plays a reciprocal role; an interference signal on the inner wires induces current on the outer surface of the shield [36].

At DC, it can be shown that the Z_t is real and is equal to a quantity called p.u.l. "transfer resistance", R_t, itself equal to the p.u.l. resistance of the shield. Then, when the frequency increases, because of the limitation of the current on the outer surface of the shield, the transfer impedance improves with a damping to zero. If the braid were a full thick cylinder, such damping would continue with the increasing frequencies. However, because overshields are made of metallic braids, the braids leave a multitude of small holes that will act as small apertures (see § Free small apertures) and let the magnetic field penetrate. Because this scattering effect is a derivative phenomenon in the time domain, the transfer impedance can be characterized by a p.u.l. quantity homologous to an inductance and called "transfer, inductance", L_t. If this scattering effect arises before the skin effect, the damping effect, also called Schelkunoff effect, does not show up [37]. Without this effect, the transfer impedance can be simplified under the form:

$$Z_t(\omega) = R_t + jL_t\omega \tag{31}$$

As far as indirect lightning is concerned, the scattering by those small holes is not relevant. However, it is relevant for higher frequencies, such as HIRF frequencies, and we must consider that cable overshields are generally installed for a wide frequency band protection.

Figure B5-1 shows the typical variation of a cable-shield transfer impedance, with and without a Shelkunoff effect.

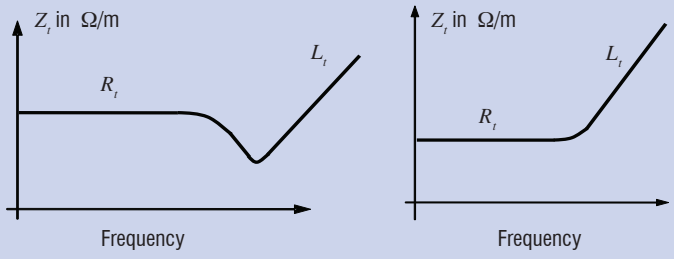

Figure B5-1 -Typical frequency variations of the transfer impedance of a shielded cable

The transfer impedance usually depends on the position of the wire in the cable-shield. In order to illustrate this point, we have shown in figure B5-2 the variation of the field inside a very specific shield design used to drive cables from the technical premises of a ship radar to the ground, in a so-called "transparent mast" [33]. This shield has a rectangle cross-shape on the left-hand side and a circular shape on the right-hand side. The inside walls are included, in order to separate volumes. In figure B5-2 the penetration of the H field is indicated with a color code. Square meshes indicate the relative amplitude only but the example allows the current redistribution effect happening also at the scale of this shield to be put to the fore. At a low frequency (10 kHz), the penetration of the shield is mainly due to Rt and is therefore homogeneous. When the frequency increases (1 MHz), due to L_t, the magnetic field begins to lower in the middle but increases along the walls, in the corners and in the middle of the circular shape. In addition, the field is quite important along the vertical wall in the half right-hand side circular volume. This behavior is accentuated at 10 MHz, for which the field significantly decreases in the middle of the straight surfaces. At very high frequencies, the internal field vanishes everywhere inside the shield. Figure B5-3 summarizes this frequency variation of Z_t at several test-points. All of the plots clearly show the R_t constant value and the start of the 20dB/decade L_t slope, but several overshoots corresponding to test points in the corners or in the middle of the half-circular surface are also displayed, as observed in Figure 13.

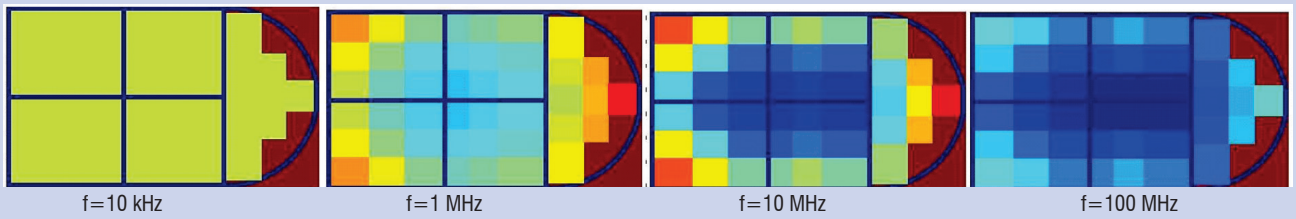

Figure B5 - 2 - Frequency variation map of the field penetration for a specific shape shield (levels are masked intentionally) – the scale color varies from dark-blue – light blue – green – orange –red. Brown stands for "not-defined"

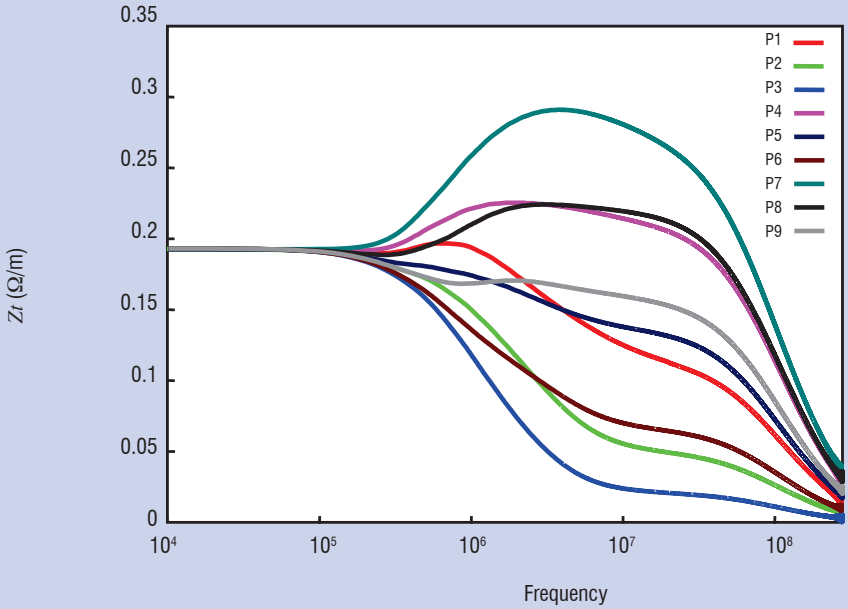

Figure B5 - 3 - Frequency variation of Z_t at various test points (P1 to P9) inside the specific shape shield in figure B5-2 (the location of the test-points is intentionally masked in Figure B5-2)

Protection with shielded cables

Cable shields have three main functions for signal cables and electrical wires: 1 – For mechanical protection, 2 – for optimizing the propagation of the signals (in order to transmit high frequency signals, for example), 3 – for providing an EM protection and making the mechanical shield become an EM shield. Here, we focus on the third function. The EM shields take the form of metallic braids that uniformly surround the cable bundles (the braid allows the overall bundle flexibility to be preserved, compared to a rigid tube). Such shields are called overshields (they may overshield cables located inside).

We have seen that current injection in the aircraft/rotorcraft structure generates equivalent common mode and mutual inductance sources in cables. In order to reduce the amplitude of those sources, the idea is interpose a shield that will act as a second shielding level after the structure shield, in terms of EM topology. However, in order to obtain this shielding level, we must allow the current to flow on this metallic conductor. This thereby requires that the shield be well connected to the mechanical ground at both of its ends in order to provide both the magnetic and the electric shielding effects (by the way, the electric shielding effect can be obtained with only one connection at one end of the shield).

Now comes the question of how to make the connection to the ground. As said for the equipment, the connection must be as short as possible, in order to lower the dynamic impedance. For the indirect lightning effect, a simple wire or braid connection is sufficient.

Nevertheless, the installation must avoid the following mistakes regularly encountered on systems:

• do not use long braids which will increase the inductance and may lead to an increase of the global shield impedance;

• if long braids must be used, do not make loops by winding them on themselves and therefore developing an "efficient" magnetic collector, likely to couple to the wiring;

• do not make the connection to a pin of the equipment chassis connector.

If the shield requires an EM protection function at higher frequencies for other EM threats (such as HIRF for example) and if it is affordable, the installation should use a 360° circular connection of the shield on the equipment connector chassis. This will avoid any inductive connection effect.

Finally, installation should be done taking the opportunity of connecting the cable overshield to the ground as often as possible. On the one hand, for regular use, this avoids resonance of the cable overshield, but this is not of real concern for indirect lightning. On the other hand, if this connection is made for each crossing of walls, this technique allows the shield induced-currents to be confined in specific zones, without transmitting them in undesired zones.

As a conclusion, we can propose the following good trade-off rules for the proper use of cable EM shields with respect to indirect lightning effects:

• always connect the cable shields at its ends at the level of the equipment;

• take advantage of intermediate connections to the ground, in order to enforce the effect of zone decoupling;

• use cables with a good resistance per unit length.

Remember also that a cable-shield that is not connected at both ends will not provide any magnetic shielding effect along the inner cables, whereas a single connection at one end provides only an electric shielding.

System level numerical simulation

As in every electrical engineering process, numerical simulation nowadays plays a major role [38], [39], [40]. The interest in using numerical simulation can be seen at two levels:

• for analyzing measurements. In this case, the simpler the model, the better the analysis. This is typically what has been shown in this article when 2D invariant models are used to understand EM coupling mechanisms on structures and cables,

• for predicting the constraints to be applied at equipment level on real systems. In this case, the model must be as precise as possible and must take into account the entire system. The trend is increasingly for the generation of such EM models to become part of industrial process for the design of the system and even the certification. Let us mention for example the significant part played by EM demonstration in the new version of ED107 for HIRF [41]. Let us also mention the HIRF-SE project, which is aimed at considering EM modeling as an integral part of the HIRF certification process [42].

In this section, we are interested in the second aspect of indirect effect modeling. Let us specify that in such cases, the objective can also be to help in the building of the experimental test program and to be able to extrapolate the test results to configurations that cannot be tested.

Indirect lightning EM modeling specificities

The numerical tools concerned by these types of heavy EM modeling processes are so-called "3D computer tools". These tools are based on a discretized resolution of Maxwell's equations [43], either in their differential form or in their integral form, applied on a discretized model of the geometry on which EM and electric characteristics are applied (the mesh). The modeling process is thereby divided into 3 usual steps:

• the generation of the mesh (geometrical and electrical model). This task is accomplished by means of tools called meshers;

- the availability of the geometrical model comes from CAD models. Two main types of geometrical models are generally considered: surface and volume meshes.

◆ on the one hand, most commonly used surface meshes generally consider only thin surfaces, which is a quite reasonable approximation for indirect lightning but they may suffer limitations if lossy volume materials must be considered. The advantage of such techniques is the good conformity of the generated meshes. However, while the generation of the outer surface is generally not a key problem, the generation of a precise model of the interior involving all of the constitutive parts is a real problem

◆ on the other hand, the most commonly used meshes are structured meshes with models discretized in small cubes. The technique for generating such geometrical models is based on the interception of a Cartesian grid with the real geometry description (CAD model). The conformity to the real shapes is therefore limited to the cubic approximation. However, small cells of about 5 to 10 cm are generally sufficient to obtain a good approximation of the external surface for indirect lightning concerns (Figure 25-a). In addition, this cubic representation becomes a real advantage compared to conformal meshes as soon as the model of the interior geometry is concerned.

- the availability of the electrical and EM models generally comes from databases (databases of materials, cable database). As seen before, Zs material models are well suited for thin surfaces; lossy materials are sufficient to describe lossy contacts. When EM scattering through holes or seams is concerned, macro-models of small apertures, as seen in § "Free small apertures", are appropriate.

- as far as cable models are concerned, models of thin wires are used; they are based on an approximation of a homogeneous current in the cross-section and they usually require to be much smaller than the cell-size. Multiconductor Transmission Line Network (MTLN) models [44], [45] can be interesting for calculating current and voltage levels precisely on specific wires or pin-connector ends. However, for indirect lightning, it is sometimes difficult to include the common mode resistance in the MTL models for the electrical parameters, because the return of the current depends on the 3D geometry (for higher frequency threats, the current mostly returns under the cables). For this reason, the application of field-to-MTL approaches, which allow coupling 3D solvers and MTLN solvers, is not fully appropriate or requires at least precautions [31], [46], [47]. From a practical point of view, coupling with 3D solvers is therefore mainly possible with shielded cables. The 3D solver calculates the current response on meshed equivalent wires of the cable-shields and MTLN models calculate the responses of wires inside the shield, using its Z_t transfer impedance (see § "Protection with shielded cables").

In Figure 18, because of the small cell-size, it has been decided to mesh the bundles as rectangular cross-sections along the Cartesian mesh, in order to better approach the real size of the cable-bundles and in particular to better approach their self-inductance. Considering the overall complexity of the problem, it is not certain that a thin wire approximation would not have given similar results.

• the resolution of Maxwell's equations for the geometrical and electrical model. The technique of resolution generally depends on the type of mesh, since the geometrical decomposition conditions the type of Maxwell's discretization. Generally, for various reasons, such as stability of numerical schemes, volume techniques are solved in time domain; the Finite Difference Time Domain technique is one of the most favored approaches for the many advantages that it provides [43]. Surface techniques are solved in the frequency domain with resolutions of the Moment Method type. Volume techniques require absorbing boundary conditions for limiting the calculation volumes, such as ML, PMLs [48], [49]: this also allows infinite wires to be considered to simulate the lightning injection channel. Surface techniques do not require such conditions, but they suffer the fact that it is impossible to consider infinitely long wires.

• the post-processing covers the usual task of displaying results in one, two or three dimensions with a specific objective to be able to handle large sets of data, especially in 2D and 3D (figure 18-b). Another specificity is the extrapolation of time domain signals to zero for time domain calculations. Indeed, due to the long calculation time, 3D calculations are generally stopped sometime after the maximum of the waveform has passed. This return to the zero signal is required, because it is the only way to determine the action integral or the frequency content at the zero frequency. Several techniques can be applied: we can mention the techniques based on autoregressive techniques (such as Prony techniques) [51] or on the decomposition of sums of biexponetial waveforms, such as the Levenberg-Marquardt technique available in the XMGRACE freeware tool [52].

Indirect lightning EM model related issues

The challenges for building and solving indirect lightning on a 3D discretized model can be synthesized as follows:

• the cleaning of the geometry, which consists in removing all parts that do no significantly participate in the EM response and the morphing of the cells, in order to correct approximations generated by the cell discretization (correction of the contacts between parts, especially).

• the correct evaluation of the contact resistances to be placed at junctions between mechanical parts. This type of information is quite difficult to obtain from a data base, because it is highly system-dependent (unlike the resistance of a cable or the characteristics of a material).

• the management of the size of the geometrical models. A usual requirement is to be able to consider the quasi-static approximation in each cell of the mesh, which commonly leads to an approximation of the type $\lambda/10$. Therefore, for indirect lightning, this condition should lead to cells of some meters only! Nevertheless, small cells are required in order to describe correctly the geometry and particularly the contacts or absence of contacts between zones or cables. For time domain resolution, stability criteria imply small time steps and lead to long resolution times. In addition, large meshes imply efficient hardware and software to display the views of the mesh, since the amount of data is generally huge (of tens of millions of cells).

• the availability of cable architecture in the CAD models. The wiring database must include at the same time the wiring topology and its constitution; unfortunately, such information is not always jointly available. In addition, the problem is to be able to run the cables (volume models or 3D models) in a consistent way. In figure 18-a, cables have been meshed in surface because they are shielded cable bundles whose radius is large compared to the cell size (0.5 cm). The difficulty is of course related to the constraints generated by the Cartesian grid. In box 2, an original and new technique of multiconductor

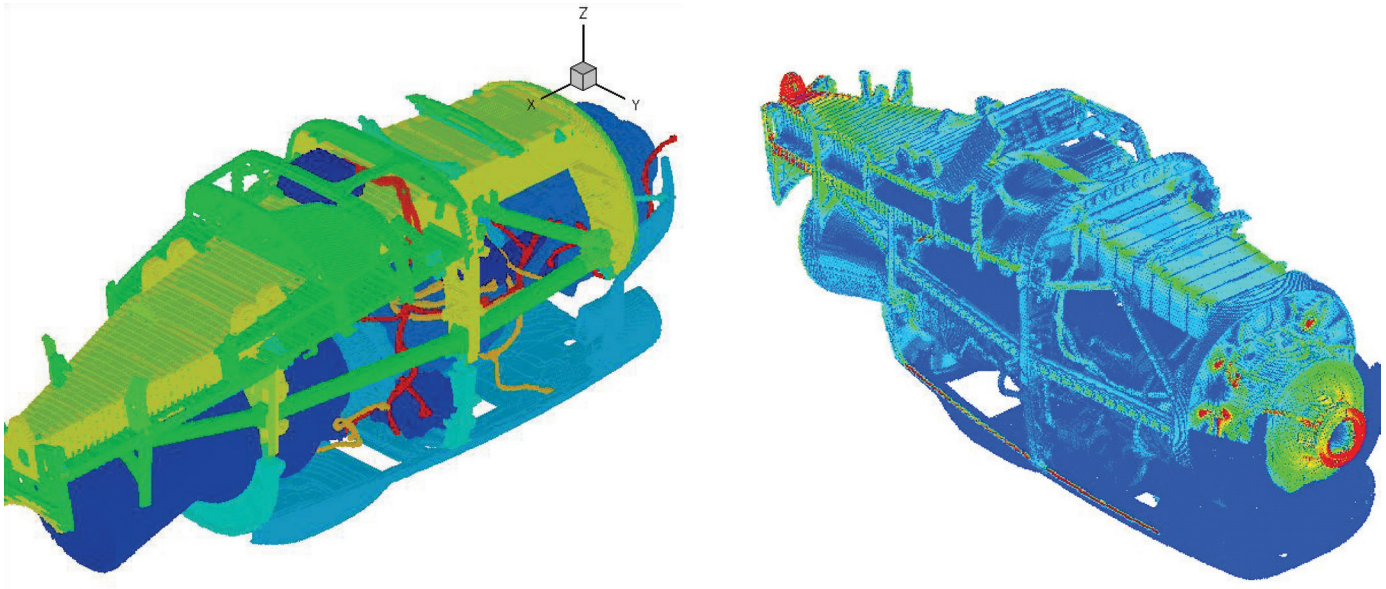

a) 3D FDTD model

b) Current distribution

Figure 18 - 3D FDTD model of the TP400 engine (from [50])- Courtesy of HISPANO-SUIZA

Box 6 - Modeling bent wires in a simulation of indirect lightning on the Falcon 7X aircraft

In [53] and [54] a very complete work is shown to describe how the methodology of indirect lightning modeling can be carried out at the level of an entire aircraft. This work, carried out within the framework of a cooperation between Dassault and Xlim in France, can be seen as an extension of several studies carried out within the framework of aircraft certification, such as the one described in [40] for the certification of the C 27J Italian aircraft. In Dassault's and Xlim's paper, the authors use an FDTD approach in [40] which gives further evidence of the robustness to carry-out extensive EM 3D calculation, as far as tackling the full complexity of an aircraft system is concerned. However, Dassault's and Xlim's authors go a step further by providing, at the same time, a solution to 3 main challenges which currently limit the application of FDTD techniques on such large problems:

Calculation of late times

As we have seen, it is essential to obtain the long times of the induced signals because they are required to have a good estimate of the action integrals and therefore of the induced energy. The French authors propose the combination of two techniques:

- the Matrix-Pencil method (MP) [55] developed by T-K. Sarkar to extrapolate long time signals using poles and residues decomposition techniques, based on the Singularity Expansion Technique (SEM)
- the Short Impulse to Large Impulse (SILI), which calculates the transfer function over a large frequency band in order to be able to determine the response of the system to any type of injected current waveform.

When these two techniques are applied for estimating current responses in cables, this technique allows the extrapolation of 50 μs responses to 1ms responses.

The positioning of cable models anywhere in the aircraft model

We have seen that realistic models of an aircraft system require the possibility of modeling a large set of cables. Of course, more and more CAD models provide cable route geometrical data, but the problem of describing it correctly in the meshed model remains. For this, the thin wire model [56] is a good approximation, but the model requires the route to follow the edges of the Cartesian grid, which results in having all of the meshed routes described in steps. In addition, the bad description of the routes is not the only limitation; the restriction of having wires along the edges implies merging some cable-links in unique equivalent cable models, which of course changes the electrical circuit followed by the flow of the current. This is why Dassault and XLIM have been working on the development of a thin bent wire model, which avoids those limitations and allows very realistic aircraft wiring systems to be obtained, as far as indirect lightning is concerned. This feature has been integrated into XLIM's FDTD 3D computer tool; wires can be placed anywhere in the FDTD Cartesian cells; several wires can even be placed in a given cell. It has been used for all of the cable results presented in [53] and [54] (figure B6-1).

The incertitude on cable-losses and end impedances

As regards indirect lightning, we have seen the relevance of two major factors:

- the common mode impedances, which depend on the material electrical characteristics and the connection impedances at junctions.
- the cable impedances. These depend on all of the elementary cables, which constitute the thin equivalent model of the cable-bundles.

Therefore, both parameters cannot be fully deterministic. [53] and [54]evaluate several designs of experiment methods to estimate extreme values of signals resulting from these uncontrolled parameters. One of the main lessons is that the Rechtschaffner method [57], based on simplified fractional plans, gives very satisfactory results compared to more exhaustive methods.

The main interest of this very complete work resides in its application to Dassault's F7X aircraft and its comparison to real measured signals, which provide a clear validation of the method for using it, for certification purposes. This is why, at the time of the publication of this article, this work may be presented as the most achieved state of the art of lightning indirect modeling at the entire aircraft level.

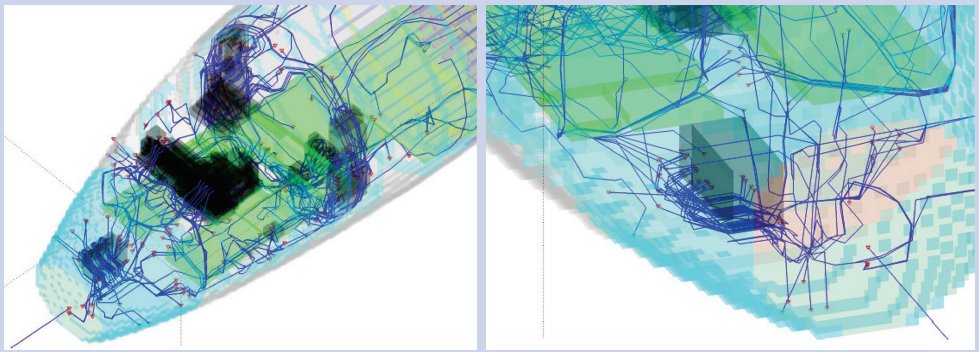

Figure B6 -1 - Details of Dassault's F7X wiring model inside the FDTD model (form [54]). Courtesy of Dassault

wires, not necessarily parallel to the Cartesian grid, has been used and opens a new field for describing the large density of cables in 3D interior geometry.

• identification of zones of electric breakdown. We have seen that it is difficult to control non-linear effects due to indirect lightning. In particular, electric breakdowns occurring between geometrical parts, especially junctions, are of particular importance. For this the determination of zones in which the electric field may be of the order of magnitude of electric breakdown in free space (typically 3 MV/m) is a very good indicator. Thus, the simulation of the electric breakdown with a thin wire with a specific resistive law may provide very good indicators in terms of design. Nevertheless, the prediction level is not achievable yet.

New trends

3D modeling is so far based on the resolution of Maxwell's equations for a geometrical model that replicates the real geometry as much as possible. Such approaches are well suited for industrial processes, for which the CAD models are prior inputs. Nevertheless, we have noticed in many of the results displayed in this article that the system response waveforms are very close to R, L, C circuit waveforms. This is particularly true because the lightning waveforms can barely excite the resonances of most of the systems under consideration. Of course, the main difficulty remains in determining the R, L and C parameters, which is almost not achievable on a complex system.

In the French Industry sponsored program called "PREFACE", such models have been investigated under the generic name of Partial Element Electrical Circuit (PEEC) methods [58]. Particular interest has been given to the so called "stick models", in which 3D structures are represented by wires supporting the circulation of currents. Each wire has a resistance and a radius that allow the determination of its self-inductance. In addition, mutual inductances are calculated analytically, as a function of the respective positions of the wires in the 3D geometry [59]. Then, the entire current response can be obtained by solving the equivalent circuit, either in the frequency or time domain (LIRIC computer code from Onera).

In [60], in order to demonstrate the capability of the approach, an A320 landing gear is modeled with such a stick model. The results are compared to measurements and a full 3D modeling performed with Onera's ALICE FDTD code. The test configuration consists in injecting an A-waveform with a lower level (all of the results are then normalized to the regular 200 kA). On the one hand, figure 19-a shows the structured 5mm-cell mesh used for the ALICE calculation. The entire mesh was made of 80 millions of cells; the time step required by the stability criterion was 25μs which led to a 15-hours total calculation time on 380 processors for passing 20% of the maximum of the response waveform. On the other hand, the equivalent stick model is shown in figure 19-b. Each constituent of the landing gear has been modeled by a wire with an equivalent radius and an equivalent length: in total, there are 56 wires and 40 connections between them. The LIRIC calculation took only a few minutes to calculate the entire signal damped to zero for long times. The advantage of such an approach clearly resides in its short calculation time, which is well suited for parameter analysis and thereby for design optimization.

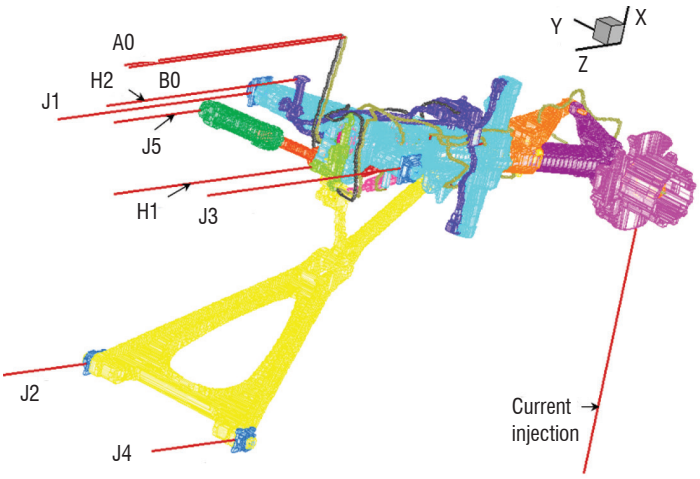

a) FDTD model

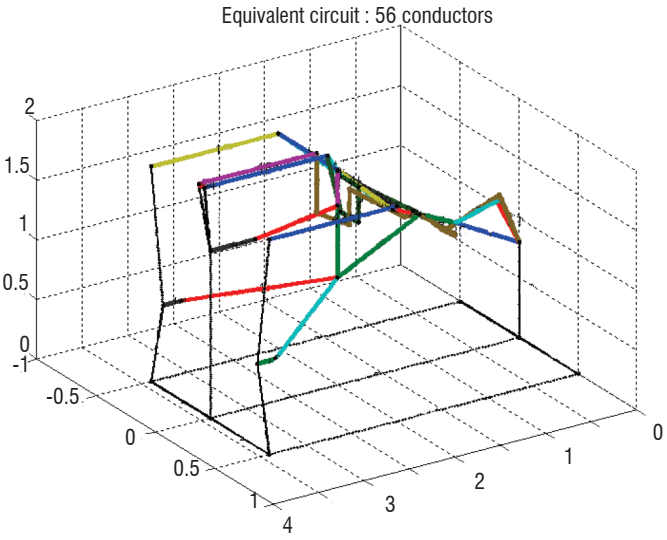

b) Stick model

Figure 19 - Models for a current injection on an A320 landing gear [60]- Courtesy of the PREFACE project

Figure 20-a shows some results obtained for the wires used to close the circuit and for shielded cables (Jx, A0 and B0 – see figure 19). Figure 20-b shows a histogram of the results of the maximum currents obtained. They first show the confidence that can be given in both modeling techniques.

Nevertheless, note that to obtain these results, either by the 3D computer code or by the stick model code, the model is significantly dependent on the values of the contact resistances between constitutive parts; these resistances had to be measured and introduced into the models. Without them, none of the models would have given the expected results.

Of course, in [60], the structure being modeled is mainly made up of a network of bars and more validations must be made for more 3D shapes, in which some 3D surfaces need to be modeled by sets of parallel wires. Nevertheless, considering the quality of the results shown in § "Cables inside and outside a realistic structure", based on the use of 2D invariant cross-sections meshed with parallel wires, there is no reason why such an extension in 3D should not give good satisfactory results. Stick models have been known for a long time. In the 80s they were the precursors of 3D full-wave models and they were used because of their low computation cost [25]. Then, the

trend to reach higher frequencies such as EMP made them become inappropriate and led to the race towards achieving increasingly efficient 3D full wave models. However, this made the numerical modeling community forget how those techniques may be efficient at low frequencies! By the way, such techniques are fast because the model itself introduces some hypotheses on the solution, by imposing the direction of the currents.

Such models are not ready to be introduced in industrial processes yet, as for some 3D full-wave calculations, but there is a good chance that the stick model approach can become part of this overall modeling process in the near future. Indeed, we can foresee a very efficient combination of these two types of full-wave and stick models:

- full wave models may be required for the first calculation, which provides reference results for mapping the current redistribution. They provide a reference calculation;
- then, the stick model decomposition can be made from this first 3D evaluation. It offers the capacity of running sensitivity analyses.

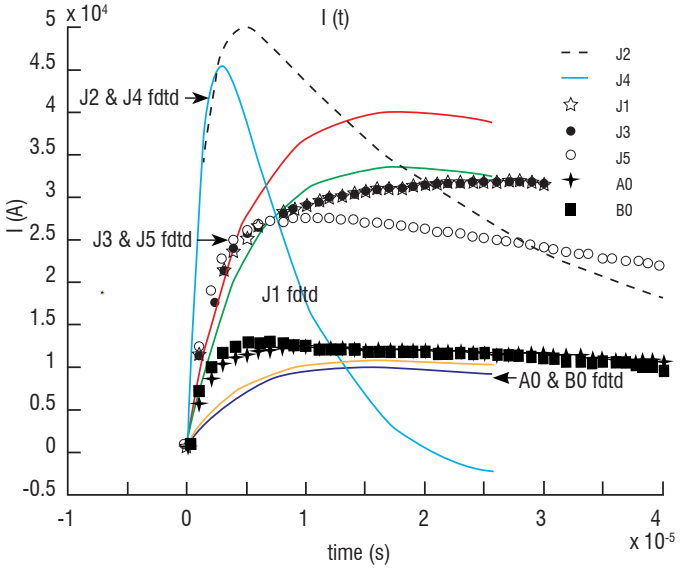

a – Global time domain waveforms

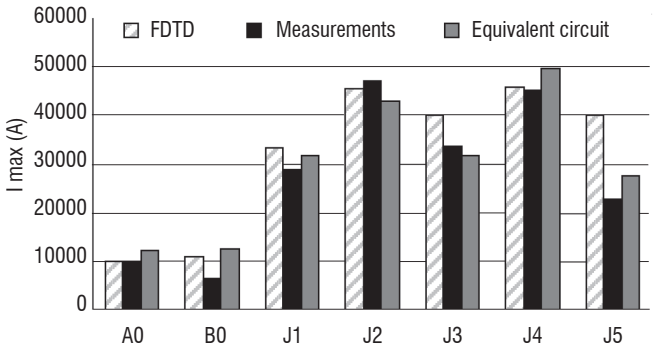

b – Maximum of the waveforms

Figure 20 - Current results on the A320 landing gear (PREFACE project) [60]

Conclusion

In this paper, we have shown that, as for direct lightning, is was impossible to consider addressing the full indirect lightning sequence and lightning analysis must be broken down into a series of independent waveforms, among which type A waveforms are the most relevant for the system, because of their energy content. This is why most of the illustrations in this paper concern this particular waveform of interest.

The elementary coupling effects are of two types: the conduction effect, which merges resistance and inductance effects on induced current lines and the scattering effect, which concerns the EM field produced through local geometries, such as apertures or junctions. Again, the electrical nature of the materials involved in this scattering is very influent on the signature of the resulting attenuation. A very important result is that, most of the time, scattering dominates against diffusion in lossy materials in closed structures, as soon as apertures are made in the structure. This analysis allows the introduction of the concept of EM shield, for which we showed that magnetic shielding was the most difficult to carry out, as far as in direct lightning is concerned, because of its low frequency content.

At system level, the analysis of the structure response is not sufficient and the electrical system response must be investigated. We showed that typical time domain responses could be reproduced by 2D invariant models and that an equivalent source model including generator and impedance could be deduced. We have seen that, for low frequency type-A waveforms, the common coupling was the most significant and could lead to the generation of significantly high amplitude voltage or current signals on cables. In addition, linear approximation is a convenient approximation, because it prevents us from considering non-linear effects, which are so difficult to control from one configuration of injection to the other. Hopefully, we illustrated through real aircraft measurements that this approximation is quite satisfactory, in the sense that it remains conservative on the levels of currents observed in cables.

Two main techniques can be used for protection against indirect lightning. One consists in acting on the installation design, in order to have EM shields contributing to block the magnetic field as much as possible and, therefore, the EM coupling on cables. The key idea to remember is that magnetic shielding requires currents to flow over surfaces as much as possible, otherwise there is no shielding effect. The installation of cable shields obeys the same rules exactly, but at the scale of the cable. Grounding and bounding are very important installation rules, in order to make this current flow possible. In addition, at the same time, they provide the confinement of currents in a volume zone, which is a key point for the maintenance and the control of system evolution in the future life of the AC/RC. Nevertheless, active protection at the level of equipment inputs cannot be avoided, because of safety issues. Indeed, topology based rules can be easily broken if new system components come to be installed on the existing system without any awareness of the rules to be applied. In addition, it must also be said that, due to the system complexity and other constraints naturally not compatible with electromagnetics (think of thermics which requires opening as many apertures as possible to evacuate heat!), perfect EM design rules are not applicable.

Finally, we have shown that EM modeling constantly makes progress, which makes it nowadays a valuable complement to scale-one tests. Nowadays, progress in the 3D modeling of indirect lightning effects is aimed towards two opposite directions: one relies on a very accurate description of the system for applying 3D full-wave solvers; the other relies on intensive simplification, introducing knowledge of the solution on the current distribution in the model as much as possible for applying light solvers, such as electrical circuit solvers. The parallel evolution of the geometrical and electrical aided design tools now

makes it possible to feed the numerical models with the relevant data required by the 3D simulation. However, some of the driving models remain very specific to a given installation and the parameters to put in the models remain inaccessible without measurements. This leads to a new way of thinking for scale-one models: to not consider them only to simulate an effect, but also to provide the model with the missing information, applying very specific configurations designed to measure the model parameters. The advantage is that, once validated, it offers more flexibility and a greater variety of injection configurations than scale-one tests.

Consequently, as a general conclusion, we can say that even if indirect lightning remains a real threat for aircraft, for which constant progress allows a better design of AC/RC to resist this threat, we must ask ourselves if the new emerging aircraft designs will not require some ways of thinking about indirect lightning to be changed. Over the past ten years, we have already seen how the trend towards full composite aircraft has imposed new design rules for allowing the dissipation of currents with new structures, because the surface could not do it properly like the metallic structure did previously. Now comes the trend toward the full electrical aircraft, which of course raises the question of the vulnerability of those new systems to indirect lightning. Because more electrical systems will have to be installed outside the surface of the structure, direct and indirect effects must be handled simultaneously, if the protection is to be properly designed. For example, new embedded de-icing systems must apply the same level of protection and surveillance as antennas. Consequently, the real question is: do we have the knowledge, the rules, the tools and the methodology for making these new systems comply with indirect lightning constraints?

Acknowledgements

The authors would like to thank:
- M. P. Foutrel from SAGEM Defence for having accepted the publication of the animation of the lightning current distribution on the AASM system
- MM. F. Tristant from Dassault and E. Perrin from XLIM for having made possible the publication of figure B6-1.
- M. C. Lair from SNECMA for having accepted the publication of figure 18

References

[1] E. WILLIAMS, S. HECKMAN - *Specific Behaviour of Positive and Negative Atmospheric Electrical Discharges*. Aerospace Lab Issue 5, December 2012
[2] *User's Manual for Certification of Aircraft Electrical/Electronic Systems Against the Indirect Effects of Lightning.* SAE International, 2001-08-01
[3] *Certification of Aircraft Electrical/Electronic Systems for the Indirect Effects of Lightning.* EUROCAE, Issued in May 1996 - Including Amendment N°1 August 1999
[4]RTCA / DO-160 E - *Environment conditions and test procedures for airborne equipment – section 22: lightning induced transient susceptibility*. RTCA Inc, December 2004
[5] *Lightning Aircraft Lightning Environment and Related Test Waveforms Standard.* EUROCAE,1997
[6] P. LAROCHE, P. BLANCHET, A. DELANNOY, F. ISSAC - *Experimental Studies of Lightning Strike to Aircraft.* Aerospace Lab Issue 5, December 2012
[7] J. GRANDO, X. FERRIÈRES, D. MULLER - *Code Alice: Introduction des joints résistifs et exploitation Transall.* Rapport Technique Onera, N° 4/6161 PN, Juin 1992. In French.
[8] V. GOBIN - *Diffraction par les ouvertures et par des objets tridimensionnels. Application à la mesure des impédances de surface des matériaux bons conducteurs*. Thèse de doctorat de 3ème cycle de l'Université de Lille III, juillet 1989. In French.
[9] C. CUILLER, J-C. ALBOUY - *Etude des effets indirects de la foudre sur une voilure réalisée en composite de carbone.* Proceedings of the 1992 French Conference on EMC, CEM 92, 3-4 June 1992, pp. 477-483. In French
[10] J.P. MARQUE, S. BERTUOL, J.P. PARMANTIER - *Modélisation et analyse de l'environnement électromagnétique induit par un foudroiement. Fonctions de transfert d'un réseau de câbles complexes*. Actes du 9ème congrès CEM. Brest, pp. B4-5-B4-10, 8-12 June 1998, in French.
[11] J. PARMANTIER, J. MARQUE, S. BERTUOL, U. THIBBLIN, and al. - *Modeling and Analysis of the Electromagnetic Environment on Aircraft and Helicopter Part 2: Coupling to Complex Cable Networks.* SAE Technical Paper 1999-01-2356, 1999, doi:10.4271/1999-01-2356.
[12] M. RENARD and al. - *Aircraft Electromagnetic Vulnerability Operative Model (MOVEA).* ICOLSE, 28-31 August 2007, paper PPR-52.
[13] L.CHEMARTIN, P.LALANDE, B.PEYROU,A.CHAZOTTES, C.DELALONDRE, B.G.CHÉRON, F.LAGO - *The Thermo Electrical effects of Lightning on Aircraft Structure: Observation and Modeling of Thermo Electro Mechanical Damaging*. Aerospace Lab Issue 5, December 2012
[14] *Aircraft Lightning Environment and Related Test Waveforms.* SAE International, Revision A, 2005-02-21
[15] *Environmental Conditions and Test Procedures for Aircraft Systems.* Version D, Chapters 22 and 23, 2006
[16] P. DEGAUQUE, J. HAMELIN - *Electromagnetic Compatibility*. Oxford, Oxford University Press, Oxford [England]; New York: Oxford University Press, 1993
[17] D.MORGAN, C.J. HARDWICK, S.J. HAIGH, A.J. MEAKINS - *Lightning Test of Aircraft: challenge and issues.* Aerospace Lab Issue 5, December 2012
[18] *Aircraft Lightning Test Methods.* Revision A, SAE International, 2005-03-17
[19] *Protection against lightning*. 2010.
[20] S. RAMO, S. WHINNERY, J.R. VAN DUZER - *Fields and waves in communication electronics.* John Wiley & Sons, 1965, 1984, 1994
[21] P.LALANDE, A.DELANNOY - *The Global Zoning.* Aerospace Lab Issue 5, December 2012
[22] *Aircraft Lightning Zoning.* Revision A, SAE International, 2005-02-16
[23] P. FOUTREL - *« Méthodologie de conception CEM d'un système avionique.* 13th International French Conference on EMC, CEM 2006, 4-6 April 2006.
[24] M.A. BETHE - *Theory of diffraction by small holes*. Phys. Rev 2nd Series 7 and 8.. 1 and 15 October 1944
[25] K.S.H. LEE - *EMP Interaction: principles.* techniques and reference data, Hemisphere Publishing Corporation, Washington, New York, London, 1986.

[26] V. GOBIN, J-P. PARMANTIER - *Chapter 3: Pénétration et couplage dans les structures tridimensionnelles*. In EM Compatibility, Collection technique et scientifique des télécommunications. Lavoisier, Hermes. Paris 2007, under the direction of P. Degauque and A. Zeddam. In French.
[27] K.F. CASEY - *Quasistatic electromagnetic penetration of a mesh-loaded circular aperture*. Interaction notes, note 387, 7 March 1980*.
[28] K.F. CASEY - *Low frequency electromagnetic penetration of loaded apertures*. IEEE Trans. Elect. Compt. Vo1.EMC-23, pp.367-377, 1981.
[29] W. H. HAYT, J. A. BUCK. *Engineering Electromagnetics*. Mc Graw Hill. 2001. Boston, New York, San Francisco, St Louis, (6th edition)
[30] V. GOBIN, J.P. APARICIO, J. GRANDO, J.C. ALLIOT - *The surface impedance: a pertinent parameter to describe finite conductivity materials in numerical codes.* Electromagnetic compatibility (EMC) Symposium, ZURICH, 12-14 mars 1991
[31] F.M. TESCHE, M.V. IANOZ, T. KARLSSON - *EMC Analysis Methods and Computational Models.* John Wiley & Sons, pp.247-266. 1997.
[32][ISS 2008] F. ISSAC - *PEA MOVEA Sous-tâche 1.3 – Fiche E3 – Dimensionnement des termes sources en BF et HF. Approche Onera*. Onera's internal report MOVEA/Onera/E3/08.2-B, 15 December 2008
[33] Y. LE-GOLVAN, G. PENSEC, D. QUILTU, J-P. PARMANTIER*, X. FERRIÈRES*, E. BACHELIER*, S. BERTUOL* - *Etude du couplage d'une onde foudre de type A sur une goulotte de descente de câbles installée à l'intérieur d'une mature intégrée pour navires militaire.* CEM France, Saint-Malo 2006, in French
[34] C. E. BAUM - *The Theory of the Electromagnetic Interference Control.* Interaction Notes. Note 478, December 1989* and, Modern Radio Science 1990, pp. 87-101, Oxford University Press
[35] F. ISSAC, E. BACHELIER, D. PROST, V. ENJALBERT, L. MOHEDANO - *Space launching site protection against lightning hazard.* Special Issue N° xx, "Lightning hazards to Aircraft and Launchers", December 2012
[36] P. DEGAUQUE, J-P. PARMANTIER - *Chapter 2: Couplage aux structures filaires.* in Compatibilité Electromagnétique, Collection technique et scientifique des télécommunications. Lavoisier, Hermes. Paris 2007, under the direction of P. Degauque and A. Zeddam.
[37] E.F. VANCE - *Coupling to Cables*. Wiley Interscience Publication. 1978
[38] M. D'AMORE, M. SARTO, A. SCARLATTI - *Radiated Susceptibility of Wiring System Aboard Lightning Struck Aircraft. Part I: sensitivity to the p.u.l. length external parameters.* Proc. 2002 IEEE Int. Symp. EMC, Minneapolis, MN, August 2002
[39] M. D'AMORE, M. SARTO, A. SCARLATTI - *Radiated Susceptibility of Wiring System Aboard Lightning Struck Aircraft. Part II: sensitivity to the distributed sources.* Proc. 2002 IEEE Int. Symp. EMC, Minneapolis, MN, August 2002
[40] M. APRA, M. D'AMORE, M. SARTO, V. VOLPI - *Lightning Indirect Effects Certification of a Transport Aircraft by Numerical Simulation.* IEEE Transactions on Electromagnetic Compatibility 50(3), pp.513, 2008.
[41] *Guide to Certification of Aircraft in a High Intensity Radiated Field (HIRF) Environment*. version A, EUROCAE, July 2010
[42] http://www.hirf-se.eu/hirf/
[43] J-P. PARMANTIER - *Numerical Coupling Models for Complex Systems and Results*. IEEE Trans. on EMC, vol 46, n°3, pp. 3594, 367 , November 2004.
[44] C. E. BAUM, T. K. LIÙ, F. M. TESCHE - *On the Analysis of General Multiconductor Transmission-Line Networks.* Interaction Notes, Note 350, novembre 1978 Interactions Notes are available at: http://www.ece.unm.edu/summa/notes
[45] C.R. PAUL - *Analysis of Multiconductor Transmission Lines*. New-York: John Wiley & Sons, 1994
[46] L. PALETTA, J-P. PARMANTIER, F. ISSAC, P. DUMAS, J.-C. ALLIOT - *Susceptibility Analysis of Wiring in a Complex System Combining a 3-D Solver and a Transmission-Line Network Simulation.* IEEE Trans. on EMC, Vol. 44, No. 2, pp. 309-317. May 2002.
[47] X. FERRIÈRES, J.P. PARMANTIER, S. BERTUOL, A.R. RUDDLE - *Modeling EM Coupling onto Vehicle Wiring Based on the Combination of a Hybrid FV/FDTD Method and a Cable Network Method.* Proc. of 15th International Zurich EMC Symposium, Zurich, février 2003, pp.465–470
[48] J.-P. BERENGER - *A Perfectly Matched Layer for the Absorption of Electromagnetic Waves*. Journal of Computational Physics, 114(2):185–200, 1994.
[49] J.P. BÉRENGER - *Improved PML for the FDTD Solution of Wave-structure Interaction Problems*. IEEE transactions on Antennas and Propagation, 45(3): pp. 466-473, mars 1997.
[50] J-P. PARMANTIER, S. BERTUOL, T. VOLPERT, C. LAIR, P. DUPRÉ, F. THEROND, G. GUTIERREZ, J.I. PLAZA GOMEZ - *Méthodologie de modélisation/simulation 3D des effets EM d'une injection foudre sur le moteur TP400.* 15th international French conference on EMC, CEM 2010, Limoges, 7-9 April 2010, in French
[51] W. L. KO, R. MITTRA - *A Combination of FD-TD and Prony's Methods for Analyzing Microwave Integrated Circuits.* IEEE Trans. On Microwave Theory and Techniques, VOL. 39, n°12, December 1991
[52] http://plasma-gate.weizmann.ac.il/Grace/
[53] E. PERRIN, C. GUIFFAUT, A. REINEIX, F. TRISTANT - U*sing Transfer Function Calculation and Extrapolation to Improve the Efficiency of the Finite-Difference Time-Domain Method at Low Frequencies.* IEEE Transactions on ElectroMagnetic Compatibility, 52(1), pp. 173, 2010.
[54] E. PERRIN - *Modélisation des effets inirects de la foudre sur avion composite.* Ph. D. report of the University of Limoges, 5 May 2012. In French.
[55] T. K. SARKAR, O. PEREIRA - *Using the Matrix Pencil Method to Estimate the Parameters of a sum of Complex Exponentials*. IEEE Antennas and Propagation Magazine, 37:48–55, 1995
[56] R. HOLLAND, L. SIMPSON - *Finite Difference Analysis of EMP Coupling to Thin Structures and Wires*. IEEE Transactions on ElectroMagnetic Compatibility, 23:88–89, 1981.
[57] R. L. RECHTSCHAFFNER - *Saturated Fraction of 2n and 3n Factorial Designs*. Technometrics, 9:569–575, 1967
[58] A. E. RUEHLI, G. ANTONINI - *The Partial Element Equivalent Circuit (PEEC) Method: Part I: General Overview and Part II: Advanced Modeling.* 16th International Zurich Symposium on EMC, Zurich 13-18 février, Switzerland, 2005
[59] A. RUEHLI, C. R. PAUL, K. GARETT - *Inductance Calculations using Partial Inductances and Macromodels.* 1995 IEEE International Symposium on Electromagnetic Compatibility, pp. 23-28, 1995
[60] D. PROST, F. ISSAC, W. QUENUM, J.P. PARMANTIER - *Lightning Induced Current Simulation using RL Equivalent Circuit: Application to an Aircraft Sub-system Design.* IEEE Trans. On EMC, To be published 2012

Acronyms

2D	(Two-dimensional)
3D	(Three-dimensional)
AC/RC	(Aircraft/Rotorcraft)
CAD	(Conception Assisted Design)
EM	(Electromagnetic)
EFIE	(Electric Field Integral Equation)
EMC	(Electromagnetic Compatibility)
EU	(European Union)
MP	(Matrix Pencil)
p.u.l.	(Per Unit Length)
SEM	(Singularity Expansion Techniques)
SILI	(Short Impulse to Large Impulse)
VCC	(Carbon Composite Wing (Voilure Composite Carbone))

AUTHORS

Jean-Philippe Parmantier obtained his engineering degree from SUPELEC in 1987. In 1988, he joined Dassault Aviation, where he obtained his Ph.D in Electromagnetic Topology from Lille University, in cooperation with The French Aerospace Lab, Onera, France and established the first basis of the CRIPTE code. In 1991, he joined Onera, where he began to apply his research to various complex systems, such as, for example, the EMPTAC test bed aircraft from 1993 to 1996. Since 1999, he has been the head of a Research Group on EMC at Onera; Toulouse, France. He is author and co-author of numerous papers on EMC and the organizer of various EMC related conferences and research projects.

François Issac obtained his Technical University Degree (DUT) in physics measurement in 1982, in Montpellier, France. He began working at Ecopol from 1983 to 1986 on lightning effects and he joined the Office National d'Etudes et de Recherches Aérospatiales (Onera) where he became involved in numerous large scale EMC experiments (in-flight lightning tests on a Transall aircraft in 1987 1990; EMPTAC tests on EM Topology, 1993-1996; joint cooperation on mode stirred chambers with DERA, 1999-2000). Nowadays, his field of interest covers a large area, from low frequency to high frequency, mainly from an experimental point of view. He is co-author of numerous papers dealing with EM measurement validations carried out at Onera.

Vincent Gobin obtained his engineering degree from SUPELEC in 1985. In 1987, he joined Dassault Aviation, where he obtained his Ph.D in Electromagnetic Modeling of Composite Materials from Lille University, in cooperation with the French Aerospace Lab Onera, France. In 1990, he joined Onera, where he continued to work on the numerical modeling of complex structures and antennas, more specifically on integral equations and a multi-domain approach. Since 2008, he has been the head of a Research Group on EMC at Onera, Toulouse, France, studying antennas, materials and EM modeling.

D. Morgan, C. J. Hardwick,
S. J. Haigh and A. J. Meakins
(Cobham)

E-mail: dan.morgan@cobham.com

The Interaction of Lightning with Aircraft and the Challenges of Lightning Testing

Aircraft are struck by lightning in flight with some regularity and are required to have demonstrated protection against this threat; much of this demonstration is provided by simulating in test the effects of lightning on aircraft structures, components and systems. Clearly these tests need to be carried out in a representative manner and guidance on how to do this is provided in the Aerospace lightning standards and guidance materials produced by the SAE/EUROCAE committees. Nevertheless, there are challenges; for example, due to dramatic differences in both scale and conditions between a lab and the inside of a cloud, achieving sufficient representation of every aspect of the lightning phenomena can be difficult. Before considering these challenges we discuss the phenomenology and effects of lightning and how they are addressed in the lightning standards, in order to provide some background.

Introduction

The incidence of lightning strikes on aircraft in civil operation is of the order of one strike per aircraft per year and it is vital, from a safety point of view, that these strikes do not endanger the aircraft. Earlier generation aircraft, which were predominantly constructed from aluminum and with mechanical controls and electromechanical instrumentation, had a greater inherent immunity to lightning effects. On modern aircraft, the structure is increasingly constructed from composite materials, in particular carbon-fiber composite. There is also an increasing reliance on electronic avionics systems for primary control of the aircraft. Both of these aspects have made aircraft manufacturers pay greater attention to lightning protection and its certification through testing and analysis. Reproducing lightning and its effects under lab conditions can present certain challenges.

In this paper we will explore the interaction of lightning with aircraft, as well as the methodology of testing and we will discuss the challenges faced in simulating the lightning-aircraft interaction in a laboratory.

The lightning threat

Lightning arises from the breakdown of air by the electric fields generated via triboelectric charging in and around cumulonimbus clouds. These electric fields are well below those required to breakdown the gaps between the cloud and ground or between clouds, however, local field enhancements within a cloud (most likely from ice particles [1], though the process is not entirely understood) can be high enough to initiate the growth of leaders (a filamentary discharge [2]) that propagate towards regions of opposite charge. Once a leader creates a conducting bridge between charged regions, the flow of a return stroke current - the 'flash of lightning' - can occur. The return stroke neutralizes all of the unfulfilled leader branches giving the perception of the classic forked lightning pattern.

Strikes on aircraft in civil operation are of the order of one strike per aircraft per year; however, the probability of an aircraft being struck while stationary on the runway in Europe is approximately one strike every hundred years. The reason for the high strike rates while airborne is

because the aircraft modifies the electric fields in its vicinity, which acts as a catalyst for lightning attachments: an uncharged aircraft located in an electric field will become polarized and the local electric field values at the aircraft surface will be magnified at those extremities aligned with the field, especially where the radius of curvature of the conducting structure is small, such as on wing tips, the tail tips, radome protection strips, etc., see figure 1.

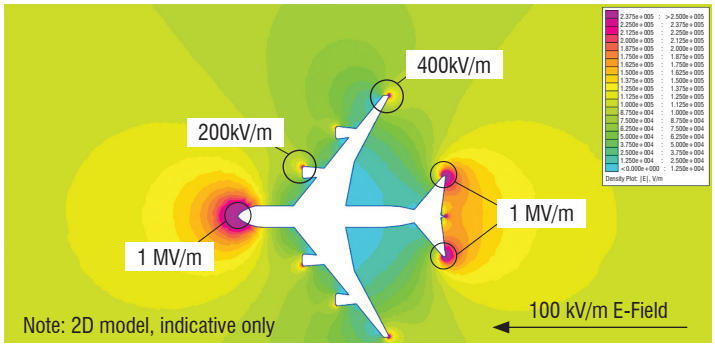

Figure 1 – An indicative 2D electrostatic model of an aircraft in a 100 kV/m ambient field. The field magnitudes at the extremities are significantly enhanced compared to the ambient field, due to charge redistribution and to the sharp curvature of the structure. In moving to a 3D model, the field values would tend to be further enhanced by additional curvature in the extra dimension

Three dimensional computer studies [3] indicate that field enhancements over the ambient of up to a hundred times can occur for some field directions, see Figure 1. Hence, ambient fields as low as 30 - 300 kV/m (typical within a thundercloud or in the vicinity of an approaching leader) will be sufficient to cause corona breakdown at the aircraft extremities.

This corona breakdown can result in the development of bi-directional leaders extending from the aircraft extremities, which may eventually connect with oppositely charged regions in the cloud, see figure 2. In the classic cloud to ground scenario, one of the charged regions would be ground. Through this process, the aircraft triggers a lightning strike, with itself being the direct path of the return stroke current flowing between the two attachment locations.

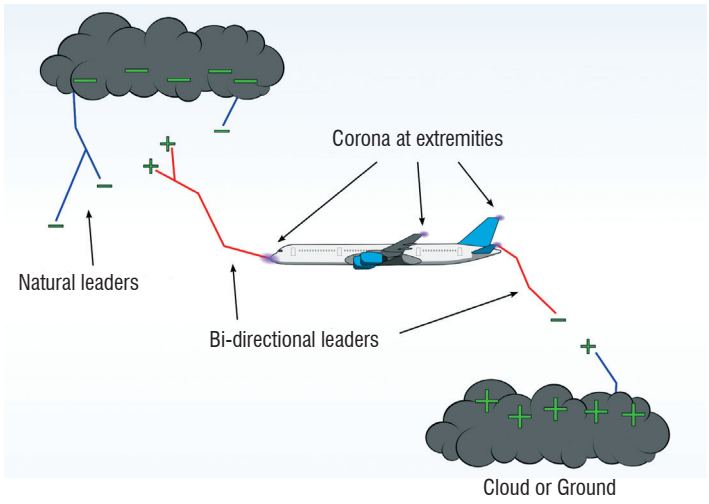

Figure 2 – Illustration of bi-directional leader development (Triggered attachment)

As well as this bi-directional leader development [4, 5] being initiated with the thundercloud field (triggered attachment); it can also be initiated by an existing natural leader channel approaching the aircraft (intercepted attachment). The former tend to be intra-cloud strikes and the latter tend to be the generally more severe cloud to ground strike. Only about 1 in 10 strikes are intercepted attachments, which explains the reason for the relatively high strike rate of airborne aircraft compared to that of those on the ground.

During the return stroke, and also during the progression of the leader from the aircraft to ground, the aircraft can move relative to the lightning channel. An attachment point to a surface therefore moves relative to the channel, causing it to be stretched along the fuselage of the aircraft. This stretching reaches a point where the gap between the channel and the aircraft surface breaks down and a new attachment is formed.

This process continues, so that the arc sweeps back along the aircraft surface in a discontinuous fashion, with dwell times at each attachment point varying according to the nature of the surface, the local geometry and the current waveform. When the lightning arc has been swept back to a trailing edge, it may remain attached at that point for the remaining duration of the flash.

Lightning testing

The leader interaction (both triggered and intercepted) and the subsequent return stroke can be thought of as two distinct phases; (i) the attachment process, which determines where the arcs (leaders) develop from the aircraft; and (ii) the high current return stroke phase.

In the first phase, the aircraft is exposed to high and fast changing electric and magnetic fields during the development of leaders. Consequences arising from this could be the breakdown of dielectric materials (for example radomes, dielectric covers and canopies during the attachment), as well as repetitive electrical transients induced on wiring. Severe damage can also be caused by the high current discharge, which follows a path made available by the HV breakdown. An internal arc through a punctured dielectric will cause physical damage to the dielectric, but also has implications for underlying systems, which may then have very large currents injected onto them. The methods used to assess susceptibility to dielectric puncture during this phase are assessed during High Voltage testing.

The second phase is the high current return stroke phase; this includes the high energy impulses of the first return stroke and the subsequent restrikes, and the long duration slow components. These different component types can have quite different effects on aircraft structure and systems.

Lightning waveforms and levels can vary widely, so an idealized lightning waveform, as defined in ED-84 (see next section on standards), is used for testing. This is shown schematically in figure 3. This idealized waveform is divided into four components, A to D. Note the huge differences in time scales and magnitudes in these four current components.

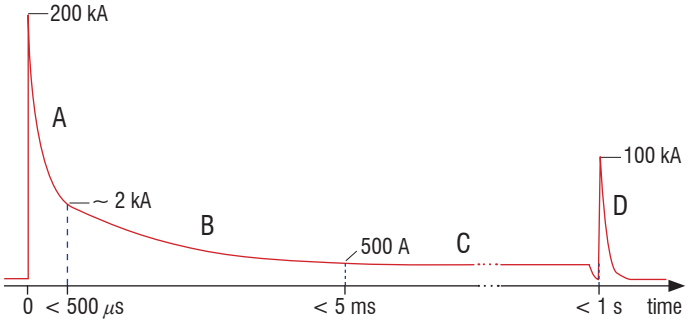

Figure 3 – Schematic of the ED-84 standard high current waveforms (note that the amplitude and time scales are not linear) [6]

Component A is associated with the initial return stroke attachment location, for instance, near the nose and tail of the aircraft. Component D is associated with a re-strike, as the arc is swept along the aircraft. The peak current of the D is half that of the component A, but its Action Integral, the energy associated with the waveform, is an 8th (2 MJ/Ω for the A and 0.25 MJ/Ω for the D). This is due to this difference in the rise and fall times of the two components.

Components B and C form the long duration slow components, also known as the intermediate and continuing currents respectively. A long component C will only be injected at trailing edges where the lightning arc hangs on and cannot sweep to a further aft location.

Fast component damage (A and D)

- Joule heating, proportional to the action integral of the lightning waveform, can cause thin conductors to fuse explosively, leading to damaging overpressures. In carbon-fiber materials, this heating can melt and vaporize the epoxy, leading to delamination damage of the carbon-fiber;
- Magnetic forces arising from the high currents can crush, or drive together/pull apart conductors;
- The acoustic shock caused by flash heating of the air by the lightning channel (thunder) can cause damaging overpressures, particularly inside radomes;
- Current flow within the structure can cause arcing and sparking across interfaces potentially igniting fuel vapor/air mixtures;
- Changing magnetic fields, created by the current flowing in the airframe, generate induced transient voltages in the wiring, which can cause damage or interruptions to the aircraft avionics systems.

Slow component damage (B and C)

- Metals, particularly aluminum alloys, are not significantly damaged by the fast components, however, the charge transfer associated with the slow component can create local melting and puncture. Similarly, carbon-fiber composite can be damaged by the heating process of an attached arc. This is especially important for fuel tank skins.

The methods used to protect against this potential damage are assessed during High Current and Induced Effects testing.

Knowing that these different components can cause different types and severity of damage, and therefore require different types of protection to be installed and tested, it is important to classify an aircraft into different zones, according to the type of lightning attachment likely to be encountered [7].

Test standards and certification

Regulations and test standards define procedures for the certification of aircraft structures and systems against lightning damage and also define the lightning characteristics to be considered.

Box - Simplified aircraft zoning

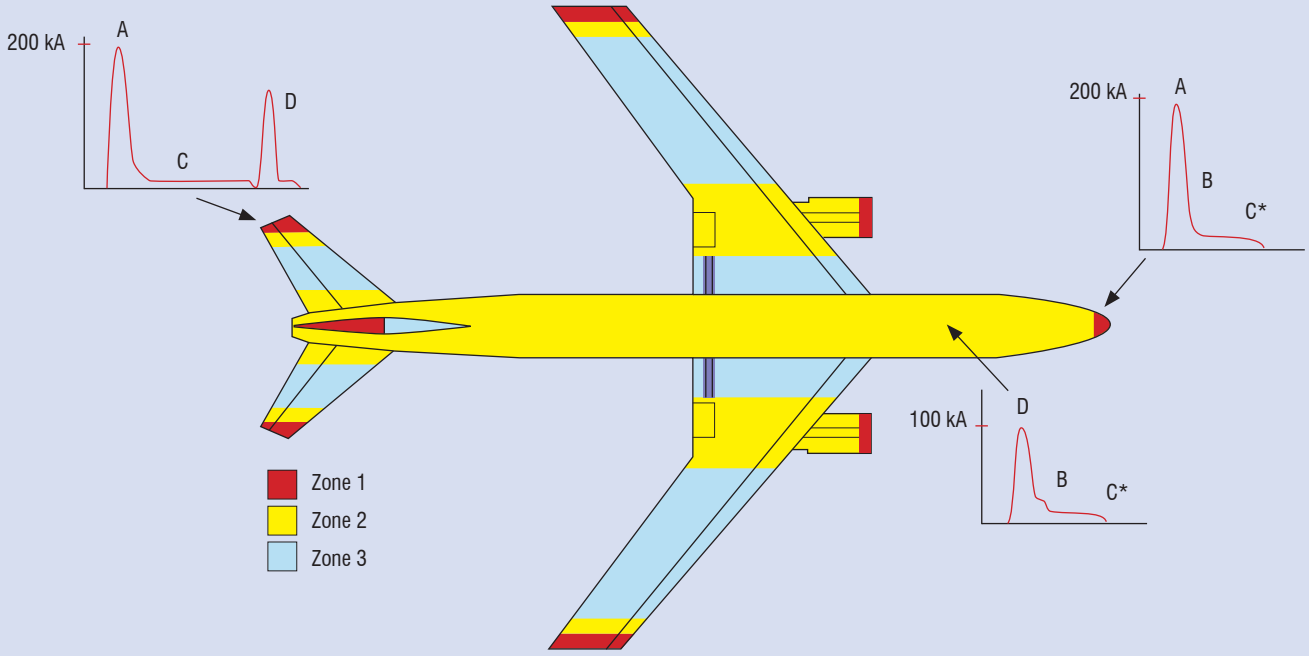

Zone 1 - High probability of initial lightning flash attachment (entry or exit).

Zone 2 - High probability of a lightning flash being swept from a point of initial attachment.

Zone 3 - Any aircraft surface other than those covered by zones 1 and 2. In zone 3 there is a low probability of a direct attachment, however, zone 3 areas may carry substantial lightning currents by direct conduction between two attachment points.

Zones 1 and 2 are further subdivided into A and B regions, depending on the probability that the flash will hang on for a protracted period of time. An A region is one in which there is a low probability that the arc will remain attached (*e.g.*, at the leading edge of a wing) and a B region is one in which there is high probability that the arc will remain attached (e.g., at the trailing edge of a wing).

The civil regulations set by the European Aviation Safety Agency (EASA) and the Federal Aviation Administration (FAA) in the USA give the basic requirements. These are short and fairly non-specific, and with little or no guidance. For example, the structural requirements of 25.581 state little more than that 'the aircraft must be protected against catastrophic effects from lightning' [8].

In order to provide guidance as to how such requirements can be achieved, the European Organization for Civil Aviation Equipment (EUROCAE) Working Group 31 and the Society of Automobile Engineers (SAE) AE2 committee in the USA were founded to produce guidance documents.

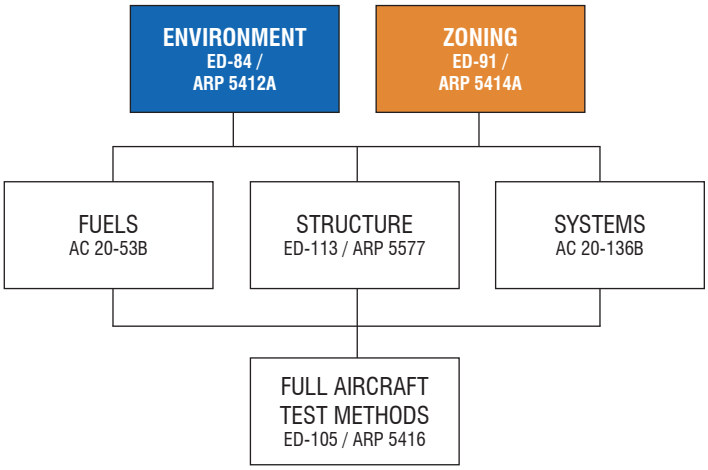

Figure 4 – Diagram showing the structure of the guidance documents produced by EUROCAE WG31 and SAE AE2 committees

The upper tier in figure 4 defines the lightning interaction with aircraft, in terms of the waveforms ED-84 [9] and the zoning ED-91 [10].

The middle tier contains procedures that the applicant can follow, to provide an acceptable route to compliance. There are separate procedures to cover the certification of Structure, Fuels and Electrical/ Avionic Systems, each of which has its own regulation.

The procedure may also include a requirement to carry out tests, and there is guidance material on this in the lower tier, mainly in the comprehensive testing document ED-105 [11].

Challenges and issues

Lightning tests need to be carried out in a representative manner and, as discussed, guidance on how to do this is provided in the Aerospace lightning standards and guidance materials produced by the SAE/ EUROCAE committees.

Nevertheless, there are challenges; for example, due to dramatic differences in both scale and conditions between a lab and the inside of a cloud, achieving sufficient representation of every aspect of the lightning phenomena can be difficult.

In the following sections, some of these challenges are outlined and the approach to mitigating them, where possible, is discussed.

Zoning

The guidance for zoning gives a series of templates for different aircraft geometries deduced from in-flight data.

There is a limited amount of data publicly available and there is also the question of data reliability, as it is not easy on a large metallic aircraft to find arc attachment points, and especially to determine the sequence of events behind the observed attachment points. Since arc attachment is a statistical process, extensive data is required to determine zone boundaries reliably.

There are various other ways of zoning an aircraft, although they each have limitations:

- **Model tests** use a scale model of the aircraft to perform multiple attachment tests in various field orientations, to determine the probability of attachment at any location. Tests must be carried out and interpreted with care, since the curvature on a model's features will be very different from the full scale aircraft and thus the local electric field won't be to scale, affecting the probability of attachment. Also, the "leaders" produced in a lab are much shorter (by an order of magnitude) than in flight;
- **Rolling sphere method** [12] is an empirical approach that uses the 'striking distance' – the closest distance that a leader can approach an object before attracting an "answering" leader– to determine initial attachment locations on an aircraft. This method, using a conservative sphere radius of 25 m, tends to predict larger areas for initial attachment than ED-91;
- **Electromagnetic modeling** uses complex electric field modeling and a model of leader development from the aircraft, offering a scientific method for deducing lightning strike zones and, in general, the results correlate with observed data [13].

In practice, a combination of these approaches may be used.

Attachment to radomes

Radomes are dielectric covers over antennas that can be subjected to high electric fields and initial lightning attachments, particularly to the nose radome. Diverters can be fixed on the radome shell, from which lightning attachments can develop, rather than from the metallic antenna beneath the radome and thus prevent the lightning from puncturing it.

The tests should address the different electric field and antenna orientations. Most strikes are triggered by the aircraft, in which case the leaders propagate out from the radome over long distances. They may also be triggered by an approaching leader, but even here it would be expected that the approaching leader would be tens of meters away before the radome leader develops. In each case, the attachment location is determined by a leader developing from the radome.

The challenge in HV testing is to perform tests with reduced breakdown gaps (typically one meter, due to equipment limitations), which correctly simulates an event that typically develops over a distance of at least tens of meters.

Historically, HV impulse tests to radomes used rod electrodes connected to a high voltage generator. This produces an electric field distribution around the radome that is dissimilar from that experienced

in natural lightning. The maximum electric field gradient will be at the rod electrode, rather than the stress raisers on the radome. Leaders are then likely to develop from the electrode, rather than from the radome, quite unlike what we expect for in-flight strikes.

The use of profiled or de-stressed electrodes is therefore preferred and this is specified in the test standard ED105. The recommended technique is to mount the radome above a large de-stressed plate electrode, which gives a more realistic electric field environment.

Where dielectric breakdown is a concern, historically a faster rising waveform, waveform A with a rise time of 1 to 2 μs, might be thought to give the most severe test. In-flight data suggests that, for initial attachments, a slower waveform, waveform D with a rise time of 50 μs to 250 μs, is more appropriate, at least for the lightning scenario involving an approaching stepped leader. Such tests have reproduced in-flight failures on some radomes that use segmented diverters. No such failures occurred when testing with the faster waveform, hence the slower waveform (waveform D) is both more appropriate and more severe; in ED-105 it is the mandatory test waveform for initial attachment regions.

Triggered lightning can occur within an even slower quasi-DC electric field environment. Work at Cobham has shown that, if the radome is held within a high DC field, corona and leader development from metal fixtures inside the radome can spray charge on the inside of the radome and this can lead to radome puncture.

A coating of an anti-static paint would prevent puncture from such fields. However, when the field causes a leader to develop from the radome, the antistatic paint would be too resistive to conduct the required charge and a connection from the leader to the aircraft would be established via a surface flashover or a radome puncture.

In DC conditions, backed strips certainly behave differently when under impulse conditions - the resistive backing strip, if present, goes into corona (as would the tip if as anti-static paint coated). However, the tests performed in the Joint Radome program [14] already suggested that the change from the A to D waveform was successful in reproducing the in-flight failures that had not been demonstrated by the earlier test standard.

The process of air breakdown is in part a statistical one, which means that repeated tests to a radome would be needed to achieve full confidence in the results. This is particularly so when the radome is negative and the leaders in the test set up approach the radome rather than develop from it, since the path of the leader tip approaching the radome will vary from test to test.

However, repeat tests will degrade the dielectric, so there is a limit to the number of tests that can be performed and the test standards suggest only 2 tests per radome/antenna orientation. Consequently, the statistics obtained in the tests are limited. Despite these reservations, radomes cleared by the latest test procedures appear to be surviving in flight strikes.

Fuel systems

One of the primary concerns with a lightning strike to an aircraft is the prevention of arcing and sparking within the fuel system, since this could potentially cause an ignition of fuel vapor. A frequent way of testing fuel system components is to monitor the fuel side of a component with a sensitive camera, while applying a simulated lightning strike to its exterior.

Whatever approach is used, it is required to be sensitive to a 200 μJ spark, since this has been considered historically to be the minimum energy that can pose a risk to aviation fuel/air mixtures. This 200 μJ electrical spark is simply a means of demonstrating the sensitivity of the diagnostic system; in reality, electrical sparks very rarely occur during fuel tank tests.

What is generally seen are highly visible “thermal sparks”, which are burning particles ejected when arcing within a fastener location hole, leading to a buildup of pressure at the fastener/carbon composite interface, with ejection of sparks and vapor. The spark trails can be faint and the question arises of whether such a spark event seen by the camera could actually cause the ignition of a fuel vapor.

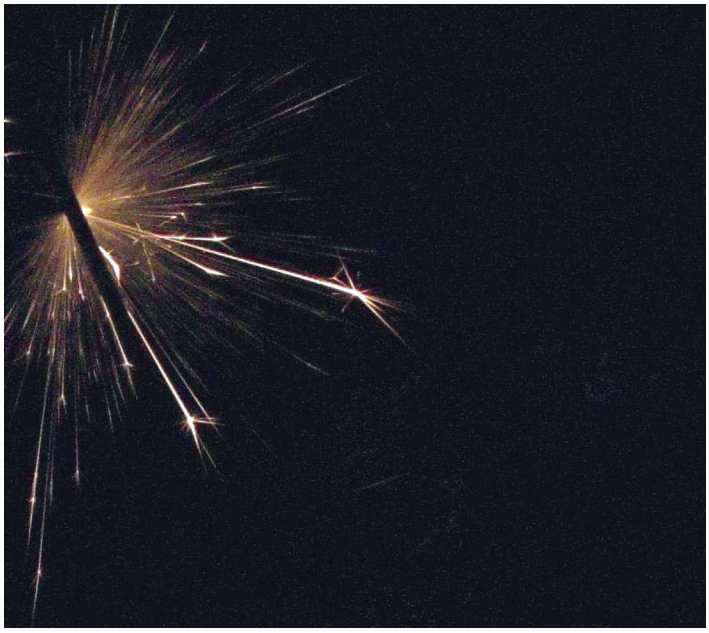

Figure 5 – Highly visible thermal sparks are sometimes seen during fuel system testing, but without necessarily igniting the gas mixture

The question is complicated, since there are many different parameters in such an event that determine whether it would cause an ignition; these are factors such as the number, speed and size of the sparks. Material is also important, since titanium and aluminum, for example, burn with much greater temperatures than steel. Although a more hazardous spark tends to appear more brightly visible on camera images, there is no reason why there should be a close correlation between visibility on film and its ignitability. However, there is good evidence to suggest that a camera capable of detecting a 200 μJ voltage spark will easily detect hazardous thermal sparks.

The conventional, and cautious, approach is to consider the observation of any spark or arc detected by the camera as a fail, but because even “safe” sparks are quite visible on film, this can lead to problems for the engineers, who require an optimum design. A solution is to use a diagnostic gas technique, in which the internal surface is encased and filled with a diagnostic gas that is shown to be sensitive to a 200 μJ voltage spark. That is, it will be ignited by such a spark with $>$ 90 % confidence.

This is an approach that is partly statistical, but with a good margin of safety, since aviation fuels would have an extremely low probability (typically < 0.1 %) of ignition from such a spark. The diagnostic mixtures are also more sensitive to ignition by the "thermal sparks" discussed above.

When gas tests are used in conjunction with cameras, they will occasionally show up faint spark trails on the cameras, without the gas igniting. This is a symptom of the high sensitivity of the cameras to thermal sparks, but for a single test (*i.e.*, with no statistical understanding of the result) such a result would normally still be considered a failure.

High current test waveforms

The high current waveforms defined in the ED-84 standard [15] are derived from natural lightning data and some aspects of the waveforms can be difficult to implement in practice. To account for this, the standard includes some leeway in the waveform definitions.

Rise time

It is very difficult to replicate both the high current and the high rise times (dI/dt) defined in ED-84 using conventional lightning generators. This is because the generator voltages required to achieve the dI/dt become impractically high (>>100 kV), giving a risk of flashovers.

For practical implementations, the standard therefore permits generators with slower rise times, typically 15 - 50 μs rather than, for example, the 6.4 μs of Component A. Historically, it has been assumed that force effects and damage caused by heating are due to the action integral and not dependent on the speed at which the energy is deposited. However, it has been conjectured that faster rise times could contribute to certain types of damage, particularly shock effects on composite skins.

Carbon fiber skins are usually protected with an external layer, such as a copper mesh, which is sacrificially vaporized during a lightning attachment. This vaporization can be explosive and create a shock effect, which is enhanced when thick paint layers are used. It has been suggested that a faster rise time can increase the effect, therefore leading to inaccurate damage replication during tests.

Although it is difficult to look at rise time effects in isolation, it is relatively simple to test the comparative effects of a given peak current or action integral using scaled Component D (12 μs rise time) and Component A (25 μs rise time) waveforms.

Figure 6 below shows how two damage effects (mesh vaporization and shock effects) respond to these parameters on a lightweight carbon composite panel protected by aluminum mesh and with a relatively thick paint layer. The vaporization damage can be seen to be mainly dependent on the action integral, not the peak current or the dI/dt. However, the shock damage is apparently related to the peak current rather than the action integral, which may indicate a dependency on the rise time. However, there is no reported evidence at this time to suggest that tests are failing to replicate the actual observed damage to composites.

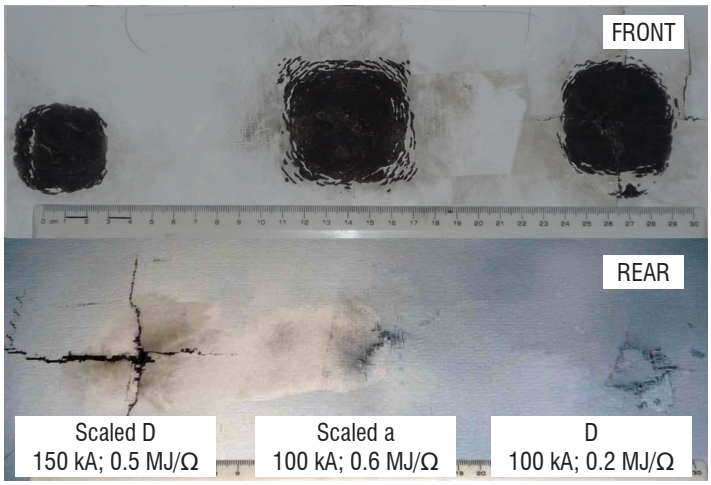

Figure 6 – Outer and inner views of a mesh protected sample tested at different levels. In such tests, the diameter of fused mesh relates closely to specific energy (action integral), but the shock effect (panel splitting) appears to be more a function of the peak current

The rise time can also have an effect on the current distribution in a sample. The current distribution is determined by both the inductive and resistive distributions of the test object. The inductive component acts to force the current to flow in the extremities of the object, away from the path of least resistance defined by the resistive distribution. The strength of the inductive response is directly related to the rate of change of the current waveform. A slower rise time can therefore have implications; on hybrid metal/composite test samples, the slower rising waveform will tend to drive a larger proportion of the current through metallic paths, which could lead to an under-test of the composite parts. Also, for high current tests, where the distribution of current is being measured for the determination of transient levels, any effect of the waveform shape should be borne in mind. The above argument also applies to damped sinusoidal waveforms, which are also allowed by the standards, since the distribution could differ significantly from a unidirectional threat.

The need to specify generic waveforms for either test or analysis purposes can lead to peculiarities. In ED84 [16], the components A and D are defined mathematically (for analytical purposes) as a simple double exponential, beginning with a high rate of rise at t=0, which gives the waveform an infinite second derivative (that is, the resulting dI/dt waveform rises to peak in zero time).

This can cause a problem for certain types of electromagnetic modeling approaches. There is also an inconsistency with one of the test voltage waveforms, which is derived from the dI/dt and would therefore be expected to have a zero rise time, which cannot occur in practice. Previously, this was addressed in the standard by placing a practical limit of 100 ns on the rise time. The standards committees have readdressed this and a modification of the double exponential is being introduced shortly. The new definition of current waveform leaves it effectively unchanged, but the infinite second derivative is removed and the dI/dt rise time becomes 340 ns. With this modification, the practical and theoretical waveforms for Induced Effects are consistent.

Test sequence

In lightning tests, the fast components are applied first (A/D) followed by the slow components (B/C). The components are applied in this order since it follows the order seen in real lightning strikes on the majority of the aircraft, *i.e.*, the initial high current attachment followed by the lingering low current phase.

However, at the trailing edges of the aircraft, where the lightning attachment exits the aircraft, the trailing edge will see the lingering slow component before the high current reattachment (component D) phase. This means the charge transfer associated with the slow component can create local melting, weakening the structure, before the high current reattachment. This weakening can amplify the damage caused by the concussive shock of the high current reattachment. Therefore, it is sometimes appropriate to apply a different ordering of the components where such an effect is possible.

Applying the components in a representative order during a test is complicated, since the different components are generated by different capacitor banks and applied as a single composite pulse. An accurate trigger system is required to ensure the correct timing. Achieving initial breakdown using the B and C components can be challenging, since these banks are usually implemented using much lower voltages than the A and D components.

Whole aircraft tests

Whole aircraft tests are a means of assessing the type and amplitude of transients induced into airframe wiring by a lightning strike. In this approach, a scaled down component A current is injected into an aircraft, or part thereof, and the internal threat is measured - for example the induced currents and voltages on wiring.

Two of the issues with these tests are how to build a test rig, which leads to a representative test, and how to ensure that the waveform provides the same coupling effects, albeit at a lower level, as the full threat. In addition, the complexity of aircraft avionics systems requires that a careful understanding of the cable harnesses be gained before making measurements.

The whole aircraft test rig includes the generator as the source of the current and a return conductor system to carry current back to the generator from the aircraft exit point. The return conductor system needs to be designed and installed in such a way that the resulting current distribution on the test object is similar to that which would be obtained during a natural strike. The usual technique is to construct a quasi-concentric cage of cables, tubes or plates around the airframe (generally co-axial).

The return cage for large transport aircraft becomes such a feat of construction that it becomes impractical; thus, a ground plane can be used as a return instead. Ground planes can cause considerable deviations from the free space current distribution, resulting in a large difference between current densities on the upper and lower surfaces of the aircraft, requiring corrections to account for the difference.

The injected current for whole aircraft testing is generally reduced, compared to the 200 kA Component A threat defined in the standards; pulse amplitudes of 1 - 20 kA with the correct 6.4/69 μs waveshape are typical. This is driven by two factors:

- Large high current generators are bulky and impractical to move to a test site;
- The desire to minimize potential damage to an airworthy aircraft.

Using a scaled waveform raises the question of representativity - the lower current levels and voltages associated with smaller generators could potentially lead to a different response to that of a full threat current. For example, arcing at material interfaces may occur with a full threat current, but not with a lower level current. Such non-linear behavior could lead to a modification in the current distribution and therefore induced transient levels.

Careful consideration must be given to any potential sources of non-linear response. For example, linkages with bearings isolated by low friction Teflon, or metal-to-metal interfaces isolated by anodizing, are structures that could produce non-linear results. Similarly, during a real strike, spark-overs might be expected to occur across tiny gaps or through paint layers; paths which would not be present in low level tests.

For some structures, empirical data is available that can be used to support a scaled current test. One such publication is the collaborative investigation between Airbus and Cobham Technical Services, which explored the linearity of a wingbox subjected to a range of injected currents that spanned 1 A to 200 kA [17]. The wingbox was constructed from a carbon composite with mesh protection. Rogowski coils and voltage sense wires were embedded in the structure to look for changes in the current distribution and induced voltages as the injected levels were varied. A high degree of linearity was observed over the whole 106 dB range of injected current. The current and voltage measurements were found to vary by $\pm$0.5 dB and $\pm$2.5 dB respectively over the injected range, with much of this variation being consistent with the measurement uncertainties in the diagnostic systems.

During whole aircraft tests, measurements of induced voltage transients will be made on selected harnesses. A wide variety of waveforms are observed, from waveforms following the injected current or its derivative (waveform 4 and 2) to transient voltage oscillations superimposed on the basic response (waveform 3) [18]. These oscillations in the airframe arise from reflections of travelling waves at impedance mismatches, where the body of the airframe meets the small radius of the arc attachment point. Similarly, oscillations in cables can be excited.

Care must be taken when interpreting these transient voltage oscillations since, in a test, the transition between the body of the aircraft and the return conductor is a short circuit. This can cause the standing waves to have a frequency and spatial distribution along the aircraft different to that expected in reality.

The measurements made during whole aircraft tests can be cable bundle currents and/or the transients on the core wires. The latter are usually made at equipment interfaces, to give the open circuit voltage and the short circuit current allowing the Thévenin equivalent generator to be deduced. These core wire measurements require disconnection of the connectors at each end, to allow measurement access to the core wire at one end and to ground the wire at the other. The screens at each of the connectors will need to be bonded to structure also and considerable care is required.

Cable bundle currents are an easier parameter to measure, however, a tricky problem is the presence of intermediate grounded bulkhead connectors in the cable run, as illustrated in figure 7. These allow currents to flow off the harness, so that different portions of the same harness can carry quite different currents. Therefore, for a complex cable run many current measurements may be required, as well as a detailed understanding of the location of the intermediate grounded connectors.

These measurements can be used to determine the current levels to be applied in screened cable tests, or used to define voltages test levels on unscreened bundles or pin test levels. The latter case also requires knowledge of the harness section lengths and transfer impedances, in order to sum [*transfer impedance (Z) x current (I) x section length (L)*] for the various sections of the one harness, see figure 7.

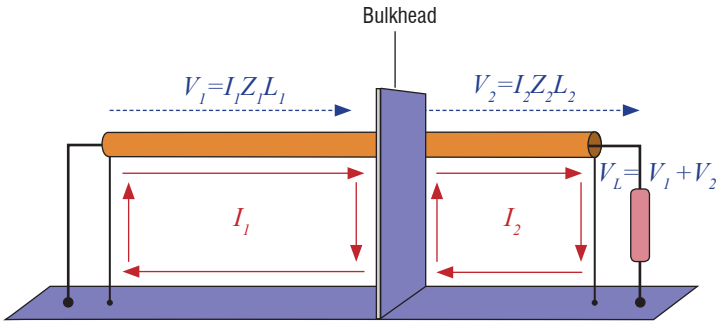

Figure 7 – The voltage at the input load (V_L) is the sum of contributions from different sections (V_1, V_2). In this example, the cable screen is effectively split into two sections, which can carry quite different currents if one has a more exposed location

Fault/Failure Simulation

On July 17th, 1996, shortly after taking off from John F. Kennedy Airport in New York, flight TW800 broke up in flight as a consequence of a center fuel tank explosion. Investigation by the U.S. National Transportation Safety Board could not identify the actual ignition source, but did suggest that this aircraft, and those of a similar age (over 25 years), exhibited considerable 'wear and tear' on bonding braids and on some of the wiring running through fuel tanks; NTSB conjectured in their report that sparking may have occurred at chafed wiring.

Following this incident, regulations for transport aircraft fuel tanks were modified, requiring that designs should incorporate a tolerance to anticipated wear & tear and installation faults. This has had a big effect on lightning test requirements, since the testing must cover not only the standard build, but also the possible fault/failure configurations that can arise during an aircraft's life. This requires the manufacturer to anticipate the possible fault and failure conditions and to address them within a manageable test program. Since it is not feasible to test every scenario, some selection of worst-cases for test must be made; of course, some test experience is required to identify what the worst cases are, given numerous variables, such as fastener type/size, skin layup and the anticipated lightning current threat, even before fault conditions, such as sealant loss, skin cracks and broken bond straps are considered. Manufacturers and test houses are working together through the SAE/EUROCAE committees to provide guidance on this and to ensure that a consistent approach is adopted.

Environment

For carbon composite structure, the uptake of moisture during its life can have an influence on its response to lightning currents. To assess this, artificial aging of samples for test purposes is achieved by moisture conditioning. Samples are kept in a very humid environment for a prolonged period of time (typically 70 °C and 95% RH for 1500 hours). Samples are then tested and the results compared against nominal samples, to determine the likely effect of aging on the protection methods. Although some additional loss of mechanical strength has been noted under some conditions, the effect on lightning currents appears to be small.

Investigations have been undertaken into the effects of rain and ice on segmented strip divertors. These are used to protect nose radomes from being punctured by attracting the strike and carrying the current safely over the outer radome surface [19]. This investigation involved setting up a lightning generator inside a wind tunnel that had a rain/icing facility. It was found that rain did not seem to affect the performance and the divertors still worked with thin layers of ice. However, with thick layers of ice ~1 cm thick, puncture of the radomes occasionally occurred.

Quantitative studies of the effect of ice have been conducted in the EM-Haz program [19]. The ice increases the flashover voltage for segmented strips by a factor about 2 to 3, depending on strip type and thickness of ice. The light-up voltage increases with ice thickness, up to the voltage gradient required to create a surface flashover on the radome surface or on the ice. In the test standards, ice and water are not usually specified, but clearly they can have an effect.

Ambient air pressure at cruising altitude is a fraction of its sea level value and, since this pressure determines breakdown voltage, it can be anticipated that lightning effects could have some different effects at altitude. For example, when using electrical isolation as a means of protection, this is usually taken into account by adding an additional safety factor. Thus, testing is normally conducted at appropriately higher amplitude, to compensate for the reduced voltage at flight altitudes. Tests could also be conducted at the reduced air pressure, although this is not normally required, since the effects of altitude on breakdown are well understood.

Other effects are less readily predicted and one of these is the occurrence of sparking when testing fuel tanks. Recent test programs have investigated the effect of ambient air pressure on the lightning protection of a fuel tank structure. The test sample was installed within a cell constructed around the skin/spar/rib fastened interface, allowing the pressure to be reduced to 140 Torr (the pressure at 40,000 ft.). No significant effect on the performance of the fuel tank was observed, which probably reflects the fact that sparking is caused by the fusing of contacts, rather than a voltage breakdown, so there is less pressure dependence.

Representativity

While it is necessary for the tests to be a representative simulation, there are advantages in testing manageable sized samples, both in terms of the ease of testing and the cost of sample manufacture. Most tests for determining the integrity of structural skins are performed with square flat panels. There is no evidence to suggest that the local structural damage is

influenced by the use of a simple test sample. However, if the skins form part of the flight control surface, then protection against other aspects of damage, such as delamination from spars and ribs, and splitting of trailing edges, will need to be demonstrated. In these cases, it is normal to test a larger scale sample, which incorporates these critical features.

In testing fuel tank structural designs, test samples are usually relatively large; for arc attachment tests, a 600 mm x 500 mm skin sample with internal structural ribs is considered large enough for the current to distribute freely around the sample, without being constrained by the sample size or set-up. However, it becomes impractical to use such samples for testing tolerance to foreseeable fault conditions, since there will be a huge matrix of design/fault combinations to be tested. A single test sample cannot usually be used for testing many variables, since conditioning of the sample can occur after only a small number of tests. In conditioning, current paths become typically more well defined after successive tests, affecting overall current distribution and hence results may not be representative.

Thus, one practical approach is to test large numbers of samples as small coupons, supported by a smaller number of tests to more representative samples, in order to validate the results. The coupon tests are a good way of making comparative assessments to determine which faults are more significant and which types of fastener, for example, are most affected.

Conclusion

There will always be practical limitations in the way in which lightning can be simulated by test and attempts are made to ensure that the most significant effects are reproduced. However, as this paper has shown, there are inevitably compromises, both in simulating the "worst-case" lightning threat (and combining the most severe parameters) and in providing samples that are manageable enough to be tested, but whose results can also be considered representative.

Challenges also exist in regard to how tests are conducted, both in terms of the waveforms used and how the tests are carried out. By bringing together aerospace companies and lightning specialists, the WG31 and SAE committees continue to drive the development of the standards and guidance material to overcome the challenges faced in this industry ■

References

[1] V. A. RAKOV and al. – *Lightning: Physics and Effects*. Cambridge University Press, p. 121, 2003.
[2] V. A. RAKOV and al. – *Lightning: Physics and Effects*. Cambridge University Press, pp. 122-137, 2003.
[3] L. W. PARKER and H.W. KASEMIR – *Predicted Aircraft Field Concentration Factors and their Relation to Triggered Lightning*. Paper 4A.9, International Conference on Lightning and Static Electricity, Orlando, 1984.
[4] H. W. KASEMIR – *Static Discharge and Triggered Lightning*. Paper 5A.24, International Conference on Lightning and Static Electricity, Fort Worth, 1983.
[5] P. LALANDE, A. BONDIOU-CLERGERIE, and P. LAROCHE – *Analysis of Available In-Flight Measurements of Lightning Strikes to Aircraft*. Paper 1999-01-2397, International Conference on Lightning and Static Electricity, Toulouse, 1999.
[6] EUROCAE ED-84 – *Aircraft Lightning Environment and Related Test Waveform Standard*. 26, 1997.
[7] EUROCAE ED-91 – *Aircraft Lightning Zoning Standard.* Amendment 2, 17-22, 2006.
[8] EASA – *Certification Specifications and Acceptable Means of Compliance for Large Aeroplanes*. Amendment 11, CS 25.581, 2011.
[9] EUROCAE ED-84 – *Aircraft Lightning Environment and Related Test Waveform Standard.* 1997.
[10] EUROCAE ED-91 – *Aircraft Lightning Zoning Standard.* Amendment 2, 2006.
[11] EUROCAE ED-105 – *Aircraft Lightning Test Methods.* 2005.
[12] C. C. R. JONES and al. – *Zoning of Aircraft for Lightning Attachment and Current Transfer*. International Conference on Lightning and Static Electricity, Dayton, 1986.
[13] H. ZAGLAUER and al. – *Definition of Lightning Strike Zones on Aircraft and Helicopters – Results of the FULMEN Programme*. Paper 1999-01-2380, International Conference on Lightning and Static Electricity, Toulouse, 1999.
[14] J. C. HARDWICK and al. – *Review of the Joint Radome Programme.* Paper 1999-02-2322, International Conference on Lightning and Static Electricity, Toulouse, 1999.
[15] EUROCAE ED-84 – *Aircraft Lightning Environment and Related Test Waveform Standard.* p. 26, 1997.
[16] EUROCAE ED-84 – *Aircraft Lightning Environment and Related Test Waveform Standard.* pp. 25&34, 1997.
[17] A. J. MEAKINS and al. – *106dB Current Linearity Study of the TANGO CFC Wingbox.* International Conference on Lightning and Static Electricity, Oxford, 2011.
[18] EUROCAE ED-84 – *Aircraft Lightning Environment and Related Test Waveform Standard*. 42-49, 1997
[19] J. A. PLUMER and al. – *Combined High Voltage and Icing Tunnel Tests on Radomes*. Paper 1999-01-2389, International Conference on Lightning and Static Electricity, Toulouse, 1999.
[20] J. C. HARDWICK and al. – *Effect of Water and Icing on Segmented Divertor Strip Performance*. Paper I03-80, International Conference on Lightning and Static Electricity, Blackpool, 2003.

Acronyms

ARP (Aeronautical Recommended Practice)
AC (Advisory Circular)
ED (EUROCAE Document)

Dan Morgan graduated from Warwick University in 2004, with a Masters in Physics. He joined Cobham in 2009 and is currently a Scientist, primarily involved in direct effect testing and the development of a new static testing facility. He has co-authored papers published in the proceedings of the International Conference on Lightning and Static Electricity (ICOLSE), in both 2009 (ILDAS, In-flight Lightning Strike Damage Assessment System, project) and 2011 (Tango project).

John Hardwick graduated from Cambridge University in 1972 and received a doctorate in Physics from the University of Liverpool in 1976. He joined Culham Lightning in 1983 and is currently a technical consultant, primarily involved in the indirect effects of lighting and radome protection and testing. He has been a member of the European Committee for Aviation Electronics (EUROCAE) Working Group 31 on lightning since its inception in 1987, until recently serving as secretary. He has authored and co-authored numerous papers published in the proceedings of ICOLSE.

Stephen Haigh graduated from Oxford University with a degree in Physics. He joined Culham Lightning in 1986 and is currently the Technical Manager and Principal Scientist. His main current role is consultancy for aircraft avionics system qualification, but he has been responsible for the group's research work on lightning fuel ignition hazards and associated test methods. He has contributed to the development of international standards for aerospace, as a member of both the EUROCAE and FAA ARC committees.

Alex Meakins graduated from Imperial College in 2002 with a Masters in Physics. Before joining Cobham in 2008, he gained his doctorate in Plasma Physics and Controlled Fusion at JET, in collaboration with Imperial College. He is presently a Senior Scientist, involved both in the development of diagnostics and in indirect and direct effect testing. He is interested in the computational modeling of lightning processes. He has papers published in Plasma Physics and Controlled Fusion and ICOLSE.

F. Issac, E. Bachelier, D. Prost
(Onera)
V. Enjalbert
(DGA)
L. Mohedano
(APAVE)

E-mail: francois.issac@onera.fr

Space Launching Site Protection against Lightning Hazards

A launching pad, because of its activity, is particularly sensitive to the risk of lightning. The use of Standard IEC62305 "Protection against lightning" establishes the general framework for the Lightning Protection System (LPS). However, the specific activity of a launching pad requires special analysis on specific points of the LPS. Indeed, it is necessary to take into account the lightning conductor system particularity on the one hand, and the launcher electromagnetic susceptibility on the other hand.

This paper presents the general methodology used to define the LPS of a launching pad. The analysis is based upon expertise, numerical simulation and experiments performed at launching pad sites.

Introduction

A rocket launching pad is, by its very nature, a zone particularly sensitive to the risk of lightning. Generally located in parts of the earth globe where lightning activity is strong, launching installations are in addition being built in obstacle-free zones measuring a few square kilometers and comprise tall structures; all of these elements unfortunately favor lightning attraction.

While the metallic structures of the launcher building complex can be used as a lightning conductor and can thus drain the lightning current in a natural way, in many cases they present the major disadvantage of being lower than the launchers that they could protect.

This is why a launcher lightning protection must be built in a specific way; the protection depends on both the launcher and on the way it is operated in its various configurations before launching.

Various lightning protection solutions can be used according to the type of launcher and its management. Protection solutions based on gantries can be used and various types of lightning rods with their specific down-conductors (draining current solution) can be implemented.

Even though there is no record of serious incidents on CSG *(Centre Spatial Guyannais, the Guyana Space Center)* launching sites, its lightning protection system has changed over the past thirty years because the obligations to take lightning risk into account have become increasingly constraining.

Consequently, the launcher protection solutions follow the changes in the international standardization and lightning risk management.

For this particular activity, though, the application of standards is not sufficient to guarantee the absence of any lightning risk. Nevertheless, standards define a minimum applicable framework for the design of the protection.

The objective of this article is, first, to briefly present the phenomenology of a lightning aggression on buildings and the specificity of a launching site subject to such an aggression. Then, the safety of the installation and evaluation of the lightning protection devices are discussed.

Lightning protection of a launcher

On November 14th, 1969, 36.5 seconds after lift-off, Apollo XII triggered a lightning discharge, followed by another stroke a few seconds later. This event is the most famous lightning strike of a rocket; by chance, it did not have serious consequences on the mission. Although the ground installations of the launching pad in Florida, with a high keronic level, had lightning protection, the risk after lift-off had clearly been underestimated. The knowledge of the attachment mechanisms in the first seconds of flight, the impact of the ionized exhaust plume on the electric field and the capacity of the rocket to trigger the lightning discharge had been very widely underestimated. This incident imposed a modification of lightning risk management after lift-off.

However, the modification of the lightning risk management rules did not prevent the loss of the Atlas Centaur rocket on March 27th, 1987, struck in flight, which led to the destruction of the rocket. This accident definitively showed that the risk of lightning is an important problem in all phases of the life cycle of a rocket.

In the rocket assembly phases, the risk of a direct lightning strike is lower because the launcher is protected inside buildings with metal framework structures, offering significant protection. However, this risk must not be underestimated because of a pyrotechnic issue, which concerns all of the Electro Explosive Devices (EED) of the rocket and also all of the electronic control devices. All the same, in these assembly phases, the analysis that must be carried out remains an indirect lightning analysis.

In the transfer phases of the rocket, when part of the rocket or the whole rocket is outside the building complex, direct lightning becomes a main risk. In such a configuration, the rocket cannot be protected by a system like a lightning conductor system and its protection can only be guaranteed by proper weather forecasting.

The difficulty lies in obtaining a reliable forecast over a period of a few hours, with weather configurations that can change very fast.

If we take the example of the CSG launching pads, the lightning forecast is based on weather radar giving the evolution of storm cells, but also on more specific devices giving information on the electric activity of these cells, namely:

- a network of field mills "MAC" (“Moulin À Champ” in French) giving the intensity of the electric field on the ground in real-time;
- the "THOR" (Thunderstorm Occurrence) system based on radio-electric interferometry techniques and giving information on the electrical activity within storm cells. This system makes it possible to follow the movement of the electric activity and makes it possible to differentiate cloud-to-cloud discharges from cloud-to-ground discharges.

In the phase before lift-off, the rocket is parked on the launching pad for several days and protection cannot be ensured by weather forecast alone. Protection is thus ensured by lightning conductors and possibly by a mobile gantry. This phase is particularly critical, on the one hand because the probability of lightning is strong due to the size of the installations and, on the other hand, because of the launcher state with all pyrotechnic systems, the loading of propellants, the control systems and the payload. In this configuration, the launcher must be protected from any direct lightning strike, but also from all significant electromagnetic coupling phenomena.

Finally, the launcher lift-off phase is rather similar to the transfer phases, since the launcher cannot be protected by an additional system. Only the weather forecasts can predict the lightning risk and thus give the authorization for rocket launch. Nevertheless, the problem here is a little different from that in a transfer phase, in the sense that only a short temporal window is required for the weather forecast.

Lightning in a few words

Lightning is a complex natural phenomenon. Before looking at the lighting protection system (LPS) of a rocket, we will recall some characteristics of the physics of lightning and of the reasoning behind the protection. It is important to note that there are many physical mechanisms related to lightning and that, in the present state of the knowledge, the physics of these has been rather well mastered. Laboratory experimentation on long gap discharges and experimentation on natural lightning have contributed to making important progress on this issue. However, in spite of the present scientific understanding of these physical mechanisms one is still not able to predict the point of the lightning impact with good accuracy. This is why, for two hundred years, the best protection for installations is still Franklin’s rod.

Lightning features

As seen in [1], the initial process leading to lightning takes place within a thunderstorm cloud, with the creation of electric charges. The electrification phenomena within the cloud generate sufficiently high electric fields to induce electrical discharges inside the cloud (cloud-to-cloud, CC discharge) or between the cloud and the ground (CG discharge). It is this last type of discharge that is of interest to us. It generally consists of the joining of two (not simultaneously emerging) propagating leaders one downward from the cloud to the ground and one upward from the ground to the cloud. Because of the two possible polarities of electrically charged particles and the two different time orderings of the formation of the leaders, we have four different types of connections between the cloud and the ground [2] [3].

Figure 1 presents the four configurations of CG lightning. The classification is first based on the behavior of the initial leader (downward or upward) and then based on the sign of the current flow of the first return stroke (when the connection of the two leaders is made).

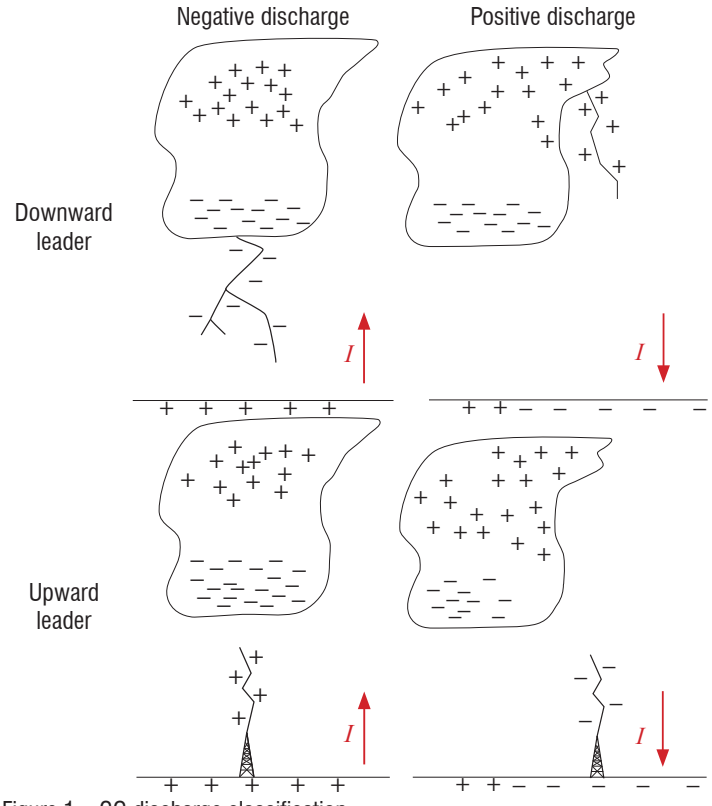

Figure 1 – CG discharge classification

In agreement with the ordering of the figures in figure 1, the most frequent discharge is the negative discharge with an initial downward leader. The propagation of the leader does not follow a simple curve, it has many separate branches. In this case, the connection point with the ground depends on local electrical conditions in the neighborhood of the nearest

branch to the ground. We will see in the following sections, that these local conditions are the basis of the models used in lightning protection for buildings.

A second type of discharge is induced by an initial upward propagating leader. In this case, the electric field intensification at the top of a structure is strong enough over a large area to initiate the propagation of the leader. In this configuration, the connection point is directly linked with the structure. This scenario is typically obtained on structures that are over 100 m high [3]. We will keep in memory that this height of 100 m is of the order of the height of the lightning protection systems of the Guyana Space Center launching pads and this point will be later used in our discussion.

The striking distance and the electro-geometric model

In the most frequent case of lightning, i.e., for a downward negative discharge, the advance of the negative leader by jumps intensifies the electric field between the head of the leader and the ground. When the negative leader approaches the ground, this field is sufficiently intense to initiate an ascending discharge from the ground. The distance in this last phase before the connection of the two leaders is called the "striking distance". This attraction distance depends on the area in which the electric field exceeds an electric breakdown value. The intensity of this value is thus quite large (about 500 kV/m [4]). The electric charge carried by the negative leader makes it possible to calculate the electric field between the head of the leader and the ground, but also the intensity of the first return stroke. From this consideration, there is a relation between the current of the return stroke and the striking distance. During the seventies [3][5], models based on experimental results made it possible to establish the following relation between the current intensity and the striking distance (1).

$$r = 10.I^{0.65} \qquad (1)$$

Where r is the striking distance and I is the current of the return stroke in kA.

In agreement with the recommendations of various standardization committees [6], this relation is used as a basis for dimensioning the lightning protection system.

The rolling sphere method

Based on the electro-geometric model, the rolling sphere method makes it possible to quickly visualize the lightning connection point of a scene (figure 2). The method consists in rolling a fictive sphere along the scene; the radius of the sphere is the striking distance for a given return stroke current amplitude. Any point of the scene coming into contact with the sphere is a possible point of lightning attraction.

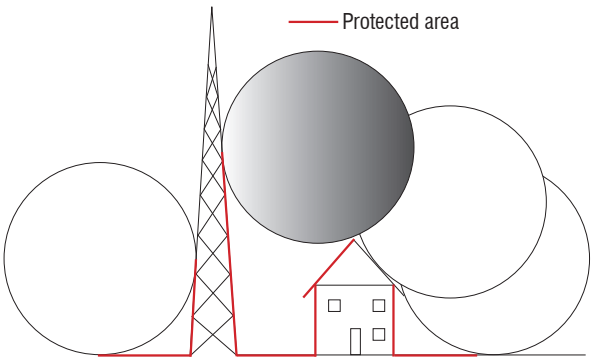

Figure 2 – The rolling sphere method (only the red parts of the drawing are protected from an attachment)

By using this method on very high structures, such as pylons, possible attachment points on relatively low parts can be diagnosed. In fact, for physical reasons, these attachment points are not probable, but the method is not able to discriminate them.

A more physical approach

The electro-geometric model is a convenient engineering tool that provides fast and efficient visualization of the risk zones, but it remains a basic model from the point of view of physics. However, for complex structures of great height, the improvement of the model precision comes together with the improvement of the understanding and the analysis of the phenomenology of lightning initiation.

Numerical approaches based on the behavior of ascending leaders give a more realistic analysis of the influence of various parameters (see [8] [9]). Comparisons between experiments of triggered lightning [10] and simulations made it possible to refine the model with, in particular, the introduction of an electric stabilization field in the zone of field intensification, which explains the behavior of the positive leader. These models are of particular interest in the case of high buildings, for which the initiation and the propagation of the positive leader will drive the attachment point.

A last point on the physics of the discharges on ground structures is their behavior during stormy activity. The latter can last several seconds and the electric field will therefore remain intense over this period. Each lightning conductor and each sharp object, as well as the vegetation, is capable of generating corona or even leaders that, in most cases, will not be followed by a lightning discharge. The ions thus created will produce a space charge with the temporary consequence of a local shielding of the emission point, contributing at the same time to a minimization of the electric field in the entire zone.

This is the reason why it remains very difficult to predict the attachment points on any structure. Some experiments have even shown that very sharp lightning conductors were less effective than round stems; indeed, the sharp shape ensures a very strong intensification of the field, but immediately generates a space charge that shields the lightning rod making it ineffective [18]. Consequently, for a complex environment, such as a launching pad with large-sized pylons, serving as lightning conductors, as well as for a significant number of lightning conductors placed on the buildings in the area, it is still very difficult to say whether the solution chosen, even though conservative, is really optimal from the point of view of the lightning conductor function.

Sizing of the protection system

The first function of the lightning protection system is to capture lightning. Though the idea that in order to protect an installation against lightning the best way is to attract it towards a controlled point is well accepted by everybody, we must concede that it is not completely intuitive and we must apply it with a lot of precautions and well documented rules.

The goal of the protection system is thus first to intercept all lightning channels in the zone of the rocket, while respecting the realization constraints related to the launcher. Studies relating to the protection system of the Guyana Space Center (CSG) launching pad began at Onera in the 90s, with studies of the ZL2 and ZL3 launching pads for Ariane4 and Ariane5 launchers respectively.

In regard to the protection of the Soyuz launching pad (ZLS), the reasoning behind the protection applied by Onera has been very similar. However, the installation constraints had changed significantly.

As we saw, the electro-geometric model is the starting point for sizing the lightning protection system, because the simulation tools for calculating the attachment points of the lightning are not mature enough to be accepted by the regulatory authorities.

The electro-geometric model is therefore applied in the design of the system, with the objective of never having lightning on the rocket. However, this objective is difficult to achieve. One of the main difficulties is the requirement to leave a free opening for the launching of the rocket.

The second function of the LPS is related to the susceptibility of the launcher due to induced EM effects generated by the currents flowing within the protection system. The objective is therefore to maintain the magnetic field within the launcher zone below an acceptable level, depending on the susceptibility of the launcher to this magnetic field.

Consequently, the most efficient protection system would be a Faraday cage. However, the problem is that such a perfect situation is not possible, because there must be an opening in order to let the launcher penetrate the LPS during its installation phase and to let it out from the top during the taking-off phase.

Protection system analysis on a model structure

To understand the mechanisms of attachment on the LPS of the ZL3 launching pad at the Guyana Space Center (CSG), experiments were carried out in France in the 90s at the Renardières (EDF) research center on a 1/20 scale model structure of the launching pad (figure 3).

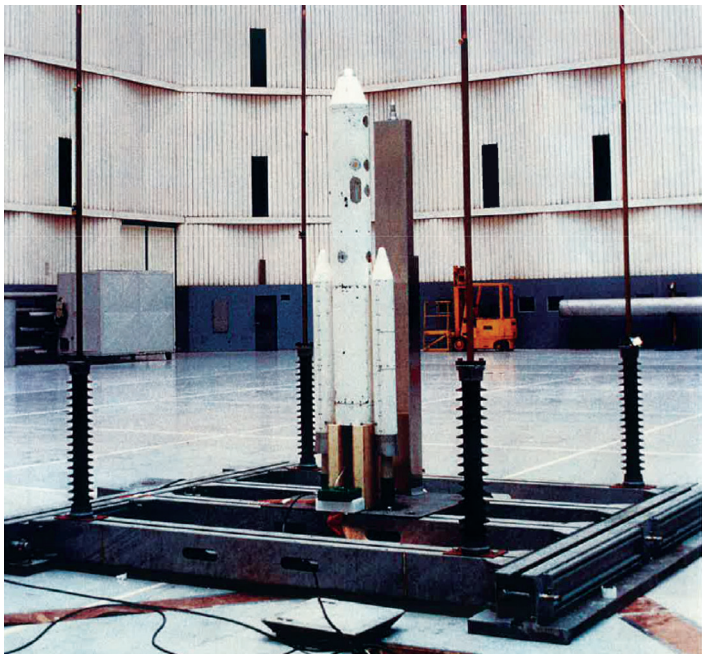

Figure 3 – Scale model of the Ariane 5 Launching pad

It was possible to generate long electric discharges with positive and negative polarities at the Renardières site. From the phenomenological point of view, these simulated discharges are very close to natural discharges. This experimental test allowed the estimation of the effectiveness of the protection system and its capacity to protect the launcher. Several measurements were made with two or four protection pylons and with different offsets between the axis of the model and the axis of the top electrode in a "needle-top-electrode/ground-plane" type arc configuration (figure 4).

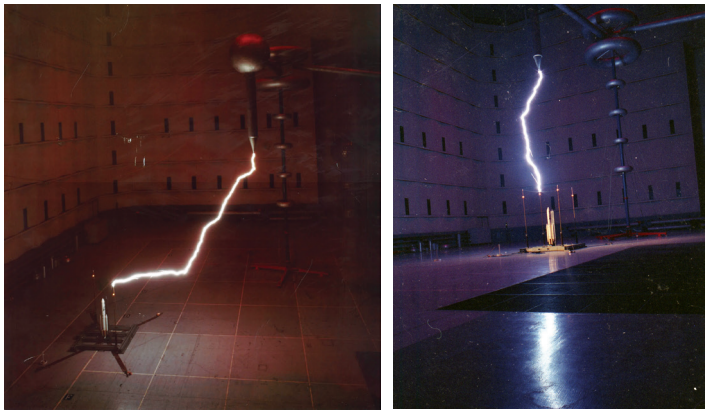

Figure 4 – Long electric discharges generated on the ZL3 mockup (launcher and protection system)

Under the laboratory conditions, the system was never put at fault (no discharge reached the launcher), but the main question was to know whether a scaling law was applicable. In particular, it is known that in the laboratory there is no direct relationship between the attachment distance and the current of the discharge; the latter being, in this case, a function of the voltage and of the internal impedance of the generator.

Later work [12] showed that, in the tested laboratory configurations, the relevant parameter is the difference of height between the pylons and the launcher. In order to test the influence of this parameter, ellipsoids with various heights have been simultaneously subjected to the same type of long electric discharge. For this, the former needle high voltage electrode was replaced by a flat metal plate, of large dimension, creating a homogeneous electric field zone at ground level (figure 5).

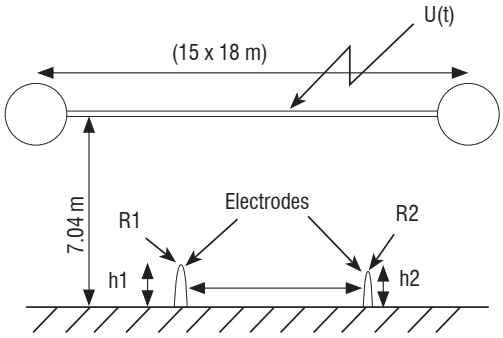

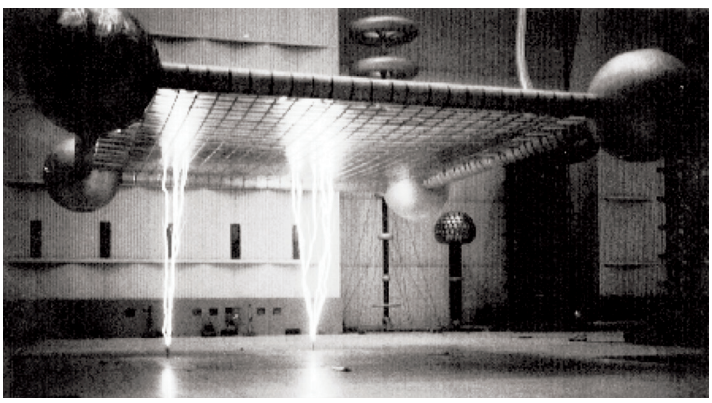

Figure 5 – Tests on ellipsoids with large plate top electrode

For ellipsoids at equal heights, their eccentricity (and therefore, their sharpness) influences the electric-breakdown statistics. However, the difference of height between the electrodes very quickly becomes the relevant parameter for ellipsoids of different heights. The explanation must be sought in the behavior of the positive discharge. A streak image of an upward positive leader measured between the two electrodes (the top plate and the ellipsoid on the ground) provides an idea of the connection between the two objects (figure 6). It is difficult to identify the start of the leader with the streak image, because of the mixing of time and space. Perhaps the ellipse with the most pointed profile starts first but, even with this hypothesis, there is a faster connection for the larger ellipse.

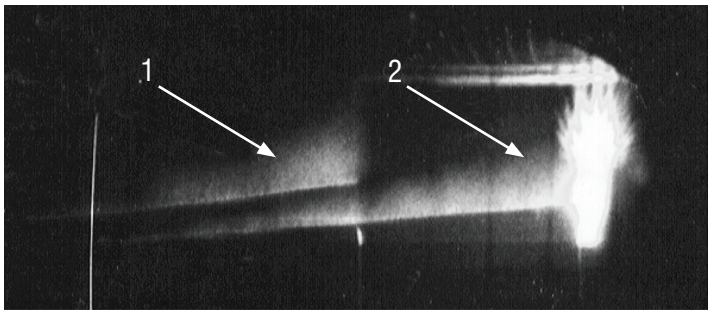

Figure 6 – Streak image of an upward positive leader at the top of the two ellipsoids

As a conclusion, the laboratory experiments do not make it possible to give the actual effectiveness of the lightning protection system. However, they contribute two important items of information:

a) The presence of two leaders on two separate objects of different height is possible. This behavior will exist for natural lightning. As far as the LPS protection is concerned, the question that arises is thus to evaluate the capacity of a leader to propagate from the top of the rocket placed inside the protection system. This specific point cannot be covered by normalization rules.

b) The laboratory discharges allowed realistic attachment models to be obtained. These models were used to analyze the leader starting configurations and can be used as a basis to answer the previous problems [11] [12].

Lightning protection system design

It is difficult to define and optimize a launcher lightning protection system using laboratory experiments and the knowledge of lightning attachment mechanisms on tall structures. This is why the design of the lightning protection system is done almost exclusively using the electro-geometric model, as defined in the international standard procedures. However, these standardized approaches cannot guarantee a total reliability of the launching pad lightning protection system.

Therefore, in order to comply with the electro-geometric model and to intercept most of the lightning strike, it is necessary to place lightning conductors in the launcher zone. With respect to the CEI 62305 standard [6], the most constraining protection level is "LPL I" 3 kA, which gives a radius of 20 m for the rolling sphere.

The installation of pylons is costly and must be taken into consideration. The smaller the number of pylons, the lower the LPS budget will be.

Several solutions are possible considering these constraints.

Umbrella

This is a system with conducting wires linked onto a single dielectric support, placed at the top of the gantry. It was the principle of the protection system used on the shuttle launching pad at the Kennedy Space Center. With such a protection system, with four electric cables descending to the ground, the electro-geometric model reveals a good protection for the high parts of the launcher. However, the application of the electro-geometric model reveals a protection default for the lower parts (figure 7). For example, if we want to protect this 50 m-high rocket with a 90m-high mast and four wires placed at 45 °, the electro-geometric model shows that the structure is not protected for lightning currents of 3 kA (radius of the sphere = 20 m); this structure is protected for 5 kA currents only (sphere of radius=30 m).

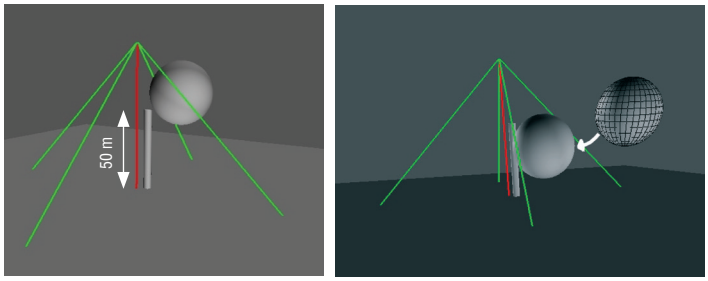

Figure 7 – Application of the electro-geometric model to an umbrella LPS

Figure 8 shows the unprotected area of the structure for a protection level “I”. Obviously, the lower part of the structure is not a lightning attachment zone for physical reasons, as we have mentioned previously; however, this solution will be eliminated, because it does not comply with the electro-geometric model. In addition, we will see hereafter (next section) that other more physics-related reasons will eliminate this solution. However, this shows one of the limitations of the model used in the standard for the umbrella type of protection system.

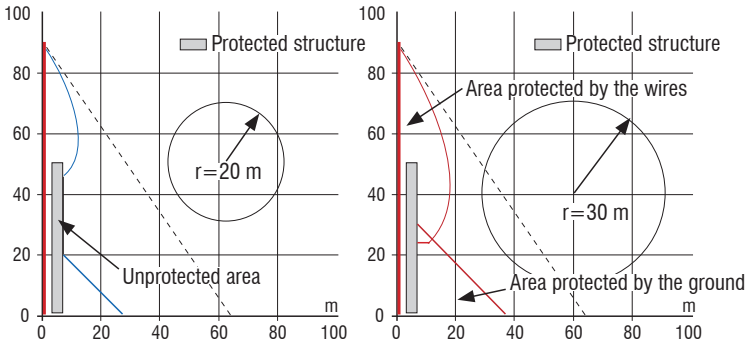

Figure 8 – Limits of the protected area

Association of lightning conductors

To protect the launcher efficiently, the simplest solution is to place several metallic pylons at a distance lower than 20 m. Solutions with three or four sufficiently high pylons both guarantee lightning

interception and comply with the electro-geometric model for lightning strokes of intensity higher than 3 kA. Under these conditions, it is rather easy to perform the lightning conductor function.

Electromagnetic sizing of the protection system

We have seen that rocket protection against direct lightning is rather easy to achieve by positioning three or four pylons of great height around the rocket. The difficulty that arises now is the susceptibility of the launcher and the critical electronic equipment to the magnetic field induced by the lightning current in the protection pylons. A launcher such as ARIANE 5 is hardened against a direct lightning strike of 5 kA, with a 4 μs rise time and a 500 μs decay time [13][14].

By the way, the hardening of the rocket on the launching pad must be evaluated with its umbilical connections, which means with all of its connections to the nearby infrastructure (in particular, the tower).

Applying Ampere's law, a 5 kA current on the rocket generates a magnetic field of around 200 A/m. Although the aggression of an indirect lightning strike does not expose the launcher to the same constraints as a direct effect, we will consider that the magnetic field produced by the lightning on the pylons should not itself exceed the value of 200 A/m in the launcher area.

This hypothesis makes it possible to simplify the study of the rocket susceptibility on the launch pad, by concentrating on the maximum field constraint to which it can be exposed.

If we choose the solution consisting of a protection system with four independent lightning conductors, installed on the four corners of a square base with 40 meter edges, a lightning current of 200 kA could appear in any pylon individually and generate a magnetic field greater than about 2 kA/m in the launcher zone. This value is not acceptable in view of the rocket susceptibility. It is thus necessary to modify the system in order to minimize this constraint.

We have seen that the solution for the LPS is to guarantee a situation as close as possible to a Faraday cage. However, it must remain at least open on one side and on the top for the regular installation and take-off phases of the rocket respectively. In the following, several solutions are proposed.

Separation function

The goal of the separation function is to reject the lightning current to the earth, as far away as possible from the launching zone. The ideal protection system is to use four pylons (for the lightning conductor function described above), each of these supporting catenary wires with insulators. The catenary wires themselves interconnect four lightning rods placed on the insulators to a faraway independent earth-termination system.

The insulator must prevent an electric discharge between the wires and the top of the pylons. This is the system that is currently in operation on the Ariane5 ZL3 launching pad.

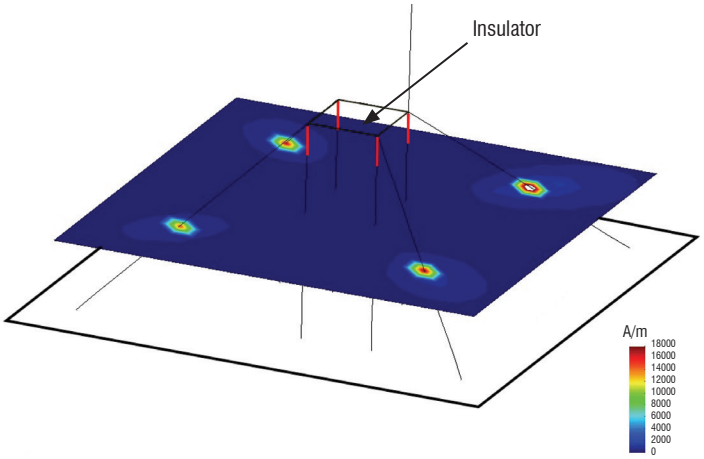

a) Transverse magnetic field plane-section at the level of the insulators

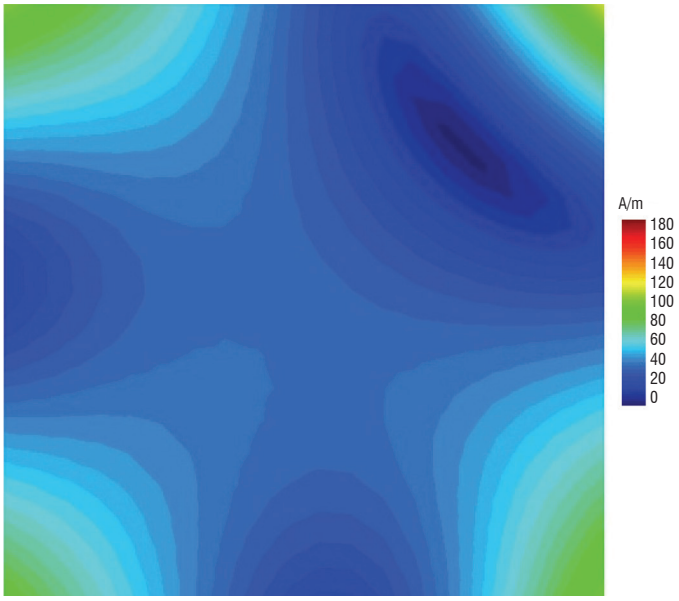

b) Transverse magnetic field plane-section at the level of 40 m

Figure 9 – Maximal magnetic field in the launcher area

This solution has the advantage of minimizing the magnetic field in the launcher area. In a nominal operating mode of this protection, it is rather easy to maintain low intensities of the magnetic field and for it to be compatible with the susceptibility of the launcher (figure 9).

However, this solution presents two disadvantages that should not be underestimated if we want to maintain the effectiveness of the lightning protection system during its entire operational life. Let us consider the example of the ZL3 again for our purpose.

The first problem concerns remote connection exiting the launching area. For example, the LOX tanks and the water tower; between these two zones and the launcher pad there are large metallic pipes. These pipes are very close to the LPS grounding system (figure 10). The potential rise going together with the lightning current in the ground can induce a current in the pipelines; this current can, firstly, modify the magnetic field on the launching pad, but it can also affect the safety of the LOX tanks.

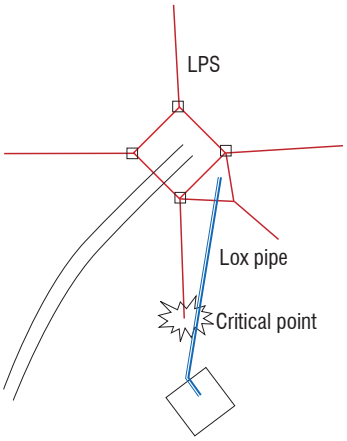

Figure 10 – Seen from above the ZL3 launch pad

The second problem is related to the maintenance of the insulators at the tops of the pylons. The efficiency of the separation function is based on the insulation capacity of the isolators. The problem is the degradation of the dielectric rigidity, on the one hand due to ageing and on the other hand because of surface pollution of the isolators. A strong lightning strike may therefore produce a breakdown of these insulators if they are not as perfect as expected; under these conditions, the pylon will become a shunt for the current due to its impedance being lower than that of the wires. A significant part of the injected current is thereby conducted to the normally protected zone!

Mesh cage

Given the cost related to the maintenance of a protection system based on the separation function, an alternative solution is to use the pylons as down-conductors for the lightning current. By connecting the top of the pylons with electric cables, we build a large-sized meshed system, close to a simplified Faraday cage. The minimization of the magnetic field in the launcher area is obtained by the current distribution through the four pylons and by the geometrical effect (*i.e.*, the canceling of the field between two conductors carrying equal currents) this guarantees a shielding effectiveness at the center of the system. The better the balance of the currents is, the better the shielding performance of the system. Figure 11 presents the ideal solution for the magnetic field of four pylons built on a square base with 60 m edges. This figure shows that the value of the magnetic field at the center of the zone is much lower than 200 A/m; this solution is thus possible from the point of view of the electro-geometric model, as well as from the point of view of the maximum acceptable magnetic field. Because only based on geometrical symmetry properties, this solution is independent of the current strike frequency spectrum.

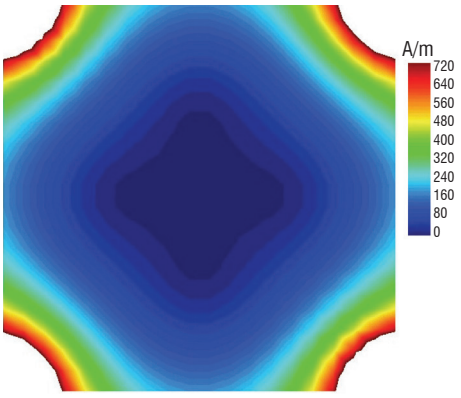

Figure 11 – Magnetic field for a perfect current balance on four pylons built on a square base with 60 m edges

In reality, the lightning connection point breaks the symmetry of the system; it is thus necessary, before making the choice of the final LPS design, to evaluate the parameter that most influences the current distribution.

With simple simulation models, it is possible to estimate the effect of the various resistances and inductances of the system on the solution. In a simple way, the LPS can be represented by figure 12 with three groups of impedances, which are the impedances of the connection cables (*Zwire*), the impedance of the pylons (*Zpylon*) and the impedance of the grounding system of these pylons (*Zground*).

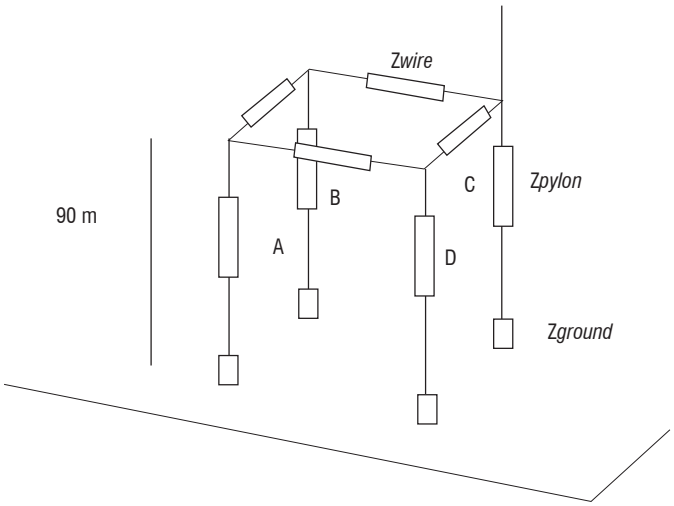

Figure 12 – Equivalent circuit of the pylons and the injection current

Taking into account the impedances of the various conductors and the point of impact of the lightning, the solution is now dependent on the spectrum of the aggression.

For a simple geometrical configuration (figure 12) and by using an electrical circuit-based simulation tool like a PEEC tool, it is easy to estimate the weight of the various impedances in the balance of the currents in the system. However, to simplify the numerical model, the current waveform used to simulate the lightning is this wave A of Standard ED84, namely:

$$i(t) = I_0\left(e^{-\alpha t} - e^{-\beta t}\right)$$

where α and β are the coefficients given in table 1.

I_0	218810	A
α	11354	s^{-1}
β	647265	s^{-1}

Table 1 – Coefficients for the waveform A

With a nonsymmetrical lightning current injection, the connection wires between the pylons have significant influence. With a low impedance value of these connections we can expect a balance distribution of the current in the four pylons. The impedance of this connection is controlled by the inductance of the wire and this inductance is higher than the pylon inductance. These connections will strongly influence the current distribution. A significant improvement of the impedance can be obtained by increasing the number of conductors between each pylon. Indeed, with several separate parallel cables we create an equivalent conductor, with a characteristic dimension much greater than the radius of the elementary wire and thus with a lower inductance.

Table 2 gives the distribution of the current in the four pylons for two configurations:

- a single connection cable between two pylons;
- four wires with 1m separation between two pylons.

With four wires, the reduction of the impedance allows a better balance of the current in the four pylons and of course a minimization of the magnetic field in the launcher zone. The result approaches the optimal solution of the perfect equal current distribution.

	Pylon A	Pylon B	Pylon C	Pylon D	Std
1 cable	26053	37907	98599	37907	32801
4 cables	34496	43324	79232	43324	19866

Table 2 – Maximal currents in Amps for a 200 kA injected current

The results in figure 13 show the improvement of the magnetic field due to the use of multiple parallel cables between the pylons.

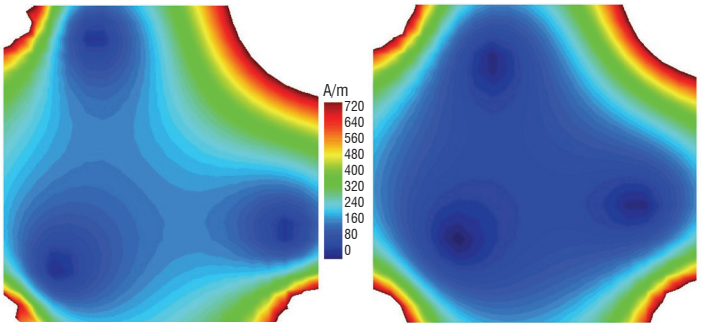

a) b)

Figure 13 – Magnetic field in the launcher area for the two configurations (a) single cable between the pylons (b) four wires, between the pylons, separated by 1m

The second element that may have a theoretical impact on the current distribution is the resistance of the pylon grounding system. However, for an aggression of waveform A (200 kA) on a given pylon, table 3 shows that the resistance value of the ground electrodes must be relatively high to obtain a well-balanced current distribution. However, a high value of the ground resistance would not be desirable for a lot of other reasons. Especially, they would not guarantee the draining of high current flows into the ground as expected of such grounding systems.

R_{ground} (Ω)	Pylon 1	Pylon 2	Pylon 3	Pylon 4	Std
1	33660	43205	79489	43205	20239
10	43690	47435	66030	47435	10077
20	46783	48800	60922	48800	6467
50	49184	49714	53348	49714	1921

Table 3 – Current distribution over the pylons for various values of the resistance of the ground electrode (R_{ground}) and standard deviation (Std) of the current for each R_{ground} configuration

Consequently, it is out of question to think of deteriorating the quality of the ground electrodes in order to improve the current balance in the pylons; the grounding system resistances cannot be an adjustable parameter to control this current distribution.

Optimization of the mesh cage

The main difficulty with this solution is the balance between the minimization of the magnetic field and the penetration of the rolling sphere.

Indeed, from the point of view of the electro-geometric model, it is necessary to bring the pylons as close as possible, but in this case we increase the residual intensity of the magnetic field induced by the lightning impact on the LPS at the level of the rocket area. A compromise must thus be sought between the maximum intensity of an acceptable strike on the launcher and an acceptable electromagnetic environment due to a strike on the LPS. To have a protection of level I according to the IEC62305 standard, the protection for a current intensity higher than 3 kA leads to a rolling sphere radius equal to 20 m. To obtain this protection, the maximum distance between the pylons must be of 40 m.

A simplified simulation of the two solutions, with 40 m or 60 m separation between the pylons, corresponding to a rolling sphere of 20 m or 30 m respectively, shows that the solution with closer pylons (20 m) cannot ensure a sufficiently low level of the magnetic field (figure 14). Moreover, one solution with pylons on a square base with sides measuring 40 m also has strong constraints, such as the proximity to the rocket during the launch.

a)

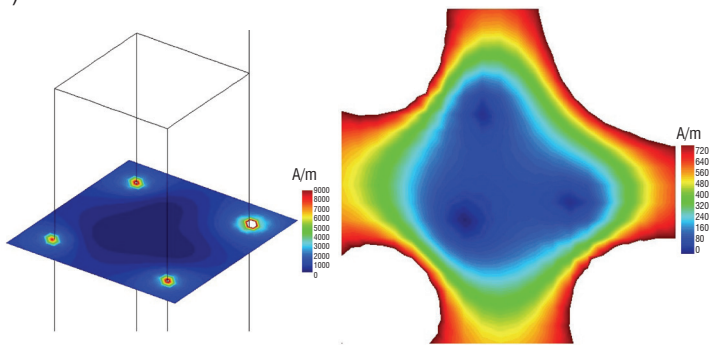

b)

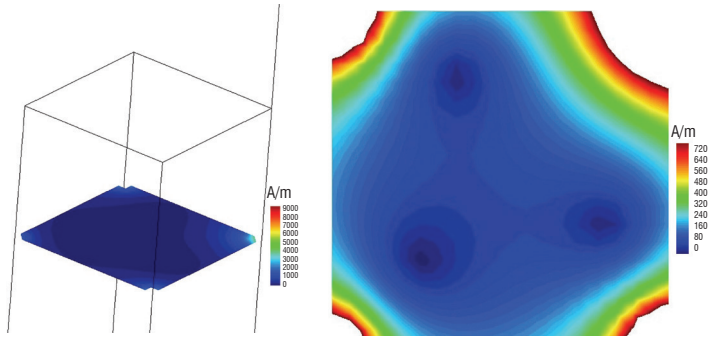

Figure 14 – Maximum magnetic field within the LPS (a) distance between pylon 40 m (b) distance between pylon 60 m

The lightning protection system is finally made of four 90 m-high pylons on a square base with sides measuring 60 m. The pylons will be connected by their tops with a set of four parallel wires.

Evaluation of the solution selected

Three main criteria have been retained for the design and the realization of the lightning protection system of the Soyuz launching pad (ZLS) in Guyana. Those are:

- the system effectiveness, namely the launcher must be protected from any lightning strike of intensity higher than 5 KA;
- the cost of the system;
- the maintenance of the system.

The effect of the last two criteria was to favor a mesh cage solution, with the use of pylons as down-conductors for the lightning current.

The preliminary study made it possible to define the broad lines of the LPS design, pointing out the important role played by the cables between the tops of the pylons in the system effectiveness.

For a current of 5 kA and a 30 m rolling sphere, the standard gives a Type II protection level, but this solution was found as the best compromise between a direct lightning strike of 5 kA on the rocket and a high level lightning strike of 200 kA on the LPS.

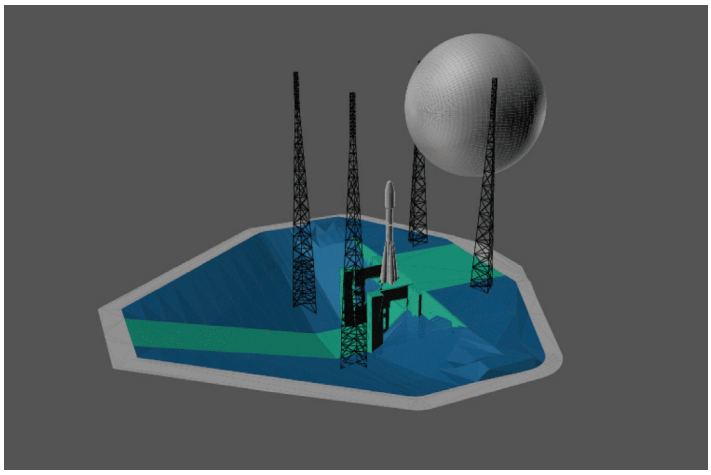

Figure 15 – Rolling sphere on the LPS of Soyuz launching pad in Guyana

Then, the adopted solution must be analyzed with the particular operating constraints of the Soyuz launching pad; for example with a gas pipe of a very large dimension (figure 16). On the one hand, this zone does not allow the location of the pylons in a perfectly symmetrical configuration and we must recall the influence of the system inductances on the balance of the currents. On the other hand, the latter analysis is unable to take into account the impedance of the grounding network; it has only shown that the ground resistance could not be a driving parameter. However, the ground network cannot be comparable to a simple local resistance on each pylon. It is thus necessary to study the global behavior of the site upon receiving a lightning strike, by taking into account the actual geometry and the ground parameters.

Impedance of the grounding network and pylons grounding

It is widely known that the grounding system is a critical point of the lightning protection system. Indeed, if one wishes to minimize the overvoltage induced by the lightning current, the ground connection must have low impedance. The element that will condition the grounding value is the ground in contact with the ground electrode and of course, the conductivity of the ground is not an easily modifiable parameter. This will impose a dimension of the ground electrode according to the conductivity of the ground, with the disadvantage of increasing the impedance with the size of the buried system for low conductivity ground.

In the case of the Soyuz lightning protection system, we have evaluated the impact of the grounding of the pylons. The problem here is very specific, but it makes possible an evaluation, in a concrete grounding configuration, of different grounding system solutions.

For mechanical reasons, the Soyuz launching pad is built on a rock zone. The ground topology and the final installation of the site result in the fact that each pylon cannot be put to ground identically. Figure 16 presents a cross-section of the ground, with the two different added dirt and rock ground layers, respectively of resistivity of 30 Ωm and 300 Ωm.

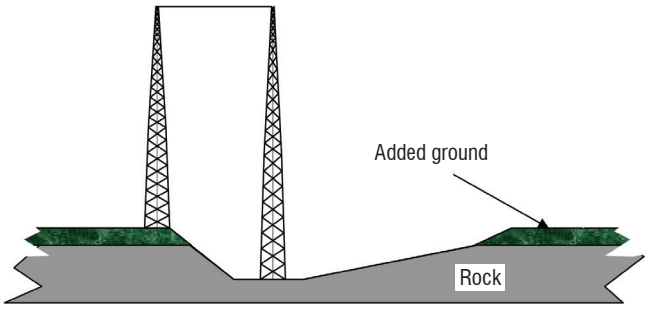

Figure 16 – Cross section geometry of the pylon installation on the Soyuz LPS and picture of the flue (flame exhaust)

From a general point of view; the launching pad ground consists of two different layers. The deepest layer has a resistivity of 300 Ωm; a more conductive ground of 30 Ωm was brought back onto this layer. The grounding of the pylons in the flue (flame exhaust) is thus more difficult to perform and is the cause of local ground electrodes of lower quality. However, since all of the grounding systems are interconnected, the value of the ground resistance of the entire site is very low. Therefore, for the low frequency components of the current spectrum the behavior of the grounding will be good; however, for the high frequency components, the inductance of the ground electrodes will deteriorate the performance of the grounding.

However, by using the impedance parameter, it is difficult to quantify the quality of the site. Indeed, this impedance is frequency dependent because of an inductive behavior.

In order to evaluate the behavior of a ground electrode subjected to a lightning excitation and to evaluate the impact of its inductive part, we will first analyze the overvoltage V related to the current flow in the grounding system. In a very simplified way, the latter can be written as follow:

$$V = RI + L\frac{dI}{dt} \qquad (2)$$

and in the frequency domain:

$$\tilde{V} = R\tilde{I} + jL\omega\tilde{I} = \tilde{V} = \left(R + jL\omega\right)\tilde{I} \qquad (3)$$

The ground makes this simple problem complicated, because the real part

and the imaginary part of the impedance are both frequency dependent. Therefore, we must first understand the frequency behavior of a ground electrode as a function of the ground conductivity.

The first important parameter of a ground electrode is its resistance. For a given ground conductivity, the ideal ground electrode is a metallic half sphere. Comparison with other ground electrodes geometries shows that a buried ring, of equivalent dimensions, leads to values close to the resistance value of a half sphere. Table 4 presents resistance values for different shapes of ground electrodes and for the two values of electric conductivities encountered in the Soyuz launching pad.

This table shows that, with the constraint of obtaining equivalent values of ground resistance, the differences in the conductivity of the layers causes a need for the size of the ground electrodes to be 10 times larger for the pylons inside the flue. However, if the ground electrode is larger, it is legitimate to raise the question of its performance for the high frequency components of the lightning waveform.

The impedance of a buried ground electrode can be analyzed using the transmission line model [10]. Although approximate, this model gives good results. A comparison between this model and a more complete electromagnetic solution yields very similar results for the value of the input impedances of buried cables [15].

The propagation coefficient inside the ground is given by:

$$\gamma = \sqrt{j\omega\mu_0\left(\sigma + k\varpi\varepsilon\right)} \rightarrow \gamma \approx \sqrt{j\omega\mu_0\sigma} \qquad (4)$$

Let us consider a single buried line of radius a, at a depth d within a ground of conductivity σ (figure 17).

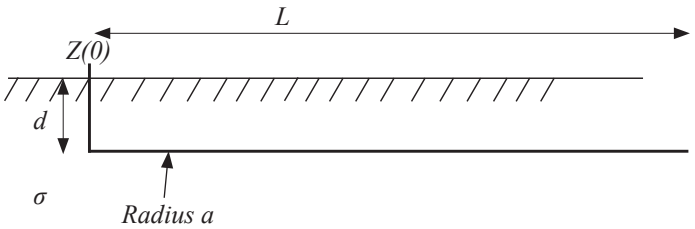

Figure 17 – Buried line

The impedance per unit of length of the transmission line model is given by:

$$Z_g \approx \frac{\omega\mu_0}{8} + j\omega\frac{\mu_0}{2\pi}\ln\left(\frac{\sqrt{2\delta}}{\gamma_0 a}\right) \qquad (5)$$

where δ is the skin depth in the ground at the frequency f.

		$\rho = \frac{1}{\sigma} = 30\ \Omega\text{m}$	$\rho = 300\ \Omega\text{m}$
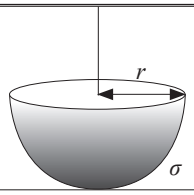	$R = \frac{1}{2\pi\sigma r}$	$r = 1$ m $R = 4.77\ \Omega$	$r = 1$ m $R = 47.7\ \Omega$
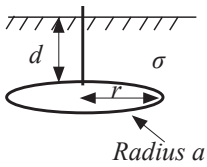	$R = \frac{1}{2\pi\sigma}\frac{1}{\pi r}\ln\left(\frac{8r}{a'}\right)$ $a' = \sqrt{2ad}$ $a \ll d$ $a \ll r$	$Radius = 1$ cm $r = 1$ m $d = 1$ m $Z = 6.13\ \Omega$	$Radius = 1$ cm $r = 1$ m $d = 1$ m $Z = 61.33\ \Omega$
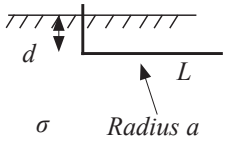	$R = \frac{1}{\pi\sigma L}\left[\ln\left(\frac{2L}{a'}\right) - 1\right]$ $a' = \sqrt{2ad}$ $a \ll d$ $a \ll L$	$Radius = 1$ cm $d = 1$ m $L = 6.28$ m $Z = 5.30\ \Omega$	$Radius = 1$ cm $d = 1$ m $L = 6.28$ m $Z = 53.0\ \Omega$
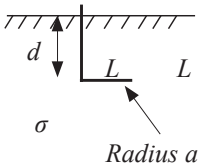	$R = \frac{1}{2\pi\sigma L}\left[\ln\left(\frac{2L}{a}\right) - 1 + \frac{L}{4d}\right]$ $a \ll d$ $L \ll d$	$Radius = 1$ cm $d = 1$ m $L = 1$ m $Z = 21.7\ \Omega$	$Radius = 1$ cm $d = 1$ m $L = 1$ m $Z = 217\ \Omega$
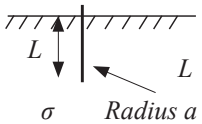	$R = \frac{1}{2\pi\sigma L}\left[\ln\left(\frac{4L}{a}\right) - 1\right]$	$Radius = 1$ cm $L = 1$ m $Z = 23.8\ \Omega$	$Radius = 1$ cm $L = 1$ m $Z = 238\ \Omega$

Table 4 – Value of the ground electrode resistance for various shapes and ground resistivity (ρ)

$$\gamma_0 = 1.781...$$
$$\delta = \frac{1}{\sqrt{\pi f \mu_0 \sigma}} \quad (6)$$

The admittance per-unit length Y_g is given by:

$$Y_g \approx \frac{\gamma^2}{Z_g} \quad (7)$$

The admittance per-unit length Z_c is given by:

$$Z_c \approx \sqrt{\frac{Z_g}{Y_g}}$$
$$Z(0) \approx \frac{Z_c}{th(\gamma l)} \quad (8)$$

By using (8), we show that the impedance of the ground electrode increases with the frequency; at low frequencies the latter is driven by the static resistance, whereas at higher frequencies the real and imaginary part of the impedance are approximately equal and both increase with the square root of the frequency. A numerical application is done for a 100 m length line, for the two values of the site ground electric conductivities (figure 18). At high frequencies, the impedance of a buried line in the ground is both resistive and inductive.

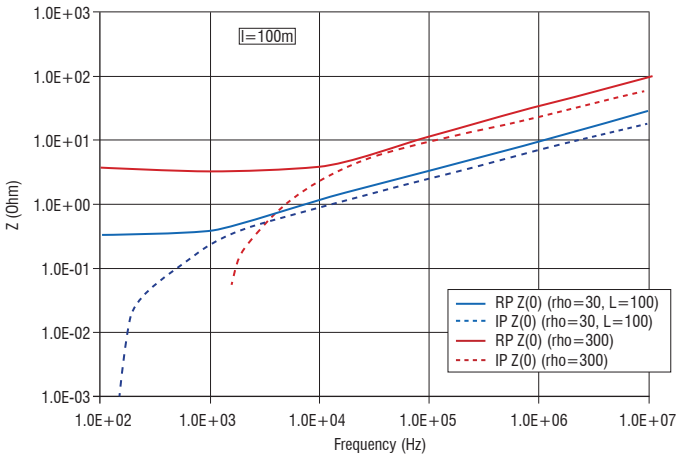

Figure 18 – Real part and imaginary part of a 100 m length buried wire, for two values of the ground electric resistivity

If we want to perform a more precise analysis of the weight of the real part compared to that of the imaginary part of the ground electrode impedance, we must choose a relevant frequency. For this purpose, we choose the frequency for which the derivative of the function $f(t) = I_a \sin(2\pi ft)$ gives the same maximum derivative value as the lightning excitation, namely:

$$\frac{dI}{dt} = 2\pi f I_a$$

The average rise time value of the lightning excitation varies depending on the standard applied. The maximum derivative value of the waveform A of the ED84 standard is significantly higher than the values listed in the other various standards. Table 5 presents a standard comparison of the values recorded for the first negative short stroke. For the analysis of the impedance, we take the value of 6.5 10^{+10} A/s given by the IEC 62305 standard. In this case, the equivalent frequency for the impedance calculation is of approximately 50 kHz.

Standard	*di/dt* (A/s)	Observation
Wave A (ED84)	13.9 10^{+10}	Maximum derivative value
ED84	3.2 10^{+10}	1st negative short stroke
IEC 62305	6.5 10^{+10}	1st negative short stroke
Stanag	4.0 10^{+10}	Negative Lightning Flash

Table 5 – Steepness value of the 1st negative short stroke

At this 50 kHz frequency, we can estimate the input impedance of a buried wire according to its length and the ground conductivity.

Figure 19 gives this input impedance for our two values of ground conductivities. For the weakest conductivity, this impedance is significantly larger and is obtained for a larger length of the buried cable.

Moreover, the characteristic length to obtain a stable value of the impedance is about the distance between two pylons.

The estimation of this impedance shows that it will be very difficult to obtain a grounding resistance of the two pylons in the flue comparable with the two other pylons anchored in a good ground. Moreover, the imaginary part of this impedance (inductance) is not negligible and we have seen that the inductances of the entire grounding systems were the main contributors for the balance of the currents at high frequencies.

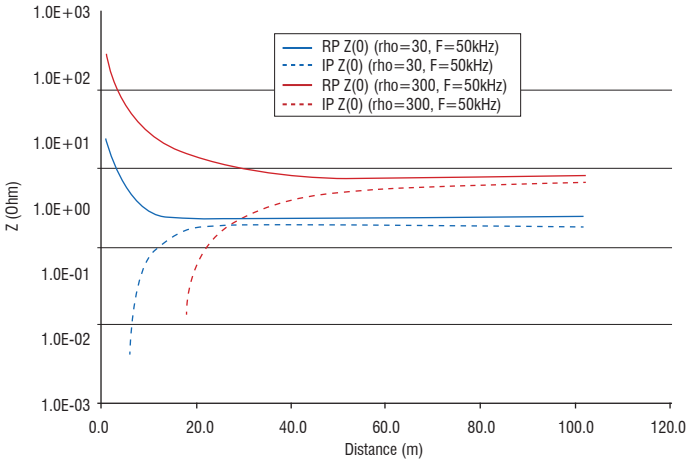

Figure 19 – Variation of the real and imaginary parts of a buried wire, as a function of its length

Numerical evaluation of the solution selected

In order to analyze the impact of the ground network on the current distribution more precisely, it is necessary to perform a global analysis of the site.

This can be done with a 3D computer code that solves Maxwell's equation. On the Soyuz LPS, this was done with the ALICE FDTD code from Onera. With the use of this method, it was possible to take into account the global geometry of the ground and of the wires buried in the ground [17]. Figure 20 presents a view of the model used. The principal

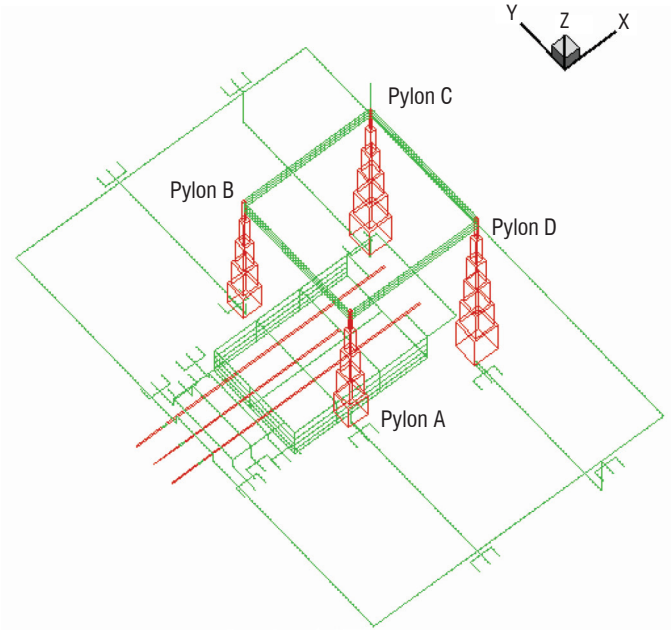

Figure 20 – FDTD numerical model of the SOYUZ launch pad

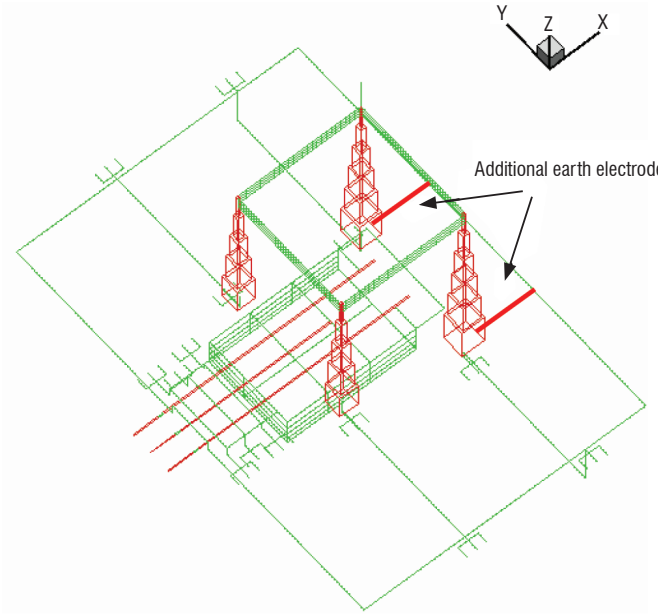

Figure 22 – Numerical model of the SOYUZ launching pad, with additional ground electrode (configuration No.2)

ground network is the bunker ground network coupled to the foundation ground network around the site. This ground network must ensure the equipotential link of the site during the lightning stroke. Because of its dimensions and of the number of buried wires, the resistive value of the ground impedance is very small but this is not the case of its inductance.

As for the pylons, these are first grounded with a local ground electrode and second with a connection to the foundation ground network by buried bare copper wires.

With an independent ground electrode for each pylon and a connection of these pylons to the global ground network, we have in this configuration No. 1 an almost optimal basic configuration that we can evaluate.

In this configuration, with a current injection in Pylon C, the 3D numerical simulation yields a first evaluation of the currents and magnetic field levels; figure 21 shows a shift of the minimum magnetic field area toward Pylons A and B, which are the closest to the bunker. This shift is the consequence of too large currents in Pylons A and B, combined with bad ground electrode values for Pylons C and D.

The results of configuration No.1 show that the grounding impedances of Pylons C and D must be decreased for better symmetry. This is why, in configuration No.2, we have placed an additional conductor between Pylons C and D and the large foundation ground electrode (figure 22).

The simulations performed in this new configuration show that the additional connection in the ground makes it possible to move the minimum magnetic field zone towards the center of the pylons (figure 23). A comparison of the intensities of the currents in the pylons for an injection in Pylon C shows that the addition of ground electrodes for Pylons C and D makes it possible to approach an optimal balance of the currents (table 6).

Pylon	Configuration No.1	Configuration No.2	LIRIC
A	49.6	43.6	34.5
B	60.5	54.4	43.3
C	52.3	60.3	79.2
D	37.4	41.6	43.3

Table 6 – Current constraint (A) of the 1st negative short stroke

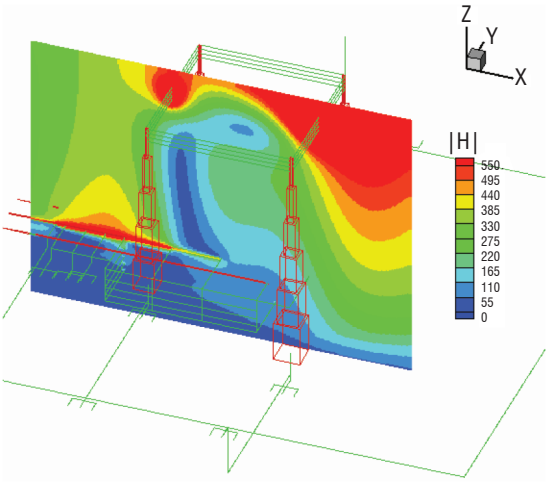

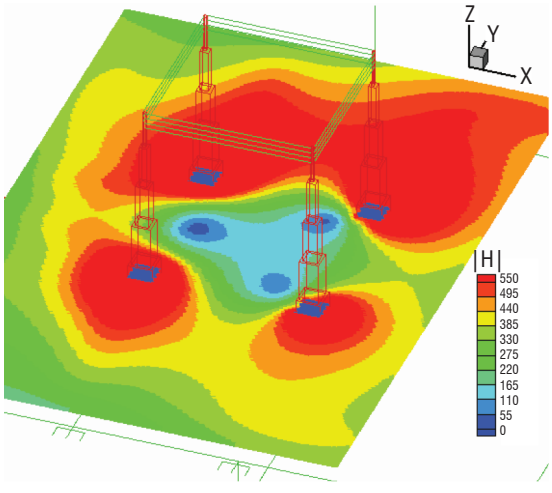

Figure 21 – Magnetic field level in configuration No.1

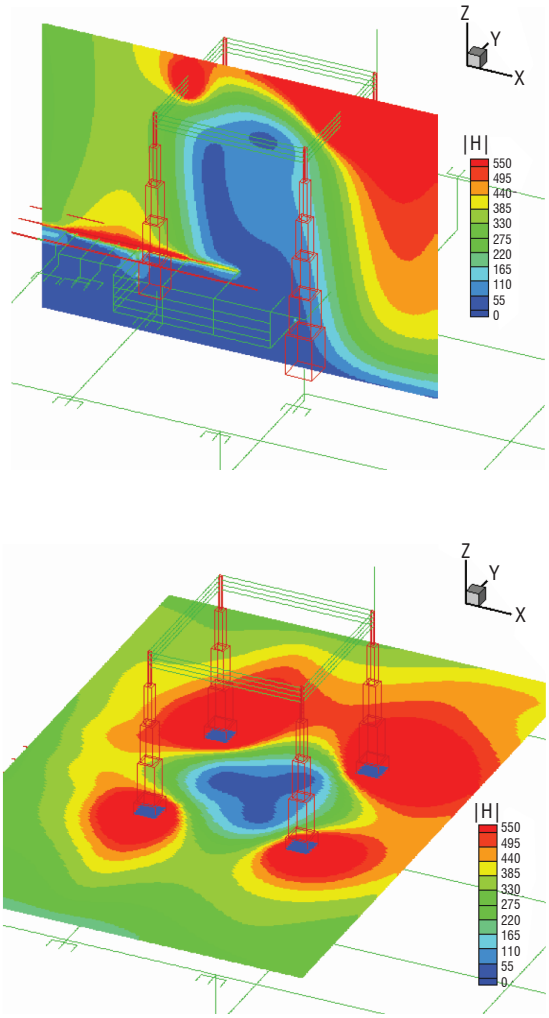

Figure 23 – Magnetic field level in configuration No.2

The entire set of simulations performed on the lighting protection system shows the three parameters influencing the magnetic field minimization in the launcher pad, namely:

- the geometry and the distance between the pylons;
- the impedance value of the connecting wires between the pylons;
- the impedance of the grounding system of the pylons.

While for the two first parameters a simple visual control can give a quick evaluation of the performance of the site, this is not the case for the buried part of the LPS. It is thus necessary to evaluate the behavior of the grounding of the pylons.

Experimental evaluation of the lightning protection system

From the point of view of the respect of the standards, various actions are carried out. The first action consists in checking whether all parts of the site are well connected. The second action consists in evaluating the resistance of the grounding of the installations. The third action is the evaluation of the magnetic field associated with the lightning strike. In many cases, the magnetic field evaluation is based on analytical formulas and numerical simulations on simplified structures, and the resistance evaluations are performed by static measurements after construction completion.

In complex sets of buildings it may be necessary to supplement the lightning paper studies by experiments. The IEC 62305-4 standard proposes an experiment with a lightning current generator.

In this chapter, we will present the principle of the test in a general case. We will show the choice of the generator to obtain an appropriate current waveform having the spectrum of a standardized lightning strike. Then, we will strive to adapt the test procedure to a site like a launching pad and we will show some results allowing a lightning qualification of the site.

As an illustration of our presentation, we will show results obtained during experimentation that we performed, in order to qualify the Soyuz launching pad for the effects of a lightning strike; thus, one of the goals was the dynamic evaluation of the LPS.

The experiment also made it possible to evaluate the susceptibility of various sensitive links, such as power networks to a lightning excitation.

The experimental principle

For physical reasons, it is not possible to inject a current having the characteristics of a real lightning current into a large building, both from the point of view of its intensity and from the point of view of its distribution onto the structure. The lightning current distribution on a structure is a function of both the point of impact and of the current dissipation paths in the ground (figure 24). If we modify one of these two parameters, we modify the current distribution in the structure.

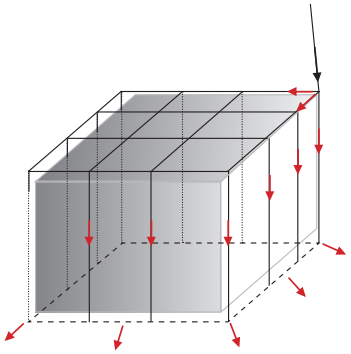

Figure 24 – Lightning current distribution in a structure and within the ground

We thus see that in the absolute, it is impossible to generate an identical current distribution between a natural lightning strike and an artificial lightning strike. The experiment requires a localized generator that induces a specific current distribution, which depends on its position and on the feeders used for the return current (figure 25). In order to obtain a distribution as close as possible to the real lightning current distribution, we must multiply the number feeders. Furthermore, this testing methodology is very constraining because it requires the placement the generator on the structure and it requires feeder installation for the return current.

There is an alternative solution to analyze the global building response to a current impulse. For this purpose, the feeders of the previous problem can be used as injection lines. In this case, we have as many excitation states as the number of feeders. The solution of the global problem is obtained by a superposition of the elementary problems (figure 26). In this new

configuration, the generator can be placed at ground level, which results in an easier configuration test. However, by decomposing the test, we highlight the ground influence in the return of the current and the interaction between the two grounding systems. Indeed, we can either use the ground as a return conductor or a wire between the grounding of the building and the generator (figure 27).

In this last case, we clearly see that the distribution of the current is influenced by this wire. In the case of an independent ground electrode for the generator, for the building ground, the influence on the current distribution will depend on the interaction between the two ground networks.

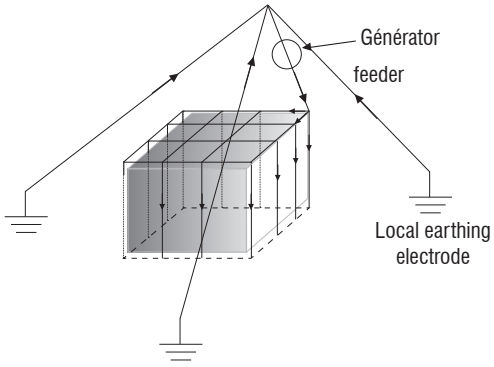

Figure 25 – Experimental feeder installation usable to inject a current in a building

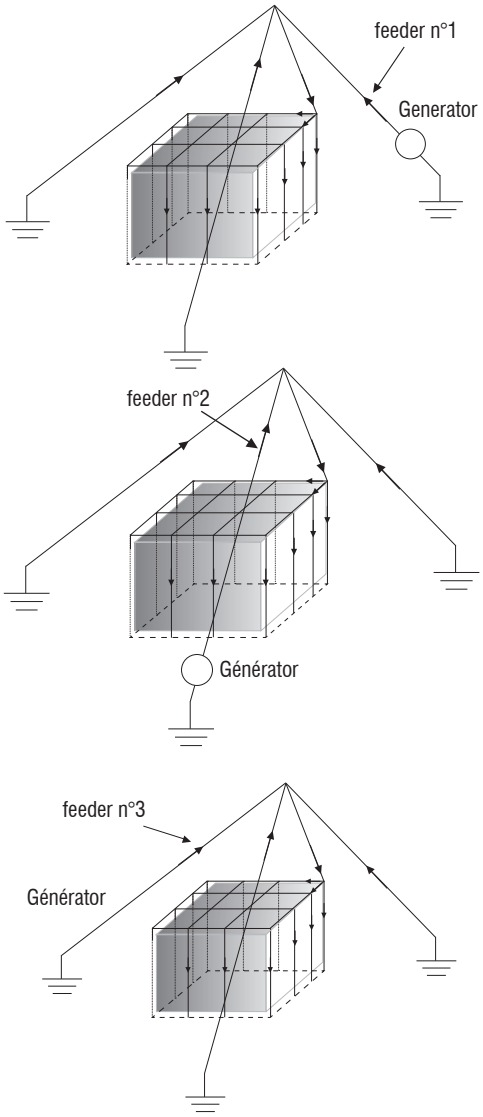

Figure 26 – Experimental feeder installation usable to inject a current in a building

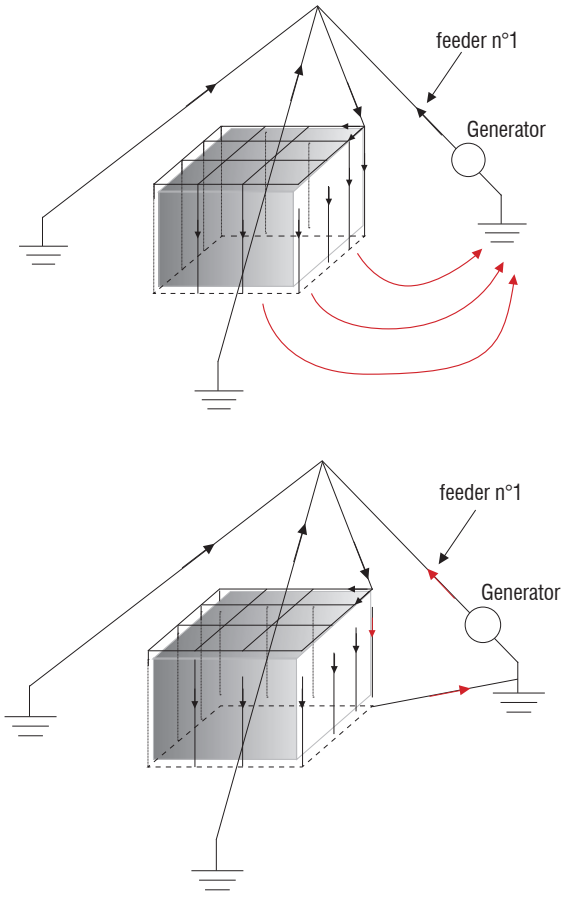

Figure 27 – The effect of the ground on the current distribution

With the same principle, a third solution consists in placing the generator far away from the building. On the one hand, in this case, the impact on the current distribution in the structure is low (figure 28); on the other hand, the constraints on the injected waveform, and more exactly on its rise time, limits the distance between the generator and the building.

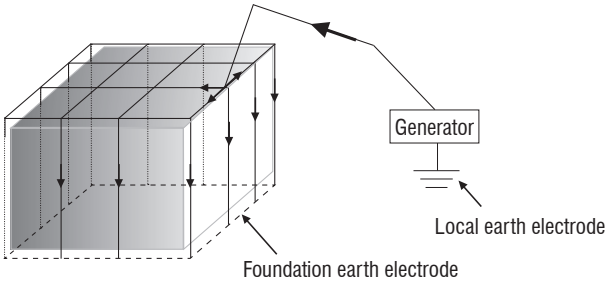

Figure 28 – Current injection on a building with separate ground system

A preliminary analysis is thus aimed at finding, with respect to the generator characteristics, an optimal distance of the generator to the building. With a generator based on a capacitive discharge (figure 29) it is easy to determine the component of the injection circuit according to the desired current waveform (waveform A).

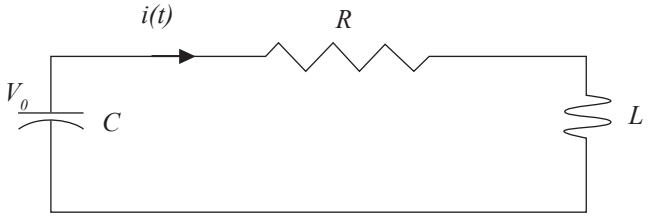

Figure 29 – Electrical circuit of a capacitive discharge

We recall that the waveform A is given by:

$$i(t) = I_0\left(e^{-\alpha t} - e^{-\beta t}\right)$$

And the current for an overdamped capacitive response is given by:

$$i(t) = \frac{V_0}{2Lp_0}\left(e^{-(a-p_0)t} - e^{-(a+p_0)t}\right)$$

with:

$$a = \frac{R}{2L}\ ,\ \omega_0^2 = \frac{1}{LC} \text{ and } p_0^2 = a^2 - \omega^2$$

By identification we have:

$$a = \frac{(\alpha+\beta)}{2} = \frac{R}{2L} \text{ and } C = \frac{1}{L\left(a^2 - p_0^2\right)}$$

In a first step, the calculation for a one-hundred-meter line gives the circuit parameters presented in table 7. The distance between the generator and the building being tested fixes the circuit inductance. This enables us to calculate the generator capacity C and the circuit resistance R to obtain a current injection waveform having the waveform A signature.

The level of the injected current will depend on the initial charge of the capacity; for our application with a voltage of 30 kV we can expect a current of 400 A in the structure.

Consequently, from a theoretical point of view, it is rather easy to determine the optimal parameters that will allow a waveform A current injection. However, the application to a real situation shows that the most influent parameter is the resistance, because it depends on the ground and in particular it depends on the ground electrode, which is not perfectly controlled.

α	β	Line inductance	Resistance	Capacitance
s^{-1}	s^{-1}	H	Ω	F
11354	647265	1.16E-04	77	1.17E-06

Table 7 – Calculation of the circuit components

Thereby, for a given site, it will be necessary to optimize the generator ground electrode and locate it as far as possible; if necessary, the introduction of an additional resistance in the circuit could lead to a significant improvement. In the same way, the impedance can also be optimized to obtain a high impulse current.

Test procedure on Soyuz LPS

In the case of the LPS of Soyuz launching pad we have had another problem, indeed it is not possible, for safety reasons, to inject directly at the top of the system and we had to adapt the test procedure to take this constraint into account.

We must thus ask ourselves the question of which information is expected in the test?

The numerical simulations showed that the relevant parameter, which is difficult to control, was the pylon grounding system impedance. We thus defined a test procedure to qualify this dynamic impedance as well as possible. Thus, the current injection was done at the base of the pylon (figure 30). In this configuration, it was possible to evaluate the pylon grounding system and the respective weight of the impedance of the aerial parts in the current distribution and the weight of the buried conductors of the LPS.

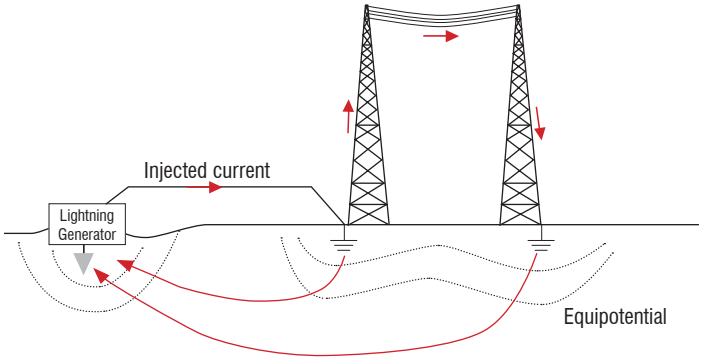

Figure 30 – Potential and current distribution for the injection at the pylon feet

In order to be able to conclude on the symmetry of the current redistribution, a global set of measurements has been recorded with the four possible successive positions of the generator (figure 31). The interest of this approach is to have a global understanding of the behavior of the system.

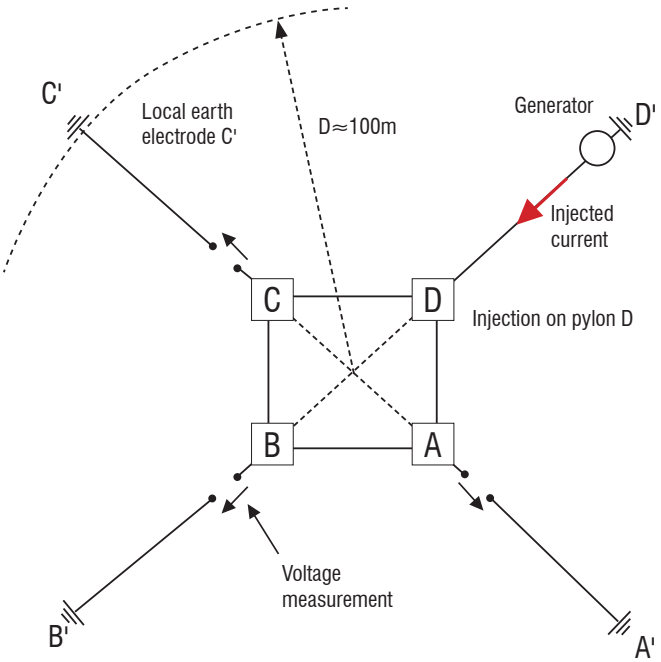

Figure 31 – Schematic representation of the injection points (here, injection in Pylon D)

The measurement lines are an electric cable installed at approximately 80 cm from the ground (figure 31). They connect the pylon and its associated reference ground electrode. They are used both to inject the current and to measure the surge voltages.

Figure 32 – Injection and measurement line

The injected current is measured in the four injection configurations. For each configuration, the overvoltages have been measured on the 3 other pylons. Voltage measurements have been based on the same local reference principle, using the same cables as for current injection. The voltage measurement was obtained by opening the cable at the level of the pylon (figure 34).

The constraints of the Soyuz launching pad environment do not make it possible to place the reference ground electrode of the generator in perfectly symmetrical position relative to the LPS the figure 33 presents the actual positions of the four ground electrodes for the four injection positions.

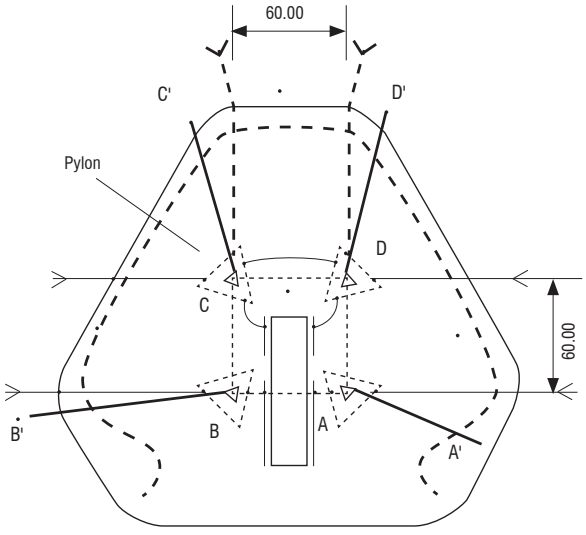

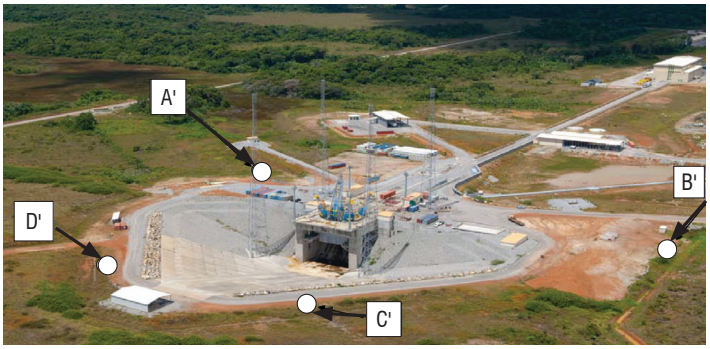

Figure 33 – Injection and measurement line

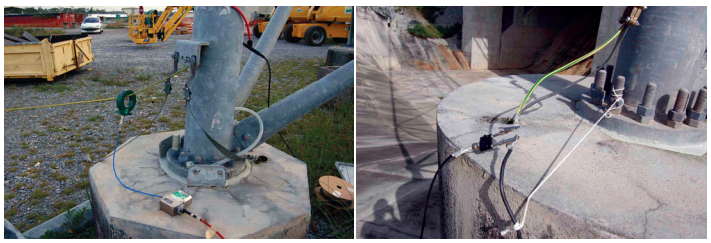

Figure 34 – Current and voltage measurement

Evaluation of the grounding impedance

Preliminary work consisted in the implementation of four reference ground electrodes, almost identical in regard to voltage measurements and current injection. The installation of identical reference ground electrodes would facilitate the analyses carried out later on. The injected current in the four configurations is shown in figure 35. The recordings show that the four injection configurations are completely comparable. An example of the voltage measured is presented in figure 36. The curves correspond to the overvoltage in Pylons A, B and C for an injection in Pylon D.

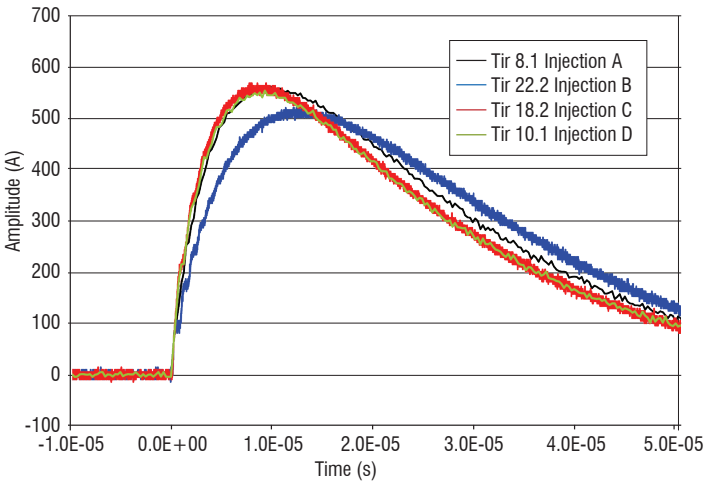

Figure 35 – Injected current in the four configurations

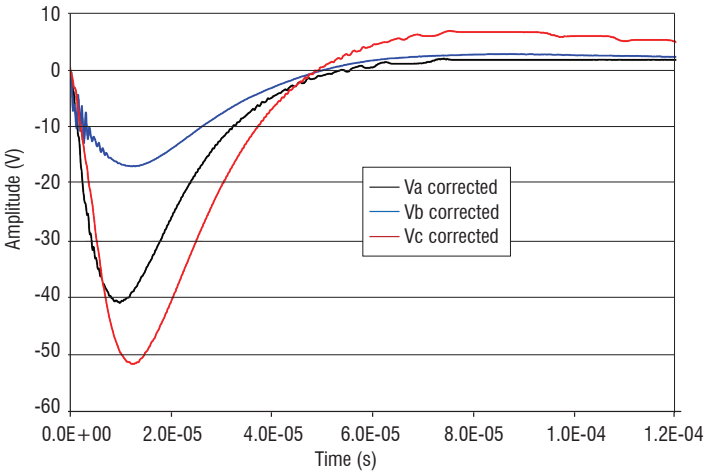

Figure 36 – Voltage measurement

For each injection position we have a measurement of the associated overvoltage in the three other pylons. Thus, we can define a coupling impedance between the voltage measured and the injected current (Z_m). This impedance provides information on the grounding of the pylons but what about exactly of this measurement.

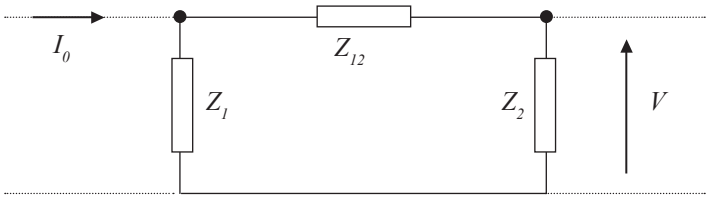

Figure 37 – Electrical diagram used for the determination of the coupling impedance

For a given voltage measurement, the equivalent electric diagram of our coupling impedance is given in figure 37; its value is given by:

$$Z_m = \frac{1}{\frac{1}{Z_1} + \frac{1}{Z_2} + \frac{Z_{12}}{Z_1 Z_2}}$$

On the one hand; the above formula shows that the coupling impedance is high in three cases that can be independent: for a high value of the impedance Z_1, a high value of the impedance Z_2 or a high value of the $Z_1 \times Z_2$ product, compared to the impedance value Z_{12} ($Z_1 Z_2 > Z_{12}$). On the other hand, Zm is small for a low value of Z_1 or a low value of Z_2, or a low value of $Z_1 \times Z_2$ compared to Z_{12}.

In fact, the value of the coupling impedance cannot be higher than the lowest value of the impedances Z_1 and Z_2. To find low values of these impedances, as shown in table 8 and table 9, we can either have low values of the grounding impedance or a strong value of the connection impedance (Z_{12}) between the pylons.

In the test, the measured coupling impedances are low. Consequently, for the lightning protection system analysis, we must differentiate between the interconnection impedance behavior and the ground electrode behavior.

	Impedance (Ω)			
	A	B	C	D
Injection A		-6.6E-3	-3.4E-3	-19.3E-3
Injection B	-6.5E-3		-11.8E-3	-6.6E-3
Injection C	-3.3E-3	-12.6E-3		-18.4E-3
Injection D	-21.6E-3	-7.2E-3	-19.1E-3	

Table 8 – Static coupling impedance (f=0 Hz)

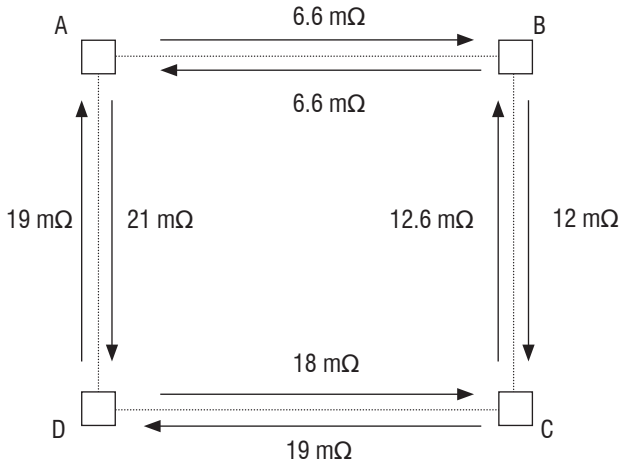

Figure 38 – Diagram of the coupling impedance (static)

	Impedance (Ω)			
	A	B	C	D
Injection A		64.0E-3	26.5E-3	64.7E-3
Injection B	63.1E-3		73.5E-3	28.7E-3
Injection C	26.3E-3	81.1E-3		92.1E-3
Injection D	71.3E-3	30.0E-3	89.9E-3	

Table 9 – Dynamic coupling impedance

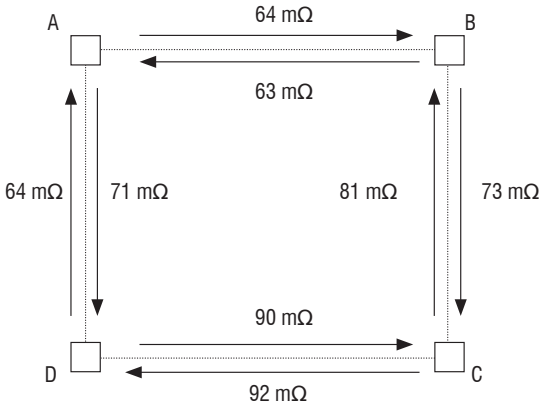

Figure 39 – Diagram of the coupling impedance (dynamic)

By construction, we know that the pylons are interconnected, by both the aerial parts of the lightning protection system and the pylon interconnections buried within the ground. Due to this status, the values of the connection impedances cannot be large. With this assumption and the measured values of the coupling impedances, we can say that the impedances of the pylon grounding system are low and with the symmetry of measurements these values must be equivalent.

The difficulty is to determine the value of the main impedances of the system circuit model with the experimental data available. The number of measurements being limited, the system that we will try to solve must be simple. In the first order approximation, the circuit is presented in figure 40, with a grounding resistance for each pylon and connecting resistances between pylons.

To solve this problem, we have six measurements of the coupling impedances and eight resistance values to evaluate.

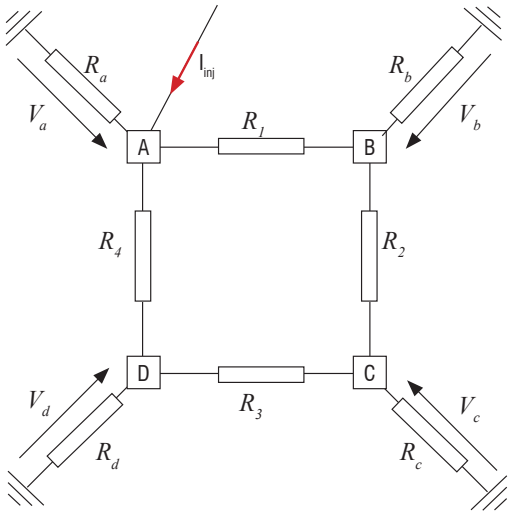

Figure 40 – Simple electrical diagram for the measurement analysis

The problem is underdetermined and the number of solutions is thus important. However, by carrying out a research of solutions by a minimization algorithm, we can show that the pylon grounding resistances are low, whatever the impedance values between the pylons may be (figure 41).

This result is also important because it shows that the grounding resistances are comparable whatever the pylon, which confirms the raw experimental measurements.

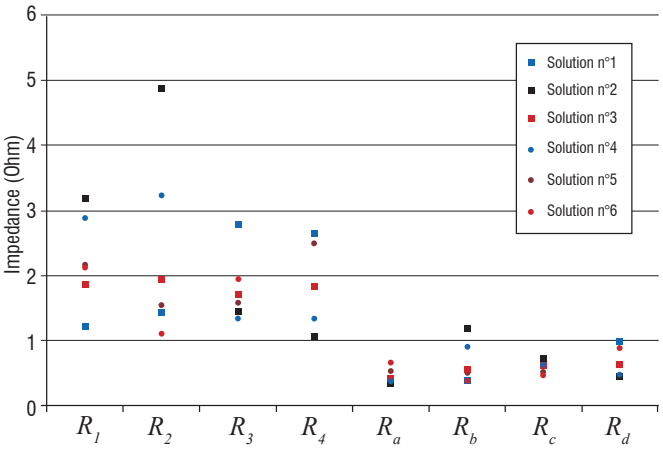

Figure 41 – Impedance values after the optimization process

This kind of analysis makes it possible to study the dynamic quality of the pylon grounding system. This analysis is supplemented by the study of the local distribution of the currents. Indeed, the grounding system is not a single system. A pylon on the Soyuz launching pad is composed of three main reinforcements bar, which are connected to the grounding system in three different ways (figure 42), namely:

- a local ground termination system;
- a local buried connection connected to the building grounding system;
- a buried connection connected to a ring ground electrode of the site.

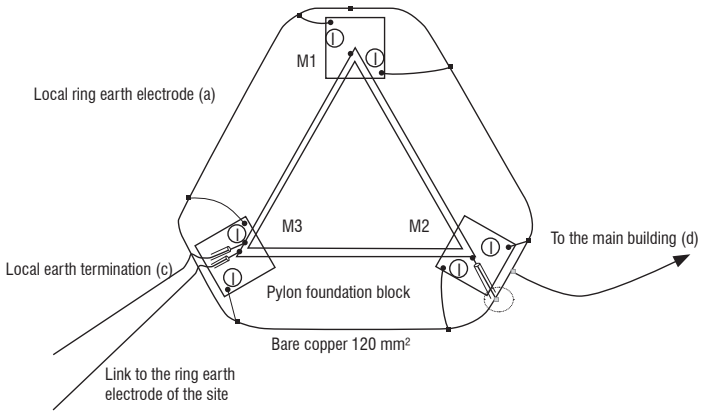

Figure 42 – Different types of grounding systems for a pylon

The currents recorded on the three bonding connections of the ground of the Pylon B (reinforcement N° 3) gives us a lot of relevant information (figure 43). It is the anchorage of the pylon which drives the maximum of current. This result is logical, the anchorage being connected to the local ring ground electrode, which is itself connected to the grounding circuit of the main building; this circuit impedance is obviously the lowest.

The share of current in the connection wire with the site ring ground electrode is less important and it drives a current at higher frequencies. The local ground electrode drives a low current but with high-frequency components.

This example clearly shows the behavior of a grounding system; at low frequencies, the entire grounding system drives the current whereas, at high frequencies, the local grounding system becomes predominant for draining the current.

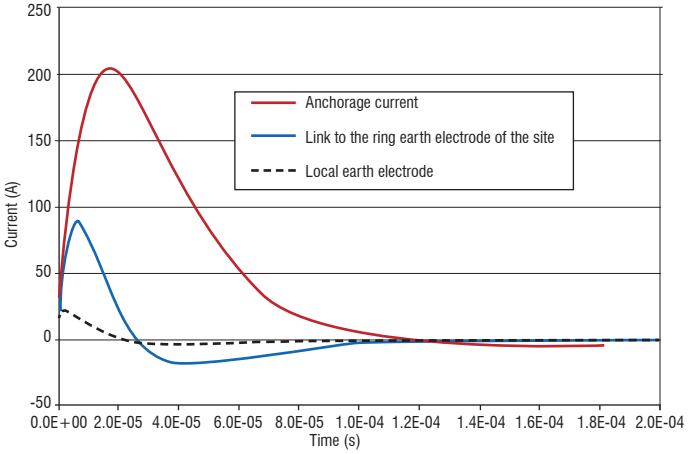

Figure 43 – Current on the bonding connections to the grounding system

Currents in power lines

With this experimental protocol we can obtain other information on the behavior of the site during a lightning strike. Overvoltages induced by the current injection on the pylon ground electrodes will induce a current on all of the external metallic links of the site area. We can mention, for example, the LOX pipelines, but also the power cables. This is all the more important because the current in these connections can induce significant perturbations inside the building.

Let us for example take a look at the power supply cable of the Soyuz launch pad. This connection consists of an armored cable, which ensures the mechanical and electric protection of the power line. The shield of the cable is connected to the ground in the power room inside the building but, for practical reasons, it is not connected to the LPS. In the building, the power line is placed inside metallic cable trays. Inside the building, we have two types of EM shields around the power line: the first shield is the mechanical shield of the cable, the second shield is provided by the cable trays (figure 44). From the inside of the building (figure 45), the cable seems to be perfectly shielded, which gives the impression that it cannot generate a disturbance!

However, the current measured around the cable tray is of about two amperes for an injected current of 500 amps in Pylon B (figure 46). This value is rather important and it is mainly the result of a bad connection between the cable shield and the lightning protection of the building (figure 47).

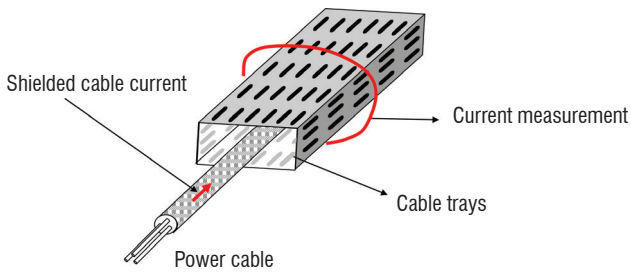

Figure 44 – Power line inside the cable tray

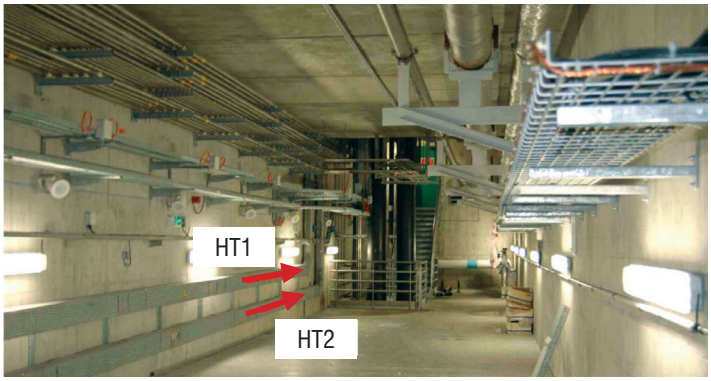

Figure 45 – Power cable trays inside the building

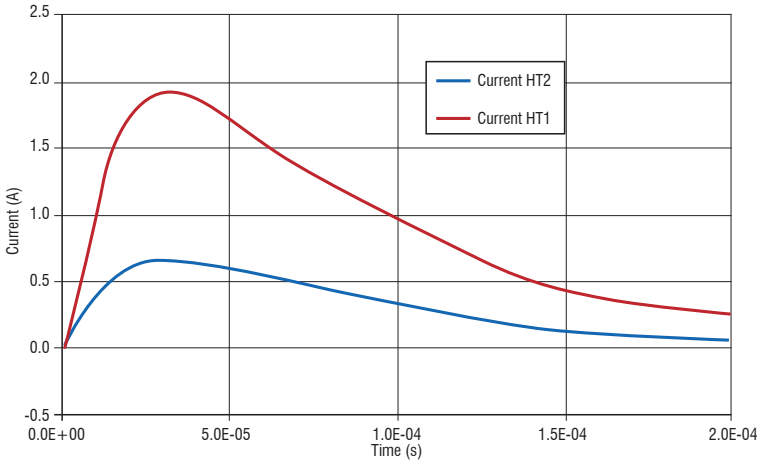

Figure 46 – Current measured around the cable tray of the power line

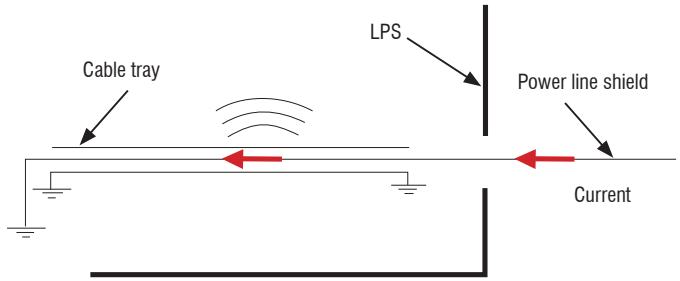

Figure 47 – Disturbance generated by the shielding current

Conclusions

The lightning protection solutions applied on the launch pad must comply with the requirements of any type of industrial site. However, the specificity of the launching pad installations requires a particular analysis suitable for the launcher protection before lift-off and for the seconds after lift-off.

In some phases of the launcher life cycle, lightning protection can only be provided by weather forecasting, which requires an efficient lightning alarm network.

However, the most significant risk is still a lightning strike in the phases before lift-off, when the launcher is on its launching pad. Indeed, the duration of this phase is significant and cannot be covered by weather forecasting.

At the present time, there are various solutions; these solutions often depend on the launcher itself and on the launching procedures.

The first solution is a protection starting with a removable gantry, which can be used for lightning protection as well as for protection against bad weather conditions. However, during the few hours, or even the few days, before launching, the gantry is removed and another protection system is absolutely required. This independent protection system is made up of several lightning conductors. The international standards based on the use of the electro-geometric model will impose a solution with three or four lightning conductors.

The protection system cannot however be summarized by the lightning conductor function. Due to electromagnetic coupling, a large number of devices are sensitive to the lightning current. For example, we can mention the propellant stored in the rocket, the pyrotechnics devices, electronic devices for launching management and, of course, the payload.

Thus, indirect lightning criteria are included in the dimensioning of the lightning protection system, in order to minimize the magnetic field in the launcher area. We must thus find a balance between positions close to the pylons, to satisfy the electrogeometric model, while keeping a low level for the magnetic field.

The first option to minimize the electromagnetic field is to use the separation function principle. In this case, we have insulators between the pylons and catenary wires, which drive the lightning current far away. However, it is difficult to ensure the efficiency of this solution for a strong lightning current.

The second solution is to use the pylon as a lightning down-conductor. In this case, to minimize the magnetic field in the launcher area, we must obtain a good balance of the current distribution on the pylons. The current balance is made first with multiple wire connections at the top of the pylons and second by a good grounding system for each pylon.

It is difficult to qualify the behavior of ground electrodes only with local experiments and, in particular, their behavior in regard to lightning current impulses. However, using complementarities of numerical simulations and experimentations, it is possible to qualify the quality of the grounding system and the impact on the current distribution, which allows an estimation of the magnetic field in the launcher area.

Finally, an on-site instrumentation of the site with a series of current and magnetic sensors would allow the monitoring of the actual lightning activity on the site and the assessment of the magnetic field mitigation ■

Acknowledgements

The authors would like to thank Mr Phippe CUROT (CNES France) for his support for this work

References

[1] S. SOULA – *Electrical Environment in a Storm Cloud*. Aerospace Lab Issue 5, December 2012.
[2] K. BERGER, R. B. ANDERSON and H. KRÖNINGER – *Parameters of Lightning Flashes.* CIGRE Electra n° 41, pp. 23-37, 1975.
[3] V. A. RAKOV and M. A. UMAN – *Lightning Physics and Effects.* Cambridge University Press, 2003.
[4] R. H. GOLDE – *Lightning*. Academic Press, 1975.
[5] R. B ANDERSON and A. J. ERIKSSON – *Lightning Parameters for Engineering Application*. CIGRE Electra n° 69, pp. 65-102, 1980.
[6] CEI 62305 – *Protection against Lightning*. 2006.
[7] P. LAROCHE and al. – *Observations of Bi-Directional Leader Development in Triggered Lightning Flash.* ICOLSE, 1991.
[8] M. BECERRA, V. COORAY and F. ROMAN – *Lightning Striking Distance of Complex Structures*. IET Gener Transm. Distrib, January 2008.
[9] L. DELLERA, E. GARBAGNATI – *Lightning Stroke Simulation by Means of the Leader Progression Model.* IEEE/PES, Long Beach California,1989.
[10] J. C. WILLETT, D. A. DAVIES and P. LAROCHE – *An Experimental Study of Positive Lightning Rocket Triggered.* Atmos. Res. 51, pp. 189-219, 1999.
[11] A. BONDIOU and I. GALLIMBERTI – *Theoretical Modeling of the Development of the Positive Spark in Long Gaps.* J. Phys. D: Appl phys., 1994.
[12] P LALANDE – *Study of the Lightning Stroke Conditions on a Grounded Structure*. Phd Onera, 1996.
[13] A.SCHAFFAR and J.L.DECIBIEUX – ESA Workshop on Aerospace EMC Florence, Italy, 2009.
[14] S. DESHAYES, S. FARGEOT, A. SCHAFFAR, P. N. GINESTE – *Calculs numériques des effets de la foudre sur l'ensemble de lancement Ariane 5 10t*. CEM04 Symposium.
[15] F. VANCE – *Coupling to Shielded Cable Edward*. A Wiley-Interscience publication.
[16] L. GRCEV and al. – *Lightning Current Distribution to Ground at a Power Line Tower Carrying a Radio Base Station.*
[17] E. BACHELIER and al. – *Simulation 3D de grands systèmes complexes: application a la definition des systèmes de protection foudre des futures sites de lancement SOYUZ et VEGA*. CEM, 2008.
[18] W. RISON and al. – *Lightning Air Terminals – Is Shape Important.* ISEMC, 2004.
[19] J. P. MARQUE – *Essai de simulation de foudroiement du site de lancement ELA au CSG.* Rapport Onera 22/6118, November 1989.

Acronyms

Cloud-to-Cloud (CC)
Cloud-to-Ground (CG)
Centre Spatial Guyannais (CSG)
Electro-explosive device (EED)
Electricité de France (EDF)
LIghtining Resistive Inductive Circuit (LIRIC)
Liquid oxygen (LOX)
Lightning Protection Level (LPL)
Lightning Protection System (LPS)
Electric Field Mills - *Moulin À Champ* (MAC)
Partial element Equivalent Circuit (PEEC)
Thunderstorm Occurrence (THOR)

AUTHORS

François Issac obtained his Technical University Degree (DUT) in physics measurement in 1982, in Montpellier, France. He began working at Ecopol from 1983 to 1986 on lightning effects and he joined the Office National d'Etudes et de Recherches Aérospatiales (Onera) where he became involved in numerous large scale EMC experiments (in-flight lightning tests on a Transall aircraft in 1987-1990; EMPTAC tests on EM Topology, 1993-1996; joint cooperation on mode stirred chambers with DERA, 1999-2000). Nowadays, his field of interest covers a large area, from low frequency to high frequency, mainly from an experimental point of view. He is co-author of numerous papers dealing with EM measurement validations carried out at Onera.

Elodie Bachelier is engineer in the EMC team of the Electromagnetism and Radar Department, at Onera Toulouse. She first studied applied mathematics, and prepared a PhD thesis on the modeling of diffusion effects of soils, with a FDTD method. In the EMC team, she works on the improvement of the numerical tools dedicated to 3D electromagnetic coupling, for complex industrial problems. During the last ten years, modeling the effects of lightning on structures has been an important part of her topics of interest.

Daniel Prost got his engineering degree from INPG (Institut National Polytechnique de Grenoble) in 1991 and obtained his Ph.D on magnetic properties of superconductors, from the Paris Sud University at LPS (Laboratoire de Physique des Solides d'Orsay) in 1994. He has been working as a Research Engineer in different industrial companies (Schneider Electric, Schlumberger), involved in different topics (circuit breakers, electric arc, magnetic sensors, simulation). He joined the French Aerospace Lab Onera in 2008 to more especially work on lightning indirect effects and other EMC concepts in the aerospace industry context.

Vincent Enjalbert is a lightning expert and test manager within the lightning department of DGA Techniques Aéronautiques since 1994. He is in charge of tests on systems. He has been led to perform and manage tests on the main civilian and military aeronautical programs. He is also in charge of test campaigns on ground structures. Today, he is carrying out expertises to the benefit of military programs managed by the Direction Générale de l'Armement (DGA) of the Ministry of Defence.

Laurent Mohedano is responsible for the communication network activity for the "région Aquitaine" at APAVE SUDEUROPE. Highly experienced, for more than 20 years he worked on lightning protection. He has, in particular participated in the European project MESA which aimed at the development and the site testing of a lightning generator. He has also written risk analyses and technical studies on lightning for the sites of VEGA and SOYUZ of the Guyana Space center. He had also provided risk analyzes and lightning technical studies of the VEGA and SOYUZ sites at the Guyana Space Center.